UNIVERSITY OF LONDON THESIS

Degree PhD Year 2006 Name of Author LASHLEY Tamaryn C.

BRI2 gene-related dementias; a morphological and biochemical study.

By Tammaryn Lashley

Thesis submitted for the degree of Doctor of Philosophy at the University of London

Department of Molecular Neuroscience
Institute of Neurology
Queen Square House
Queen Square
London
WC1N 3BG

ProQuest LLC
789 East Eisenhower Parkway
P.O. Box 1346
Ann Arbor, MI 48106-1346

Abstract

Aspects of the neurodegenerative mechanism in AD remain unknown; therefore studies on alternative models of cerebral amyloidosis, such as familial British dementia (FBD) and familial Danish dementia (FDD) may contribute to a better understanding of the neurodegenerative process. FBD and FDD are neurodegenerative disorders caused by mutations in the *BRI2* gene. Both mutations cause elongation of the precursor proteins, the furin-like cleavage of which results in the formation of amyloidogenic peptides, ABri in FBD and ADan in FDD.

Extensive morphological examinations of FBD and FDD were undertaken using antibodies recognising ABri and ADan, establishing a regional distribution of CNS peptide deposits in either amyloid or pre-amyloid configuration in both diseases, including cerebral amyloid angiopathy (CAA) formation.

Amyloid associated proteins (AAP) are able to modify Aβ aggregation and are implicated in AD pathogenesis. Establishing whether AAPs are implicated in the pathogenesis of other cerebral amyloidoses, AAP deposition was investigated and found associated with ABri and ADan amyloid and preamyloid parenchymal lesions. Inflammatory mechanisms, including activation of the complement pathways, initiated by Aβ deposition strongly are implicated in AD pathogenesis. The presence of the complement pathways were shown in FBD and FDD, highlighting the importance of chronic inflammation in the neurodegenerative diseases. Biochemical analysis of extracted ABri and ADan species indicates that as solubility of the deposits decrease heterogeneity and complexity of extracted peptides increases, including post-translational modification of glutamate to pyroglutamate.

The production and cellular origin of the precursor proteins and the localisation of furin expression were investigated. Evidence is presented that BRI2 mRNA and furin are found in neurons and glia, suggesting that cleavage of the wild type and mutated precursor proteins can take place in these cells. The absence of BRI2 mRNA in cerebrovascular cells indirectly supports the drainage hypothesis of CAA.

For my Dad

Acknowledgements

I would like to thank my supervisors, firstly Professor Tamas Revesz for encouraging me to undertake this work, believing that I could do the work and supporting me all the way. Dr Janice Holton and Dr Jorge Ghiso for giving me support and advice when needed. I would also like to thank Professor Blas Frangione and Dr Jorge Ghiso for allowing me to visit their laboratory in New York to undertake part of my studies and making me feel so welcome. I would like to thank Dr Gordon Plant for the clinical analysis and allowing me to use the FBD cases for this study. Dr Marie Bojsen-Møller and Dr Hans Braendgaard for the clinical analysis and allowing me to use the FDD cases for this study, and the families of the cases for allowing me to study these two very interesting diseases. I would like to thank everyone in the Division of Neuropathology for the help their help they gave me at various points throughout my studies. Especially Catherine Strand, Milan Ganguly and Hilary Ayling who have helped in numerous ways to keep me going throughout my studies. Steve Durr and Trinnete Pearce who have listened to my moans and groans without any complaint and both been invaluable.

I would like to thank Yasushi Tomidokoro and Doug Ng who made me feel at home in New York and for their help with and completion of the biochemical techniques and endless trips to McDonalds to fetch lunch!!

I would like to thank all the staff at the Queen Square Brain Bank especially Linda Parsons for her help with everything including sending endless parcels to New York and using all her controls samples and Dr Ann Kingsbury for her help with radioactive work. I would like to thank all at the Reta Lila Weston Institute, including Rina Bandopadhyay, Rohan de Silva, Drew Hope and Alan Pitman for their help and guidance and making me so welcome in their laboratory.

Finally, I would like to thank my family, Pauline Johnson (my mom) for helping in any way she could. Looking after Eden and Ethan and just being there when I needed her. Lastly, my husband Andrew for providing all the help, support and encouragement needed and ofcourse my kids (Eden and Ethan) for providing much needed interruptions to get me through.

Publications

Original papers related to thesis

1. **Tammaryn Lashley**, Tamas Revesz, Gordon Plant, Rina Bandopadhyay, Agueda Rostagno, Nick Wood, Rohan De Silva, Blas Frangione, Jorge Ghiso, Janice Holton. Expression of *BRI2* mRNA, BRI precursor protein and furin in normal human brain and familial British dementia: their relevance to the pathogenesis of disease. To be submitted.

2. **Tammaryn Lashley**, Janice L. Holton, Marcel M Verbeek, Agueda Rostagno, Marie Bojsen-Møller, Guido David, Jack van Horssen, Hans Braendgaard, Gordon Plant, Blas Frangione, Jorge Ghiso, Tamas Revesz. Molecular chaperons, amyloid and preamyloid lesions in the *BRI2* gene-related dementias: a morphological study. Neuropathology Applied Neurobiology In Press.

3. Ghiso J, Rostagno A, Tomidokoro Y, **Lashley T**, Bojsen-Moller M, Braengaard H, Plant G, Holton J, Revesz T, Frangione B. Genetic Alterations of the BRI2 gene: Familial British and Danish dementias. Brain Pathol 2006;16:71-79.

4. Tomidokoro Y, **Lashley T**, Rostagno A, Neubert TA, Bojsen-Moller M, Braendgaard H, Plant G, Holton J, Frangione B, Revesz T, Ghiso J. Familial Danish dementia: co-existence of Danish and Alzheimer amyloid subunits (ADan AND A{beta}) in the absence of compact plaques. J Biol Chem. 2005 Nov 4;280(44):36883-94.

5. Rostagno A, Revesz T, **Lashley T**, Tomidokoro Y, Magnotti L, Braendgaard H, Plant G, Bojsen-Moller M, Holton J, Frangione B, Ghiso J. Complement activation in chromosome 13 dementias. Similarities with Alzheimer's disease. J Biol Chem. 2002 Dec 20;277(51):49782-90. Epub 2002 Oct 17.

6. Holton JL, **Lashley T**, Ghiso J, Braendgaard H, Vidal R, Guerin CJ, Gibb G, Hanger DP, Rostagno A, Anderton BH, Strand C, Ayling H, Plant G, Frangione B, Bojsen-Moller M, Revesz T. Familial Danish dementia: a novel form of cerebral amyloidosis associated with deposition of both amyloid-Dan and amyloid-beta. J Neuropathol Exp Neurol. 2002 Mar;61(3):254-67.

7. Ghiso JA, Holton J, Miravalle L, Calero M, **Lashley T**, Vidal R, Houlden H, Wood N, Neubert TA, Rostagno A, Plant G, Revesz T, Frangione B. Systemic amyloid deposits in familial British dementia. J Biol Chem. 2001 Nov 23;276(47):43909-14. Epub 2001 Sep 13.

8. Holton JL, Ghiso J, **Lashley T**, Rostagno A, Guerin CJ, Gibb G, Houlden H, Ayling H, Martinian L, Anderton BH, Wood NW, Vidal R, Plant G, Frangione B, Revesz T. Regional distribution of amyloid-Bri deposition and its association with neurofibrillary degeneration in familial British dementia. Am J Pathol. 2001 Feb;158(2):515-26.

Review papers related to thesis

1. Rostagno A, Tomidokoro Y, **Lashley T**, Ng D, Plant G, Holton J, Frangione B, Revesz T, Ghiso J. Chromosome 13 dementias. Cell Mol Life Sci. 2005 Aug;62(16):1814-25. Review.

2. Revesz T, Ghiso J, **Lashley T**, Plant G, Rostagno A, Frangione B, Holton JL. Cerebral amyloid angiopathies: a pathologic, biochemical, and genetic view. J Neuropathol Exp Neurol. 2003 Sep;62(9):885-98. Review.

3. Revesz T, Holton JL, **Lashley T**, Plant G, Rostagno A, Ghiso J, Frangione B. Sporadic and familial cerebral amyloid angiopathies. Brain Pathol. 2002 Jul;12(3):343-57. Review.

4. Ghiso J, Revesz T, Holton J, Rostagno A, **Lashley T**, Houlden H, Gibb G, Anderton B, Bek T, Bojsen-Moller M, Wood N, Vidal R, Braendgaard H, Plant G, Frangione B. Chromosome 13 dementia syndromes as models of neurodegeneration. Amyloid. 2001 Dec;8(4):277-84. Review.

5. Frangione B, Revesz T, Vidal R, Holton J, **Lashley T**, Houlden H, Wood N, Rostagno A, Plant G, Ghiso J. Familial cerebral amyloid angiopathy related to stroke and dementia. Amyloid. 2001 Jul;8 Suppl 1:36-42. Review.

Orginal papers unrelated to thesis

1. Yue-Shan Piao, Chun-Feng Tan, Keisuke Iwanaga, Akiyoshi Kakita, Hiroki Takano, Masatoyo Nishizawa, **Tammaryn Lashley**, Tamas Revesz, Andrew Lees, Rohan de Silva, Mitsuhiro Tsujihata, Hitoshi Takahashi. Sporadic 4-repeat tauopathy with frontotemporal degeneration, parkinsonism and motor neuron disease. Paper accepted in Acta Neuropath.

2. Rohan de Silva, **Tammaryn Lashley**, Catherine Strand, Anna-Maria Shiarli, Jing Shi, Kathryn L Bailey, Eileen H Bigio, Kunimasa Arima, Eizo Iseki, Shigeo Murayama, Hans Kretzschmar, Manuela Neumann, Carol Lippa, Glenda Halliday, James MacKenzie, Rivka Ravid, Dennis Dickson, Zbigniew Wszolek, Takeshi Iwatsubo, Stuart M Pickering-Brown, Janice Holton, Andrew Lees, Peter Davies, Tamas Revesz, David MA Mann. An immunohistochemical study of cases of sporadic and inherited Frontotemporal lobar degeneration using 3R- and 4R-specific tau monoclonal antibodies. Paper submitted to Brain.

3. Hope AD, **Lashley T**, Lees AJ, de Silva R. Failure in heat-shock protein expression in response to UBB+1 protein in progressive supranuclear palsy in humans. Neurosci Lett. 2004 Apr 8;359(1-2):94-8.

4. Bandopadhyay R, Kingsbury AE, Cookson MR, Reid AR, Evans IM, Hope AD, Pittman AM, **Lashley T**, Canet-Aviles R, Miller DW, McLendon C, Strand C, Leonard AJ, Abou-Sleiman PM, Healy DG, Ariga H, Wood NW, de Silva R, Revesz T, Hardy JA, Lees AJ. The expression of DJ-1 (PARK7) in normal human CNS and idiopathic Parkinson's disease. Brain. 2004 Feb;127(Pt 2):420-30.

5. de Silva R, **Lashley T**, Revesz T, Lees A, Powers JM. Detecting tau isoforms in archival cases. Acta Neuropathol (Berl). 2004 Feb;107(2):181-2.

6. de Silva R, **Lashley T**, Gibb G, Hanger D, Hope A, Reid A, Bandopadhyay R, Utton M, Strand C, Jowett T, Khan N, Anderton B, Wood N, Holton J, Revesz T, Lees A. Pathological inclusion bodies in tauopathies contain distinct complements of tau with three or four microtubule-binding repeat domains as demonstrated by new specific monoclonal antibodies. Neuropathol Appl Neurobiol. 2003 Jun;29(3):288-302.

7. Morris HR, Gibb G, Katzenschlager R, Wood NW, Hanger DP, Strand C, **Lashley T**, Daniel SE, Lees AJ, Anderton BH, Revesz T. Pathological, clinical and genetic heterogeneity in progressive supranuclear palsy. Brain. 2002 May;125(Pt 5):969-75.

8. Houlden H, Baker M, McGowan E, Lewis P, Hutton M, Crook R, Wood NW, Kumar-Singh S, Geddes J, Swash M, Scaravilli F, Holton JL, **Lashley T**, Tomita T, Hashimoto T, Verkkoniemi A, Kalimo H, Somer M, Paetau A, Martin JJ, Van Broeckhoven C, Golde T, Hardy J, Haltia M, Revesz T. Variant Alzheimer's disease with spastic paraparesis and cotton wool plaques is caused by PS-1 mutations that lead to exceptionally high amyloid-beta concentrations. Ann Neurol. 2000 Nov;48(5):806-8.

9. Hirst EM, **Johnson TC**, Li Y, Raisman G. Improved post-embedding immunocytochemistry of myelinated nervous tissue for electron microscopy. J Neurosci Methods. 2000 Feb 15;95(2):151-8.

Abstracts

1 Bandopadyay, R, Coulter,I, Kumaran, R, **Lashley, T**, Kingsbury, A, De Silva, R, Holton, J, Revesz, T, Lees, A. DJ-1 (PARK-7) protein in neuronal and glial inclusions in neurodegenerative disorders. *Neuropathol Appl Neurobiol In press 2006.*

2 De Silva, R, **Lashley, T,** Strand, K, Shirli, AM, Revesz, D, Mann, DMA. An immunohistochemical study of sporadic and inherited fronto-temporal lobar degeneration using 3R- and 4R-specific monoclonal tau antibodies. *Neuropathol Appl Neurobiol In press 2006.*

3 **Lashley, T**, Holton, JL, Frangione, B, van Horssen, J, Rostagno, A, Verbeek, MM, Ghiso, J, Revesz, T. Amyloid-associated proteins (AAPs) in familial British dementia (FBD)and familial Danish dementia (FDD). *Neuropathol Appl Neurobiol 31*: 2005

4 Rostagno, A, Zhao, ZH, Ng, D, **Lashley, T**, Holton, J, Frangione, B, Revesz, T, Ghiso, J. Familial British and Danish dementias: BRI2 gene and protein expression by human cerebral cells. *Neurobiology of Aging* 25: 2004. Suppl. 2

5 **Lashley, T**, Holton, JL, Frangione, B, Bandopadhyay, R, Ghiso, J, Rostagno, A, Revesz, T. The possible origin of the amyloid peptides in the BRI2 gene-related dementias. *Neurobiology of Aging* 25: 2004. Suppl. 2

6 **Lashley T**, Holton JL, Rostagno A, Strand C, Plant G, Bojsen-Moller M, Braendgaard H, Frangione B, Ghiso J, Revesz T. Morphological evidence of *in vivo* activation of the complement pathways in the *BRI2* gene-related dementias. *Neuropathol Appl Neurobiol* 29: 183, 2003.

7 Holton JL, Ghiso J, **Lashley T**, Ganguly M, Strand C, Rostagno A, Plant G, Frangione B, Revesz T. Familial British dementia (FBD): a cerebral amyloidosis with systemic amyloid deposition. *Neuropathol Appl Neurobiol* 28:148, 2003.

8 Revesz T, **Lashley T**, Ganguly M, et al. Familial British dementia (FBD), a form of cerebral amyloidosis with systemic amyloid deposition. *Neurobiology of Aging* 23:1759, 2002.

9 Tomidokoro Y, Fleire S, Rostagno A, Frangione,B, Ghiso J, **Lashley T**, Holton J, Houlden H, Revesz T, Bojsen-Moller M, Braendgaard H, Plant G. Co-existence of amyloid ADan and amyloid-beta in familial Danish dementia. *Neurobiology of Aging* 23:1663, 2002.

10 Holton J, **Lashley T**, Revesz T, Rostagno A, Frangione B, Ghiso J. Morphological evidence of the activation of the classical complement pathway in the BRI gene-related dementias. *Neurobiology of Aging* 23:774, 2002.

11 Holton JL, **Lashley T**, Vidal R, Rostagno A, Gibb G, Anderton BH, Braendgaard H, Plant GT, Bojsen-Moller M, Ghiso J, Frangione B, Revesz T. Familial Danish dementia (FDD): a novel form of cerebral amyloidosis associated with deposition of two amyloidogenic peptides. *J Neuropathol Exp Neurol* 60:131, 2001.

12 Revesz T, **Lashley T**, Vidal R, Rostagno A, Gibb G, Anderton BH, Plant G, Frangione B, Ghiso J, Holton JL. Deposition of amyloid-Bri (ABri) is associated with neurofibrillary pathology in familial British dementia (FBD). *J Neuropathol Exp Neurol* 60:132, 2001.

13 Holton JL, **Lashley T**, Vidal R, Rostagno A, H. Ayling, Braendgaard H, Plant GT, Ghiso J, Frangione B, Bojsen-Moller M, Revesz T. Immunohistochemical and immuno-electron microscopic (iEM) study of familial Danish dementia (FDD), a novel form of cerebral amyloidosis. *Neuropathol Appl Neurobiol* 27:147, 2001.

14 Holton JL, **Lashley T**, Vidal R, Rostagno A, Guerin C, Houlden H, Plant G, Frangione B, Ghiso J, Revesz T. Familial British dementia: immunohistochemical and immunoelectron microscopic study. *Brain Pathol* 10(Suppl): 713-714, 2000.

15 Revesz T, Houlden H, Holton JL, Baker M, Vowles GH, **Lashley T**, Wood NW, Scaravilli F, Swash M, Hardy J, Geddes JF. Alzheimer's disease with spastic paraparesis due to deletion of exon 4 and a P436E point mutation of exon 12 of the presenilin 1 gene. *Brain Pathol* 10(Suppl): 633, 2000.

16 Revesz T, Holton JL, Vidal R, Rostagno A, **Lashley T**, Plant G, Frangione B, Ghiso, J. Cerebral deposition of ABri amyloid in familial British dementia. *Neurobiol Aging* 21 (Suppl 1S): S191, 2000.

17 Revesz T, Holton JL, Vidal R, Rostagno A, Houlden H, **Johnson T**, Ayling H, Martinian L, Plant GT, Frangione B, Ghiso J. The distribution of ABri cerebral amyloid in familial British dementia. *Neuropathol Appl Neurobiol* 26:193, 2000.

Table of contents

List of Figures

List of Tables

Chapter 7

Chapter 8

Abbreviations

Aβ	Beta-amyloid protein
AβPP	Beta-amyloid precursor protein
AAP	amyloid associated proteins
ABri	Amyloid-Bri
ABriPP	British precursor protein
ABC	Avidin biotin complex
ACys	Amyloid-Cystatin
AcN	Acetonitrile
ACT	α-1-antichymotrypsin
AD	Alzheimer's disease
ADan	Amyloid-Dan
ADanPP	Danish precursor protein
ADAM10	disintegrin metalloproteases 10
ADAM17	disintegrin metalloproteases 17
ADDL	Aβ-derived diffusible ligands
AGel	Amyloid-Gelsolin
AN	Abnormal neurite
ApoE	Apolipoprotein E
ApoJ	Apolipoprotein J
ATTR	Amyloid-transthyretin
BACE	β-SITE APP cleaving enzyme
BBB	Blood brain barrier
BriPP	Wild type Bri precursor protein

BSA	Bovine serum albumin
C1INH	C1 inhibitor
CAA	Cerebral amyloid angiopathy
CBD	Corticobasal degeneration
CCPR	Complement control protein repeat
CLAC	collagen-like Alzheimer amyloid plaque component
CNS	Central nervous system
CSF	Cerebral spinal fluid
Cys	Cysteine
DAB	di-aminobenzidine
DAF	decay-accelerating factor
DEPC	diethyl pyrocarbonate
DNA	deoxyribonucleic acid
DS	Down's syndrome
DTT	Dithiothreitol
ECL	enhanced chemiluminescence
EDTA	ethylenediaminetetra acetic acid
EM	Electron microscopy
ER	Endoplasmic reticulum
FA	Formic acid
FAF	Familial amyloidosis Finnish type
FAP	Familial amyloidoitic polyneuropathy
FBD	Familial British dementia
FDD	Familial Danish dementia
FISH	fluorescence *in-situ* hybridisation

FTDP	Fronto-temporal dementia
FTDP-17	Fronto-temporal dementia linked to chromosome 17
GAG	glycoaminoglycans
GAPDH	glyceraldehydes-3-phosphate dehydrogenase
GSS	Gerstmann-Sträussler syndrome
GCL	Granular cell layer
HCCAA	Hereditary cystatin C amyloid angiopathy
HCHWA-D	Hereditary cerebral haemorrhage with amyloidosis of Dutch type
HCHWA-I	Hereditary cerebral haemorrhage with amyloidosis of Icelandic type
HSPG	Heperan sulphate proteoglycans
H&E	Haemotoxylin and Eosin
KPI	Kunitz-type serine protease inhibitor
LRP-1	low-density lipoprotein receptor related protein-1
MAPs	microtubule associated proteins
MAC	membrane attack complex
MES	(2-(N-morpholino)ethane sulphonic acid)
Mg	Magnesium
MOPS	(3-(N-morpholino) propane sulphonic acid)
mRNA	messenger ribonucleic acid
MS	Mass spectrometry
NFT	neurofibrillary tangle
NT	neuropil thread
PBS	Phosphate buffered saline
PC	Pressure Cook
PCo	Proprotein convertase

PG	Proteoglycans
PHF	Paired helical filament
PS1	Presenilin 1
PS2	Presenilin 2
PSP	Progressive supranuclear palsy
PVDF	Polyvinydene diflouride
PVC	Parvopyramidal cell clusters
RAGE	receptor for advanced glycation end products
RCA	Regulators of complement activation
RNA	Ribonucleic acid
RT-PCR	reverse transcriptase polymerase chain reaction
sAβ	Soluble Amyloid-Beta
SAP	serum amyloid P
SDS	Sodium Dodeccasulphate
SR	Scavenger receptor
SSC	Sodium chloride- sodium citrate buffer
SSPE	saline sodium phosphate EDTA buffer
TACE	Tumour necrosis factor alpha-converting enzyme
TBS	Tris buffered saline
TFA	Trifluoracetic acid
TTR	Transthyretin
Vn	Vitronectin

Chapter 1

Introduction

Chapter 1 Introduction.

1.1 Cerebral amyloidosis and neurodegeneration

Amyloidosis is a term that covers many disorders involving abnormal protein conformations leading to aggregation and fibrillization. A diverse group of proteins which are normally present as soluble precursor proteins are able to assemble into amyloid fibrils by adopting a β-pleated sheet conformation, producing insoluble deposits. To date there are over 25 different proteins identified that are able to form amyloid fibrils (Westermark *et al.*, 1999; Revesz *et al.*, 2003). Although these amyloid forming proteins are the product of normal genes, several amyloid precursors do contain abnormal amino acid substitutions causing an unusual potential for self-aggregation. Of all the identified amyloid proteins, less than half are known to result in amyloid deposition in the central nervous system (CNS), which can result in cognitive decline, dementia and stroke.

Cerebral amyloid angiopathy (CAA) is a term used to define the deposition of amyloid within the walls of leptomeningeal and cortical arteries, arterioles and less frequently capillaries and veins (Vinters, 1987), commonly associated with Alzheimer's disease (AD) and Down's syndrome (DS). Familial conditions in which amyloid is deposited as CAA include hereditary cerebral haemorrhage with amyloidosis of Icelandic type (HCHWA-I), familial CAA related to mutations of the *APP*, *PS1* or *PS2* genes including hereditary cerebral haemorrhage with amyloidosis of Dutch type (HCHWA-D), transthyretin-related meningocerebrovascular amyloidosis, gelsolin related CAA and the recently described *BRI2* gene-related dementias in the British and Danish kindreds which form the subject of this thesis.

CAA in AD may go beyond a contribution of ischaemia to the clinical and pathological manifestations of the disease, suggesting that CAA may be involved in the development of plaques and tangles, the pathological hallmarks of AD (Weller *et al.*, 1998). Clues to the relationship between amyloid and neuronal dysfunction may well arise from research involving other mutant peptides in addition to Aβ. Particularly the novel molecules ABri and ADan which originate from different mutations in the *BRI2* gene and were not previously known to be related to human neurological disorders. Therefore different amyloid peptides are able to trigger similar neuropathological changes leading to neuronal loss and dementia, supporting the notion that amyloid peptides may be of primary importance in the initiation of neurodegeneration.

1.2 Familial British dementia (FBD)

1.2.1 Clinical features of FBD

FBD was first described by Worster-Drought and colleagues as a familial presenile dementia with spastic paralysis (Worster-Drought *et al.*, 1944; Worster *et al.*, 1940). In subsequent studies FBD was referred to as an example of atypical AD (Aikawa *et al.*,), Gerstmann-Sträussler syndrome (GSS) (Masters *et al.*, 1981; de Court & Mandybur, 1987; Keohane *et al.*,) or as a form of primary CAA and classified together with the Icelandic and Dutch types of HCHWA (Vinters, 1987). It was also considered to be a form of hereditary spastic paraparesis (Baraitser, 1990).

Following the original pedigree studied by Worster-Drought et al (Worster *et al.*, 1940), a number of additional families have been described. Griffiths et al (1982) described two siblings with pathological changes that were identical to those observed in the cases described by Worster-Drought et al. Plant et al (1990) discovered that the two families

were part of the same larger pedigree, by reference to a house physicians family history in the archive case notes of a patient seen at the National Hospital for Neurology in 1924. In 1982 a case of 'familial cerebellar ataxia with amyloid angiopathy' was published by Love and Duchen. It has long been suspected that this patient suffered from the same disease despite there being no report of dementia. This case has also been linked to the main Worster-Drought family (Mead *et al.*, 2000). A pedigree of 372 individuals has so far been assembled from the Worster-Drought pedigree (Mead *et al.*, 2000) (figure 1.1).

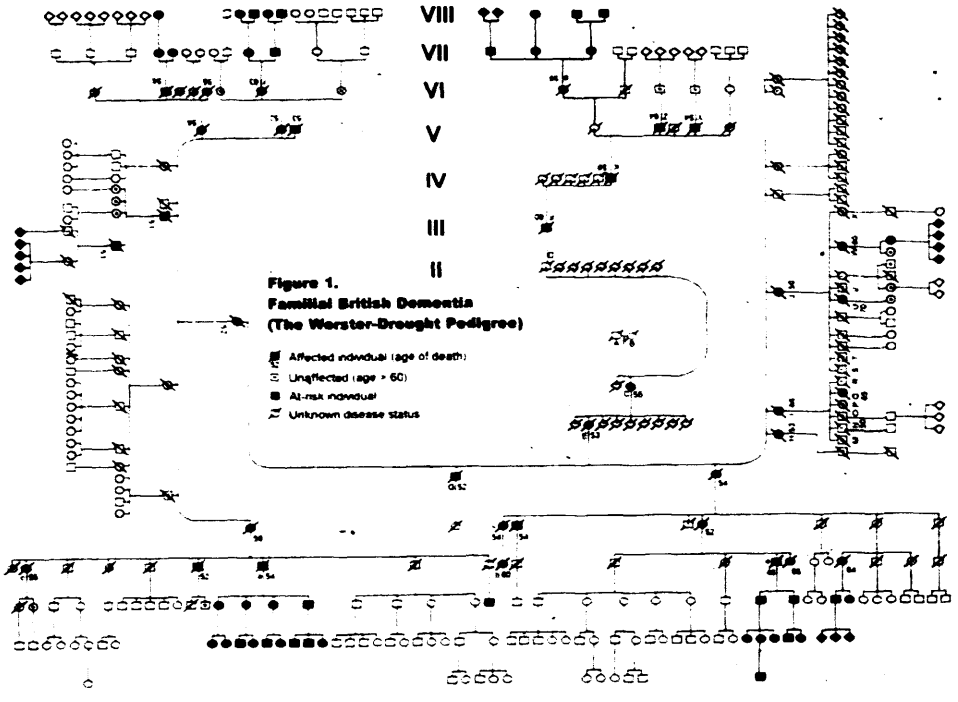

***Figure 1.1:** Worster-Drought pedigree (Mead et al 2000)*

A second pedigree, reported in abstract form by Doshi et al 1996, has been studied in detail in an attempt to find a common ancestor with the Worster-Drought pedigree (figure 1.2). Only two members are affected. The family was traced back to a generation born in 1840s but a link has not yet been found. A third pedigree has also been

identified recently with typical clinical presentation and the *BRI2* gene mutation in affected members. Although it cannot be traced at present to the Worster-Drought pedigree, ancestors of this and the Worster-Drought family are believed to have lived in the same village (unpublished data).

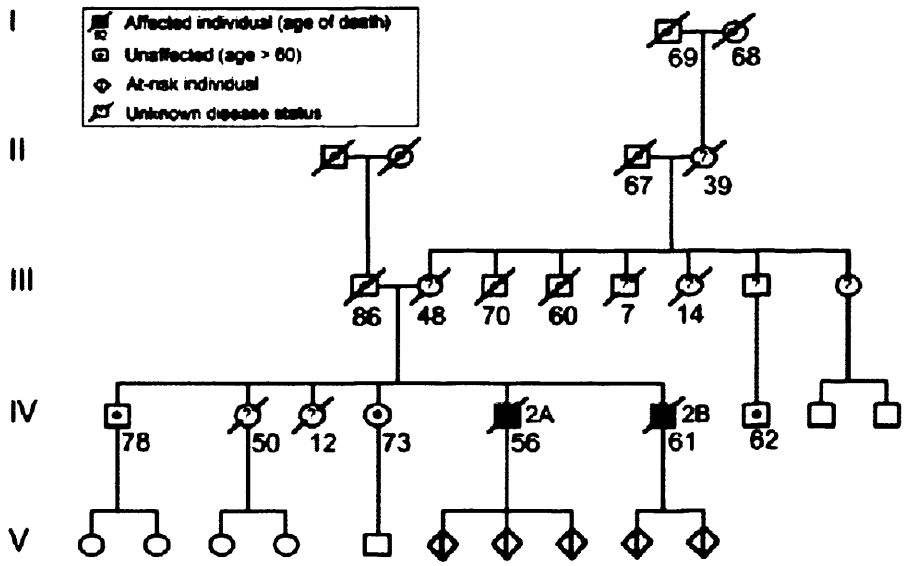

***Figure 1.2**: Familial British Dementia - second pedigree (Mead et al 2000)*

Analysis of clinical details of 6 living affected patients and 35 historical cases have shown a median age of onset of clinical symptoms is 48 years (range 40-60) and the median age of death 56 years (range 48-70) (Plant *et al.*, 1990) (table 1). Psychometric assessment early in the course of the disease has shown marked impairment of memory ultimately progressing to global dementia. Many of the cases developed personality change as an early manifestation. Spastic paralysis is characteristic and is far more profound than is seen in GSS or in variant AD. All patients have progressed to a mutism, unresponsiveness, quadraplegia and incontinence and finally to a chronic vegetative state.

Case (Worster-Drought)	Sex	Age at onset of symptoms (years)	Age at death (years)
II1	F	40	53
II2	F	-	-
III1	F	-	52
III2	M	57	60
III3	F	44	54
III4	F	48	53
III5	F	48	66
III6	F	48	50
IV1	M	40+	53
IV2	F	42	52
IV3	F	46	56
IV6	M	45	51
IV9	F	50	56
IV12	F	44	54
IV13	M	46	54
IV15	F	44	56
IV17	F	43	-
V2	F	57	63
V4	F	54	61
V7	M	50	56
V15	M	45	51
V28	F	50	55
V32	M	-	52
V33	M	48	50
V41	F	56	65
V45	F	42	64

***Table 1:** Age of onset and age of death of individuals affected by FBD (Plant et al 1990)*

1.2.2 Neuropathology of FBD

The neuropathological changes have been reported in detail in six historical cases of this condition (Worster-Drought *et al.*, 1944; Worster *et al.*, 1940; McMenemey, 1952; McMenemey, 1970; Griffiths *et al.*, 1982; Love & Duchen, 1982; Plant *et al.*, 1990). The brains are of normal or slightly reduced overall weight with leptomenigeal thickening and mild to moderate diffuse atrophy of both the cerebral and cerebellar hemispheres. The cerebral cortex is relatively well preserved in slices of the fixed brain but the white matter is reduced in bulk, diffusely discoloured and contains small cystic infarcts. The brain stem and spinal cord appear normal to the naked eye. The main histological finding is severe and widespread amyloid deposition in the walls of small

leptomeningeal arteries and arterioles of gray and white matter. In addition, there are numerous parenchymal amyloid plaques together with ischaemic white matter damage and the presence of numerous neurofibrillary tangles (NFTs), particularly in the hippocampus (Plant *et al.*, 1990). CAA affects vessels of small size usually less than 100μm in diameter. The vessels affected by CAA are narrowed or occluded and a significant proportion of them show concentric fibrotic thickening of their wall, fragmentation of the elastic lamina or the morphological phenomenon of double barrelling.

Two types of amyloid plaques are found: a) large plaques are about 150μm in diameter with a central congophilic core with radiating spicules of amyloid emerging from it and a finely fibrillar rim: b) small plaques with appearances similar to the core of the large plaques without the rim (Plant *et al.*, 1990). Some of the large plaques are related to capillaries. The large plaques are most numerous in the dentate fascia, CA3 and CA4 regions of the hippocampus, presubiculum and basolateral nucleus of the amygdala. Perivascular plaques occur chiefly in the cerebral and cerebellar cortex and white matter, while small plaques are numerous in CA1 and part of CA2 regions of the hippocampus and less common in the granular cell layer of the cerebellar cortex (Mead *et al.*, 2000).

NFTs are seen in most of the remaining pyramidal neurons of the hippocampus and are also observed in the subiculum, entorhinal cortex, amygdala and occasionally elsewhere in the cortex and in the basal nucleus of Meynert. In the cerebellar cortex neuronal axonal torpedoes, neuronal cell loss and severe gliosis are observed. The dentate nucleus also shows neuron loss and deep cerebellar white matter ischaemic lesions. In the medulla there is long tract degeneration in the pyramids and inferior cerebellar peduncles, neuron loss and gliosis in the inferior olive and in the medial accessory

olive. The spinal cord shows pallor of myelin staining in all columns of white matter, a few large amyloid plaques in grey and white matter and amyloid containing vessels.

The white matter changes are considered to be secondary to CAA in arterioles penetrating through the cortex to supply the white matter. The white matter changes are thought to contribute to the dementia. The plaque formation, NFTs and neuron loss in the hippocampus are sufficient to account for amnesia; cerebellar plaques and ischaemic lesions for the ataxia and cerebral deep white matter and spinal cord pathology for the spasticity (Mead *et al.*, 2000). Although the pathological changes were originally thought to be confined to the CNS deposition of the amyloid protein in systemic organs has been added to the list of morphological abnormalities that occur in FBD (Ghiso *et al.*, 2001).

1.3 Familial Danish dementia (FDD)

1.3.1 Clinical features of FDD

Strömgren (1981) described 9 cases from 3 generations of an autosomal dominant inherited disorder. The family originated from the Djursland peninsula Northwest of the city of Aarhus in Denmark with most members now living in Aarhus. Previously known as heredopathia ophthalmo-oto-encephalica (Stromgren *et al.*, 1970; Stromgren, 1981) then as familial CAA with deafness and ocular haemorrhage (Danish type). The clinical picture of FDD is unique with early cataract formation (around the age of 20) followed by deafness (around the age of 30) and progressive ataxia and dementia beginning in the fifth and sixth decades. Progression to death occurs within ten years following the onset of neurological symptoms. The ages at onset of the different symptoms are summarized in Table 2 (Stromgren, 1981).

Designation in pedigree	Ages at onset of disturbances				Age at death
	Visual	Auditory	Neurological	Psychiatric	
II-2	<46	None	?	?	~73
III-1	~20	~43	?	53	62
III-2	48?	47	60	59	60
III-3	32	42	56	56	58
III-5	27	42	<50	<55	57
III-6	Congenital	<28	<20	56	57
III-7	27	?	?	?	34
IV-2	<19	25	40	<42	?
IV-5	10	28	37	54	60

***Table 2:** Ages of disturbance onset in FDD*

An up to date pedigree of the family with FDD is shown in figure 1.3. Case 3 corresponds to III-6 and Case 2 corresponds to IV-5 in table 2. Cases 1, 2 and 3 shown in figure 1.3 were available for the study presented in this thesis.

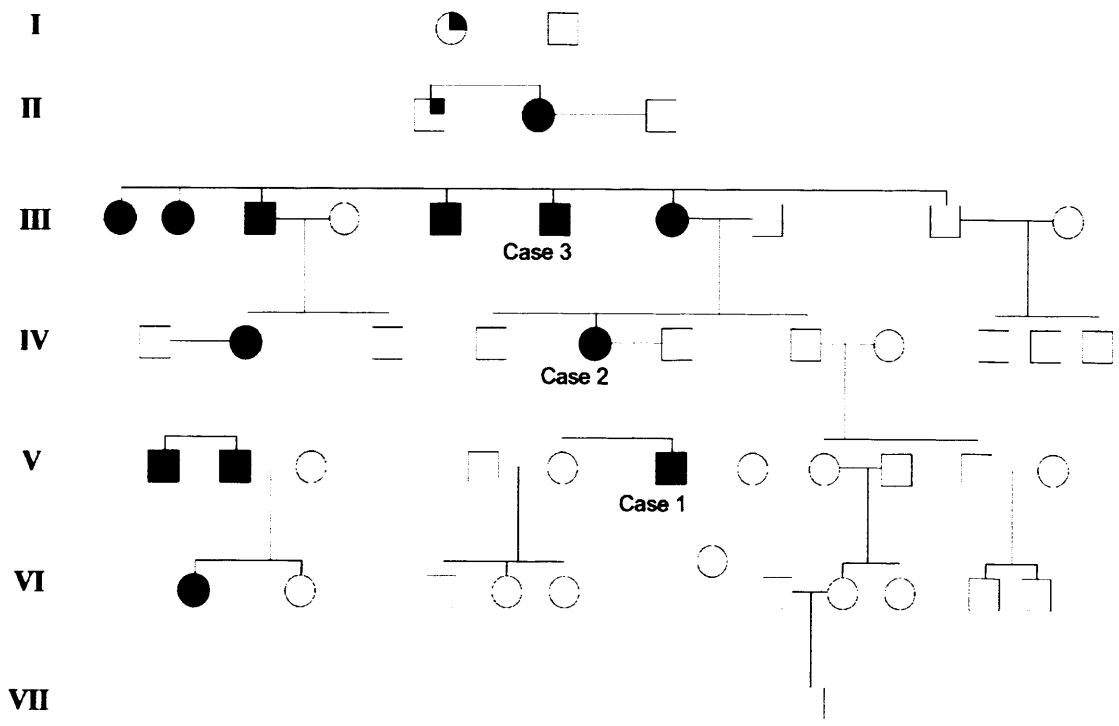

***Figure 1.3**: FDD pedigree (Holton et al 2002)*

1.3.2 Neuropathology of FDD

The published report by Strömgren in 1981 described accumulation of 'lipid' in the blood vessel walls and parenchyma but subsequent studies have shown the presence of CAA in FDD (Stromgren, 1981), in the cerebrum, cerebellum, spinal cord and retina (Bek, 2000). The disease is neuropathologically characterized by a uniform diffuse atrophy of all parts of the brain and very severe chronic diffuse encephalopathy mostly in the cerebellum, cerebral cortex and white matter. The presence of plaques and NFTs is the major histopathological finding in the hippocampus, whereas the cerebral white matter also shows some ischemic lesions (Stromgren *et al.*, 1970; Stromgren, 1981).

1.4 Genetic alteration of *BRI2* in FBD and FDD

1.4.1 Identification of ABri protein and ABriPP

In 1995 Ghiso et al investigated a case of FBD with immunohistochemical techniques using antibodies to known amyloid proteins and suggested that the disease 'familial cerebral amyloid angiopathy (British type), might be due to the deposition of a novel amyloid protein (Ghiso *et al.*, 1995). The identification of the amyloid protein was achieved by using a combination of formic acid solubilization and gel filtration chromatography from isolated leptomeningeal blood vessels (Vidal *et al.*, 1999). MS analysis indicated the presence of a peptide of Mr 3,935. Analysis of the protein sequence also revealed that the amyloid protein was a fragment derived from a larger precursor molecule in which the longest open reading frame predicted a protein of 266 amino acids with a calculated Mr of 30,329.05 and a theoretical pI of 4.86. Hydropathy analysis indicated the presence of a putative single transmembrane spanning domain between amino acids 52 and 74, indicating that the molecule is a type-II integral

transmembrane protein with the C-terminal part being extracellular and a potential N-glycosylation site identified at asparagine 170.

```
          gcgagatccctaccgcagtagccgcctctgccgccgcggagcttcccgaa    -  119
cctctcagccgcccggagccgctcccggagcccggccgtagaggctgcaatcgcagccgg    -  59
gagcccgcagcccgcgccccgagcccgccgccgcccttcgagggcgccccaggccgcgcc    -  1
atggtgaaggtgacgttcaactccgctctggcccagaaggaggccaagaaggacgagccc       60
 M  V  K  V  T  F  N  S  A  L  A  Q  K  E  A  K  K  D  E  P
 1                                                          20
aagagcggcgaggaggcgctcatcatccccccccgacgccgtcgcggtggactgcaaggac      120
 K  S  G  E  E  A  L  I  I  P  P  D  A  V  A  V  D  C  K  D
 21                                                         40
ccagatgatgtggtaccagttggccaaagaagagcctggtgttggtgcatgtgctttgga      180
 P  D  D  V  V  P  V  G  Q  R  R  A  W  C  W  C  M  C  F  G
 41                                                         60
ctagcatttatgcttgcaggtgttattctaggaggagcatacttgtacaaatattttgca      240
 L  A  F  M  L  A  G  V  I  L  G  G  A  Y  L  Y  K  Y  F  A
 61                                                         80
cttcaaccagatgacgtgtactactgtggaataaagtacatcaaagatgatgtcatctta      300
 L  Q  P  D  D  V  Y  Y  C  G  I  K  Y  I  K  D  D  V  I  L
 81                                                        100
aatgagccctctgcagatgccccagctgctctctaccagacaattgaagaaaatattaaa      360
 N  E  P  S  A  D  A  P  A  A  L  Y  Q  T  I  E  E  N  I  K
 101                                                       120
atctttgaagaagaagaagttgaatttatcagtgtgcctgtcccagagtttgcagatagt      420
 I  F  E  E  E  E  V  E  F  I  S  V  P  V  P  E  F  A  D  S
 121                                                       140
gatcctgccaacattgttcatgactttaacaagaaacttacagcctatttagatcttaac      480
 D  P  A  N  I  V  H  D  F  N  K  K  L  T  A  Y  L  D  L  N
 141                                                       160
ctggataagtgctatgtgatccctctgaacacttccattgttatgccacccagaaaccta      540
 L  D  K  C  Y  V  I  P  L  N  T  S  I  V  M  P  P  R  N  L
 161                                                       180
ctggagttacttattaacatcaaggctggaacctatttgcctcagtcctatctgattcat      600
 L  E  L  L  I  N  I  K  A  G  T  Y  L  P  Q  S  Y  L  I  H
 181                                                       200
gagcacatggttattactgatcgcattgaaaacattgatcacctgggtttctttatttat      660
 E  H  M  V  I  T  D  R  I  E  N  I  D  H  L  G  F  F  I  Y
 201                                                       220
cgactgtgtcatgacaaggaaacttacaaactgcaacgcagagaaactattaaaggtatt      720
 R  L  C  H  D  K  E  T  Y  K  L  Q  R  R  E  T  I  K  G  I
 221                                                       240
cagaaacgtgaagccagcaattgtttcgcaattcggcattttgaaaacaaatttgccgtg      780
 Q  K  R  E  A  S  N  C  F  A  I  R  H  F  E  N  K  F  A  V
 241                                                       260
gaaactttaatttgttct[illegible]acagtcaagaaaaacattattgaggaaaattaatatcac      840
 E  T  L  I  C  S  -
 261          266
agcataaccccacccttacattttgtgcagtgattatttttaaagtcttctttcatgt
aagtagcaaacagggctttactatcttttcatctcattaattcaattaaaaccattacct
taaaatttttttctttcgaagtgtggtgtcttttatatttgaattagtaactgtatgaag
tcatagataatagtacatgtcaccttaggtagtaggaagaattacaatttctttaaatca
tttatctggatttttatgttttattagcattttcaagaagacggattatctagagaataa
tcatatatatgcatacgtaaaaatggaccacagtgacttatttgtagttgttagttgccc
tgctacctagtttgttagtgcatttgagcacacattttaattttcctctaattaaaatgt
gcagtattttcagtgtcaaatatatttaactatttagagaatgatttccacctttatgtt
ttaatatcctaggcatctgctgtaataatattttagaaaatgtttggaatttaagaaata
acttgtgttactaatttgtataacccatatctgtgcaatggaatataaatatcacaaagt
tgtttaactagactgcgtgttgtttttcccgtataataaaaccaaagaatagtttggttc
ttcaaatcttaagagaatccacataaaagaagaaactatttttaaaaattcacttctat
atatacaatgagtaaaatcacagatttttctttaaataaaaataagtcattttaataac
taaaccagattctttgtggatactattaaagtaacatttaagcctcaaccttg
```

***Figure 1.4**: Nucleotide sequence and predicted amino-acid of BriPP. Single transmembrane spanning domain highlighted in red. A potential N-glycosylation site identified at Asp173 indicated in blue. The normal stop codon located at 267 indicated in green.*

The *BRI2* transcript was mapped to human chromosome 13 by fluorescence *in-situ* hybridisation (FISH) analysis (Vidal *et al.*, 1999). Measurements of chromosome 13 also showed that the *BRI2* gene is located 34% of the distance from the centromere to the telomere of chromosome 13q corresponding to the band 13q14. The predicted nucleotide sequence of the *BRI2* gene, contains six exons is shown in figure 1.4 (Vidal *et al.*, 1999). Hybridisation of the clone of the human precursor protein to Northern blots identified a major mRNA transcript of ~2.0 kb and a second transcript of 1.6 kb which were expressed in most regions of the human brain as well as in several peripheral tissues (Vidal *et al.*, 1999).

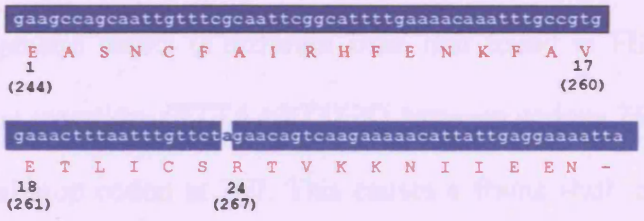

***Figure 1.5**: Nucleotide sequence of the British mutation*

Nucleotide sequence analysis of the *BRI2* gene revealed a single nucleotide transition (T for A) at position 267 resulting in the presence of an arginine residue instead of the normal stop codon, producing an open reading frame 33 nucleotides longer and a precursor protein of 277 amino acids instead of the wild type 266 (Vidal *et al.*, 1999) (figure 1.5).

This nucleotide substitution is associated with FBD and is not seen in unaffected family members or individuals with unrelated neurological disorders. Furthermore, the stop codon that is altered in the British family is conserved in the murine homolog,

indicating that the nucleotide substitution is a pathogenic mutation rather than an innocent polymorphism. Once the identity of the amyloid protein had become known polyclonal antibodies were raised against the last ten residues of the ABri sequence (Vidal *et al.*, 1999) and such antibodies (anti-ABri) were shown to recognise amyloid deposits in FBD. This immunoreactivity co-localized with Congo red staining showing that the anti-ABri antibody was in fact staining the amyloid material.

1.4.2 Identification of ADan protein and ADanPP

Using the same strategy, as in FBD, the amyloidogenic protein was isolated from leptomeningeal blood vessels in FDD and demonstrated to have homology to ABri (Vidal *et al.*, 2000b). Genetic analysis of the *BRI2* gene in the Danish kindred showed that the genetic defect is different from that found in FBD. In FDD there is a 10-nt duplication insertion, (TTTAATTTGT) between codons 265 and 266, one codon before the normal stop codon at 267. This causes a frame shift mutation, which abolishes the normal stop codon generating an 11 amino acid longer precursor protein. The amyloid subunit (ADan) is produced, similar to ABri, by cleavage of the last 34 C-terminal amino acids of the mutated precursor protein (figure 1.6). However the twelve C-terminal amino acids of the peptide are different from those of ABri. Using MS analysis a peak was found at 4,046 Da for ADan, which corresponded to the estimated mass of the peptide. Another major peak was also found at 3,883.7 Da, which matched the molecular mass of the amyloid molecule extending from residues 1-33 with a cyclic pyroglutamate at the N terminus and a detyrosinated C-terminus. Other peaks were also found which matched peptides starting at position 3 and extending to residues 28, 33 and 34.

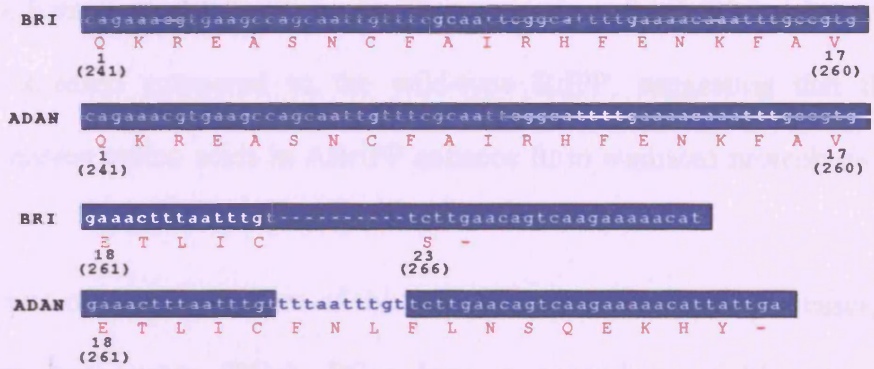

Figure 1.6: *Nucleotide sequence of the Danish mutation*

From the discovery of the amyloidogenic peptide, ADan, a polyclonal antibody (Ab5282) was raised using a synthetic peptide homologous to residues 22-34 (CFNLFLNSQEKHY) of the ADan peptide, which is mutation specific (Vidal *et al.*, 2000b). A limited immunohistochemical study was carried out using Ab5282 and the amyloid and preamyloid lesions were visualized for the first time. Ab5282 was found to label Congo red positive structures including parenchymal and vascular amyloid lesions. In addition Congo red negative, Ab5282 positive deposits were also found in the brain tissue of FDD cases. Tau immunoreactive structures were numerous in the hippocampus where abnormal neurites, mostly around affected blood vessels, NFTs and neuropil threads (NTs) were seen in large numbers (Vidal *et al.*, 2000b).

1.4.3 Generation of ABri and ADan by proteolytic processing

The mechanism of cleavage of both the wild-type and mutated precursor proteins has been investigated using *in vitro* studies in cell cultures. These have shown a furin-like cleavage of the wild-type BriPP between Arg243 and Glu244, generating a C-terminal 23 amino acid fragment. ABriPP and ADanPP, the mutated precursor proteins, are also

cleaved at the same site producing the amyloidogenic peptides ABri and ADan (Kim *et al.*, 1999; Kim *et al.*, 2002) (figure 7). The processing of ABriPP has been shown to be greatly increased compared to the wild-type BriPP, suggesting that the carboxyl terminal eleven amino acids in ABriPP enhance furin mediated proteolysis (Kim *et al.*, 1999).

Furin is one of seven members of the calcium dependent serine proteases, also called proprotein convertases (PCo). PCos have a general recognition motif sequence $(R/R)x_n(R/K)$ where n=0,2,4,or 6 and X is any amino acid except Cys and rarely Pro (Seidah & Chretien, 1999). Furin, a type 1 transmembrane protein, is synthesized as profurin and during progression from the endoplasmic reticulum to the *trans*-Golgi network, undergoes activation by two sequential autoproteolytic cleavages, the second of which permits dissociation of the propeptide providing the final step in enzyme activation (Thomas, 2002; Nakayama, 1997). Furin has been shown to be essential for embryonic development as gene knockout results in death between embryonic days 10.5 and 11.5 (Roebroek *et al.*, 1998). Several studies have shown that furin has a wide tissue distribution (Seidah & Chretien, 1994; Schalken *et al.*, 1987; Hatsuzawa *et al.*, 1990) and *in-situ* hybridisation studies using rat brain have demonstrated the presence of furin mRNA in neuronal cells (Cullinan *et al.*, 1991; Day *et al.*, 1993). Furin protein expression has been confirmed immunohistochemically in hypothalamic nuclei (Dong *et al.*, 1997).

Furin is involved in the processing of a wide variety of precursor proteins including serum proteins, growth factors, receptors, extracellular matrix proteins, bacterial toxins and viral coat proteins. In addition, it has been associated with the proteolytic processing of the precursors of molecules associated with cerebral amyloid deposition. These include BACE, which cleaves AβPP to produce the N-terminus of the Aβ peptide

in AD; ADAM10 and ADAM17 which have been implicated in α-secretase activity leading to the cleavage within the Aβ sequence of AβPP (Lopez-Perez *et al.*, 2001); gelsolin, the precursor protein for the amyloidogenic peptide AGel, deposition of which results in a form of familial CAA.

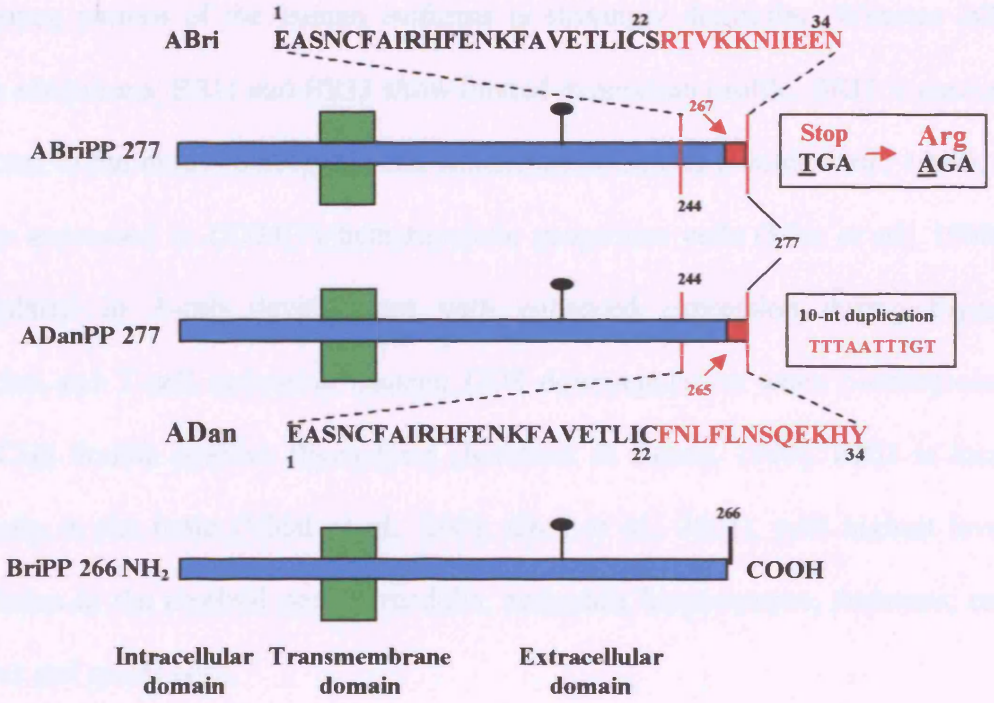

Figure 1.7: *Mutations in the BRI2 gene. Mutations in FBD and FDD are situated on chromosome 13 which encodes the 266 amino acid long precursor protein BriPP. Both mutations extend the open reading frame resulting in novel 277 amino acid proteins, ABriPP and ADanPP. The amyloidogenic peptides ABri and ADan are derived by furin-like proteolytic cleavage of the C-terminal 34 amino acids.*

1.4.4 The BRI gene family

The *BRI* gene belongs to a multigene family comprising at least three homologues in both mice and humans, *BRI1*, *BRI2* and *BRI3*. Which have also been referred to as *ITM2A*, *ITM2B* and *ITM2C*, or *E25A*, *E25B* and *E25C* respectively (Deleersnijder *et al.*, 1996; Pittois *et al.*, 1998; Vidal *et al.*, 1999; Vidal *et al.*, 2001). *BRI* gene homologues

have also been found in other vertebrate and non-vertebrate animals suggestive of an evolutionarily conserved gene family (Deleersnijder *et al.*, 1996; Sanchez-Pulido *et al.*, 2002; Vidal *et al.*, 2001). Each of the family members was mapped to a different chromosome by fluorescence *in-situ* hybridisation: the human *BRI1* gene is located on chromosome X (Pittois *et al.*, 1999): *BRI2* gene on the long arm of chromosome 13 (Vidal *et al.*, 1999) and *BRI3* gene on chromosome 2 (Vidal *et al.*, 2001). The gene expression pattern of the human isoforms is strikingly dissimilar. Whereas BRI2 is highly ubiquitous, BRI1 and BRI3 show limited expression profile. BRI1 is particularly restricted to the mouse osteogenic and chondrogenic tissues (Pittois *et al.*, 1998). BRI1 is also expressed in CD34(+) hematopoietic progenitor cells (Mao *et al.*, 1998) and upregulated in T-cell development with enhanced expression during thymocyte selection and T-cell activation causing CD8 downregulation when overexpressed in CD4/CD8 double positive thymocytes (Kirchner & Bevan, 1999). BRI3 is localised primarily in the brain (Vidal *et al.*, 2001; Choi *et al.*, 2001), with highest levels of expression in the cerebral cortex, medulla, amygdala hippocampus, thalamus, caudate nucleus and spinal cord.

The *BRI2* gene locus is on the long arm of chromosome 13, specifically at 13q14, as demonstrated by fluorescence *in-situ* hybridisation analysis (Vidal *et al.*, 1999). It is broadly expressed in peripheral organs, with high levels of expression in heart, kidney, pancreas, liver, placenta as well as brain, where it shows a more abundant distribution in the hippocampus and cerebellum compared with cortex (Vidal *et al.*, 1999). *In-situ* hybridisation of human cells in culture showed BRI2 mRNA is widely distributed in different cerebral cell populations and its presence can be demonstrated in neurons, astrocytes and microglial cells, as well as smooth muscle and cerebral endothelial cells.

No *in vivo in-situ* hybridisation data on the expression of BRI2 mRNA within human brain has been shown to date.

1.4.5 The BRI proteins

At the protein level the human and mouse BRI isoforms share over 90% homology with the same isoform in the other species, with a less pronounced amino acid similarity among the different isoforms within each species. Very little is known about the physiological functions of the BRI proteins. Database scans for possible functional roles revealed a BRICHOS domain, a conserved motif common to members of the BRI, ChM-I, SP-C and CA11 protein families (Sanchez-Pulido *et al.*, 2002). The conserved BRICHOS domain is located within the pro-peptide region, which is removed after proteolytic processing by pro-protein convertases and which includes a pair of conserved cysteine residues that most likely form a disulphide bridge, with the blocks or sequence conservation located predominantly around these cysteines. It has been postulated that this domain may be involved in the targeting of the respective proteins to the secretory pathway or in intracellular processing. Although all the proteins described as possessing the BRICHOS motif are dissimilar in proposed functions they share two common features: 1) they are all type II transmembrane proteins and 2) they are all processed by furin-like endoproteases.

Studies aimed at determining the brains topographical distribution of BRI2 in humans demonstrated its presence in normal pyramidal neurons in the CA3 and CA4 of the hippocampus as well as in Purkinje cells in the cerebellar cortex (Akiyama *et al.*, 2004). In pathological conditions, BRI2 was detected in dystrophic neurites in senile plaques and around ischemic lesions derived from axons and dendrites in AD tissues, and it was highly positive within Lewy neuritis in dementia with Lewy bodies and PD cases

(Akiyama *et al.*, 2004). Although this study did not look at normal controls or FBD and FDD cases.

Although the function of BRI2 remains unknown, its cellular distribution throughout the brain and its presence in dystrophic neuritis in various neurodegerative conditions (Akiyama *et al.*, 2004), along with its morphological distribution within neuronal cell bodies and axons and its axonal localisation in BRI2 transfected neurons (Choi *et al.*, 2001) suggest a role in transport along neuronal processes and a putative role in nerve terminals.

1.5 Alzheimer's disease

1.5.1 Introduction

AD is the most common form of CAA. Therefore, FBD and FDD closely mimic the morphological features of AD and will therefore be compared with AD throughout the thesis. In 1907, Alois Alzheimer a German psychiatrist, using the newly developed Bielschowsky's silver impregnation method, described the occurrence of NFTs in the brain of a 55 year old woman dying after a 4 year history of progressive dementia. Almost a century later AD is recognized as a leading cause of disability and decreased quality of life among the elderly (Kawas & Brookmeyer, 2001).

The clinical diagnosis of AD depends on the inclusion and exclusion of certain features, an extensive clinical workup is performed including clinical history, physical examination, neuroimaging, neuropsychological evaluation and analysis of CSF. Despite extensive clinical evaluatation, the final definite diagnosis of AD depends upon the neuropathological evaluation.

Gross anatomical changes are observed in AD; cortical atrophy noted at autopsy varies between AD cases and may correlate with cognitive decline (Mouton *et al.*, 1998).

Atrophy exemplified by narrowing of the gyri and widening of the sulci is observed in the frontal, temporal and parietal lobes also revealed by tissue sections, while relative sparing of the occipital cortex is common. Another feature of AD is often disproportionate enlargement of the temporal horns of the lateral ventricles, together with severe atrophy of the hippocampus and amygdala.

1.5.2 Histology, immunohistochemistry and electron microscopy of AD

1.5.2.1 Neurofibrillary tangles

One of the major histopathological hallmarks of AD are NFTs, intracellular inclusions often occupying the cell body of the neuron. NFTs are not specific to AD and are found in aged individuals, progressive supranuclear palsy (PSP) (Li *et al.*, 1998), GSS (Ishizawa *et al.*, 2002) and DS (Wegiel *et al.*, 1996). NFTs are an important pathological feature of AD as they correlate with cognitive decline and remain a key diagnostic feature of AD. Although NFTs may be apparent on H&E staining other stains are required for their optimal visualisation, which include a variety of silver impregnations e.g Gallyas or Bielschowsky's method or by immunohistochemistry using antibodies raised against hyperphosphorylated tau.

The general shape of NFTs differs depending on the neuron within which it is formed. For example tangles in the pyramidal neurons of the Ammon's horn in the hippocampus are usually flame shaped. Whereas in the rounder neurons of the nucleus basalis of Meynert or locus coeruleus they have a more globose appearance. NFTs, particularly in the CA1 of the hippocampus and the entorhinal cortex, may survive long after the neurons have died and lost their cell membranes. These are termed 'ghost' or 'extracellular tangles' and are still detectable on silver stains or by tau immunohistochemistry.

It has been seen with EM that tangle bearing neurons exhibit a progressive change. Early stages show accumulation of perinuclear aggregates of paired helical filaments (PHF) and other filaments. These changes progress to a densely compacted mass of PHFs within the cell body and apical dendrite impinging upon the nucleus and cytoplasmic organelles. PHFs have been extensively studied and have been shown to be composed of two filaments measuring around 20nm in diameter. Although initially thought to represent twisted tubules (Terry *et al.*, 1964), this observation changed with Kidd's finding that PHFs consisted of two filaments wound in a double helix (Kidd, 1964). Phosphorylated tau protein was shown to be a major constituent of PHFs within NFTs, plaque-related neurites and NTs (Delacourte & Buee, 1997). PHFs contain epitopes spanning the entire length of tau (Iwatsubo *et al.*, 1994a) and multiple phosphorylation sites have been identified.

The topographical distribution of neuropathological changes has been studied in AD by several groups (Braak & Braak, 1991; Delacourte *et al.*, 1998). It has been found that NFTs tend to occur most frequently in the amygdala, hippocampal formation, parahippocampal gyrus and the temporal, frontal and parietal cortices. NFTs generally occur in a predictable laminar distribution, with some laminae being severely affected while others are spared. For example in the entorhinal cortex NFTs are always present in neurons of layers II and IV, whereas layers III, V and VI have relatively few NFTs. In the association cortex, the pyramidal neurons in layers II, III and V are similarly affected. In general NFT bearing cells are large pyramidal neurons, primarily glutamatergic and frequently marked by antibodies to phosphorylated neurofilaments (Schmidt *et al.*, 1996) and in contrast other neuronal populations appear to be spared. Braak and Braak in 1991 observed that the progression of neurofibrillary changes follows a predictable pattern (Braak & Braak, 1991). From examining brains of

demented and non-demented individuals, they found a characteristic distribution of NFTs and NTs. This allowed the differentiation of six stages exemplified by progression from the transentorhinal to the isocortex. The first two stages involve NFTs in the entorhinal, transentohinal and CA1/ subicular portions of the hippocampal formation. In stages III and IV increasing numbers of NFTs accumulate in the limbic system and stages V and VI in isocortical areas.

1.5.2.2 Neuropil threads

NTs are thread like structures in the neuropil distributed widely in the grey matter in AD. The frequency of NTs correlates with the severity of dementia and the numbers of NFTs. They are also frequently associated with ghost or extracellular tangles in the hippocampus (Yamaguchi *et al.*, 1991b). Although observed near dendrites of NFT bearing neurons (Braak & Braak, 1988), threads may also involve distal dendrites or axons in the amygdala or entorhinal cortex unassociated with local tangle-bearing cell bodies (Schmidt *et al.*, 1993).

Like NFTs, NTs are also observed in other disorders; including PSP (Probst *et al.*, 1988), corticobasal degeneration (CBD) (Ksiezak-Reding *et al.*, 1994) and Pick's disease (Cochran *et al.*, 1994).

1.5.2.3 Senile plaques

The other major histopathological hallmark of AD are senile plaques which are near spherical structures ranging in diameter from 4 to 200μm. The amyloid portion of senile plaques is apparent in many silver stains but may also be distinguished from other substances using Congo red stain or the fluorescent dye thioflavine-S. Immunohistochemical preparations using Aβ antibodies also highlight the senile

plaques along with diffuse plaques. Although plaques have been classified based on their morphological appearance, Aβ immunohistochemistry does not distinguish between the conformational state of the Aβ peptide.

1.5.2.3.1 Neuritic plaques

Neuritic plaques display clusters of abnormally distended, radially orientated, neuronal processes often surrounding well-formed extracellular Aβ cores found in the limbic and association cortices. The fine structure of neuritic plaques highlights their complexity, with amyloid cores surrounded by radiating spikes of fibrillar amyloid. Amyloid is often seen in coated vesicles within the cytoplasm (Roher *et al.*, 1993) suggesting a process of receptor mediated endocytosis. Lamellar or dense bodies are a major component of plaque neurites and have been shown to contain acid phosphatase (Suzuki & Terry, 1967) suggesting a lysosomal origin. These structures co-exist in varying proportions with clusters of PHFs. Astrocytes and microglia are often seen surrounding neuritic plaques and entwined within the extracellular amyloid. This relationship between glial cell and plaques is not yet fully understood.

The Aβ contained within the neuritic plaques tends to be the species ending at amino acid 42 (Aβ42). This longer, more hydrophobic form is prone to aggregation. However, the Aβ species ending at the amino acid 40 (Aβ40) which is normally more abundantly produced by cells than Aβ42 usually co-localises with Aβ42 within the plaques.

1.5.2.3.2 Diffuse plaques

In contrast to neuritic plaques, diffuse plaques or pre-amyloid plaques are more amorphous and lack the thickened neurites and well-defined amyloid cores (Ikeda *et al.*,

1989; Yamaguchi *et al.*, 1989) of neuritic plaques. In fact diffuse plaques have little or no ultrastructurally detectable fibrillar amyloid (Yamaguchi *et al.*, 1991b). They are not or weakly detected with silver stains, and show very weak staining with fluorescent amyloid dyes, but show immunoreactivity with Aβ antibodies.

Many investigators believe that the diffuse plaques, often seen before the occurrence of neuritic plaques, represent earlier stages of plaque development and eventually evolve into neuritic plaques (Dickson *et al.*, 1988). This notion may be supported by the observation that the distribution of the diffuse plaques is similar to that of neuritic plaques i.e. limbic and association cortices. An alternative hypothesis is that the individual plaque types develop independently of each other (Armstrong, 1998). From immunohistochemical studies it was determined that the Aβ peptides deposited in the diffuse plaques are Aβ42 and no or little Aβ40 immunoreactivity was found. This is in contrast to the mixed deposits generally found in neuritic plaques.

1.5.3 Amyloid cascade hypothesis

With the deposition of two aggregated proteins in AD there continues to be a debate about which of the two lesions might precede the other and has a primary role in neurodegeneration. Many studies support the hypothesis that amyloid fibrils drive neurodegeneration in AD, known as the amyloid cascade hypothesis (Hardy & Selkoe, 2002). The hypothesis raised by Hardy et al (1992) suggested that the deposition of Aβ, whether it is due to overproduction or insufficient clearance, is the causative agent of AD pathology and that the NFTs, cell loss, vascular damage and dementia are consequences of this.

The initial step in this proposed pathway (Figure 1.8) is the accumulation of Aβ into amorphous deposits. The longer Aβ peptide (1-42) is the most amyloidogenic and

earliest peptide species to deposit. This initial deposition acts as a seed for further deposition of the shorter less amyloidogenic peptide Aβ 1-40. With the toxic Aβ peptides accumulating, an inflammatory response is triggered. Amyloid associated proteins may also play an indirect role in this process by accelerating amyloid filament formation. The amyloid deposits induce tangle formation, neuritic degeneration and ultimately neuronal loss. These final steps in the pathogenesis of AD remain undefined since the mechanisms for neurodegeneration and neuronal death in AD are still not fully understood.

Several developments have supported the amyloid cascade hypothesis including: the identification of rare cases of familial AD caused by mutations in the *APP, PS1 or PS2* genes and the production of transgenic mice exhibiting some AD like pathology. On the other hand mutations found within the tau gene do not lead to AD. Instead these mutations are associated with frontotemporal dementia and parkinsonism linked to chromosome 17.

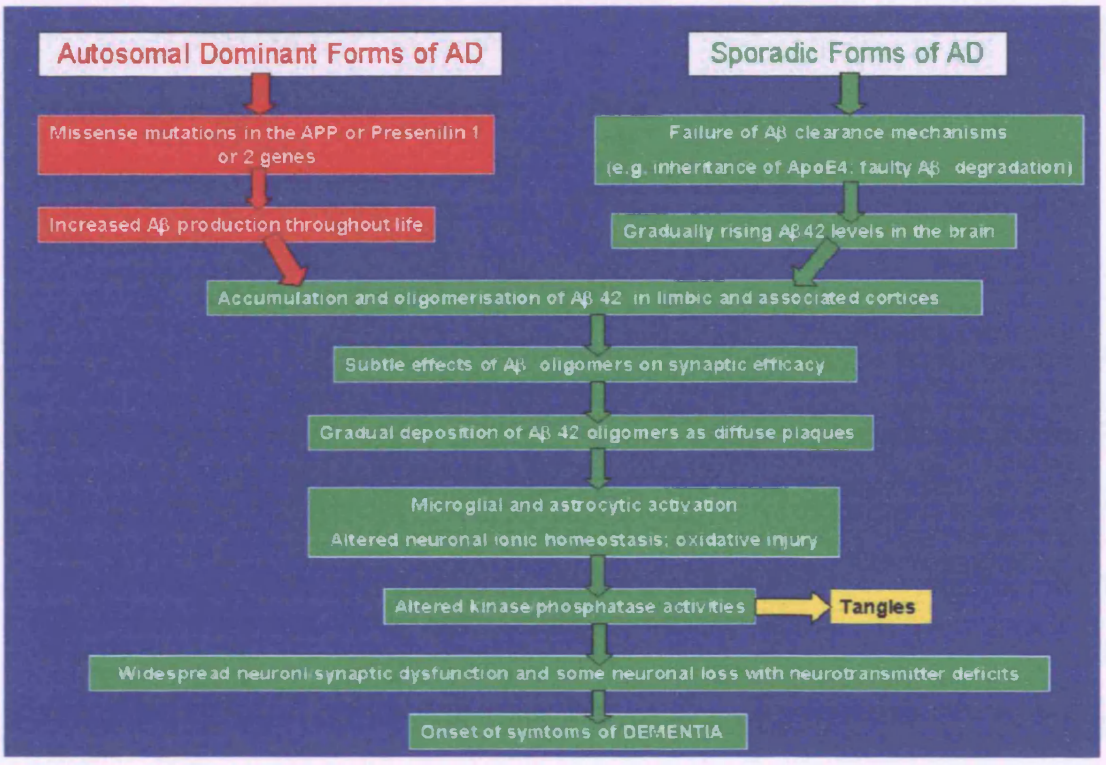

***Figure 1.8**: Amyloid cascade hypothesis (Selkoe et al 2002)*

Although the amyloid cascade hypothesis offers the framework to explain AD there are still details lacking. A long-standing controversy surrounds the relative contribution of plaques to the loss of neuronal function, because there is a relatively poor correlation between the numbers of plaques and the degree of cognitive decline (Hyman, 1992; Berg *et al.*, 1998). A significant correlation between soluble Aβ levels in the brain parenchyma and the severity of the disease has been shown (McLean *et al.*, 1999), which is in contrast to the total Aβ load appearing to only signify the presence of the disease.

Although the amyloid cascade hypothesis is a framework of events that try to explain the mechanism behind AD, the same cascade could be implicated in FBD and FDD. Both hereditary diseases have an accumulation of a peptide capable of forming amyloid deposits, both have NFTs present. Whether the intermediate steps proposed in the

amyloid cascade hypothesis are present, for example microglial and astrocytic activation, is part of the focus of this study.

1.5.4 AβPP processing and the generation of Aβ

Aβ is derived from its large precursor protein AβPP. The *APP* gene is composed of 18 exons and can be alternatively spliced to create 10 isoforms ranging from 563 to 770 amino acid residues (Coulson *et al.*, 2000).

AβPP is a type 1 integral membrane protein with a large ectodomain, a single membrane spanning domain and a short cytosolic domain (Kang *et al.*, 1987). The ectodomain consists of an N-terminal region that forms an extracellular globular structure which is followed by a sequence rich in positively charged residues (acidic domain) and a glycosylated region.

AβPP is co-translationally translocated into the endoplasmic reticulum (ER) via its signal peptide. Then post-translationally modified through the secretory pathway. The α-secretase was identified as the first proteolytic cleavage site located 12 amino acids N-terminal to the transmembrane domain of AβPP between residues 687 and 688, releasing a large soluble N-terminal fragment α-APP into the lumen/ extracellular space with retention of the 83-residue C-terminal fragment in the membrane.

This is followed by cleavage around residue 712 by a γ-secretase, releasing the non-pathogenic fragment p3 fragment. Although this pathway is considered to be non-pathogenic p3 has been shown to be present in amyloid plaques (Higgins *et al.*, 1993). This sequence of events does not lead to the generation of Aβ, as the α-secretase cleaves within the Aβ domain itself. To initiate the formation of Aβ the AβPP molecule is cleaved by a β-secretase that cuts 28 residues from the transmembrane domain,

between residues 671 and 672, releasing a smaller derivative, β-APP, and retaining a 99 residue fragment within the membrane. This is followed by the γ-secretase cleavage yielding Aβ. The key to this pathway is the γ-secretase. If it cleaves at residue 712 then Aβ 1-40 is produced, but if it cleaves after residue 714 then Aβ 1-42/43 are produced. Efforts have been directed towards the identification of α-, β-, and γ-secretases involved in the processing of AβPP. The α-secretase cleavage corresponds to a secretory pathway, which predominates in all non-neuronal cells including mammalian cells (Sisodia *et al.*, 1990). ADAM10, ADAM17, MDC-9 and TACE, all of which belong to the family of disintegrin metalloproteases have been proposed as α-sectretase candidates in mammalian cells (Buxbaum *et al.*, 1998; Koike *et al.*, 1999; Lammich *et al.*, 1999). β-secretase cleavage constitutes the first step in the formation of Aβ peptides, its action leaves the Aβ peptide anchored to the membrane with its N-terminus free. Five groups independently identified a candidate for the β-site AβPP cleaving enzyme BACE1 (Vassar *et al.*, 1999; Yan *et al.*, 1999; Sinha *et al.*, 1999; Lin *et al.*, 2000). The BACE polypeptide sequence contains two conserved motifs that form the active site of aspartic proteases of the pepsin family. BACE is an unusual aspartic protease because it has a C-terminal transmembrane domain and is therefore membrane bound. Extensive studies by the five groups demonstrated that BACE exhibits all the characteristics of β-secretase; firstly it is expressed in all tissues, but at higher levels in neurons of the brain; BACE is localized within acidic intracellular compartments; over-expression of BACE in cells increases β-secretase cleavage products; anti-sense inhibition of BACE in cells decreases β-secretase cleavage; purified forms of BACE cleave APP substrates *in vitro* with correct β-secretase specificity. Soon after the discovery of BACE, a homologous gene *BACE2* (also called Asp1 or Memapsin1) was

also identified (Solans *et al.*, 2000). BACE1 and BACE2 share 64% homology and both have a C-terminal transmembrane domain. The *BACE1* gene is localised to chromosome 11q23.3 a locus not yet seen to be associated with AD, while *BACE2* is localised to chromosome 21 (Solans *et al.*, 2000). Recent work has shown that although BACE2 can cleave AβPP at the β-secretase site, the enzyme cuts more efficiently within the Aβ domain and therefore may limit the production of pathogenic Aβ species (Farzan *et al.*, 2000).

Activity of γ-secretase is required to release both Aβ and p3 peptides from the cell membrane. γ-Secretase can cleave at multiple positions generating Aβ peptides of different lengths. γ-Secretase cleavage occurs within the predicted transmembrane domain of AβPP requiring the enzyme to either cleave within the lipid bilayer or change the conformation of the C99 fragment (Selkoe, 1999). It has been recently reported that a large complex exhibits γ-secretase activity on C99 like substrates and that this complex catalyses both 40 and 42 cleavage at a ratio similar to that found in intact cells. It has been shown that the activity of the complex is inhibited by γ-secretase pathway inhibitors. Antibodies raised against PS1 inhibit soluble γ-secretase activity, indicating that PS1 protein is physically associated with the γ-secretase enzyme complex (Li *et al.*, 2000). These data can be explained by the hypothesis that PS1 and PS2 are themselves γ-secretase (Wolfe *et al.*, 1999).

1.5.5 Amyloid conformational states

A number of proteins are able to undergo specific aggregation into amyloid fibrils *in vivo*, leading to different pathological disorders. The Aβ amyloid found in AD, under normal physiological conditions, is a soluble protein (sAβ). Due to unknown factors the soluble protein forms insoluble fibrils with a β-pleated sheet conformation. In the last

decade the leading hypothesis in AD has been that dementia derives from neurotoxins comprising self-associated Aβ peptides (Selkoe, 2001). After a decade of investigation into amyloid toxicity the question of which specific neurotoxic structures derived from Aβ self-association contributed to AD pathogenesis still has to be answered.

It has been shown that amyloid fibrils are not the only neurotoxic species derived from Aβ monomers (Klein *et al.*, 2001). Neurotoxicity was found in ADDLs (Aβ- derived diffusible ligands) these are globular oligomers of Aβ formed from Aβ42 monomers ranging in size from trimers to 24-mers (Chromy *et al.*, 2003). They are able to kill differentiated CNS neurons with the toxicity being cell type specific. Neurotoxic activity has also been found in assemblies known as protofibrils (Hartley *et al.*, 1999; Walsh *et al.*, 1999). Protofibrils were identified several years ago as intermediates in fibrillogenesis (Harper *et al.*, 1997; Walsh *et al.*, 1997), they are rod like rather than globular in structure, 10 times the size of ADDLs, with diameters of ~5nm and often display a beaded appearance. For protofibrils to form they need high concentrations of Aβ monomers. It is unknown whether these different conformational states of Aβ interconvert freely. The idea that AD pathogenesis has less to do with the amyloid fibril but more with the non-fibrillar conformational states is consistent with the imperfect correlation between amyloid plaque burden and dementia. The amyloid fibril may be the end stage of a process in which the key pathological events have occurred earlier mediated by intermediated conformational states of the Aβ peptide.

It has been proposed that mutations already known to affect the *AβPP* gene cause the soluble Aβ to aggregate to a greater extent than in normal individuals. Other factors that may affect or initiate this process are post-translational modifications, concentrations of soluble Aβ, low pH, tissue factors, metal ions and amyloid associated proteins (AAPs).

The pathway involved in fibril formation is not unique to Aβ. Among others, the formation of soluble oligomers, protofibrils and then amyloid like fibrils of ABri can also be produced experimentally (El Agnaf *et al.*, 2001; Kim *et al.*, 1999b). Although ABri and Aβ have no sequence homology the key features of their neuropathology and fibril assembly pathways are similar. There is, as yet, no biochemical evidence of non-fibrillar forms of ADan: however immunohistochemical evidence of non-fibrillar (ADan positive and Congo red negative) material in FDD, suggests the presence of pre-amyloid conformational states. The similarity between the two peptides (ABri and ADan), with identical 22 amino acid N-terminal sequences and the potential for identical disulphide bonding suggests that ADan and ABri may, or are likely to, follow a similar pathway to fibril formation.

1.6 Genetics of familial Alzheimer's disease.

The prevalence of inherited forms of AD has been documented to be around 5% of all cases, with three genes found to be associated with familial AD; *AβPP*, *PS1* and *PS2*. Furthermore the apolipoprotein E (ApoE) gene has been shown to be a risk factor for sporadic AD and some early onset familial AD. Studying the mutations within these genes may provide an insight into the mechanism of AD by examining genotypic to phenotypic relationships.

1.6.1 Mutations in the *AβPP* gene

The location of mutations within the *AβPP* gene and their genotype-to-phenotype relationship have provided critical insights into the pathogenesis of AD and CAA. Mutations in *AβPP* are clustered around the three-secretase cleavage sites; immediately before the β-secretase site; after the α-secretase site or C-terminally to the γ-secretase

site. The mutations exert their pathological effects through different mechanisms and often have characteristic clinical and pathological phenotypes. The double Swedish mutation [KM670/671NL] affects the two residues located just before the N-terminus of Aβ, immediately preceding the β-secretase cleavage site (Johnston *et al.*, 1994; Axelman *et al.*, 1994) (figure 1.9), producing Aβ plaques as well as extensive NFT pathology (Bogdanovic *et al.*, 2002). This mutation induces increased cleavage by the β-secretases generating more Aβ40 and Aβ42, although the main species deposited in this disease is Aβ42 (Mann *et al.*, 1996). Mutations occurring around the γ-secretase cleavage site, including the London mutation (V717I) and the Florida mutation (I716V) enhance the production of Aβ42 (Hardy, 1997; Selkoe, 2001). The phenotypes of these mutations are that of classical AD including extensive NFT pathology. Whereas mutations that occur in the middle of the Aβ sequence between residues 21 and 23 are associated with a clinical presentation that includes heamorrhagic and ischemic strokes and a pathological presentation of severe CAA. The first of these latter mutations to be described was HCHWA-D.

The other known mutations that occur around the same region of the Aβ protein include Flemish (A692G), Italian (E693K), Arctic (E693G) and Iowa (D694N) mutations (figure 1.9). As well as the mutations within the *AβPP* gene, an extra copy of the structurally normal *AβPP* owing to elevated gene dosage in DS leads to the premature occurrence of classical AD neuropathology (Holtzman & Epstein, 1992).

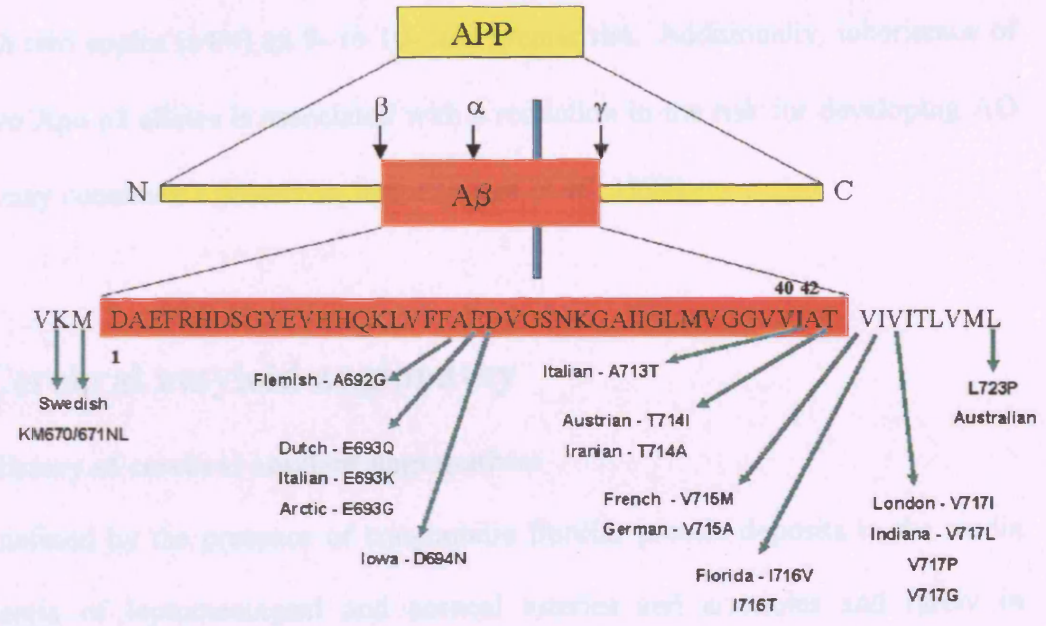

***Figure 1.9**: Mutations in the APP gene that cause AD like phenotypes. Mutations in the APP gene are clustered around the three secretase cleavage sites. The above diagram illustrating the orientation of the Aβ peptide in the AβPP peptide and its orientation across the membrane. The three-secretase cleavage sites are highlighted on the Aβ peptide and the mutations shown on the Aβ peptide sequence.*

1.6.2 Genetic risk factors for AD

Mutations in the *PS1*, *PS2* and *AβPP* genes are known to cause familial AD. It has also been shown that the possession of an ε4 allele of the *ApoE* gene is a genetic risk factor for late onset AD, being over represented in subjects with AD compared with the general population. A strong association between the inheritance of the Apo ε4 and both sporadic AD and late onset familial AD has also been described (Corder *et al.*, 1993; Strittmatter *et al.*, 1993a). *ApoE* is a single gene located on chromosome 19q 13.2, and has three major allelic variants (ε2, ε3 and ε4) encoding three protein isoforms (Emi *et al.*, 1988). There are six possible genotypes ε2/2, ε2/3, ε2/4, ε3/3, ε3/4, ε4/4 and compared with people without the ε4 allele individuals with one copy of the Apo ε4

allele (ε2/4, ε3/4) have approximately a 2- to 3- fold greater risk of developing AD and those with two copies (ε4/4) an 8- to 10- fold greater risk. Additionally, inheritance of one or two Apo ε2 alleles is associated with a reduction in the risk for developing AD and thus may constitute a protective factor (Lippa *et al.*, 1997).

1.7 Cerebral amyloid angiopathy

1.7.1 History of cerebral amyloid angiopathies

CAA is defined by the presence of congophilic fibrillar protein deposits in the media and adventia of leptomeningeal and cortical arteries and arterioles and rarely in capillaries and veins. After the first description by Divry in 1941 of amyloid deposition in senile plaques in AD, came the recognition by Scholz in Germany that amyloid can also be found in cerebral blood vessels in the brains of elderly patients. The earliest English language description of CAA was by Worster-Drought et al in 1940 when they first described FBD. In the 1970's it was recognised that CAA is a major cause of cerebral haemorrhage in the elderly, ischemic lesions and dementia, as well as being associated with cerebral haemorrhage, CAA has also been documented as one of the pathological hallmarks in AD (Frangione *et al.*, 2001). The fibrillar deposits found in CAA of AD, DS and normal elderly subjects are composed of Aβ. As well as the deposition of the Aβ protein in blood vessel walls in sporadic AD, CAA can also be severe in variants of familial AD caused by mutations of the *AβPP* or *PS1* genes. Other proteins are also involved in familial CAAs, including mutated cystatin C in hereditary cerebral haemorrhage with amyloidosis of Icelandic type (HCHWA-I), variant transthyretins in meningo-vascular amyloidosis, mutated gelsolin in familial amyloidosis of Finnish type and ABri and ADan in the *BRI2* gene-related dementias.

The cellular mechanisms involved in CAA which result in the degeneration of the microvessel wall are poorly understood. It is also unknown whether the mechanisms involved in various types of CAAs are similar or unrelated.

1.7.2 Morphological appearances

Amyloid deposition most frequently affects leptomeningeal and cortical small and medium sized arteries and arterioles, resulting in an acellular thickening with a smudgy appearance of the blood vessel wall. As a rule capillaries and veins tend to be less often affected than arterial blood channels. Amyloid laden blood vessels show positivity with Congo red, with an apple green birefringence when viewed under polarized light and green fluorescence when stained with thioflavine-S. Both stains are highly specific, for they are dependent on the β-pleated sheet conformational state of the amyloid peptides. The deposition of amyloid within blood vessels is a multistep process. Amyloid initially appears in the basement membrane around smooth muscle cells in the abluminal area of the media and adventia (Vinters, 1992). This phase is followed by a progressive loss of smooth muscle cells and the appearance of vascular degenerative changes. The preservation of endothelial cells is usually a feature. A grading system has been proposed by Vonsattel et al (1991) which may be useful for both diagnostic and research purposes (Vonsattel *et al.*, 1991). Briefly if amyloid is seen in the media without significant destruction of smooth muscle cells it is classified as 'mild' CAA. The smooth muscle cells are mainly absent in 'moderate' CAA, while together with the loss of smooth muscle cells and the presence of degenerative changes such as double barrelling, microaneurysm formation, fibrinoid necrosis and leakage of blood through the blood vessel walls constitutes 'severe' CAA.

Ultastructural examination of blood vessels in cases of AD has shown that randomly orientated amyloid fibrils are first laid down in the abluminal aspect of the basal lamina around smooth muscle cells, which gradually spread towards the internal elastic lamina of arteries and the endothelium of arterioles. As these deposits increase in size the luminal smooth muscle cells may show degenerative features. In capillaries amyloid fibrils are found within the basal lamina with larger deposits extending into the adjacent neuropil. In HCHWA-D immunoelectron microscopy demonstrated that the initial phase of Aβ deposition the basal lamina shows increased electron density and reticular structures with amyloid fibrils being observed in more advanced lesions.

1.7.3 Sporadic cerebral amyloid angiopathy

The majority of CAA is sporadic and is found in elderly individuals with or without morphological evidence of AD. CAA can also be associated with other neurological manifestations including transient neurological symptoms, CAA-associated vasculitis and it has also been suggested to be a cause of dementia (Greenberg *et al.*, 2000). Recent epidemiological studies have been shown to support vascular factors playing a role in the pathomechanism of dementia in AD (Pfeifer *et al.*, 2002). Further studies are needed to elucidate the pathogenic mechanisms by which CAA affects cognition, but it seems likely that ischemia related to CAA plays a significant part in this process (Cadavid *et al.*, 2000; Winkler *et al.*, 2001; Natte *et al.*, 2001). This proposal is supported by clinicopathological studies demonstrating that the presence of extensive CAA alone is sufficient to cause dementia in some cases of HCHWA-D (Natte *et al.*, 2001).

The overlapping biology of sporadic CAA and AD suggests that the two conditions share common risk factors. With the occurrence of both diseases steadily increasing with age, the incidence of CAA may be as high as 46% in elderly individuals over the

age of 70 (Bergeron *et al.*, 1987; Esiri & Wilcock, 1986; Glenner *et al.*, 1981). Compared with non-AD cases the presence of AD further increases the frequency and severity of CAA pathology and vascular amyloid deposition can be observed in more than 80% of all AD cases. CAA is of moderate degree in about a quarter of all such cases (Ellis *et al.*, 1996). The ApoE ε4 allele that has been identified as an important risk factor in AD, has also been related to sporadic and AD related CAA (Greenberg *et al.*, 1995; Premkumar *et al.*, 1996). Increasing doses of ApoE ε4 have been shown to be associated with increasing amounts of Aβ40 per affected cortical blood vessel without increasing the proportion of amyloid laden blood vessels (Alonzo *et al.*, 1998). From these observations, the hypothesis was proposed that ApoE ε4 enhances the accumulation of Aβ40 in blood vessels previously seeded by Aβ42. The ApoE ε2 allele has been demonstrated to be associated with CAA related cerebral haemorrhage in which, through an unknown mechanism, amyloid-laden blood vessels undergo vasculopathic changes leading to their rupture (Nicoll *et al.*, 1997).

1.7.4 Cerebral amyloid angiopathy in familial AD

1.7.4.1 Mutations in *AβPP*

Familial AD is the single most important hereditary condition that is associated with CAA. Mutations located in the middle of the Aβ protein between residues 21 and 23 cause severe CAA. In the autosomal dominant condition HCHWA-D (E693Q) patients develop strokes including cerebral haemorrhage and white matter changes (Bornebroek *et al.*,). Some patients present with dementia in the presence or absence of strokes suggesting that severe CAA associated with this mutant has a significant role in the dementing process in these individuals. In the Italian (E693K) and Arctic (E693G)

(Nilsberth *et al.*, 2001) variants in which the mutations affect the same site severe CAA has also been described. Carriers of the Flemish mutation (A692G) develop early onset AD or cerebral haemorrhage, and their pathological phenotype is unique in that it includes neurofibrillary degeneration and AD type Aβ plaques with a large amyloid core (Kumar-Singh *et al.*, 2000). The Iowa mutation (D694N) has been described with a clinical phenotype characterized by dementia and pathological changes including severe CAA (Grabowski *et al.*, 2001). Abundant NFTs and dystrophic neurites, often occurring around amyloid-laden blood vessels are present. Sparse parenchymal plaques of diffuse morphology, composed of Aβ40 have been described (Grabowski *et al.*, 2001).

Despite the close localization of these mutations with similarities in the clinical presentation, experimental studies suggest that the Dutch and Iowa mutations exert their pathological effects through a mechanism that is strikingly different from that found in the Flemish mutation. Neither the Iowa nor the Dutch mutations seem to affect the processing of AβPP, but instead have an effect on the aggregation and toxicity of these modified peptides. In contrast, the main affect of the Flemish mutation is that it interferes with the normal processing of AβPP and leads to an increased production of Aβ by the β-secretase homologue BACE2 (Farzan *et al.*, 2000).

1.7.4.2 Mutations in the *PS1* and *PS2* genes

As well as mutations found within the *AβPP* gene some mutations associated with the *PS1* and *PS2* genes cause severe CAA. A recent study has suggested that *PS1* mutants in which mutations are located after codon 200 have more severe CAA than those located before codon 200 (Mann *et al.*, 2001a). In cases with Δ9 and Δ183/ΔM84 mutations of the *PS1* gene the clinical phenotype can include spastic paraparesis

(variant AD) and the neuropathological changes include cotton wool plaques together with extensive and severe CAA (Crook *et al.*, 1998; Steiner *et al.*, 2001; Houlden *et al.*, 2000). CAA has also been identified to be a prominent feature and in at least one case cerebral haemorrhage was documented in a Volga-German family with familial AD due to the N141I mutation in the *PS2* gene (Nochlin *et al.*, 1998; Levy-Lahad *et al.*, 1995).

1.7.4.3 Aβ in sporadic and familial AD

Aβ species deposited in the blood vessel walls in sporadic AD and familial AD related CAAs are pathogenic variants of a constitutive host protein, sAβ. Aβ and sAβ have identical primary sequences but have different secondary structures, which could be responsible for their different physiochemical properties, including the generation of β-pleated sheet conformations resulting in aggregation and formation of insoluble amyloid fibrils. The Aβ species deposited in the blood vessel walls show both C and N-terminal heterogeneity, as well as post-translational modifications that can be demonstrated with specific antibodies. Both immunohistochemically and biochemically Aβ40 has been shown to be predominantly deposited in the blood vessel walls in both sporadic and familial AD as well as in HCHWA-D (Levy *et al.*, 1990a). Pathological observations reported in both humans and transgenic animals suggest that the first Aβ species deposited in the blood vessel wall ends at position 42 which seeds the subsequent deposition of Aβ40 (Lemere *et al.*, 1996). The N-terminal heterogeneity of Aβ with a potential of such N-terminally truncated species for enhanced aggregation has also been documented (Iwatsubo *et al.*, 1996; Pike *et al.*, 1995; Tekirian *et al.*, 1998).

The biochemical and toxicological properties of the Aβ peptide deposited in HCHWA-D and other variants have been extensively studied. In HCHWA-D the amyloid deposited as CAA is composed of both variant (E22Q) and wild-type Aβ (Prelli *et al.*, 1990). Compared with wild-type Aβ both the Dutch and Iowa Aβ40 synthetic peptides rapidly assemble to form fibrils in solution, while the Flemish Aβ40 peptide does not (Wisniewski *et al.*, 1991; Van Nostrand *et al.*, 2001). A further feature of the Dutch and Iowa synthetic peptides is that they induce robust pathologic responses in cultured human cerebrovascular endothelial cells and are also toxic to smooth muscle cells (Miravalle *et al.*, 2000). Similar to Aβ parenchymal lesions, vascular Aβ deposits are also associated with deposition of AAPs, including complement components, serum amyloid P component (SAP), ApoE, α-1-antichymotrypsin (ACT), glycosaminoglycans, extracellular matrix proteins and complement inhibitors such as ApoJ and vitronectin. Whether these unrelated proteins are key elements for the mechanism of fibre formation or represent innocent bystanders is not known.

1.7.5 Other hereditary cerebral amyloid angiopathies

1.7.5.1 Acys in HCHWA-I

HCHWA-I also known as hereditary cystatin C amyloid angiopathy (HCCAA) is an autosomal dominant condition with an early onset (Ghiso *et al.*, 1986). Individuals may clinically present with a cerebral haemorrhage, followed by cognitive decline and dementia. Pathological examination shows severe CAA of leptomeninges, cerebral cortex, basal ganglia, brainstem and cerebellum (Gudmundsson *et al.*, 1972; Jensson *et al.*, 1989). In addition, amyloid deposits can be found in peripheral tissues including skin, lymphoid tissues, salivary glands and testes (Benedikz *et al.*, 1990; Lofberg *et al.*,

1987). The amyloid deposited is an N-terminal truncated degradation product of cystatin C bearing a single glutamine for leucine substitution, due to an A for T point mutation at codon 68 of the *cystatin C* gene, located on chromosome 20p11.2 (Levy *et al.*, 1989; Ghiso *et al.*, 1986; Schnittger *et al.*, 1993). In patients with HCHWA-I the CSF levels of cystatin C were found to be higher than those of healthy individuals (Bjarnadottir *et al.*, 2001). The structural differences between the variant (L68Q) and wild-type cystatin C account for the susceptibility of the variant protein to unfolding, proteolysis and fibrillogenesis (Calero *et al.*, 2001).

1.7.5.2 Transthyretin

Amyloidoses due to mutations of the transthyretin (*TTR*) gene, located on chromosome 18, are late onset autosomal dominant systemic diseases in which the deposition of one of the many variant transthyretin proteins (TTR) takes place in multiple organs (Benson, 1996; Nilsberth *et al.*, 2001; Ghiso *et al.*, 1994). The TTR molecule has an extensive β-structure, the TTR monomer has eight β-strands arranged in anti-parallel configuration in two planes. It has also been suggested that single amino acid substitutions predispose TTR to fibril formation as they destabilize it by lowering the energy requirement for tetramer dissociation (Koo *et al.*, 1999). The most common phenotype associated with mutations in *TTR* gene is a condition identified as familial amyloidotic polyneuropathy (FAP). The systemic organs most commonly affected by amyloid-TTR (ATTR) deposition are heart, eye and kidney and can be affected individually or in various combinations with the involvement of the peripheral nerve. Involvement of the CNS is exceptional, but a few variants are known. A Hungarian kindred carrying a D18G mutation has been reported (Garzuly *et al.*, 1996) in which affected individuals are

reported to have memory loss, decreased hearing and signs of cerebellar involvement and pyramidal dysfunction.

1.7.5.3 Gelsolin

Gelsolin related amyloidosis or familial amyloidosis, Finnish type (FAF) is an autosomal dominant condition characterized by systemic deposition of the amyloid protein gelsolin (AGel). This disease has been documented worldwide (Kiuru, 1998) with the majority of cases being found in Finland. The major clinical presentation of FAF includes ophthalmologic, dermatological and neurological symptoms (Kiuru, 1998). Two point mutations are known within the *gelsolin* gene, either G654A or G654T. In all Finnish patients studied the G654A mutation has been found, whereas the G654T mutation is found in pedigrees from Denmark and Czechoslovakia (Haltia *et al.*, 1990; Levy *et al.*, 1990b; de la *et al.*, 1992). Gelsolin is a unique protein which occurs in a cytoplasmic 80kDa form and a plasma 83kDa form, both of which are generated by alternative transcriptional initiation sites and mRNA processing from a single gene located on chromosome 9 at q32-34 (Kwiatkowski *et al.*, 1986). The two forms differ from one another by the presence of an N-terminal 25 amino acid extension in the secreted plasma form (Yin *et al.*, 1984). AGel deposited in tissues of FAF patients is composed of internal proteolytic fragments of the mutated proteins spanning positions 173-243 or 173-225 of the secretory form of gelsolin (Ghiso *et al.*, 1990; Maury, 1991). Gelsolin itself appears to have a low amyloidogenic potential, indicated by secondary structure predications (de la *et al.*, 1992). In contrast, substitution of the charged amino acid aspartic acid (187) by an amino acid with an uncharged (asparagine) or hydrophobic side chain (tyrosine) creates an amyloidogenic sequence, suggesting that residue 187 is a critical site for amyloidogenesis (Maury *et al.*, 1994). Because of the

charge change in the gelsolin molecule it is postulated the susceptibility to proteases alters thereby rendering the molecule amyloidogenic. The deposition of AGel amyloid in most tissues with a predilection for blood vessel walls and basement membranes takes place. The prominent amyloid angiopathy involves arteries of nearly every organ including the CNS. Small and medium sized arteries and arterioles and capillaries are mainly affected, but veins show only occasional involvement. The production of gelsolin by vascular smooth muscle cells is of specific interest, as it may relate to one of the most characteristic pathological findings in FAF the prominent and widely distributed amyloid angiopathy.

1.7.6 CAA in *BRI2* gene related dementias

FBD has been documented as showing severe and widespread CAA (Plant *et al.*, 1990; Revesz *et al.*, 1999). Widespread deposition of amyloid in the cerebral arteries, arterioles and capillaries has been found, but amyloid deposition rarely affects veins. Establishing the pattern and distribution of ABri deposition forms part of the subject of this study. Despite the severe CAA significant cerebral haemorrhage is relatively rare (Mead *et al.*, 2000; Plant *et al.*, 1990) unlike in HCHWA-D and HCHWA-I in which cerebral haemorrhage is a common clinical manifestation. In FDD the only information available suggests that ADan is deposited in both blood vessels and parenchyma (Vidal *et al.*, 2000b). However, no systematic investigation has been previously carried out about ADan deposition in FDD CAA. Co-deposition of Aβ in FDD has been described briefly within ADan positive vascular amyloid mainly in the form of perivascular plaques (Vidal *et al.*, 2000b).

1.7.7 Mechanisms of CAA: Systemic verses local origin

The origin of the different amyloid proteins in cerebral blood vessels is not fully understood and a number of hypotheses have been proposed, which mainly deal with the origin of Aβ in sporadic and AD related CAAs. As most cell types are able to produce AβPP several theoretical possibilities can be considered for the origin of the Aβ deposits in cerebral blood vessels.

1) Aβ depositing in cerebral blood vessels may be derived from the circulation. In support of such a hypothesis is the observation that AβPP is expressed by megakaryocytes, is present in platelets and sAβ is present in plasma (Gardella *et al.*, 1992; Mackic *et al.*, 1998; Zlokovic *et al.*, 1993). Furthermore there is a bi-directional receptor-mediated transport across the blood brain barrier (BBB), and exchanges of Aβ between the CNS, blood and CSF play an important role in determining Aβ concentration in the CNS (Zlokovic, 2002). A number of receptors including RAGE (receptor for advanced glycation end products), LRP-1 (low-density lipoprotein receptor related protein-1), SR (scavenger receptor) and megalin receptors have been implicated in this process (Mackic *et al.*, 1998; Shibata *et al.*, 2000; Zlokovic *et al.*, 1996). RAGE-mediated Aβ transport is present at the luminal side of the BBB facilitating Aβ transport in a luminal to abluminal direction and allowing a significant influx of Aβ into the brain. In contrast the LRP-1 receptor mediated transport is initiated at the abluminal side and has a role in eliminating Aβ from the cerebral interstitial fluid. It is of note that one of the modulators of this process is the LRP-1 ligand ApoE, which is also one of the risk factors of CAA and sporadic AD (Zlokovic, 2002).

Another source of Aβ in CAA could be the CSF where it is present in both normal individuals and AD patients. The arguments against a blood borne derivation of cerebrovascular Aβ include the finding that Aβ is first detectable morphologically in the

abluminal basement membrane of blood vessels (Yamaguchi *et al.*, 1992). The more common involvement of arteries than veins and smaller arteries than larger ones in the subarachnoid space are arguments against a CSF origin of Aβ in CAA (Weller *et al.*, 1998). Furthermore systemic overexpression of a C-terminal fragment of the human AβPP in transgenic mice, which has high levels of sAβ in the plasma, does not result in CAA or deposition of Aβ in brain parenchyma (Tamaoka *et al.*, 1998).

2) The vascular hypothesis proposes that Aβ may derive from cerebrovascular cellular elements and this proposition is supported by morphological observations showing that Aβ deposits are closely associated with cerebrovascular smooth muscle cells (Kawai *et al.*, 1993; Vinters *et al.*, 1996). Furthermore it has been demonstrated that isolated cerebral microvessels and meningeal blood vessels are able to produce Aβ. Arguments against the vascular hypothesis include the finding that Aβ deposits in capillaries, which lack smooth muscle cells, and also that of larger arteries, which have several layers of smooth muscle cells are less affected (Wisniewski & Wegiel, 1994).

3) The drainage hypothesis proposes that Aβ, produced primarily by CNS neurons, is drained along the periarterial, perivascular spaces of the brain parenchyma and leptomeninges and CAA occurs due to deposition of Aβ along these drainage pathways (Weller *et al.*, 1998). Degenerative changes that commonly affect aged individuals could have a deleterious effect on the perivascular flow of interstitial fluid and contribute to vascular deposition of Aβ. The presence of CAA in some of the transgenic animal models of AD in which AβPP is expressed by neurons could support the drainage hypothesis (Van Dorpe *et al.*, 2000).

Data suggest that some of the amyloid peptides implicated in familial CAAs for example ACys, ATTR and AGel may derive from the circulation as they all deposit in systemic organs (Kiuru, 1998; Olafsson *et al.*, 1996; Garzuly *et al.*, 1996), but the origin of ABri and ADan deposited in the brain parenchyma and cerebral blood vessels is unknown. The possibilities include that they are derived from the circulation like some other amyloid forming peptides, are produced solely by cellular elements within the CNS, which is similar to that found with AβPP in AD, or that both mechanisms may be present. Observations to date have shown that ABri is found in the circulation and is deposited systemically in FBD (Ghiso *et al.*, 2001), which raises the possibility that peripherally produced ABri species could also be a source of CNS amyloid deposits. Although the familial forms of CAA are usually rare disorders, some of these disorders such as the *BRI2* gene-related dementias might provide an insight into the link between cerebral vascular and parenchymal amyloid deposition and neurodegeneration.

1.8 Tau

1.8.1 Tau protein and normal function

Tau, a microtubule-associated proteins (MAPs), functions to stabilize microtubules within cells. Microtubules have two general functions 1) they form the primary structural component of the mitotic spindles and 2) organise the cytoplasm.

1.8.2 Tau deposition

Insoluble tau isolated from neurodegenerative diseases is hyperphosphorylated and does not bind to microtubules (Lovestone & Reynolds, 1997; Grundke-Iqbal *et al.*, 1986; Morishima-Kawashima *et al.*, 1995). The major effect of tau hyperphosphorylation may

be the destabilization of microtubules. Tau knock-out mice develop almost normally indicating that loss of tau function may be compensated by other MAPs (Harada *et al.*, 1994). Hyperphosphorylated tau is able to bind normal tau and other MAPS leading to microtubule disruption (Alonso *et al.*, 1996). A number of protein kinases and protein phosphatases have been implicated in the abnormal phosphylation of tau. These include a number of stress activated protein kinases.

NFTs develop intracellularly and consist of PHFs which are formed by hyperphosphorylated tau. With time the neurons containing PHF tau die leaving behind extracellular ghost tangles (Bancher *et al.*, 1989; Braak *et al.*, 1994). Various components have been associated with these extracellular ghost tangles including growth factors (Tooyama *et al.*, 1993), proteoglycans (Alonso *et al.*, 1996; Snow *et al.*, 1992) and complement components (McGeer *et al.*, 1989; Schwab *et al.*, 1996b).

1.9 Role of complements in cerebral amyloid diseases

Evidence suggests that cerebral inflammation is associated with AD pathogenesis (Akiyama *et al.*, 2000) and inflammatory mediators, immunologic factors and activators of the complement pathways have been implicated in this process (Berkenbosch *et al.*, 1992). Complement proteins have been shown by previous studies to be associated with Aβ plaques (Head *et al.*, 2001; Stoltzner *et al.*, 2000; Webster *et al.*, 1997) amyloid-laden blood vessels (Verbeek *et al.*, 1998) and NFTs (Alonso *et al.*, 1996; Shen *et al.*, 2001; Schwab *et al.*, 1996b) *in vivo*. Aβ has been shown to bind to C1q and activate the classical pathway (Afagh *et al.*, 1996; Rogers *et al.*, 1992b) and the alternative pathway, through the hydrolysis of C3 (Bancher *et al.*, 1987; Pangburn & Muller-Eberhard, 1983).

1.9.1 Introduction to the complement cascades

Complement proteins are a group of serum and cell surface proteins that interact together and with other immune system molecules in a highly regulated manner, providing many of the effector functions of humoral immunity and inflammation. There are two complement pathways; one is the phylogenetically older 'alternative' pathway, which is initiated on microbial surfaces without the requirement for specific immune responses. The second pathway, called the 'classical' pathway, is usually initiated by binding of complement proteins to antibody-antigen complexes. Both pathways converge to a common final pathway generating the assembly of the membrane attack complex (MAC) (figure 1.10).

The functions of the complement pathways fall into two broad categories 1) cell lysis by the MAC and 2) biological effects of proteolytic fragments of complement. It has been described how complement activation on cell surfaces leads to the insertion of the MAC into lipid bilayers causing osmotic lysis of the cell. Many other effects of complement in immunity and inflammation are mediated by the proteolytic fragments generated during complement activation. These proteolytic fragments may remain membrane bound to the same cell surface to where complement has been activated or may be released into the fluid phase (blood or extracellular).

1.9.1.1 Classical pathway

The 'classical' pathway is activated principally by the binding of C1 to the Fc portion of antibody molecules that have bound antigens. There are stringent requirements for antibody mediated C1 activation that ensures the pathway is activated only under certain conditions. Activation of C1 requires specific regions of certain antibodies, with examples including the Cγ2 domains of IgG or Cμ3 domains of IgM. Furthermore a

single C1 molecule must bind simultaneously to at least 2 Fc portions of Ig to induce a conformational change in the C1 molecule, inducing enzymatic activity. C1 is a large multimeric protein complex ~750kDa, composed of C1q, C1r and C1s subunits. The catalytic functions of C1 are mediated by C1s-C1r-C1r-C1s tetramer that is non-covalently associated with the C1q subunit. C1r and C1s are serine esterases that remain inactive until the C1 molecule binds to an immune complex

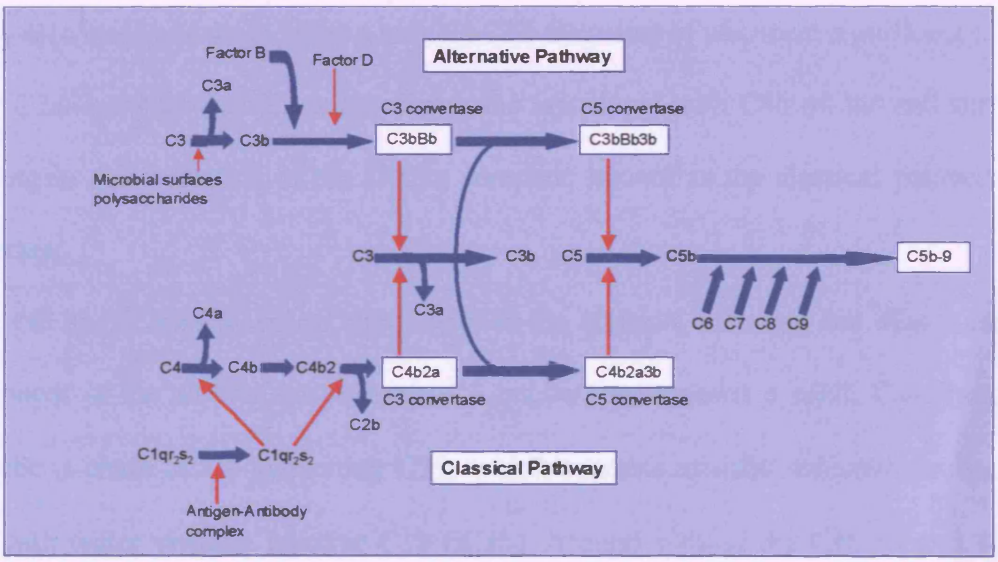

***Figure 1.10**: Alternative and classical complement pathways. The diagram shows how the alternative pathway is activated by microbial surfaces and the classical pathway by antigen-antibody complexes. Both pathways converge by catalysing the conversion of C5 to C5b and the formation of the MAC complex.*

Once bound C1r is enzymatically activated, this then cleaves and activates C1s. Which in turn acts on the next two components of the classical pathway, C4 and C2. C4 is the next serum complement protein to be activated in the classical pathway, participating in the formation of the C3 convertase. In addition, it is critical for keeping subsequent activation steps localized to the initial site where the antibody is bound. C4 consists of 3 polypeptide chains α,β and γ. The α chain contains a thioester bond similar to C3 keeping the C4 molecule localized to the antigen-antibody binding site. The α chain of

the soluble C4 is cleaved by the active C1s component yielding a large short-lived, C4b molecule and a small C4a fragment that diffuses from the cell surface. C4b contains a thioester bond in the α chain and is highly susceptible to nucleophilic attack. Most C4b molecules are inactivated by rapidly reacting with water.

C2 is the third soluble serum component of the classical pathway. It is involved in the formation of the C3 convertase. It is a single chain polypeptide that binds to cell surface bound C4b molecules in the presence of Mg^{++}. Once bound to C4b, C2 is cleaved by a nearby C1s molecule to generate a soluble C2b fragment of unknown significance. The larger C2a fragment that is produced remains associated with C4b on the cell surface, resulting in the formation of the C4b2a complex, known as the classical pathway C3 convertase.

C3 is the fourth soluble serum component in the classical pathway, but also a central component of the alternative pathway. C3 convertase removes a small C3a fragment from the α-chain of C3 generating C3b, which contains unstable thioester bonds that react with water yielding inactive C3b (iC3b). Around 10% of the C3b formed forms covalent bonds with cell surfaces or with Ig to which the C3 convertase is bound resulting in the formation of C4b2a3b known as the classical pathway C5 convertase. C5 convertase catalyses the cleavage of C5, which intiates the formation of the MAC.

Proteins involved in the terminal pathway include C5, C6, C7, C8 and C9. This part of the process is initiated by the cleavage of C5 by either of the C5 convertases from the alternative or classical pathway. Further steps in these pathways do not involve enzymatic degradation, but require the binding and polymerisation of intact proteins. C5 is then cleaved into a small C5a fragment that is released and a two chain C5b fragment that remains bound to the cell surface. C6, C7, C8, and C9, which are the remaining components of the cascade, are structurally related proteins. C5b maintains its

conformational shape ready to bind C6 and the stable C5b-6 complex is produced and remains loosely associated with the cell surface. Once C7 is bound the resulting molecule becomes highly lipophilic and is inserted into the hydrophobic lipid bilayer of cell membranes. Once inserted into the membrane one C8 molecule is bound. The formation of the highly lytic and microbicidal MAC is accomplished by binding of C9. C9 is a monomeric serum protein that polymerises at the site of the bound C5b-8. MACs with just four C9 molecules bound have full lytic capabilities.

1.9.1.2 Alternative pathway

The alternative pathway is activated in the absence of antibodies and is, therefore, a mechanism of innate immunity. This pathway is in a continuous state of low-level activation due to the reactivity of soluble C3 with water. This fluid phase activation is sometimes called C3 tickover, which then goes on to promote solid phase activation. The fluid phase activation is initiated when the internal thioester bond of C3 is hydrolysed by water to form an unstable intermediate called C3i, which binds to the alternative pathway protein factor B. Once bound to C3i factor B is susceptible to proteolysis by factor D, a serine protease that circulates at very low concentration in the serum. Factor D proteolytically cleaves bound factor B, releasing a small fragment (Ba), leaving a larger fragment Bb attached to C3i. This C3iBb complex is unstable and rapidly decays unless it is bound to properdin. Properdin may also bind to C3i before factor D, and promote the binding of factor B. The stable complex formed by the binding of both properdin and factor B is the initial alternative pathway C3 convertase, where the Bb fragment functions as a serine protease capable of cleaving C3.

1.9.2 Regulation of pathways

The complement cascades have evolved to permit rapid, self-amplified activation on microbial surfaces, which is necessary for effective defence against infection. The requirement for tight regulation of both pathways is needed, without which complement activation could lead to deleterious consequences. About half the protein components of the complement system function as regulatory molecules, showing how tightly the system is controlled. As complement activation involves both the fluid phase and localized membrane events, the regulatory mechanisms have evolved to include both soluble and integral membrane proteins. The majority of regulatory mechanisms are directed toward the C3 convertase activity, which is the central feature of both the classical and alternative pathways.

Inhibition of the initiation of the classical pathway is undertaken by C1 inhibitor (C1INH). C1INH functions by presenting a 'bait' sequence that mimics the normal substrates of C1r and C1s. Most of the C1 found in the blood is non-covalently bound to C1INH (which is present at seven times the molar concentration of C1). However, once C1 binds to antigen-complexed antibody, via the C1q subunit the C1INH is released and the classical pathway can proceed.

If the classical and alternative pathways are activated, they have the potential to generate millions of C3b molecules by the action of the C3 convertases. Several of the proteins involved in C3/C5 convertase regulation are members of a family of proteins called regulators of complement activation (RCA). All these proteins also share a structural feature, the presence of multiple copies of a 60 amino acid long, cysteine-rich module called a complement control protein repeat (CCPR). Molecules involved in this regulation include Factor I, which is a plasma serine protease that cleaves C3b and C4b preventing their insertion into the convertases. Factor H and C4-binding protein are two

RCA members that serve as important cofactors for Factor I-mediated proteolysis. Factor H and C4BP work in a similar fashion by binding to the fluid phase C3b and C4b respectively, and inhibiting the formation of the C3 convertases. The second major mechanism in the regulation of C3/C5 convertases is the destabilization of the enzyme complexes themselves. The major host cell membrane bound protein is decay-accelerating factor (DAF), which is also a member of the RCA family. DAF is expressed on most blood cells, endothelium and epithelial cells, being covalently linked to the outer leaflet of the plasma membrane by a phosphatidyl-inositol linkage. DAF functions by binding either C3 convertases and causing rapid release of Bb from C3b, or C2a from C4b.

Even after the formation of the convertases, excessive complement mediated cell lysis is prevented by a number of proteins that act at the level of MAC. The presence of MAC inhibitory molecules on host cells distinguishes them from most microbes and protects cells against lysis. In addition, at the C5b-7 stage, the growing MAC complexes have the ability to insert into neighbouring cell membranes besides the membrane on which they were generated. Therefore, inhibitors are needed in the host cell membranes and at the plasma level to ensure innocent bystander cell lysis does not occur. A major membrane inhibitor of MAC is CD59 (membrane inhibitor of reactive lysis). It is also, like DAF inserted into the membrane by a phosphatidylinosital linkage. CD59 works by inserting itself into the growing MAC complex after the insertion of C5b-8, thereby inhibiting C9 membrane insertion. Soluble inhibitors of MAC include vitronectin (S protein) and ApoJ (Clusterin, SP40-40). Vitronectin functions by binding C5b-9 complex preventing their insertion into the cell membrane. Like vitronectin, ApoJ inhibits MAC formation by binding to soluble C5b-7 complexes and preventing membrane insertion.

1.9.3 Vitronectin

Vitronectin (Vn) is a multifunctional protein that has been reported to have roles in cell adhesion, regulation of complement cascades and blood coagulation. It is present in serum at 200-400 μg/ml, and is also present in many tissues as a component of the extracellular matrix. As a complement inhibitor it can bind to the nascent C5b-7 terminal complement pathway components therefore preventing the insertion and assembly of the C5b-9 membrane attack complex into cellular membranes. Vn generally localizes at the site of complement activation and has also been visualized in AD brains, in which it co-localizes with Aβ containing plaques and NFTs. It is bound to cells that express a group of integrin receptors that recognises the Arg-Gly-Asp amino acid motif. Although primarily produced in the liver other tissue cells can express Vn mRNA including brain, heart, and skeletal muscle and cerebellar Purkinje cells (Walker & McGeer, 1998).

1.10 Amyloid Associated Proteins (AAPs)

The amyloid structures found in the neurodegenerative diseases mentioned above are not a result of the accumulation of the amyloid proteins alone, but such structures also contain a number of other components, generally referred to as AAPs. Attention was first placed on the senile plaques found in AD and the presence of a variety of proteins associated with such lesions was documented (Wisniewski & Frangione, 1992). These included complement factors and their inhibitors, acute phase proteins, proteoglycans and ApoE and it was proposed that most of these proteins are deposited as a result of amyloid deposition.

There are two possible roles for the AAPs in the pathogenesis of Aβ deposition in plaques and/or CAA. They may trigger or facilitate Aβ deposition and/or fibrillization

(Ghiso & Frangione, 2002), or, as a secondary effect, increase Aβ induced cytotoxicity and tissue damage. Theoretically, it is also possible that they do not have any biological effect.

1.10.1 Apolipoprotein E

ApoE is a 34-kDa product of a 4 exon gene located on the long arm of chromosome 19, and is central to cholesterol metabolism (Mahley, 1988). It is classed as a very low-density lipoprotein, which is synthesized primarily by the liver. In addition to cholesterol metabolism it is also important in local circuits of lipid turnover that are involved in membrane repair. In humans, the *ApoE* gene is polymorphic, leading to three major ApoE isoforms (E2, E3 and E4). ApoE3, the most common isoform, has a cysteine at position 112 and an arginine at position 158; ApoE2 is the least frequent isoform, with cysteine at both positions, whereas ApoE4 presents arginine at both sites (Mahley, 1988). The role of ApoE in the pathogenesis of AD is unclear, given the multiple functions of ApoE that are already known. It has been proposed that ApoE functions as a 'pathological chaperone' in AD (Wisniewski & Frangione, 1992). This term describes a process in which a protein binds to another, inducing and/ or maintaining an altered or intermediate folding state that leads to an incorrect fate *in vivo*. ApoE has also been shown to be present in systemic amyloid deposits, which are not related to Aβ, therefore ApoE most likely has a general role in amyloidogenesis. ApoE binds to Aβ only after it has been cleaved from AβPP and acts as a glue to foster plaque maturation, making it resistant to degradation. Such a role is consistent with immunohistochemical studies on ApoE distribution among different types of amyloid deposits (Sheng *et al.*, 1996; Gallo *et al.*, 1994). There have been several studies that have shown ApoE is able to enhance Aβ polymerisation and aggregation. (Sanan *et al.*,

1994; Ma *et al.*, 1994). The different isotypes have been shown to bind to Aβ at different rates (Yang *et al.*, 1997), with the ApoE3/ApoE2 isoforms binding more avidly to Aβ than the ApoE4 isoform. Furthermore the density of Aβ deposition is directly related to the inheritance of an ε4 allele (Schmechel *et al.*, 1993), therefore the inability of ApoE4 to bind Aβ efficiently may result in the accumulation of Aβ leading to its deposition.

Transgenic mice carrying the $A\beta PP^{V717F}$ mutation show large fibrillar Aβ deposits surrounded by plaque-associated dystrophic neurites. In the $A\beta PP^{V717F}$ apo E-/- mice extensive nonfibrillar Aβ deposits were observed and the neuritic degeneration was relatively rare, suggesting that the presence of ApoE is required for the formation of amyloid plaques. However when astrocyte-specific expression of human apoE3 or apoE4 was introducted in such animals, fibrillar Aβ deposition could be restored (Holtzman *et al.*, 2000a). ApoE has also been shown to be a ligand for LRP-1 (Beisiegel *et al.*, 1989), and is also a constituent of high-density lipoproteins which are associated with soluble Aβ in the CSF (Koudinov *et al.*, 1996) and bind to LRP-1 (Fagan *et al.*, 1996). It has been shown that Aβ is internalized via a pathway that shows close relationship to the metabolism of ApoE-containing lipoproteins, via LRP-1 and other lipoprotein receptors (Urmoneit *et al.*, 1997).

1.10.2 Apolipoprotein J

ApoJ is a multifunctional disulfide linked heterodimeric glycoprotein composed of two ~40 kDa subunits, named α- chain and β- chains (de Silva *et al.*, 1990a). The final ApoJ structure is generated by post-translational cleavage at peptide bond Arg ^{205}- Ser^{206} and stabilized by five interchain disulfide bonds. A single gene on chromosome 8 produces

a single mRNA that codes for a 449 amino acid chain containing a leader sequence and the α and β subunits (Kirszbaum *et al.*, 1989). ApoJ mRNA is found within almost all mammalian tissues (Collard & Griswold, 1987) as well as in all body fluids (Aronow *et al.*, 1993). ApoJ is mainly a secreted glycoprotein although an intracellular form has been described (Jin & Howe, 1997). It was first isolated from ram rete testis and named clusterin because of its ability to elicit clustering of Sertoli cells (Blaschuk *et al.*, 1983; Fritz *et al.*, 1983). Since then this multifunctional ubiquitous protein has been purified from several tissues where it apparently exhibits different functional properties. ApoJ has been implicated in the following normal functions; as a phagocyte recruitment signal (Buttyan *et al.*, 1989); it promotes aggregation and adhesion of cells (Silkensen *et al.*, 1995); involoved in spermatogenesis (Hermo *et al.*, 1994); development (French *et al.*, 1993); complement inhibition (Jenne & Tschopp, 1989) and lipid transport (de Silva *et al.*, 1990b).

The CNS is a major site of ApoJ mRNA, although regional differences have been observed (Danik *et al.*, 1993). High levels are found in neuron rich layers including the granular cell layer of the hippocampal formation, whereas the cortical layers show ApoJ mRNA is also expressed by astrocytes.

In pathological conditions, such as AD, an increase of mRNA and protein expression is observed (Duguid *et al.*, 1989). Immunohistochemical staining for ApoJ has been shown to co-localise with amyloid lesions in the brain and peripheral organs, including many diffuse lesions found in the cortex of AD and DS cases (McGeer *et al.*, 1992). It has also been shown that ApoJ immunoreactive, NFT-free neurons appear to be relatively resistant to neuronal death in AD, suggesting a neuroprotective role for Apo J in AD (Giannakopoulos *et al.*, 1998).

1.10.3 Serum amyloid P component

SAP component was named because of its amyloid binding capacity. SAP is a component of all amyloid deposits including those of AD. SAP is known as a pentraxin because of its capacity to aggregate in a non-covalent fashion into flat pentameric discs. Pentraxins are also able to activate the classical complement pathway in an antibody independent manner (Hicks *et al.*, 1992). It has been presumed that SAP is primarily produced by liver hepatocytes (Gabay & Kushner, 1999) and that the presence of SAP within cerebral amyloid lesions is due to a damaged BBB (Kalaria *et al.*, 1991). However, this proposition has been disputed by some (Caserta *et al.*, 1998) as it has been shown that SAP mRNA is present several organs (Yasojima *et al.*, 2000), and was also found in other cell types such as macrophages and neurons. SAP has also been reported to be a normal constituent of basement membranes and it may have a normal physiological role as well as being a response protein in pathological situations (Zahedi, 1997). Its strong binding to glycosaminoglycans would explain its appearance in all forms of amyloid but would not explain its association with pathological structures such as NFTs (Schwab *et al.*, 1997). Immunohistochemical staining of SAP usually mirrors that seen for C4d (McGeer *et al.*, 1991), but its deposition on NFTs has been found to precede the appearance of C4d (Schwab *et al.*, 1997).

Using immunoelectron microscopy SAP has also been shown to be associated with Aβ fibrils (Holm *et al.*, 2000). Positivity for SAP was seen on the surface of *in vitro* formed mature Aβ42 fibrils, whereas protofibrils, representing earlier stage in fibrillogenesis did not show any positive immunoreactivity.

1.10.4 α-1-antichymotrypsin

ACT is an inhibitor of chymotrypsin-like serine protease and is normally produced in the liver as part of the acute phase response to inflammation. ACT is overexpressed in astrocytes in brains of AD patients (Pasternack *et al.*, 1989). With the deposition of ACT in amyloid laden blood vessels and plaques the question can be raised whether inflammation was merely a response to the disease or whether it was an essential cause of the disease. *In situ* hybridisation studies in AD brain revealed that ACT is produced mainly by reactive astrocytes located around senile plaques (Abraham, 2001). Virtually all plaque types, including the diffuse ones, are stained with antibodies to ACT, suggesting that ACT first appears in early diffuse plaques. Rozemuller et al (1991) found that ACT immunoreactivity was associated with congophilic plaques and in amorphous plaques and resembled the staining pattern of Aβ. They also found infrequent staining of NFTs. An antibody directed against an inactive form of ACT was found to be negative on pathological structure and vascular amyloid was negative with all the ACT antibodies.

Amino acids 1-12 of Aβ closely resemble the conserved active site of serine proteases, the natural target for protease inhibitors such as ACT. In contrast to ACT, ApoE is found to be associated with all cerebral and systemic amyloids, apparently reflecting a more general affinity for the β-pleated sheet conformation characteristic of amyloid filaments. ACT was not detected in amyloid deposits occurring in other amyloidoses studied so far, raising the possibility of a special interaction between ACT and Aβ. This can be tested in the two novel diseases, FBD and FDD with ABri and ADan amyloid lesions respectively

1.10.5 Cystatin C

Cystatin C, also known as γ-trace protein, is an alkaline protein composed of one non-glycosylated 120 residue polypeptide chain (Grubb & Lofberg, 1982), belonging to a group of potent, non-covalent, competitive inhibitors of cysteine proteinases of the papain superfamily and is present in all body fluids with the highest concentrations in the CSF and seminal fluid (Bobek & Levine, 1992). It has a molecular weight of ~14KDa and mRNA levels of cystatin C were found at varying levels in different tissues with highest expression levels in pancreas, testis and brain. The human *cystatin C* gene has been mapped to chromosome 20p11.2 (Abrahamson *et al.*, 1989; Schnittger *et al.*, 1993). Mutant cystatin C is associated with HCHWA-I (see section 1.7.5.1) and the possibility that cystatin C may have a role in the pathogenesis of other amyloidosis was raised by the observation that it is present in Aβ parenchymal and vascular amyloid lesions in AD (Levy *et al.*, 2001). Furthermore, a polymorphism in the *cystatin C* gene may confer a greater risk of developing AD (Crawford *et al.*, 2000; Finckh *et al.*, 2000).

1.10.6 Heperan sulphate proteoglycans (HSPGs)

HSPGs are a small subgroup of the larger group of proteoglycans (PG). PG molecules are composed of proteins and carbohydrates and are distributed throughout the body. Being found intracellularly, on cell surfaces and in the extracellular matrix. By definition a PG is a molecule where at least one glycosaminoglycan (carbohydrate) side chain is covalently attached to the protein core of the molecule. EM studies have shown that PGs have a bottlebrush-like structure, with the 'bristles' non-covalently attached to a filamentous hyaluronic acid backbone and are composed of a core protein to which glycosaminoglycans are covalently linked. To date there have been 25 different core proteins found in the rat brain (Herndon & Lander, 1990).

The carbohydrate moieties of PG are called glycosaminoglycans (GAG). They are a group of polysaccharides of major structural importance in vertebrate animals. All are unbranched polymers composed of repeating disaccharide units, in which one of the sugars is either N-acetylgalactosamine or N-acetylglucosamine. The major GAGs are chrondroitin sulphate, dermatan sulphate, keratan sulphate and heperan sulphate. The extended structures of PGs together with their polyanionic character of their GAG components cause them to be highly hydrated.

Protein Family	Name	~MW core protein	GAG type	Cellular origin	Tissue location
Lecticans	Aggrecan	225-250	CS in brain	Unclear	Cartilage
	Versican	400	CS	Neurons (chick)	Connective tissue
	Neurocan	245	CS	Neurons Glia	CNS
	Brevican	140 soluble	CS	Glia	CNS
Syndecans	Syndecan-1	50	HS/CS	Not known	Cerebellum
	Syndecan-2	48,90	HS	Neurons	
	Syndecan-3	120	HS	Neurons	
Glypicans	Glypican-1	64	HS	Neurons	CNS
Others	NG2	300	CS	Glia	CNS
	Perlecan	400	HS(CS)	Blood vessels, glia	Basement membrane, cartilage
	Agrin	220	HS	Neurons	Basement membrane

Table 3: *Table of HSPG's Showing cellular origin and tissue location; CS- chondroitan sulphate, HS- Heperan sulphate, MW – Molecular weight*

PGs can be split into different categories (table 3), large extracellular PG's include aggrecan, versican, neurocan and brevican. Cell-associated PGs form a variable group of molecules with many functions, which include syndecans and phosphatidyl inositol anchored proteoglycans. Nervous tissue proteoglycans include NG2, agrin and perlecan. One important feature of PGs is their ability to form non-covalent interactions with other proteins through their GAGs. One such protein that PGs have been shown to interact with is Aβ. Binding of sulphated GAG to Aβ has been found to decrease Aβ

degradation and this process is thought to be catalysed by insulin degrading enzyme. Aβ has also been shown to bind to the core protein of HSPGs (Buee *et al.*, 1993). This is mediated by a heparin binding consensus sequence (VHHQKL) located towards the N-terminal end of the Aβ peptide (Snow *et al.*, 1995). Aβ easily self-aggregates to form amyloid fibrils *in vitro* and the binding of HSPGs to Aβ (11-28 and 1-28) enhances this aggregation (Fraser *et al.*, 1992).

GAGs and PGs have been found to be present in senile plaques and CAA in AD, and it has been suggested that they might enhance the polymerisation of Aβ into fibrils. Such fibrils would become resistant to proteolytic cleavage and could therefore stimulate further deposition of Aβ. It has been suggested that oligomeric and protofibrillar intermediates of Aβ, which are said to be highly neurotoxic, may preferentially associate with sGAG resulting in the formation of dense filamentous inclusions in which Aβ molecules are prevented from interacting with neuronal membranes. According to this hypothesis the generation of senile plaques in AD would be a partially protective response aimed at reducing Aβ neurotoxicity.

Several PGs and sGAGs have previously been shown to be associated with pathological lesions in AD. Syndecans and glypicans reside in the cell membrane but differ in core protein structure and type of attachment to the cell membrane. Syndecans are transmembrane PGs and have a cytoplasmic domain, whereas glypicans are anchored to membrane lipids via glycosylphosphatidyl inositol molecules. Members of both families have been shown to be associated with senile plaques and CAA related to Aβ depostion (van Horssen *et al.*, 2001), although differences were seen between members of each group. There are six members in the glypican family (GPC1 to GPC6), which have been identified in mammals (Veugelers *et al.*, 1999). The size of the core protein is similar in

all (60-70 kDa) and the homology is moderate. All 14 cysteine residues are conserved so therefore all may have a similar structure.

Agrin and perlecan are HSPGs associated with the extracellular matrix and have been studied in relation to AD. Perlecan was first isolated from the Englebreth-Holme-Swarm tumor in 1980, and consists of a large core protein carrying 3 heparan sulphate side chains (Costell *et al.*, 1997). It is a major HSPG present in basement membranes and cartilage and was originally reported not to be present in the CNS. Some studies have shown it to be present in normal CNS vessels but not in CAA or SP (van Horssen *et al.*, 2001), while others have suggested that it is present in amyloid-laden vessels and plaques (Snow *et al.*, 1994). Agrin, with a molecular weight of 500 kDa (200KDa protein core) is a major basement membrane derived extracellular HSPG of the brain and has an important role in synaptogenesis at the neuromuscular junction (Cole & Halfter, 1996). *In vitro* studies, using sGAG, have shown that they are important for the enhancement of Aβ fibril formation (Castillo *et al.*, 1999) and that the deposition and accumulation of other PG's/GAGs at sites of Aβ deposition may also participate in the enhancement of Aβ fibrillogenesis. Agrin has also been shown to contain nine protease inhibiting domains and may therefore, protect the protein aggregates in senile plaques against extracellular proteolytic degradation leading to the persistence of these deposits (Verbeek *et al.*, 1999).

1.11 Hypothesis

There are common pathogenic events occurring in cerebral amyloid diseases irrespective of the amino acid sequence of the amyloid peptide. Therefore, my main hypothesis investigated in this thesis is that FBD and FDD provide alternative models of AD.

1.12 Questions and approaches

To investigate the main hypothesis of this thesis and issues related to FBD and FDD which had not been addressed previously in the literature as outlined in the introduction. The questions raised and the approaches taken are summarized below;

A) What are the pathological features of FBD and FDD?

A1) What is the distribution of ABri fibrillar and nonfibrillar lesions in FBD and what is their relationship to neurofibrillary pathology, astroglial and microglial responses?

To address these questions in this study of FBD cases the topographical distribution and patterns of ABri deposition were studied by immunohistochemistry. To determine the conformational state of the protein deposits ABri immunohistochemistry was combined with thioflavine-S and evaluated by confocal microscopy. The distribution and relationship of neurofibrillary degeneration to ABri deposits were investigated with tau immunohistochemistry alone and in combination with Ab338. The astrocytic and microglial responses to ABri deposits were studied by a double immunohistochemical approach. The ultrastructural characteristics of the ABri protein deposits were studied by immunoelectron microscopy.

A2) What is the distribution and conformational patterns of ADan deposition in FDD and their relationship to neurofibrillary pathology, astroglial and microglial responses?

The topographical distribution of ADan deposition was studied in FDD cases using immunohistochemistry. To determine the conformational state of the protein deposits, ADan immunohistochemistry was combined with thioflavine-S and evaluated by

confocal microscopy. The distribution and relationship of neurofibrillary degeneration to ADan deposits were investigated by tau immunohistochemistry. The astrocytic and microglial responses to ADan deposits were studied by a double immunohistochemical approach. The ultrastructural characteristics of the ADan deposits were analysed by immunoelectron microscopy.

B) What other protein components are associated with ABri and ADan lesions?

B1) Are 'amyloid associated proteins', which are known to co-localise with Aβ deposits in AD and some other cerebral and systemic amyloidoses, present in amyloid and pre-amyloid lesions in FBD and FDD?

As the presence of AAPs in Aβ lesions in AD has been linked to the process of Aβ fibrillogenesis, this study aimed to establish whether such proteins are also associated with ABri and ADan lesions thus raising the possibility of a more general role for these proteins in amyloid fibril formation. This question was addressed by an immunohistochemical study investigating the distribution of Apolipoprotein E (ApoE), Apolipoprotein J (ApoJ), α-1-antichymotrypsin (ACT), serum amyloid P component (SAP), cystatin C and various heparan sulphate proteoglycans (HSPGs), including agrin, perlecan, glypican-1 and syndecans.

B2) Are the complement pathways activated and complement products implicated in the pathogenesis of FBD and FDD?

In relation to Aβ deposition activation of the complement pathways has been documented with implications for fibrillogenesis, host response and the mechanism of neurodegeneration. This study investigates the presence of complement components of both the classical and alternative pathways and complement inhibitors in FBD and FDD, and seeks to establish whether the binding of the recognition protein C1q to ABri and ADan is dependent on the conformational state of these amyloid proteins. For this C1q immunohistochemistry was combined with thioflavine-S stain and evaluated by confocal microscopy.

C) Is there biochemical heterogeneity of the ABri and ADan peptide species deposited in the morphologically different lesions?

As correlation exists between the N- and C- terminal heterogeneity of the Aβ peptide species and different lesion types in AD, the question was addressed whether similar

heterogeneity occurs in FBD and FDD. In this study, ABri and ADan species deposited in blood vessels and parenchymal lesions were isolated and biochemically characterised. In addition, the heterogeneity of the Aβ species co-deposited in the parenchyma and CAA in FDD was also studied by immunohistochemistry, utilising a panel of antibodies specific for N- and C-terminally modified Aβ species.

D) What is the origin of ABri and ADan proteins in FBD and FDD?

Understanding the origin of the ABri and ADan peptide could provide further information about the evolution of the parenchymal and vascular lesions. To test the hypothesis that the brain is a major source of these amyloid peptides a study was undertaken to establish the cerebral distribution of BriPP and the enzyme (furin) implicated in its processing. For this study *in-situ* hybridisation, immunohistochemistry and biochemical methods were used.

Chapter 2

Material and methods

Chapter 2 – Material and Methods

2.1 Tissue Processing

2.1.1 Paraffin embedded tissue

Representative areas of formalin fixed brain and spinal cord tissue were processed as shown in table 4.

Step	Reagent	3 Day Time
1	70% alcohol	6.00 hrs
2	90% alcohol	6.00 hrs
3	90% alcohol	6.00 hrs
4	Absolute alcohol	6.00 hrs
5	Absolute alcohol	6.00 hrs
6	Absolute alcohol	6.00 hrs
7	Absolute alcohol	6.00 hrs
8	Chloroform	6.00 hrs
9	Chloroform	6.00 hrs
10	Wax	6.00 hrs
11	Wax	6.00 hrs
12	Wax	6.00 hrs

***Table 4:** Processing of paraffin tissue. Reagents and times used*

After processing tissue was embedded in paraffin wax and stored until required. Paraffin sections were cut using a Leica sledge microtome at 7μm, placed onto 30% alcohol solution and floated out onto warm water. The sections were picked up on superfrost slides (BDH) or Vectabond coated slides (Vector), and left to dry at 37°C for several hours followed by an overnight incubation at 60°C.

2.2 Immunohistochemistry on paraffin embedded tissue

Sections were deparaffinized in three changes of xylene for 5 minutes, followed by rehydration using graded alcohols (100%, 95% and 70%). For all immunohistochemical staining the endogenous peroxidase activity was blocked using 0.3% H_2O_2 in methanol

for 10 minutes followed by washes in distilled water for at least 5 minutes. Sections were subjected to various pretreatment protocols depending on the antibody used (see section 2.2.1). Non-specific protein binding was blocked using 10% non-fat milk in PBS (0.05M pH7.2) by incubating the sections for 30 minutes at room temperature. The milk was then replaced with the required primary antibody and incubated for 1 hour at room temperature or overnight at 4^0C (table 5) depending on the primary antibody used, followed by two washes in PBS. Incubation with the relevant secondary antibody was carried out for 30 minutes at room temperature, followed by washing in distilled water and two changes of PBS. Sections were incubated in avidin-biotin complex (ABC, Dako) for 30 minutes at room temperature, followed by washes in distilled water and two changes in PBS. The antigen-antibody reaction was visualized using di-aminobenzidine (DAB, Sigma) as the chromogen. Sections were placed in a 500µg / 100ml PBS DAB solution that was activated with 32µl H_2O_2 (30% solution, BDH) for 4 minutes and the colour intensity checked. Sections could also be replaced into the DAB solution if darker colour intensity was required. Sections were counterstained with Mayers haematoxylin (BDH) for 10 seconds, washed in distilled water and finally dehydrated through 70%, 95% and absolute alcohol before being cleared in two changes of xylene and permanently mounted with Depex (BDH).

2.2.1 Pretreatments used for paraffin embedded tissue sections

Different pretreatments were used for the retrieval of various antigens that may have been obscured by fixation or processing of the tissue. The pretreatments were carried out after the endogenous peroxidase was blocked with methanol (see section 2.2). The following pretreatments were used with the different antibodies as appropriate (see table 5);

- **Formic acid (FA)** – Sections were placed in 99% FA for 10 minutes followed by several washes in distilled water.
- **Pressure cooking (PC)** – Sections were placed in boiling citrate buffer pH 6.0 for 10 minutes once maximum pressure is reached.
- **Trypsin** – Sections were placed in distilled water at 37°C for 5 minutes, and then transferred to 0.1% trypsin (Sigma): 0.1% $CaCl_2$ (BDH) solution in distilled water for 10 minutes at 37°C.
- **Microwave** – Sections were placed in citrate buffer pH 6.0 for 20 minutes on high power in a 900W microwave.
- **Formic acid and pressure cooking (FA + PC)** – Sections were first pretreated in FA as above, washed in distilled water for 10 minutes. This step was followed by pretreatment as described above in the pressure cooker.

2.2.2 Double immunohistochemistry for light microscopy

Double immunohistochemical staining was carried out on paraffin sections and frozen sections using both a monoclonal antibody and a polyclonal antibody, or using two polyclonal antibodies. The protocol was followed as in section 2.2 or 2.4 depending on whether paraffin or frozen sections were used. The antibody was visualized with the glucose oxidase method as described in section 2.14.7. This was followed by incubation with the second primary antibody overnight at 4^0C. The relevant secondary and ABC were applied as in section 2.2 and the antibody visualized with Novored (Vector) for 2 minutes at room temperature. Sections were then washed in distilled water, dehydrated, cleared in xylene and mounted in DEPX (BDH).

Antibody	Source	Conc.	Species	Pretreatments	Incubation Period
CR3/43	Dako	1:200	M	PC	One hour
Amyloid P	Novacastra	1:200	P	FA + PC	Overnight at 4°C
Apo E	Autogen Bioclear	1:200	M	FA + PC	One hour
Apo J	Santa Cruz	1:600	P	FA + PC	One hour
α-1-antichymotrypsin	Neomarkers	1:500	P	PC	Overnight at 4°C
α-1-antichymotrypsin	Novacastra	1:500	P	PC	Overnight at 4°C
Vitronectin	Quidel	1:300	M	FA + PC	One hour
IC3b	Quidel	1:1500	M	FA + PC	One hour
Cystatin C	Gift from Dr Ghiso	1:200	P	FA + PC	Overnight at 4°C
AT8	Autogen Bioclear	1:600	M	Microwave	One hour
Aβ-40	Autogen Bioclear	1:100	P	FA + PC	One hour
Aβ-42	Autogen Bioclear	1:100	P	FA + PC	One hour
5282	Gift Dr Ghiso	1:1000	P	FA	One hour
338	Gift Dr Ghiso	1:2000	P	FA	One hour
CD-68	Dako	1:150	M	Trypsin	One hour
GFAP	Dako	1:1000	P	Trypsin	One hour
A4	Dako	1:100	M	FA + PC	One hour
C1q	Dako	1:100	P	Trypsin / free floating	Overnight at 4°C
Aβ1-16	Biosource	1:4000	M	FA + PC	One hour
Aβ17-26	Biosource	1:4000	M	FA + PC	One hour

***Table 5**: Antibodies used on paraffin sections. M- Mouse monoclonals; P- Rabbit polyclonals; FA- Formic acid; PC- Pressure cook.*

2.3 Immunohistochemistry of free floating sections

Paraffin sections were cut on a Leica sledge microtome at 30μm and collected in Eppendorf tubes until required. The sections were dewaxed in xylene and rehydrated in graded alcohols (100%, 95% and 70%). Sections were blocked for endogenous peroxidase in 0.3% H_2O_2 in methanol for 10 minutes. Followed by the required pretreatment needed for the antibody used (see section 2.2.3) and blocking for non-specific protein binding by incubating the tissue in 10% non-fat milk at room temperature. Incubation with the primary antibody in 10% non-fat milk containing 0.1% Tween-20 (BDH) was carried out overnight at 4°C. The tissue was washed in PBS on a shaker for 1 hour with 6 changes of PBS, followed by incubation with the relevant secondary antibody for 1 hour at room temperature, and extensive washes in PBS (6 x 10 mins). The tissue was placed in ABC (Dako) for 45 minutes at room temperature, followed by extensive washes in PBS. The antigen was visualized as above with DAB (see section 2.2).

2.4 Immunohistochemistry on frozen sections

Frozen sections were cut at 10μm from either flash frozen or slow frozen material, using a cryostat (Bright), and mounted onto either superfrost slides (BDH) or vectabond coated slides (Vector), depending on the size of the sections collected. Sections were air dried for 30 minutes, frozen at –80°C and stored until needed. Sections were removed from the freezer and placed on foil and air dried for 10 minutes, post-fixed in either 4% paraformaldehyde, or acetone depending on the antibody used (table 6) for 30 minutes at room temperature. This was followed by washes in distilled water and two washes in PBS.

Antibody	Antigen	Source	Conc.	Species	Post fixation
338	ABri	Dr Ghiso	1:1000	P	4% Para
5282	ADan	Dr Ghiso	1:1000	P	4% Para
340	ABriPP	Dr Ghiso	1:500	P	4% Para
Furin	Furin	Affinity Biochemicals	1:50	P	Acetone
NeuN	NeuN	Chemicon	1:2000	M	Acetone/ 4% Para
GFAP	GFAP	Chemicon	1:1000	M	Acetone/ 4% Para
Sc5b-9	Membrane attack complex	Quidel	1:50	M	Acetone
C5b-9	Membrane attack complex	Quidel	1:50	M	Acetone
C4d	C4d	Quidel	1:1000	M	Acetone
C3d	C3d	Quidel	1:50	M	Acetone
Bb	Bb	Quidel	1:20	M	Acetone
JM72	Agrin	Ref; Verbeek	1:500	M	Acetone
BI31	Agrin	Ref; Verbeek	1:750	G	Acetone
1948	Perlecan	Ref; Verbeek	1:500	R	Acetone
3G10	Pan-HSPG	Ref; Verbeek	1:300	M	Acetone
JM13	Heparan sulphate side chains	Ref; Verbeek	1:100	IgM	Acetone
JM403	Heparan sulphate side chains	Ref; Verbeek	1:300	IgM	Acetone
10H4	Syndecan 2 (ectodomain)	Ref; Verbeek	1:300	M	Acetone
2E9	Syndecan -1,-3 (cytoplasmic domain)	Ref; Verbeek	1:500	M	Acetone
1C7	Syndecan-3 (ectodomain)	Ref; Verbeek	1:100	M	Acetone
S1	Glypican-1 (core protein)	Ref; Verbeek	1:50	M	Acetone

***Table 6**: Antibodies used on frozen tissue. M- Monoclonal; P- polyclonal; G- goat polyclonal; R- Rat polyclonal.*

The endogenous peroxidase activity was blocked using 0.3% H_2O_2 in methanol for 10 minutes followed by washes in distilled water and two changes of PBS. The non-specific protein was blocked using 10% non-fat milk for 30 minutes at room temperature. The sections were incubated with the primary antibody for 1 hour at room temperature and the remaining protocol was followed as described in section 2.2.

2.5 Highman's Congo red staining.

Highman's Congo red stain was used to demonstrate protein deposits in amyloid conformation. Sections were dewaxed, rehydrated in graded concentrations of alcohol and then placed in water (section 2.2). Staining with Congo red solution (0.5% Congo red (BDH) in 50% alcohol) was carried out for 10 minutes and differentiated with alcoholic potassium hydroxide solution (0.2% KOH in 80% alcohol) for 3-10 seconds, followed by washing in distilled water. Nuclei were counterstained with alum haematoxylin (BDH) and the sections placed in running tap water for 5 minutes. Sections were then dehydrated in graded alcohol solution, cleared in xylene and mounted using Depex (BDH). Congo red staining was viewed under a polarized light.

2.6 Thioflavine-S staining

2.6.1 Single staining with thioflavine-S.

Sections were dewaxed and rehydrated as described in section 2.2, and stained in aqueous 1.0% thioflavine-S (Sigma) solution for 7 minutes. Sections were differentiated with 70% ethanol for 5 minutes and left to wash overnight in PBS before cover slipping in aqueous mountant (BDH) and viewed under a fluorescent microscope (Zeiss Axioskop MC80DX).

2.6.2 Double staining with thioflavine-S and immunohistochemistry

Sections were dewaxed and rehydrated as described in section 2.2. Immunohistochemistry was carried out on the sections before the thioflavine-S staining. Single fluorescent staining was carried out as described in section 2.7.1 and the antigen visualised was using the tetramethylrhodamine kit (NEN) to give a red fluorescence against the green fluorescence of the thioflavine-S. If FA pretreatment was required for the immunohistochemical staining then only a 70% solution was used for 10 minutes, as in control experiments using tissue sections with known amyloid deposits, higher FA concentrations abolished specific staining with thioflavine-S.

2.7 Fluorescence immunohistochemistry

Fluorescence immunohistochemistry was carried out using a number of antibodies to demonstrate the co-localization of specific antigens. Single and double immunohistochemistry was undertaken and the methods are described below;

2.7.1 Single staining

Paraffin sections were prepared as described in section 2.1.1. Immunohistochemistry was carried out as described in section 2.2 up to the washing step following the ABC incubation. The sections were incubated for 10 minutes at room temperature with either tetramethylrhodamine kit (1:500: NEN) to give the red fluorescence or the tetramethylfluorescein kit (1:200: NEN) to give the green fluorescence and viewed on a fluorescence microscope (Zeiss Axioskop MC80 DX).

2.7.2 Double Staining

Double fluorescent staining was carried out on paraffin sections and frozen sections using both a monoclonal antibody and a polyclonal antibody, or using two polyclonal

antibodies. The protocol was followed as in section 2.7.1 for single fluorescent staining. The antibody was visualized with tetramethylrhodamine (1:500, NEN) for 10 minutes at room temperature. This was followed by incubation with the second primary antibody overnight at 4^{0}C. From this point forward all sections were kept in the dark to avoid the first fluorescent chromogen fading. The relevant secondary and ABC were applied as in section 2.7.1 and the antibody visualized with tetramethylfluorescein (1:200, NEN) for 10 minutes at room temperature. Sections were then washed in distilled water, mounted in aqueous mountant (BDH) and viewed under a fluorescent microscope (Zeiss Axioskop MC80 DX).

2.7.3 Confocal microscopy

Fluorescent immunohistochemistry was carried out as described above (sections 2.7.1 or 2.7.2). Sections were then viewed with a Leica TCS4D confocal microscope using a 3-channel scan head and argon/krypton laser (UCL confocal imaging unit).

2.8 Immunoelectron microscopy

2.8.1 Tissue processing for electron microscopy

Tissue specimens were fixed overnight at 4°C in buffered gluteraldehyde (2.5% in 0.05M sodium cacodylate buffer). After fixation tissue was cut into 1-2 mm thick blocks, rinsed in 0.1M sodium cacodylate buffer, transferred to 1% osmium tetroxide and left for 3 hours at 4°C. The osmium was discarded and the blocks were placed in fresh 0.1M sodium cacodylate buffer. The tissue was dehydrated by being placed through increasing grades of alcohol, 70% alcohol for 10 minutes, 90% for 10 minutes and finally 3 changes of absolute alcohol for 10 minutes. For each alcohol change the tissue was agitated on a rotator.

While continuing to be agitated the tissue was transferred to propylene oxide for two 15 minute incubations. The tissue was then placed in a 1:1 mixture of propylene oxide: epoxy resin for 1 hour, followed by an overnight incubation in neat epoxy resin rotating in the fume hood. The epoxy resin was prepared in the following way; 20ml of Araldite CY212 (Resin: Agar) is mixed with 25ml DDSA (Hardener: Agar) in a plastic beaker, followed by 0.8ml DMP30 (accelerator: Agar). The whole mix is then thoroughly mixed with a wooden tongue depressor. When the colour changed from pale yellow to a deeper orange, a magnetic stirrer was placed in the beaker and the mixture was mixed on a warm plate for approximately 20 minutes. When mixed sufficiently the resin was ready for processing and the tissue was embedded in epoxy resin and left in a 60°C oven in a fume cupboard for 48 hours in order to achieve polymerization.

2.8.2 Immunoelectron microscopy for ABri

2.8.2.1 Ab338 immunohistochemistry on semi-thin sections

Resin blocks were trimmed and semi-thin sections (2μm) were cut using an ultramicrotome (Du pont MT6000), collected onto superfrost glass slides (BDH) and left to dry on a hotplate for at least 30 minutes. Sections were etched with saturated sodium ethoxide (15.25g NaOH/ 200ml Absolute alcohol) solution for 1 hour at room temperature, rinsed in three changes of absolute ethanol followed by three changes of distilled water. The sections were then placed in 4.7% sodium periodate solution for 1 hour at room temperature, followed by four changes of distilled water. The endogenous peroxidase was blocked with 0.3% H_2O_2 solution in methanol for 10 minutes followed by 10 minutes rinse in PBS. Sections were pre-treated in 99% FA for 10 minutes followed by three washes in distilled water, followed by incubation for 30 minutes in 10% non-fat powdered milk in PBS to block non-specific protein binding. The primary

antibody Ab338 was applied at 1:3000 and incubated at 4°C overnight, followed by washes in distilled water for at least 30 minutes. Biotinylated anti-rabbit (1:200 Dako) secondary antibody was applied, for 30 minutes followed by washing in distilled water for 30 minutes. ABC (Dako) was applied for 30 minutes and sections were washed in distilled water for 30 minutes. The chromogen was then developed using DAB (Sigma) for 4 minutes to give a brown precipitate.

2.8.2.2 Ab338 immunohistochemistry for electron microscopy

Sections were cut at 0.88μm from the main blocks using an Ultramicrotome (Du pont MT6000) with a diamond knife (Diatome) and mounted onto pre-prepared nickel grids (400 mesh thin bar, Agar Scientific). The nickel grids were prepared by soaking in chloroform for 10 minutes, transferred to 20% glacial acetic acid in pure distilled water for 2 minutes, washed in 95% ethanol for 2 minutes and allowed to dry. The sections were incubated at room temperature in 4.7% sodium metaperiodate (BDH) for 1 hour and rinsed twice in Tris-buffered saline (TBS, 0.5M pH7.4) containing 1% Triton X-100, followed by rinsing the grids in TBS-BSA (TBS containing 1% BSA and 0.05% sodium azide). The grids were incubated for 60 minutes at room temperature in 10% normal goat serum in TBS-BSA buffer, then transferred onto Ab338 antibody (1:20,000) overnight at 4°C. The grids were then washed on droplets of TBS-BSA before incubation with goat anti-rabbit IgG gold conjugate (1:15 in TBS, Sigma) with particle size of 20nm at room temperature for 60 minutes. This was followed by four washes in TBA-BSA buffer. The grids were then post-fixed in 2.5% gluteraldehyde in sodium cacodylate buffer for 10 minutes, washed in distilled water and allowed to dry. Sections were counterstained with uranyl acetate (25% uranyl acetate in methanol) for 3 minutes followed by three washes in methanol/ distilled water washes. The grids were

dried on clean fiber-free paper, stained in lead citrate (see appendix) for 10 minutes at room temperature, washed in three changes of filtered distilled water and dried on fiber-free paper.

2.8.3 Immunoelectron microscopy for ADan

2.8.3.1 Ab5282 immunohistochemistry on semi-thin sections.

The blocks were trimmed, cut and prepared as described in section 2.8.2.1. The primary antibody Ab5282 was applied at 1:1000 to the sections and left at 4°C overnight. The sections were washed in distilled water and the protocol was followed as described in section 2.8.2.1.

2.8.3.2 Ab5282 immunohistochemistry for electron microscopy

Ultrathin sections were cut and mounted onto nickel grids as described in section 2.8.2.2. The grids were etched as described in section 2.8.2.2, once blocked they were transferred onto droplets of Ab5282 (1:50) for 72 hours at 4^0C. The grids were then washed on droplets of TBS-BSA and transferred onto droplets on biotinylated swine anti-rabbit secondary (1:200, Dako) for 30 minutes at room temperature, then washed in TBS-BSA. The grids were incubated for 30 minutes at room temperature in ABC complex (Dako) followed by three changes of TBS-BSA buffer, followed by incubation in biotinylated tyramide (1:200, NEN) for 10 minutes at room temperature and washed in three changes of TBS-BSA buffer. The grids were incubated with anti-biotin gold (20nm, Agar) for 1 hour at room temperature and washed thoroughly in TBS-BSA.

The grids were then post-fixed for 10 minutes with 2.5% gluteraldehyde in sodium cacodylate buffer. Washed in distilled water and allowed to dry and counterstained with uranyl acetate and lead citrate as previously described in section 2.8.2.2.

2.8.4 Immunoelectron microscopy for Aβ

2.8.4.1 Aβ immunohistochemistry on semi-thin sections

The protocol was followed as described in section 2.8.2.1 for Ab338 immunohistochemistry on semi-thin sections up to the incubation step with the primary antibody. The primary antibody Aβ 17-26 (Biosource International) was used at 1:4000 and the sections left at 4°C overnight. The sections were then washed in distilled water for 30 minutes. Biotinylated anti-mouse (1:200 Dako) was applied for 30 minutes followed by another 30 minutes wash in distilled water. ABC (Dako) was then applied for 30 minutes. Sections were again washed in distilled water for 30 minutes. DAB was used as described previously to visualize the antigen.

2.8.4.2 Aβ immunohistochemistry for electron microscopy

The protocol was followed as described in section 2.8.2.2 up to the point of incubation with the primary. The grids were transferred onto Aβ 17-26 antibody (Biosource International 1:100) and incubated overnight at 4^0C. The grids were then washed on droplets of TBS-BSA before incubation with goat anti-mouse IgG gold conjugate (1:15) with particle size of 10nm for 60 minutes at room temperature (Sigma). The grids were then washed again in TBA-BSA buffer and post fixed for 10 minutes with 2.5% gluteraldehyde in sodium cacodylate buffer, washed in distilled water and allowed to dry. The grids were then counterstained with uranyl acetate and lead citrate as described in section 2.8.2.2.

2.8.5 Double immunoelectron microscopy for Aβ and ADan

For double staining with Ab5282 and Aβ17-26, the protocol above for single staining with Aβ was followed up to the incubation with the gold conjugate. After that step the grids were incubated on droplets of Ab5282 (1:50) for 72 hours at 4^0C. The rest for the protocol was followed as in section 2.8.2.2 for single staining with Ab5282. The grids were also post-fixed and counterstained as previously described.

2.9 Evaluation of immunohistochemistry

2.9.1 Evaluation of pathological analysis of CAA

The presence and frequency of parenchymal deposits and CAA were evaluated in different anatomical regions using a semi-quantitative approach. For CAA a four tiered scoring system was used such that score 0 was given for unaffected areas; '+' if a proportion of the arterioles/ small arteries were affected, but no or only an occasional capillary was stained; '++' if the majority of arterioles as well as minority of the capillaries were positive; and '+++' for areas in which the majority of the arterioles and capillaries were positive for either ABri or ADan.

2.9.2 Evaluation of pathological analysis of parenchymal deposits

For the quantitation of parenchymal deposits, Ab338 or Ab5282 positive, Congo red positive and thioflavine-S positive structures with or without an associated blood vessel were considered to represent amyloid deposits (plaques). Diffuse deposits were ill-defined, Ab338 or Ab5282 positive, Congo red negative structures, which were weakly stained if at all with thioflavine-S. Using a x 10 objective plaques and diffuse deposits were scored separately in each case following a principle similar to that recommended by 'The Consortium to Establish a Registry for Alzheimer's disease' (CERAD) for quantitating neuritic plaques in AD. Score 0 described the absence of either plaques or diffuse deposits, score '+' corresponded to sparse, score '++' to moderate and score '+++' to frequent plaques or diffuse deposits.

2.9.3 Evaluation of tau pathology

The severity of NFT, NT and AN pathologies was evaluated separately in a semi-quantitative manner using a x10 objective; score 0 was used if the pathological change was absent, '+' was used if it was sparse, '++' moderate, and '+++' if the change was severe.

2.9.4 Controls for immunohistochemistry

To demonstrate the specificity of the immunohistochemistry used in the following chapters various controls were included. Firstly all primary antibodies were ommited from the protocols and replaced with PBS (pH7.4). This method was used to determine

whether secondary antibodies were binding to any antigens in the tissue. Secondly, where the primary antibody was not obtained from a commercial supplier (where it was assumed rigourous quality control checks would have been carried out) the antibody was absorbed with the immunising peptide. This approach is expected to reduce any specific staining (see section 8.2.3). Preimmune serum from the same animals used to produce the antibodies was also used as a control.

2.9.5 Methods of consistency for semi-quantiative analysis

Several methods of assessing the consistency of the immunohistochemical staining and the semi-quantitative methods were used in these studies. In every immunohistochemical experiment to be used for semi-quantitative analysis a control section (FBD material) was stained with Ab338 and evaluated for the intensity of the DAB staining. The intensity of the staining was therefore standardised for this section so that sections stained in different immunohistochemical runs could be analysed together.

Scores were assigned to the different immunohistochemical stains according to the scoring systems described in 2.9.1, 2.9.2 and 2.9.3. The scores given were obtained by a consensus agreement between 3 observers (two neuropathologists and TL), the consistency of which was further verified with repeat evaluation with a minimum of 75% of the slides stained.

In a pilot study scores were established in a manner similar to that recommended for determining Aβ plaque density by CERAD (Mirra SS *et al* 1991).

2.10 Protein extraction

2.10.1 Crude protein extraction

Approximately 1g tissue of sample, from fresh frozen tissue, was dissected from various cerebral regions. Separating white and gray matter and recording the weight of each individual sample. Any visible blood vessels were collected separately. To each sample 10mls of Tris buffer saline (20mM Tris-HCl/150 mM NaCl, pH 7.4) containing protease inhibitors (protease inhibitor cocktail tablets- Roche) was added and homogenized by hand, to limit disruption of the blood vessels. Blood vessels were collected, by filtration through a 53μm mesh, from the gray and white matter and pooled

together with larger blood vessels collected from earlier dissection of the same region. The blood vessel samples were washed in Tris buffer containing protease inhibitors and centrifuged for 10 minutes at 4^0C at 4,000 RPM (Beckman J-6B). The supernatant was discarded and the pellet homogenized with a mechanical homogeniser to disrupt all the blood vessels. Samples obtained were centrifuged for 1 hour at 35,000 RPM (112,500 x *g*) at 4^0C in a Beckman XL-100k ultracentrifuge using a 70.1 Ti rotor.

The supernatant (S1) was collected and stored at 4^0C for further analysis by immunoblotting and mass spectrometry. The pellet was homogenized in collagenase buffer (50mM Tris, 10mM $CaCl_2$, 3mM NaN_3) and subjected to collagenase digestion (0.3mg/ml Collagenase EC.3.4.24.3; Sigma) for 16 hours at 37^0C. The samples were then placed on ice for 10 minutes followed by centrifugation for 1 hour at 35,000 RPM (112,500 x *g*) at 4^0C. The supernatants (S2) were collected and stored at 4^0C for further analysis. Using a mechanical homogeniser the pellet was resuspended in 20mM Tris/ 2% SDS. The samples were centrifuged for 1 hour at 35,000 RPM (112,500 x *g*) at 10^0C. The supernatant (S3) was removed and kept at 4^0C for further analysis. The pellets were then washed with three changes of Tris buffer to remove any excess SDS before re-suspending in 500µl of 20mM Tris buffer. The samples were centrifuged at 14,000 RPM (21,000 x *g*) for 30 minutes at 4^0C in Eppendorf tubes using an Eppendorf centrifuge 5417R. The buffer was removed and discarded and 400µl of 70% FA was added to the pellets, which were left overnight at 4^0C. The samples were centrifuged at 14,000 RPM for 15 minutes, the supernatant (S6) removed and kept at 4^0C for further analysis.

To verify generation of undesired degradation products due to reagents included in the protocol, parallel experiments were carried out under similar experimental conditions were the collagenase step was omitted.

2.10.2 Protein purification from supernatants S1, S2 and S3.

Two different methods were used to purify supernatants S1, S2 and S3 for further mass spectrometry and sequence analysis: 1) reverse-phase batch purification and 2) immunoprecipitation.

2.10.3 Reverse-phase batch purification

C18 beads (25mg; Millipore) were placed in an Eppendorf tube; 90% acetonitrile (AcN) was added to the beads to wet them before centrifugation for 3 minutes at 14,000 RPM. The 90% AcN was removed and this step was repeated once. The beads were then washed in 60% AcN followed by 20% AcN / 0.1% trifluoroacetic acid (TFA), 900µl aliquots of S1 and S2 were placed into separate Eppendorf tubes, to which 100µl 1% TFA and 200µl of 20% AcN was added. The samples were then added to the Eppendorf tubes containing the C18 beads and left overnight at 4^0C to allow the proteins to attach to the beads. The samples were centrifuged at 14,000 RPM for 3 minutes to form a pellet of beads with conjugated protein. The beads were then washed 5 times with 0.1% TFA/ 5% methanol to remove any tissue debris. The bound proteins were eluted from the beads with 300µl of 0.1% TFA/ 90% AcN. The absorbance for each sample was read at 280nm to confirm the presence of protein and estimate recovery. For the S3 samples the SDS was first removed using SDS-out sodium dodecyl sulfate precipitation kit (Pierce). Briefly, to 1ml of sample we added 50µl of SDS-out reagent and placed on ice for 20 minutes. The sample was transferred to a microfilter and centrifuged at 4,000 RPM for 10 minutes. The protein was then extracted from the supernatant as described above.

2.10.4 Immunoprecipitation experiments

Fifty microliters of paramagnetic beads coated with either goat anti-rabbit IgG or anti-mouse IgG (Dynabeads M-280; Dynal) were allowed to interact for 12 hours at 4^0C inder constant end-to-end rotation with 6µg of purified IgG from either antiserum 338 or 5282 or with a combination of 3µg each of 4G8 and 6E10 for the immunoprecipitation of ABri, ADan and Aβ, respectively. After washing three times in

PBS, beads were blocked in 0.1% (w/v) bovine serum albumin in PBS. Antibody-coated beads were incubated with either 20µl (~4% of the total fraction) of FA-extracted amyloid previously neutralized in ~800 µl of 0.5 M Tris-base, pH 11, or 20% of the total volume of each PBS-soluble or SDS-extracted fractions (S1-S3). As indicated above for the case of the SDS-extracted fractions, SDS was mostly removed prior to immunoprecipitation with SDS-out SDS precipitation reagent employing the same conditions. Elution of the bound material from the beads was performed by different methods, according to the technique used for the studies that followed. For mass spectrometry analysis, beads were subsequently washed three times with PBS and three times with water, and the bound peptides were eluted in 5 µl of a 4:4:1 mixture of isopropyl alcohol/water/formic acid. For Western blot analysis, beads were suspended in 20 µl of Tris-Tricine SDS sample buffer (Bio-Rad) containing 10% (v/v) β-mercaptoethanol (Sigma) and directly applied onto the 16% Tris-Tricine gels for SDS-PAGE analysis. In some cases, 5µl of 1 M dithiothreitol (Sigma) was used for sample reduction instead of β-mercaptoethanol.

2.11 Mass spectrometry

Mass analysis of the isolated material was carried out using matrix-assisted laser desorption ionization time-of-flight MALDI-TOF mass spectrometry. Extracted peptides from PBS, SDS, and FA fractions S1, S2, S3 and S6 were subjected to direct mass spectrometry analysis using 5-10 µl of sample or subjected to further purification by immunoprecipitation, as described above. Due to the abundance of ABri, ADan and Aβ, the use of immunoprecipitation was not always necessary in FA fractions. However, for the PBS and SDS fractions, it was a required step for proper mass spectrometry identification; the combination of low peptide recovery (due to low

availability) with high dilution of the samples resulted in a concentration that, for direct assessment, was below the sensitivity of the MALDI-TOF. In some cases, particularly for the FA extracts, samples were further purified by micro-reverse-phase chromatography using Zip-TipC4 (Millipore) according to the manufacturer's protocol. Briefly, tips were first wet by aspirating and dispensing 60% AcN three times into the tip. The tip was then equilibrated by washing three times with 10µl equilibration buffer (0.1% TFA). The samples were passed through the tips by pipetting and dispensing the sample (10 µl) 10 times into the tip, allowing the attachment of the peptides to the reverse-phase. After washing 5 times with 20µl of a mixture of 0.1% TFA/ 5% methanol, retained peptides were eluted using 5µl of 90% AcN/ 0.1% TFA. MALDI-TOF mass spectrometry analysis was performed at the New York University Protein Analysis Facility. Samples were analyzed in a 10 mg/ml α-cyano-4-hydroxycinnamic acid matrix (Sigma) prepared in 50% acetonitrile and 0.1% trifluoroacetic acid (feasible for ~10,000-Da mass range) using a Micromass Tof- Spec-2E MALDI-TOF mass spectrometer in linear mode using standard instrument settings. Under these experimental acidic conditions, which also render noncovalent binding unobservable, mostly monomeric species of ABri, ADan and Aβ were detected. Internal and/or external calibration was carried out using human adrenocorticotropic hormone peptide 18–39 (average mass 2,465.68 Da) and insulin (average mass 5,733.49 Da) as standards. FindPept tool from the ExPASy Proteomics server (www.us.expasy.org/tools) was used to assign the experimental mass values to specific peptide sequences and to search for the presence of posttranslational modifications.

2.12 Western blot analysis of amyloid peptides

For western blots, samples obtained after immunoprecipitation (see section 2.10.2.2) or from the direct S1, S2, S3 and S6 extracts (10µl previously lyophilized and reconstituted in 40µl of Tricine sample buffer) were used for the experiments. Five µl of dithiothreitol (DTT), the reducing agent, was added to each sample and they were boiled for 3 minutes in a water bath. Samples, control peptides (synthetic ABri, ADan, or Aβ) and a molecular mass standard (rainbow marker, Amersham Pharmacia Biotech) were loaded onto a 16.5% Tris-Tricine acrylamide gel and electrophoresed overnight at 50V. After electrophoresis, proteins were transferred onto methanol/water pre-wet polyvinylidene difluoride (PVDF, Millipore) membranes using 3-cyclohexylamino-1-propanesulphonic acid pH 11 buffer (CAPS), containing 10% (v/v) methanol for 1 hour at 400 mA. After blocking non-specific binding sites for 1 hour at RT with 5% low-fat dried milk in PBS /0.1% Tween, membranes were incubated with the pertinent antibodies in the appropriate dilution overnight at 4^0C (Table 7). After 4 washes of 10 minutes each with PBS / 0.1% Tween, membranes were incubated in horseradish peroxidase-labeled goat anti-mouse or anti-rabbit 1:3000 (Amersham) depending on the primary used. Antibody binding was visualized using an enhanced chemiluminescence (ECL) detection kit and exposed to Hyperfilm ECL (Amersham).

Antibody	Antigen	Source	Concentration	Species
Ab338	ABri	Dr J Ghiso	1:5000	Polyclonal
Ab5282	ADan	Dr J Ghiso	1:4000	Polyclonal
4G8	Aβ 17-24	Signet	1:2000	Monoclonal
6E10	Aβ 1-17	Signet	1:2000	Monoclonal

***Table** 7: Antibodies used for western blot analysis of amyloid peptides.*

2.13 Northern blot analysis

2.13.1 Gel preparation

In a sterile conical flask 1.5g agarose, 109ml DEPC water and 15ml x10 MOPS-acetate-EDTA buffer (pH 7.0, Sigma) were mixed and boiled to dissolve the agarose. When the solution was hand hot 27ml formaldehyde was added, mixed, poured into the gel apparatus and allowed to set. Once set the apparatus was filled with gel buffer (1x MOPS-acetate-EDTA buffer pH 7.0 buffer in DEPC water) to completely submerge the gel.

2.13.2 RNA extraction for northern blot analysis

For RNA extraction approximately 1g of flash frozen tissue was weighed out and used. The RNA was extracted following a published protocol (Chomczynski & Sacchi, 1987). In brief the samples were homogenized in 4M guanidium thiocyanate, 25mM sodium citrate, pH 7, 0.5% sarcosyl and 0.1 M 2-mercaptoethanol (solution D) in 10 times the homogenate weight. Samples were homogenized using an electric homogeniser for 10 seconds at a time and cooled on ice in between homogenizing. 3.6ml aliquots of homogenate were transferred to 15ml sterilized Falcon tubes, 0.36ml sodium acetate (2M; pH4), 3.6ml of water saturated phenol and 0.72ml of chloroform: isoamyl alcohol were added mixing well before each addition. The tubes were capped and the final suspension was vigorously shaken for 10 seconds, and cooled on ice for 15 minutes. The samples were then centrifuged at 10,000g for 20 minutes (at 4°C).

The aqueous phase was carefully transferred to a sterile Eppendorf tube avoiding contamination with the DNA interface and an equal volume of isopropanol (-20°C) was added. Each tube was shaken vigorously and left at –20°C overnight. Samples were removed from the freezer, thawed and centrifuged at 10,000g for 20 minutes (4°C). The supernatant was decanted and the tube blotted to remove excess liquid. The pellet was then dissolved in 0.3ml solution D and transferred to a sterile Eppendorf tube. After adding an equal volume of isopropanol the Eppendorf tubes were then shaken vigorously, and then placed at –20°C for ≥ 1 hour. The samples were sedimented in a microcentrifuge, the supernatant removed and the pellet left to air dry. The pellet was washed in 1ml 75% ethanol (–20°C) and recentrifuged. This washing step was repeated and the pellet allowed to dry. The pellet was redissolved in 0.5% SDS at 65°C for 15 minutes with periodic mixing.

2.13.3 Spectrophotometric standardization

The RNA samples obtained from section 2.13 were diluted with DEPC water, vortexed and read absorbance at 260nm and 280nm. Blanks were 0.5% SDS treated in an identical manner to the sample. The spectrophotometer was zeroed at 280nm and the blanks read at 260nm before reading samples. The general rule was followed that the ratio A_{260}/A_{280} is an indication of the purity of the preparation and that the higher the ratio, ideally around two, the better the quality of RNA. Since RNA solutions of 40μg/ml give an A_{260} value of 1 AU, the concentrations of unknown RNA's can be calculated as shown below:

Unknown RNA concentration (μg/μl) = A_{260} x 40 x (dilution factor/1000)

2.13.4 Sample preparation and electrophoresis

The RNA samples were mixed with a sample mix (10x MOPS, formaldehyde, formamide) before being loaded onto the gel. To 48μl of sample mix, 12μl of RNA sample (diluted to give the required μg) was added. The RNA size marker (Invitrogen, section 2.14.5) was prepared by mixing 7μl with 5μl 0.5% SDS and 48μl sample mix. Samples and size markers were heated at 55°C for 15 minutes, and then placed on ice. 6μl gel loading solution (Invitrogen) was added to each sample, mixed and 40μl loaded into each well. RNA size markers and samples were loaded in adjacent wells. The gel was run at 60V until the bromophenol blue of the gel loading solution had migrated approximately 8cm.

2.13.5 Northern transfer: capillary blot

A glass Pyrex dish was filled with 1 litre of saline-sodium phosphate-EDTA buffer (SSPE, 0.2M phosphate buffer, pH7.4, 2.98M NaCL and 0.02M EDTA) and a glass platform was placed within the dish to elevate the gel above the buffer within the Pyrex dish. The platform was then covered with a wick (Whatman paper) and saturated with SSPE buffer. The surface of the wick was flattened using a clean pipette. The gel was removed from the gel apparatus and one corner cut to identify the orientation of the gel. The gel was placed onto the wick with the RNA side (bottom of the gel) facing up. The gel was surrounded with cling film to prevent short-circuiting of the blotting buffer. Hybond-N plus nylon membrane was used for the transfer and cut to the same size as

the gel. The membrane was pre-wet in SSPE buffer, then gently placed on top of the gel avoiding air bubbles. The same corner was cut as was cut on the gel. Three sheets of Whatman paper were cut to the same size as the membrane, pre-wet with SSPE buffer and placed on top of the membrane; again avoiding any air bubbles. A stack of hand towels were cut to the same size and placed on top of the filter paper, followed by a glass plate and a 0.5kg weight. The capillary transfer was allowed to proceed overnight. The towels and filter papers were removed and the membrane was exposed to UV light to allow cross linking of the RNA and then air dried for at least 1 hour.

2.13.6 RNA integrity

To 16μl of sample mix containing ethidium bromide (EtBr); 4μl of sample (diluted in 0.5% SDS to give approx. 1.5μg/μl) was added. This was then heated at 55°C for 15 minutes and placed on ice. 2μl gel loading solution was added, mixed and 20μl loaded into wells. The agarose gel (section 2.14.1) was run at 100-120 V for 0.5 - 1 hour.

2.13.7 RNA marker

A 0.24-9.5 Kb RNA ladder (Invitrogen) was used as the RNA marker, which contains a mixture of six synthetic poly (A)-tailed RNA's which gives bands at 0.24, 1.35, 2.37, 4.40, 7.46 and 9.49kb.

2.13.8 cDNA probes used for northern blot analysis

The cDNA probes used for the northern blot analyses were obtained from whole plasmids containing the BRI sequence (Dr Jorge Ghiso) and a separate plasmid containing the GAPDH sequence (Dr Drew Hope). The cDNA was amplified using the PCR method described in section 2.16.3, and ran on a gel as described in sections 2.16.4 and 2.16.5. The primers used for both the BRI and GAPDH amplifications are shown in table 8

Transcript	Sense	Antisense	bp
BriPP	CGTTCAACTCCGCTCTGGC	GCAAACTCTGGGACAGGCACAC	378
GAPDH*	ACCACAGTCCATGCCATCAC	TCCACCACCCTGTTGCTGTA	433

***Table 8**: PCR primers used in analysis of BriPP gene transcription. Primers marked with * are based on previously published data (Lee et al 2002).*

2.13.9 Labelling of cDNA probes

cDNA probes were labelled using ^{35}S and a High Prime kit (Roche). The cDNA was prepared to 25ng/μl. 1μl of the cDNA was taken and the volume was made up to 11μl using sterile water. This was then denatured by heating in boiling water for 10 minutes and chilling on ice. High Prime was mixed according to the manufacturers instructions and then 4μl was added to the denatured DNA, followed by 5μl 50μCi ^{35}S and incubated for 20 minutes at 37°C. The reaction was stopped by adding 2μl 0.2M EDTA (pH 8.0).

2.13.10 Separation of labelled probes on Sephadex G50

The labelled probe was placed on a Sephadex column to remove any unicorporated deoxyribnucleoside triphosphates. Sephadex G50 was prepared in TE pH 8.0 buffer (10mM Tris, 1.0mM EDTA). A 2ml syringe was lightly plugged with baked glass wool and then loaded with Sephadex solution to a total volume of 2ml and this was allowed to settle. The column was washed gently with 2x 1ml of TE (10mM Tris, 1.0mM EDTA pH8.0) buffer. The labelled probe in TE buffer was loaded on top of the column and the eluate collected until the drops stopped (fraction 1). The column was then washed with 2x 200μl of TE buffer and the eluate was collected separately (fractions 2 & 3). This was followed by further washing with 2 x 400μl TE buffer and samples were collected as separate fractions (fractions 4 & 5), these two fractions will contain 70% of the labelled probe. Further washes were done with 2 x 200μl TE buffer and separate fractions were collected (fractions 6 & 7). 1μl was taken from each fraction and counted using a scintillation counter to locate the labelled probe.

2.13.11 Methylene blue staining

A 1% methylene blue stock solution was made (0.5g methylene blue dissolved in 50 mls of 0.5M sodium acetate) and kept in the dark. A 0.04% working solution was made from the stock solution (0.4mls of stock solution diluted into 96 mls 0.5M sodium acetate) when needed. The membrane obtained from the northern blot capillary transfer (section 2.14.3) was soaked in 5% acetic acid solution for 15 minutes at room temperature and transferred to the working solution (0.04% methylene blue solution) for 5-10 minutes. Excess dye was rinsed out by soaking the membrane in sterile water. Sharp distinct bands should be seen corresponding to the RNA bands.

2.13.12 Hybridisation of membranes

Before hybridisation the bands that were shown with the methylene blue were marked with a pencil along with the RNA marker so they could be lined up later in the procedure. The membranes were placed in a sterile hybridisation cylinder and wet with 2x SSC by filling the cylinder. After two minutes the 2x SSC was replaced with 10mls of the pre-hybridisation solution (SSPE, Denhardts solution, formamide, SDS, DEPC water). The cylinder was placed on a rotating wheel in the hybridisation oven for 30 minutes at 42°C. The pre-hybridisation buffer was then replaced with the hybridisation buffer (5mls: pre-hybridisation buffer) containing 800µl the labelled probe and left to hybridise overnight at 42°C in the hybridisation oven.

2.13.13 Washing of membranes

The hybridization buffer was removed from the hybridization cylinder and replaced with pre-heated 2x SSC solution containing 0.1% SDS. The membranes were washed 3 x 10 minutes in this solution and 2 x 15 minutes in 0.5x SSC containing 0.1% SDS at 55°C.

2.13.14 Visualisation of RNA

The membranes were transferred to a cassette containing x-ray film and exposed for 10 days. The cassette also contained an intensifying screen (Amersham) that concentrated the signal omitted from the labelled probe. The film was then developed using an automated x-ray film processor (Kodak, Radiography department, NHNN).

2.14 In-situ hybridisation

2.14.1 Tissue samples

Flash frozen tissue was removed from the -80°C freezer and mounted onto cork pieces using OCT (BDH) in a class 1 micro-cabinet. The mounted blocks were then placed in the cryostat (Bright) at -20°C and left for several hours for the temperatures to equilibrate before cutting. Sections were cut at 15µm and placed on sterile superfrost (BDH) or Vectabonded (Vector) slides and dried on a hot plate for about 30 minutes before storing at –80°C until required. In between each tissue sample the blade was

cleaned with three changes of absolute alcohol to avoid cross contamination of mRNA between the different samples.

2.14.2 Probes

Three oligonucleotide sense probes (Invitrogen) were used corresponding to three different regions of the *BRI2* gene. Table 9 shows the region of the *BRI2* gene recognized by each probe.

Probe	Region of cBRI gene	Sequence	bp
1	28-68	CCGCTCTTGGGCTCGTCCTTCTTGGCCTCCTTCTGGGCCAG	40
2	609-648	ACCCAGGTGATCAATGTTTTCAATGCGATCAGTAATAACC	39
3	802-836	TATTAATTTTCCTCAATAATGTTTTTCTTGACTGT	34

***Table 9**: BRI2 probes used for in-situ hybridisation*

2.14.3 Labelling of probes

The above oligonucleotides were labelled using the DIG oligonucleotide 3'- end labelling kit (Roche). 100pmol of oligonucleotide were added to sterile double distilled water to a final volume of 10µl in a reaction vial. The reaction buffer, $CaCl_2$ solution and DIG ddUTP solution were added to the oligonucleotides according to manufactures directions and vortexed. 2µl of terminal transferase was added to the mix and left to incubate at 37°C for 1 hour. The oligonucleotides were placed on ice and 4µl of EDTA pH8.0 was added to stop the reaction.

2.14.4 Hybridisation.

All solutions used in the hybridisation method were sterile and all procedures were carried out at room temperature unless otherwise stated. The slides were removed from the freezer and allowed to air dry for up to 10 minutes face up on a sheet of aluminum foil. The sections were then fixed in 4% paraformaldehyde in PBS for 5 minutes. Slides were washed twice in PBS for 2 minutes per wash and then washed in sterile saline for 1 minute to remove any phosphates deposited by the PBS. Sections were then dehydrated by immersion in 60%, 80% and 95% EtOH in DEPC treated water for 2

minutes each, then removed from the alcohol and allowed to air dry for a minimum of 30 minutes. The hybridisation buffer was allowed to warm to room temperature before the probe was added. Sections were incubated with the DIG-labelled probe diluted in hybridization buffer (Sigma) to a concentration of 200fmol/µl, with 0.1mg/ml salmon sperm (Invitrogen) added. 50µl of diluted probe was added to each slide and covered with parafilm to prevent the slides drying out. They were then hybridised overnight at 37°C, in a humidified chamber.

2.14.5 Post-hybridisation washes

A water bath was heated to 55°C and 4-5 liters of 1x SSC in distilled water was prepared. All solutions for post hybridisation steps could be made up in non-sterile water. Four glass troughs were placed into the water bath, filled with 1 litre of 1x SSC and warmed to 55°C. Three glass containers were prepared for floating off the parafilm. All three were filled with 1x SSC solution; the first was used for floating the parafilm carefully off the glass slide and to remove the majority of the hybridisation buffer followed by two quick rinses in the other two glass troughs. Once all the slides have had the parafilm removed the rack of slides was placed in the first 55°C wash for 15 minutes. This procedure was repeated 3 x 15 minutes at 55°C, followed by two more washes in 1x SSC at room temperature for 30 minutes and in distilled water, to remove the remaining salts.

2.14.6 Immunohistochemistry to visualize the probes

Once washed the sections were ready to visualize. First blocking was carried out in 10% non-fat milk / PBS for 30 minutes at room temperature, followed by an overnight incubation with the primary anti-DIG antibody (Roche 1:250) at 4°C overnight, followed by several changes of PBS. The sections were then incubated in biotinylated anti-mouse antibody (Dako 1:200) for 30 minutes at room temperature followed by a 30-minute incubation in ABC. The sections were washed several times in PBS. Finally visualization was carried out using the G.O.D method described in section 2.15.7.

2.14.7 Glucose oxidase nickel DAB method

Sections were washed in 0.1M PBS for 30 minutes, rinsed in 0.1M acetate buffer (pH 6.0) and incubated in the reaction solution as follows:

- O.1M acetate buffer pH6
- 0.05% DAB
- 0.04% ammonium chloride
- 2.5% nickel ammonium sulphate
- 0.25% β-D-glucose
- 0.001% Glucose Oxidase

Sections were incubated in the reaction solution for around 15 minutes and placed in PBS to stop the reaction. Sections could be returned to the reaction solution and left for a longer period if a darker precipitation product was required.

2.14.8 0.1% Nuclear fast red counter stain

5g aluminum sulphate was dissolved in 100ml H_2O and 0.1g nuclear fast red (BDH) was added. Sections were immersed in a filtered solution for 1 minute then washed in running water, dehydrated in graded alcohol solutions, cleared and mounted.

2.14.9 Controls used for in-situ hybridisation

To verify that the sense probes used in the in-situ hybridisation experiments several control experiments were undertaken. Anti-sense probes were labelled and used in the same manner as the sense probes described in section 2.14.3. Excess unlabelled probe was added to the DIG labelled sense probe (1:100 dilution) which competed with the labelled probe and significantly reduced the amount of positive staining observed. Control experiments were also carried out for all the steps of the immunohistochemical method used to visualise the probe. For that the anti-DIG and biotinylated secondary antibodies were replaced with PBS in consecutive experiments. All control experiments carried out provided negative or significantly diminished positive staining.

2.15 Western blot analysis of BriPP and furin

2.15.1 Sample preparation from tissue

Approximately 1g of tissue was weighed and homogenised in 10mls PBS/ Complete (Protease inhibitor, Roche), and kept on ice. The samples were aliquoted into 1ml Eppendorf tubes and centrifuged at 14,000rpm for 5mins. Excess samples were stored at –80°C until required.

2.15.2 Gel electrophoresis

To 13µl of the supernatant from the sample obtained in section 2.15.1, 5µl of 4x NuPAGE LDS sample buffer (Invitrogen) was added along with 2µl of NuPAGE reducing agent (0.5M DTT, Invitrogen). The samples were vortexed and heated to 70°C for 10mins. The samples were then loaded onto NuPAGE Bis-Tris pre-cast gels (Invitrogen) and the manufacturers instructions followed. In brief, the 20µl of sample were loaded into the wells of the gel and the gel was run at a constant 200V for approximately 35mins. To allow for maximum separation at the lower molecular weight end MES running buffer (Invitrogen) was used. A SeaBlue marker (Invitrogen) was used with every gel run.

2.15.3 Gel transfer

The sponge pads, and pre-cut filter paper (cut to the same size as the gel) were pre-soaked in NuPAGE transfer buffer (Invitrogen) containing methanol according to manufacturers instructions. A PVDF membrane was cut to the gel size and pre-wet in methanol for 30 seconds before being transferred to the NuPAGE transfer buffer. Once the gel had run for 35mins, it was removed from the pre-cast mould and placed between

the sponge pads, filter paper and membrane according to the manufactures instructions. The transfer then took place at 30V for 2 hours.

2.15.4 Development of blots

The membranes were removed from the transfer chamber and rinsed twice in PBS, followed by incubation in 10% non-fat milk for 1 hour at room temperature. Incubation with the relevant primary antibody (Table 42 section 8.2.2) took place overnight at 4°C, taking care that the membranes did not dry out. The membranes were then washed for 1 hour in 5 changes of PBS-Tween (0.1%), followed by incubation with the relevant HRP-conjugated secondary antibody (Invitrogen, 1:1000) for 1 hour at room temperature. The membranes were again washed in PBS-Tween (0.1%) for 1 hour before the antibody binding was visualized using enhanced chemiluminescence (ECL) detection kit and exposed to Hyperfilm ECL (Amersham).

2.16 Polymerase chain reaction (PCR)

2.16.1 Reverse transcription of RNA

Production of single stranded cDNA from RNA template was achieved using Avian Myeloblastosis Virus (AMV) reverse transcriptase (RT). The RNA pellets were dissolved in 10µl of a solution containing 1mM dNTPs and 50µg/ml Oligo dT primers, and incubated at 65^{0}C followed by at least 1 min at 4^{0}C, allowing the primers to anneal to the poly-A tails of mRNA in the samples. This was followed by the addition of 4µl 5x AMV RT buffer (Promega), 4µl 25mM magnesium chloride and 40 units RNasin (Promega) and the mixture was heated to 42^{0}C. Finally 10 units AMV RT (Promega) were added, and the incubation continued at 42^{0}C for 50 mins. The reaction was stopped by incubating at 70^{0}C for 15 minutes. The cDNA was then treated with 10 units RNase H (Sigma-Aldrich) for 30 mins at 37^{0}C to remove the RNA template, and then the reaction was inhibited by 70^{0}C incubation for a further 10 min. cDNA preparations were stored at -20^{0}C and used as templates for PCR reactions.

2.16.2 RT-PCR

Single stranded cDNA templates were prepared by reverse transcription as described in section 2.16.1. Primers were designed for specific amplification of cDNA fragments from genes of interest, with glyceraldehyde-3-phosphate dehydrogenase (GAPDH) being used as a house keeping gene control. The samples were prepared for RT-PCR by mixing with various other components as described in table 9.

Product	Source	Quantity
Sample	-	1µl
10x PCR buffer	Promega	5µl
25mM MgCl2	Promega	1.5µl
Sense primer	Invitrogen	1µl
Anti-sense primer	Invitrogen	1µl
10mM dNTP mix	Promega	1µl
Taq DNA polymerase	Promega	0.4µl
Q solution	Invitrogen	3µl

Table 9: Quantities used for RT-PCR reaction.

As templates were of low concentration the PCR method was modified to enhance their amplification by using 'touch-down' annealing temperatures. After an initial 5 min at 95^{0}C, cycling with 30s at the annealing temperature, 30s at 72^{0}C and 30s at 95^{0}C was performed. The annealing temperature for the first cycle was 60^{0}C and was reduced by 0.5^{0}C in each subsequent cycle until reaching 50^{0}C at the twentieth cycle. Subsequent cycles utilised 50^{0}C as the annealing temperature. The PCR products were separated by 1% agarose gel electrophoresis (section 2.16.5) and densitometrically analysed using Kodak 1D software (Labtech International).

2.16.3 Gel preparation for RT-PCR

In a sterile conical flask 1g agarose and 100ml TAE buffer (40mM Tris-HCL pH8.0, 20mM acetic acid, 1mM ethylenediamine tetracetic acid (EDTA) were mixed and boiled to dissolve the agarose. When the solution was hand hot 1µl of ethidium bromide was added, mixed, poured into the gel apparatus and allowed to set. Once set the apparatus was filled with 1x TAE buffer to completely submerge the gel.

2.16.4 Primers used for RT-PCR

The primers used for the RT-PCR reactions for *BRI2* and GAPDH are shown in table 10.

Transcript	Sense	Antisense	bp
BriPP	CGTTCAACTCCGCTCTGGC	GCAAACTCTGGGACAGGCACAC	378
GAPDH*	ACCACAGTCCATGCCATCAC	TCCACCACCCTGTTGCTGTA	433

*Table 10: PCR primers used in analysis of BriPP gene transcription. Primers marked with * are based on previously published data (Lee et al 2002).*

Chapter 3

Regional distribution of ABri amyloid and preamyloid deposition and its relationship with neurofibrillary degeneration in FBD.

Chapter 3 – Hypothesis and specific questions

In this chapter, I wished to investigate the hypothesis that deposition of the ABri amyloid peptide is closely related to the neurodegenerative process in FBD. The specific questions I wished to concentrate on were: 1) What is the distribution of ABri fibrillar and nonfibrillar lesions in FBD; 2) What is their relationship to neurofibrillary pathology, astroglial and microglial responses?

To address these questions in this study of FBD cases the topographical distribution and patterns of ABri deposition were studied by immunohistochemistry. To determine the conformational state of the protein deposits ABri immunohistochemistry was combined with thioflavine-S and evaluated by confocal microscopy. The distribution and relationship of neurofibrillary degeneration to ABri deposits were investigated with tau immunohistochemistry alone and in combination with Ab338. The astrocytic and microglial responses to ABri deposits were studied by a double immunohistochemical approach. The ultrastructural characteristics of the ABri protein deposits were studied by immunoelectron microscopy.

3.1 Introduction

The neuropathological hallmarks of FBD include extensive CAA, cerebellar degeneration and parenchymal amyloid plaques as described in section 1.2. The unique mutation involved in FBD has led to the generation of a specific antibody (Ab338) produced using a synthetic peptide comprising the last ten residues of the ABri sequence (Vidal *et al.*, 2000b). Ab338 is therefore able to recognise both conformational states of the ABri peptide, amyloid and preamyloid. Pathological analysis carried out prior to the identification of ABri only gave a limited insight into the distribution of the ABri lesions (Griffiths *et al.*, 1982; Plant *et al.*, 1990; Worster *et al.*, 1940). Previous pathological anaylsis using Bielschowsky silver impregnation showed the majority of the hippocampal plaques to be non-neuritic, but the presence of smaller amyloid plaques associated with abnormal neurites was also noted (Revesz *et al.*, 1999). Therefore using the ABri specific antibody the topographical distribution of the ABri lesions within the CNS could now be asscessed.

One of the central issues of AD research is to establish a possible relationship between Aβ deposition and formation of NFTs. Neurodegeneration in AD with the formation of

NFTs, NTs and ANs is generally considered to be secondary to Aβ deposition, which has been shown to produce a toxic environment (Selkoe, 1994). A close anatomical relationship between hippocampal amyloid plaques and cytoskeletal changes has been noted in FBD, suggesting that mechanisms documented in AD may also be present in this condition. However, with the anti-ABri antibody available it would now be possible to study the relationship between ABri and tau deposition in depth.

The importance of activated microglia in AD, which produce pro-inflammatory cytokines, reactive oxygen species and other potentially toxic substances has been reported (Dickson, 1997; Dickson *et al.*, 1993). Evidence in rodents indicates that microglia can be activated by neuronal degeneration, suggesting that microglial activation may be secondary to neurodegeneration. This indicates that microglial activation in AD may be secondary to neurodegeneration and, once activated, microglia may participate in a local inflammatory cascade promoting tissue damage and contribute to amyloid formation. Prominent astrocytic response has been shown to be associated with amyloid deposits in FBD (Revesz *et al.*, 1999). A close relationship between microglia and astrocytes has been shown within AD, suggesting that astrocyte derived growth factors may promote microglial growth (Lee *et al.*, 1994). In addition, astrocytes are the source of other important substances contributing to neuronal damage including ApoE and ApoJ (Boyles *et al.*, 1985).

The purpose of this study was to investigate the distribution of ABri using Ab338 immunohistochemical techniques and gain a detailed pathological analysis. The conformational state of ABri lesions, as to whether amyloid or pre-amyloid were present, was also assessed with double anti-ABri immunohistochemistry and thioflavine-S fluorescent staining to examine the correlation between the lesion type and the conformation of the protein present.

The distribution of NFTs, NTs and ANs was investigated immunohistochemically with anti-tau antibody AT8. Double immunohistochemistry was also carried out to establish their distribution in relation to different ABri lesions, using Ab338 and AT8.

To establish the extent of glial response to ABri lesions glial fibrillary acidic protein (GFAP) and microglial response using CD68 and CR3/43. Double immunohistochemistry was also carried out using the glial cell markers with Ab338 to determine the presence of the glial cells within ABri deposits, followed by staining with thioflavine-S to investigate the glial response with the conformational state of ABri.

3.2 Material and Methods

3.2.1 Tissue

Brain and spinal cord from five cases of FBD, five sporadic AD cases and three age-matched controls were used for these studies. The pathological diagnosis of AD was made using standard criteria (Mirra *et al.*, 1991). FBD cases 1-3 were from the original pedigree (Worster *et al.*, 1940) (we thank Professor Margeret Esiri for providing material from case 3), case 4 from a second pedigree with identical clinical and pathological features (Mead *et al.*, 2000a) and case 5 is from a recently identified third family with typical clinical presentation and mutation of the *BRI* gene in affected members (Table 10) (Mead *et al.*, 2000a).

Case	Age	Sex	Cause of death	Diagnosis
1	56	F	Not recorded	FBD
2	65	F	Bronchopneumonia	FBD
3	N/A	N/A	N/A	FBD
4	60	M	Cardiac failure	FBD
5	68	F	Bronchopneumonia	FBD
6	69	F	Acute tracheobronchitis	AD
7	92	F	Pneumonia	AD
8	88	M	Bronchopneumonia	AD
9	89	F	AD	AD
10	85	F	Acute tracheobronchitis	AD
11	56	M	Cardiac failure	Control
12	33	M	Acute bronchopneumonia	Control
13	75	F	Head injury	Control

***Table 10**: Cases used in FBD pathology study*

For immunoelectron microscopy (iEM) selected tissue samples from the hippocampal formation (cases 1 and 5) and temporal neocortex (case 5) were fixed in 3% buffered gluteraldehyde.

3.2.2 Antibodies and immunohistochemistry

The antibodies used for this study are listed in table 11. Immunohistochemical analysis was carried out at the light microscopy level using the standard protocol (section 2.2). To determine the relationship between protein deposition and amyloid formation sections were double stained with Ab338 and thioflavine-S, as described in section 2.6.2 or double stained with Ab338 and Congo red as described in section 2.5. Tissue sections from the hippocampal formation, amygdala, and cerebellum including the dentate nucleus, cerebral cortex and white matter were used for double staining with Ab338 and either GFAP or CD68 (section 2.7.2). iEM was carried out using Ab338 to establish whether ABri was of fibrillar or non-fibrillar nature in the different structures (section 2.8).

Antibody	Source	Species	Pretreatment	Dilution
338	Dr J Ghiso	Polyclonal	Formic acid	1:2000
338 Abs	Dr J Ghiso	Polyclonal	Formic acid	1:2000
338 PI	Dr J Ghiso	Polyclonal	Formic acid	1:2000
AT8	Autogen Bioclear	Monoclonal	Microwave	1:600
GFAP	Dako	Polyclonal	Tyrpsin	1:1000
CD68	Dako	Monoclonal	Trypsin	1:200

Table 11: *Antibodies used for the pathological study of FBD. Abs: Antibody preabsorbed with synthetic peptide used for immunisation, PI: Pre-immune.*

3.2.3 Evaluation of Ab338 and AT8 immunohistochemistry

3.2.3.1 Semi-quantitation of CAA

The presence and frequency of Ab338 positive plaques and CAA were evaluated in different anatomical regions using a semi-quantitative approach (section 2.9.1).

3.2.3.2 Semi-quantitation of parenchymal deposits

The presence of Ab338 positive parenchymal plaques were defined as Ab338-, Congo red-, and thioflavine-S positive structures with or without an associated blood vessel, whereas diffuse deposits were often ill-defined, Ab338 positive, Congo red- negative structures, which were only weakly stained, if at all, with thioflavine-S. The method of quantitation was followed as described in section 2.9.2.

3.2.3.3 Semi-quantitation of tau pathology

The severity of NFT, NT and AN pathologies were evaluated separately in a semi-quantitative manner as described in section 2.9.3.

3.3 Results

3.3.1 Distribution of ABri in parenchymal amyloid lesions

Amyloid plaques, defined as Congo red and thioflavine-S positive structures, were seen in many of the CNS areas. Importantly Ab338 stained all plaques types described by previous studies using silver impregnation techniques (Griffiths *et al.*, 1982; Plant *et al.*, 1990; Revesz *et al.*, 1999). Such plaque types included the large and small plaques of the hippocampal formation (figure 3.1A - C) and also the parenchymal amyloid plaques in the cerebellum (figure 3.1E) and dentate nucleus (figure 3.1F). In the majority of the hippocampal and cerebellar amyloid plaques there was a very good overlap between Ab338 and thioflavine-S double staining (figure 3.2A-F). Ab338 immunohistochemistry, Congo red and thioflavine-S methods combined with semi-quantitative evaluation, showed little variation between cases; therefore they will all be described together (tables 12 - 14). The hippocampus and cerebellum were the most

severely affected regions by amyloid plaques, but considerable numbers of amyloid plaques were present in structures such as the hypothalamus, amygdala, locus coeruleus, inferior olive and the cerebellar dentate nucleus. Between the hippocampus and third temporal gyrus Ab338 positive deposits affected all allocortical areas and also the isocortical fusiform gyrus. An anatomically determined sharp transition between two staining patterns was noted at the junction between the subiculum and presubiculum. The subiculum contained a significant number of Ab338, Congo red, and thioflavine-S positive amyloid plaques. In many cerebral and cerebellar areas and also in the spinal cord Ab338 stained subpial deposits, which were variably positive on Congo red or thioflavine-S preparations. Clearly defined fibrillar staining was also seen associated with the basolateral aspect of the ependyma (not shown).

3.3.2 Distribution of Ab338 parenchymal pre-amyloid structures

Examples were found where Ab338 positivity was observed without corresponding thioflavine-S or Congo red staining, suggesting that the protein conformational state was pre-amyloid (non-fibrillar) (figure 3.2G-I, arrow). This was also seen in the cerebellum, particularly in the granular cell layer of the cerebellar cortex, where Ab338 often stained structures more extensively and/or intensely than thioflavine-S and Congo red did. This staining pattern was also apparent in a proportion of the perivascular protein deposits (figure 3.2J-L, arrow). Diffuse deposits were also noted in varying numbers in other areas such as the entorhinal cortex, tectum, periaqueductal gray, the medullary pyramids, spinal cord gray and white matter and neocortex where they appeared randomly distributed throughout the cortical laminae. In the cerebral cortices loosely arranged diffuse deposits were also seen to surround neurons, often with an accentuation of staining adjacent to the perikaryon.

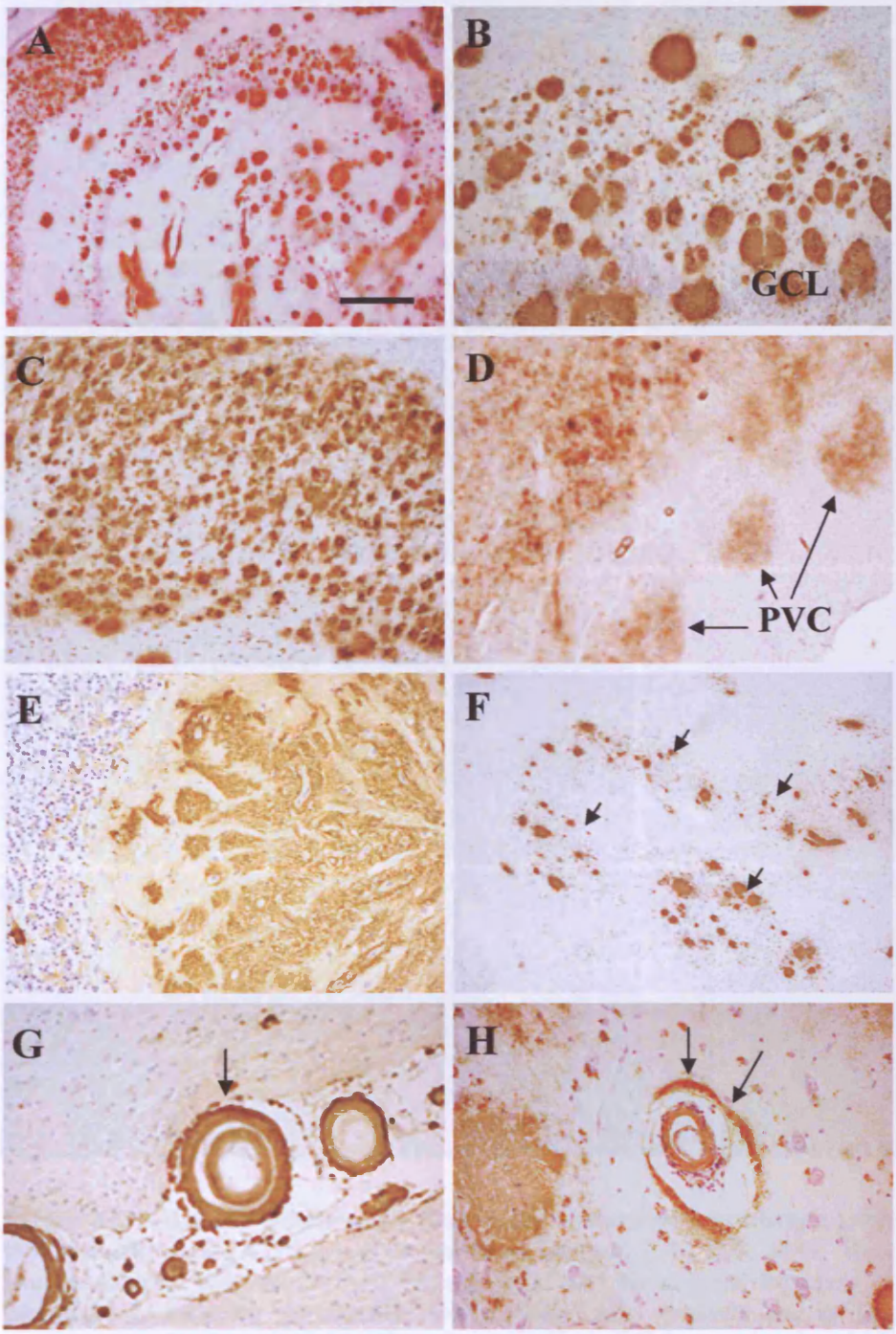

Figure 3.1: Distribution of ABri in FBD shown by Ab338 immunohistochemistry. A: There are numerous structures outlining the anatomical regions of the hippocampus. **B:** Large plaques are mainly found in the CA4 and granular cell layer (GCL). **C:** Small plaques are characteristic in CA1. **D:** Diffuse deposits are present in the parvopyramidal cell clusters (PVC) of the pre- and parasubiculum. **E:** The cerebellar cortex is severely affected by ABri plaques often forming confluent deposits **F:** ABri plaques outline the cerebellar dentate nucleus (arrows) **G:** Vessels are affected by ABri deposition throughout the CNS often showing degenerative changes such as double barrelling (arrow). **H:** Perivascular parenchymal ABri deposits were frequently found (arrows). Bar in panel A represents 1000μm in A, 500μm in E, 250μm in panels B,C and D and 100μm in F,G and H.

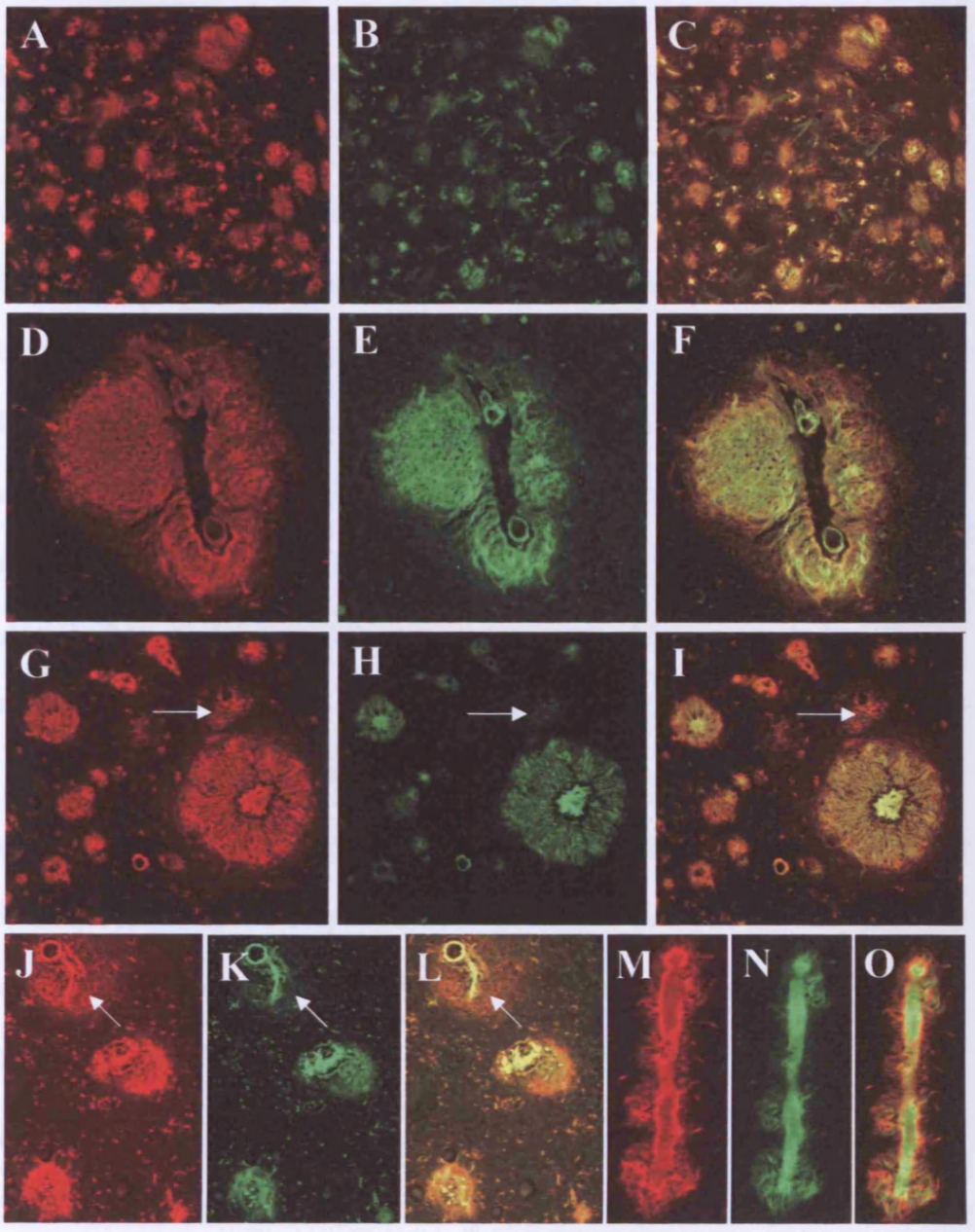

Figure 3.2: ABri and thioflavine-S fluorescent immunohistochemistry (ABri:red; thioflavine-S: green; C,F,I,L and O combined images): A-C, D-F, M-O: The good overlap of ABri with thioflavine-S (A and B, M and N) suggests that most of the parenchymal, including perivascular and vascular ABri deposits are in amyloid conformation (fibrillar). **G-I; J-L:** However, parenchymal (G-I, arrow) and perivascular (J-L: arrow) preamyloid (non-fibrillar) deposits are also present. Original magnifications A-C x 10 and D-O x 20.

This phenomenon was found at several other locations, including in the pyramidal and granular cell layers of the hippocampus, around Purkinje-cells, anterior horn cells of the cord, and neurons of the inferior olive.

A delicate membranenous staining pattern highlighting neuronal cell margins was noted most readily in hippocampal pyramidal cells. In the CA1 region and subiculum a number of less compact NFTs, not associated with visible neuronal nucleus or plasma membrane (extracellular tangles) were stained with Ab338 and a few such structures seemed to have been incorporated into amyloid plaques. The presubiculum and the parasubiculum had an ill-defined diffuse staining pattern. The size and shape of the Ab338 positivity closely matched the anatomical boundaries of the pre and para subicular parvopyramidal cell islands. In the entorhinal cortex the deposits were predominantly of the diffuse type with a striking bilaminar distribution. There was an inner wide band, occupying the deeper cortical laminae, with an ill-defined, confluent staining pattern and a narrower outer band composed of often better circumscribed deposits. The outer Ab338 positive band closely overlapped with the Pre-α neuronal clusters and with the Pre-α neurons themselves gradually descended in the transentorhinal cortex to form a single band of well-defined Ab338 positive, mainly diffuse deposits in the deeper laminae of the fusiform gyrus.

Ab338 also stained subependymal areas around the ventricles and cerebral aqueduct in a diffuse pattern. The cerebral, cerebellar, and spinal cord white matter showed mostly diffuse deposits although perivascular amyloid plaques were also noted.

3.3.3 Regions unaffected by ABri deposition

The striatum, globus pallidus, substania nigra and pontine raphe, which also lacked CAA, were entirely unaffected by parenchymal deposits whereas the degree (none to mild) of thalamic involvement varied between cases. Other areas including the optic chiasm, pontine base and sacral cord lacked any parenchymal deposits but were affected by CAA (tables 12 - 14).

3.3.4 Control immunohistochemistry

No staining of vascular amyloid, plaques or diffuse deposits of the FBD cases was observed in controls using the pre-immune serum, the Ab338 pre-absorbed with synthetic peptide or when the primary antibody was omitted. Immunohistochemical staining with Ab338 of brain tissues from individuals with AD or normal controls were also negative.

3.3.5 Distribution of ABri staining of CNS blood vessels.

All affected blood vessels stained with Congo red and thioflavine-S were also Ab338 positive (figure 3.2M-O). Furthermore on preparations double stained with Ab338 and thioflavine-S there was generally a good overlap between the different staining patterns, although a smaller proportion of affected blood vessels, especially those with perivascular plaques were more extensively stained with Ab338 (figure 3.1H). Many of the leptomeningeal and parenchymal small arteries (figure 3.1G), arterioles and capillaries were stained throughout the CNS, although the severity of CAA varied considerably in the different areas; the striatum, globus pallidus, and substantia nigra were entirely unaffected, in the thalamus and pontine base CAA was of moderate severity, whereas in other areas such as the hippocampus and cerebellar cortex it was

severe. In the cerebellum there was a difference in the staining pattern of the blood vessels of the deep white matter in that, with the exception of those found in the vicinity of the dentate nucleus, they were more rarely stained with Ab338 than those of the white matter in the cerebellar folia.

The majority of the Ab338 positive blood vessels were arterial, but a proportion of venous channels were also affected. These latter was more frequent in the leptomeninges, but were also found in the parenchyma. Although small arteries with a diameter of up to 1mm were stained with the Ab338, the majority of the affected blood vessels were smaller than 300μm. The larger vessels were usually less affected in that Ab338 primarily stained the abluminal aspect of the media and the adventitia. In contrast, in many of the small arteries and arterioles Ab338 positivity was seen throughout the full thickness of the wall, often with severe disruption of its normal structure and sometimes occlusion of the lumen. An accentuation of the staining in the outer perimeter of some small arteries and arterioles was noted.

Longitudinal sections of affected arterioles and capillaries showed that Ab338 often stained blood vessels walls in a linear manner although the full length was not always affected. Other staining patterns included the presence of globular deposits along blood vessel walls or fine Ab338 positive spicules radiating from the walls of affected arterioles and capillaries. In all regions the glia limitans around many affected blood vessels was stained with an extension into the adjacent parenchyma, often giving rise to plaques like structures previously described as perivascular plaques.

	TYPE OF LESION					
	Plaques, including perivascular	**Diffuse deposits**	**CAA**	**NFT**	**AN**	**NT**
Olfactory bulb	++	+++	++	+	+	+
Retina	+	+	++	0	0	0
Optic nerve	+	++	++	N/A	0	0
Optic chiasm	0	0	+	N/A	0	0
Optic tract	+	+	+	N/A	0	0
Hippocampus	+++	+++	+++	+++	+++	+++
Amygdala basal	+++	+++	+++	+++	+++	+++
Amygdala lateral	+	+++	++	+	+	++
Uncus	++	+++	++	++	++	+++
Entorhinal cortex	+	+++	++	+++	+	+++
Fusiform gyrus	+	+++	++	+++	0	+++
1^{st}, 2^{nd}, 3^{rd} temporal gyri	+	+	++	+	0	+
Frontal cortex	0 - +	+	++	0	0	0
Cingulum	+	+	++	+	0	+
Insular cortex	+	++	++	+	+	++
Parietal cortex	+	+	++	0	0	0
Occipital cortex	0	+	++	0	0	0
Cerebral white matter	+	++	++-+++	N/A	0	0
Hypothalamus	++	++	++	0	0	0
Striatum	0	0	0	0	0	0
Globus pallidus	0	0	0	0	0	0
Claustrum	+	++	++	+	0	+
Meynert nucleus	0	+	+	++	0	+
Thalamus	0-+	0-+	+	0	0	0
Subthalamus	+	+	++	0	0	0

Table 12: *Distribution of the different ABri lesion types and tau pathology in FBD. CAA- cerebral amyloid angiopathy; NFT- neurofibrillary tangle; AN- abnormal neurite; NT- neuropil thread; N/A – not applicable*

	TYPE OF LESION					
	Plaques, including perivascular	**Diffuse deposits**	**CAA**	**NFT**	**AN**	**NT**
Tectum	0	++	++	+	0	0
Periaqueductal gray	+	++	+	+	0	+
Midbrain raphe	0	+	+	+	0	+
Substantia nigra	0	0	0	+	0	+
Red nucleus	++	++	+++	0	0	0
Cerebral peduncle	+	++	++	N/A	0	0
Locus coeruleus	+++	+++	+++	+	0	0
Pontine raphe	0	0	0	++	0	++
Pontine base	0	0	+	0	0	0
Inferior olive	+-++	+-++	++	0	0	0
Pyramid	0	+-++	++	N/A	0	0
Cerebellar cortex	+++	++	+++	0	0	0
Cerebellar white m.	0-+	0	++	N/A	0	0
Dentate nucleus	+++	+	+++	0	0	0

***Table 13**: Distribution of the different ABri lesion types and tau pathology in FBD.*

CAA - cerebral amyloid angiopathy; NFT - neurofibrillary tangle; AN - abnormal neurite; NT - neuropil thread LC - lateral column; PC - posterior column; VC - ventral column; GM - gray matter.

	TYPE OF LESION					
	Plaques, including perivascular	**Diffuse deposits**	**CAA**	**NFT**	**AN**	**NT**
Cervical cord LC	0-+	+++	++	N/A	0	0
Cervical cord PC	0-+	+-++	++	N/A	0	0
Cervical cord VC	0-+	0-++	+-++	N/A	0	0
Cervical cord GM	+	+-++	++	0	0	0
Thoracic LC	+	+++	++	N/A	0	0
Thoracic PC	+	+	+	N/A	0	0
Thoracic VC	0	0-+	+	N/A	0	0
Thoracic GM	0	0-+	+	0	0	0
Lumbar LC	0	0	+	N/A	0	0
Lumbar PC	+	0-+	0-+	N/A	0	0
Lumbar VC	0	0-+	+	N/A	0	0
Lumbar GM	0-+	++	++-+++	0	0	0
Sacral LC	0	0	+	N/A	0	0
Sacral PC	0	0	++	N/A	0	0
Sacral VC	0	0	+	N/A	0	0
Sacral GM	0-+	++	++	0	0	0

***Table 14**: Distribution of the different ABri lesion types and tau pathology in FBD spinal cord.*

CAA - cerebral amyloid angiopathy; NFT - neurofibrillary tangle; AN - abnormal neurite; NT - neuropil thread; LC - lateral column; PC - posterior column; VC - ventral column; GM - gray matter

3.3.6 Distribution of ABri within the retina

There was substantial vascular amyloid in many retinal blood vessels and, similar to the subpial deposits, there were small amyloid plaques and diffuse deposits along the retinal limiting membrane. No gross decrease in cell numbers could be discerned in any of the retinal layers and the photoreceptor outer segments and retinal-pigmented epithelial cells appeared identical to age matched control. There was an increase in GFAP expression in Muller's glial cells.

3.3.7 Tau pathology in relation to ABri deposition

Severe involvement by NFTs and NTs of mediotemporal and other limbic structures, including the hippocampus, subiculum, entorhinal and transenthorhinal cortices, amygala, uncus, cingulum and insular cortex was readily noted using AT8 immunohistochemistry (figure 3.3A and 3.3B). Double AT8 and Ab338 immunohistochemistry also revealed that the amyloid plaques, occurring in these anatomical areas, tended to be surrounded with ANs, many of which were fine and thread like and were often incorporated within the large hippocampal amyloid plaques in a radial pattern. ANs clustering around an occasional blood vessel with amyloid deposition were also seen in the hippocampus, amygdala and temporal neocortex. There was a strikingly similar distribution of AT8 positive structures and Ab338 positive amyloid plaques within the amygdala in that both pathologies affected the basal nucleus more severely than the lateral nucleus. Occasional NFTs and NTs were seen in the parvopyramidal clusters of the pre and parasubiculum. In the entorhinal cortex, which was rich in non-fibrillar ABri and contained only relatively few amyloid plaques, the Pre-α and Pri-α neurons were severely affected containing frequent NFTs and NTs, which because of their large numbers, produced darkly stained bands in both cell layers.

The Pre-β and Pre-γ neurons also contained moderate numbers of NFTs. In the six-layered fusiform gyrus, there were numerous NFTs and NTs. These gradually decreased in number toward the neighbouring third temporal gyrus, which, similar to the first and second temporal gyri contained only sparse NFTs and NTs. Other neocortices, except the cingulum and insular cortex, were unaffected. The hypothalamus, claustrum, midbrain tectum, periaqueductal gray and locus coeruleus contained sparse and the pontine raphe moderate numbers of NFTs. The cerebellum and spinal cord were unaffected by tau pathology (table 12 - 14).

3.3.8 Correlation between Ab338, CD68 and GFAP staining and lesion types

A prominent microglial reaction was demonstrated with CD68 immunohistochemistry in different brain regions. Microglial cells were also stained with the CR3/43 antibody suggesting that microglia were activated (figure 3.3C). Such cells localized around amyloid laden (Ab338 positive) blood vessels and amyloid plaques, which were also permeated by microglial processes. A similar picture was seen with GFAP immunohistochemistry showing severe gliosis in all regions affected by amyloid lesions (figure 3.3D). Sections stained with CD68 and counterstained with Congo red (figure 3.3E and 3.3F) proved the close association of microglia with the amyloid structures. Tissue sections double stained with Ab338 and CD68 and examined by confocal microscopy showed a good co-localization between cells of microglial/macrophage lineage and both amyloid plaques (figure 3.4A and 3.4B) and vascular amyloid. However such cells were few in areas in which diffuse deposits were predominant. A similar relationship between GFAP positive astrocytes and Ab338 positive structures was seen on preparations double labelled with Ab338 and GFAP (figure 3.4C and 3.4D).

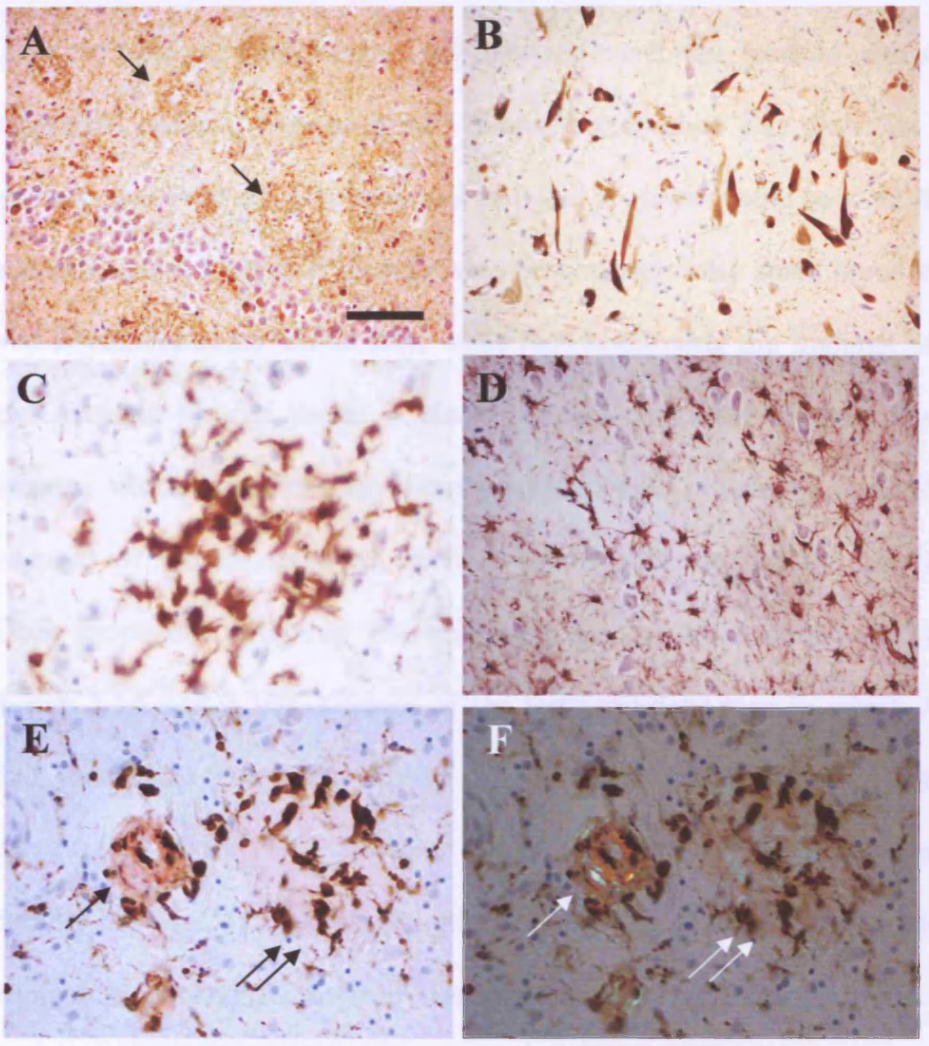

Figure 3.3: Tau, GFAP, CD68 and CR3-43 immunohistochemistry in FBD. A & B: AT8 immunohistochemistry showing numerous NFTs, NTs and ANs in the hippocampus (arrows pointing to large plaques permeated by abnormal neurites). **C:** CR3/43 immunohistochemistry demonstrating reactive microglia response associated with ABri deposits. **D:** Extensive astrocytic reaction in the hippocmapus affected by severe ABri deposition. **E & F (viewed in polarized light)** CD68 immunhistochemistry and Congo red staining shows clustering of microglia around amyloid parenchymal deposits (double arrow) and an amyloid-laden vessel (arrow). Extensive GFAP immunohistochemistry in the hippocampus. Bar in panel A represents 100μm in A, B and D, 45μm on panels E and F, 28μm on panel C.

3.3.9 Immunoelectron Microscopy

Ultrathin sections from the hippocampus and temporal neocortex, labelled with Ab338 using immunogold method, were examined. Tissue preservation was such that blood vessels, neurons, astrocytes and both neuronal and glial processes could be identified. In the hippocampus frequent amyloid plaques were present and many small blood vessels had amyloid fibrils deposited within their walls thus confirming the findings of light microscopy. Amyloid plaques varied in size and were composed of short fibrils of ~10nm diameter, which were randomly distributed but varied in density, some plaques being composed of loosely arranged fibrils were consistently heavily labelled by Ab338. Glial processes containing intermediate filaments were often seen within plaques (figure 3.5A and 3.5B). Regions of the temporal neocortex in which Ab338 positive, but thioflavine-S negative diffuse deposits had been identified in semithin sections were selected for iEM. In these areas amyloid plaques were identified ultrastructurally; however, extracellular immunogold labelling was seen to be associated with amorphous electrondense material that was sometimes accompanied by small numbers of loosely arranged fibrils resembling the amyloid fibrils of plaques (figure 3.5C). Such electron dense material was not found in association with hippocampal amyloid plaques.

Small blood vessels showed labelling of the basal lamina by Ab338. Several blood vessels had normal segments of basal lamina adjacent to areas in which a low level of labelling was present in its central part. The basal lamina then often became expanded into regions with a greater labelling density, in which amyloid fibrils became apparent. In some blood vessels the intensity of labelling was greatest on the abluminal aspect of the basal lamina reflecting the accentuation of Ab338 staining seen around the outer perimeter of some blood vessels using light microscopy.

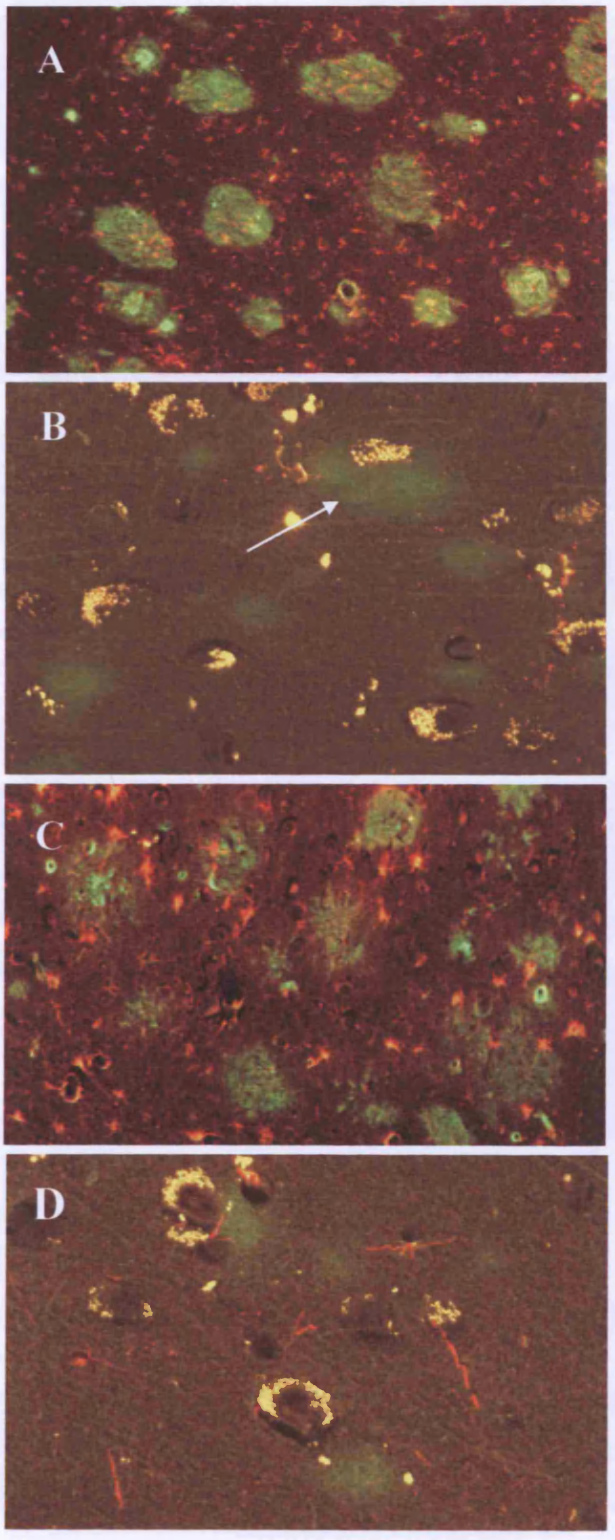

Figure 3.4: Microglial and astrocytic response in FBD. Confocal images A & B; Ab338 (green) and CD68 (red) double immunohistochemistry showing a marked microglial response around hippocampal amyloid plaques **(A),** but a sparse reaction in the entorhinal cortex where the protein deposits are predominantly non-fibrillar **(B). C & D;** Ab338 (green) and GFAP (red) double immunohistochemistry showing a similar pattern of astrocytic reaction in the same areas. Original magnifications x10 (A and C), x40 (B and D).

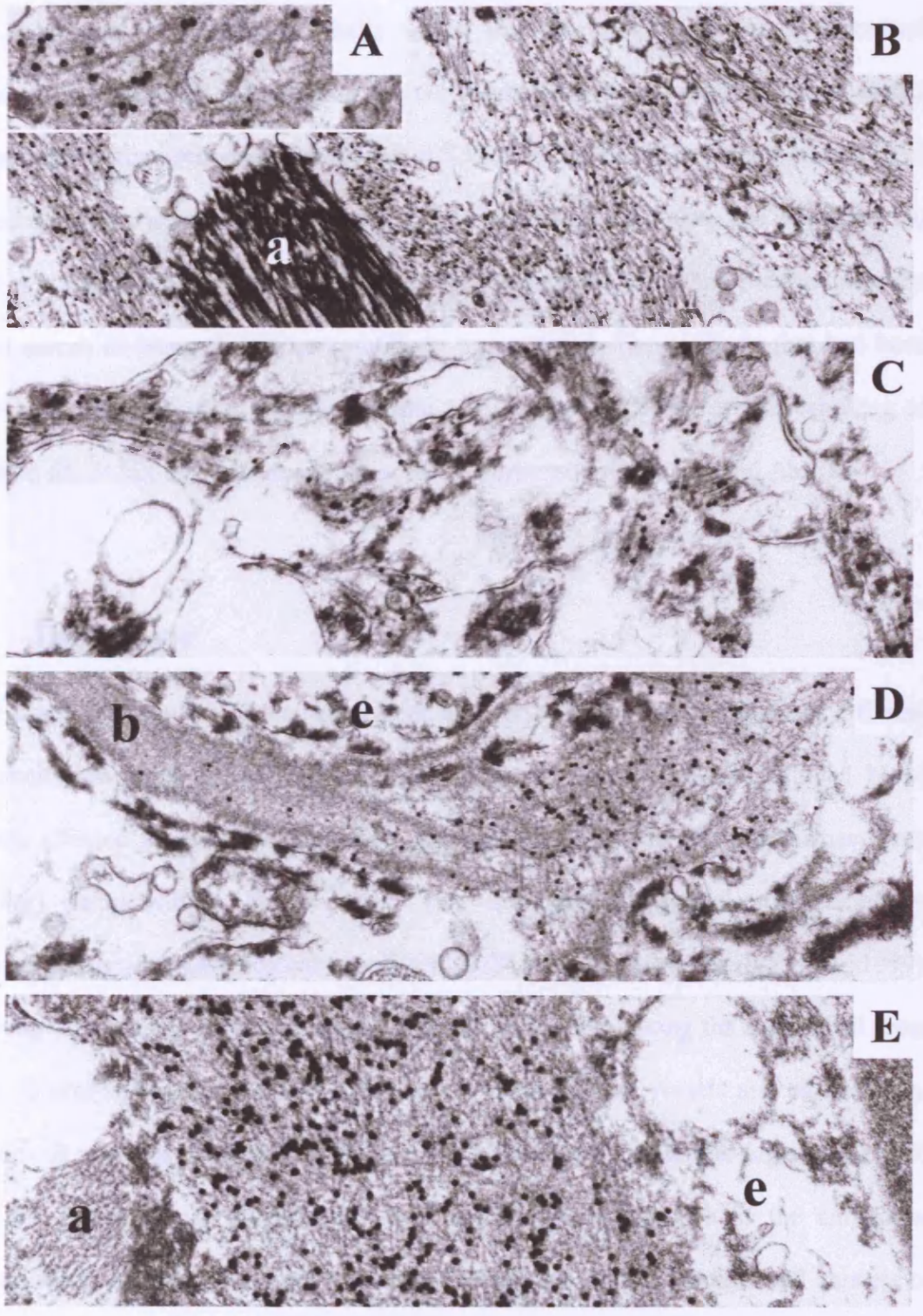

Figure 3.5: Ab338 immunoelectron microscopy. B: Bundles of labelled fibrils in a hippocampal plaque. An astrocyte process (a) is unlabelled. **Insert A** showing labelled fibrils with high magnification. **C:** Amorphous electron-dense material together with sparse fibrils is decorated with Ab338 in a thioflavine-S negative area of temporal neocortex. **D:** Small vessel showing labelling of the basal lamina (b), which is focally disrupted by amyloid fibrils. **E:** A vessel showing extensive deposition of labelled fibrils in the basal lamina. **D** and **E:** Endothelial cells (e) are unlabeled. Original magnifications: x16,000 (**A**); x6,600 (**B**); x10,000 (**C**); x8,300 (**D**); and x13,000 (**E**).

The accumulation of amyloid fibrils within the basal lamina produced increased expansion and eventual disruption of the abluminal surface whereas the luminal aspect of the basal lamina remained intact (figure 3.5D and 3.5E). NFTs composed of paired helical filaments were frequently found in both neuronal cell bodies and processes but these were unlabelled by Ab338. No labelling was found using the preimmunization rabbit serum or when the primary antibody was omitted. The antibody that had been previously absorbed using the immunizing peptide showed some residual labelling of amyloid fibrils but this was greatly reduced in comparison with untreated Ab338.

3.4 Discussion

Of 5 cases of FBD Ab338 stained a large number of pathological lesions of different morphological types throughout the CNS. The pathological lesions included blood vessels affected by amyloid deposition, amyloid (fibrillar) plaques and diffuse (non-fibrillar) parenchymal ABri deposits. This immunohistochemical study confirms findings of previous pathological examinations (Plant *et al.*, 1990; Revesz *et al.*, 1999), showing that in FBD the hippocampus and cerebellum are among the anatomical areas most severely affected by amyloid deposition in both blood vessels and parenchymal plaques. It was also possible to show that ABri is widely deposited throughout the CNS and that it deposits in anatomically well defined structures such as the amygdala, hypothalamic nuclei, inferior olive, dentate nucleus and parvopyramidal cell clusters of the pre- and parasubiculum. Using the same antibody (Ab338) for iEM examination we confirmed that bundles of amyloid fibrils in both plaques and blood vessel walls were also strongly labelled. In areas with diffuse parenchymal deposits, non-fluorescent with thioflavine-S, Ab338 decorated amorphous, electron dense extracellular material, which was interspersed with sparse fibrils, but not with bundles of fibrils. As such tinctorial,

optical and ultrastructural appearances are thought to represent protein deposits in a nonfibrillar configuration, or pre-amyloid, the presence of such lesions demonstrates that ABri deposits in both fibrillar and nonfibrillar forms throughout the CNS in FBD.

With the use of the AT8 antibody, which recognises phosphorylated serine 202/threonine 205 epitopes of tau (Su *et al.*, 1994) it was possible to show that there is a rich network of fine thread-like processes permeating the large amyloid plaques and also that tau positive dystrophic neurites are also present in relation to the ABri amyloid plaques.

When the conformational state of ABri was taken into account it was established that while NFTs and NTs occurred in association with both amyloid plaques and diffuse deposits, ANs only occurred in association with amyloid lesions, mostly around plaques but occasionally in relation to amyloid-laden blood vessels. A number of NFTs with appearances of extracellular tangles were stained with Ab338 in the hippocampus and subiculum, which are among the structures with the highest parenchymal ABri load. It has been shown that in AD Aβ deposition within extracellular tangles, taking place in the vicinity of senile plaques, is a secondary phenomenon (Yamaguchi *et al.*, 1991a; Schwab *et al.*, 1998) and it is likely that a similar mechanism is found in FBD.

The predominantly limbic distribution of the tau pathology together with mild involvement of the temporal cortex would suggest that the NFT pathology corresponds to stage IV in the system recommended by Braak and Braak for staging NFT pathology in AD (Braak & Braak, 1991). However, in FBD the severity of the limbic involvement exceeds that expected in stage IV of AD and the presence of NFTs in structures such as the granular cell layer of the dentate fascia and substania nigra suggests that in FBD the progression of NFT pathology may be different from that seen in AD. Although the mechanism of NFT formation in FBD remains to be investigated, the close topographic

association of both fibrillar and nonfibrillar ABri with neurofibrillary pathology in limbic structures may support the notion that NFTs are present because of ABri mediated neurotoxicity and not because of conformational differences. This hypothesis is supported by our finding of colocalization of reactive astrocytes and microglial with ABri in β-sheet conformation, which is strikingly similar to the findings in AD, in which a relationship between the presence of these cell types and the neurodegenerative events have been suggested (el Hachimi *et al.*, 1991; Pike *et al.*, 1995; Selkoe, 1999). Despite the close association between neurofibrillary pathology and ABri deposition in limbic structures, the absence of apparent neurodegeneration in some other well defined protein bearing regions such as the dentate nucleus and inferior olive, points to the importance of other biological variables in this process.

Ab338 positive congophilic angiopathy of variable severity was widespread and was only absent in the striatum, globus pallidus and substantia nigra. In FBD the overall patterns of amyloid deposition in cerebral blood vessels are similar to those seen in congophilic angiopathies related to other amyloid peptides, in particular Aβ, in which arteries and arterioles are more frequently affected than veins.

FBD with CAA, parenchymal amyloid plaques, and diffuse deposits as well as neurofibrillary degeneration mimics important morphological features of AD, although there are distinct features in both diseases. Limbic structures are severely affected by both parenchymal amyloid deposition and neurofibrillary degeneration in both conditions, although in AD neocortical involvement is much more prominent than in FBD. The cytoskeletal pathology in FBD, immunohistochemically, ultrastructurally and biochemically, is indistinguishable from that found in AD. The morphology of limbic plaques shows some similarities with AD as the large plaques of FBD noticeably resemble the cotton wool plaques seen in variant AD with spastic paraparesis associated

with PS1Δ9 or PS1 exon 4 DelIIM mutations. However, there are differences between the two lesions as the cotton wool plaques are mainly Congo-red negative, whereas the large hippocampal plaques of FBD are Congo red and thioflavine-S positive. CAA resulting in white matter degeneration is not a unique feature of FBD as this can be associated with a similar pathological picture in AD.

It is also possible that the immunoreactivity detected by Ab338 does not solely represent the presence of ABri because the specific epitope (TVKKNIIEEN) is shared by ABri, its precursor ABriPP and potential truncated fragments generated by the proteolytic processing of either species. The heterogeneity of the ABri peptide within the different lesion types has not previously been studied. Since antibodies to differentiate N- and C-terminally truncated ABri species are not yet available we used a biochemical approach to differentiate ABri species as described in chapter 7.

These morphological studies have also provided observations that may be relevant to the understanding of the origin of the amyloid peptide ABri. Further investigations into the orgin of ABri were carried out in Chapter 8.

Therefore the study of FBD, including future development of different transgenic animal models, may result in a better understanding of the link between amyloid deposition and neurodegeneration.

Chapter 4

Regional distribution of ADan and Aβ deposition and its association with neurofibrillary degeneration in FDD

Chapter 4 – Hypothesis and specific questions

In this chapter, I hypothesised that, similar to ABri in FBD, the deposition of the ADan peptide is closely related to the neurodegenerative process in FDD. The specific questions I wished to concentrate on included: 1) What is the distribution and conformational patterns of ADan deposition in FDD?; 2) Is there a relationship between ADan deposition and neurofibrillary pathology, astroglial and microglial responses?

To answer these questions the topographical distribution of ADan deposition was studied in FDD cases using immunohistochemistry. To determine the conformational state of the protein deposits, ADan immunohistochemistry was combined with thioflavine-S and evaluated by confocal microscopy. The distribution and relationship of neurofibrillary degeneration to ADan deposits were investigated by tau immunohistochemistry. The astrocytic and microglial responses to ADan deposits were studied by a double immunohistochemical approach. The ultrastructural characteristics of the ADan deposits were analysed by immunoelectron microscopy.

4.1 Introduction

FDD, previously described as heredopathia ophthalmo-oto-encephalica by Strömgren et al (1970, 1981), is a rare, dominantly inherited neurodegenerative disease. The original description of the disease, as described in section 1.3, provided only scanty neuropathological data based on the examination of a single case. Suggesting the presence of a uniform, diffuse atrophy of the brain, thin and demyelinated cranial nerves, as well as 'histological involvement' including a vasculopathy of the cerebellum, cerebral cortex and white matter (Stromgren, 1981).

Like FBD it has been shown to be associated with a mutation in the *BRI2* gene; however FDD is associated with a decamer duplication occurring between codons 265 and 266 (Vidal *et al.*, 2000b), resulting in a frameshift abolishing the normal stop codon and the production of a 277 amino acid long precursor protein (ADanPP), from which a 34 amino acid peptide (ADan) is cleaved by a furin-like proteolysis from the C-terminus. The amyloidogenic subunit ADan has been shown to be deposited in leptomeningeal and cerebral blood vessels and also as the major component of parenchymal lesions. The hippocampal deposits found within FDD are mainly Congo red negative suggesting that the protein deposited is predominantly in a nonfibrillary

structure. As well as the deposition of ADan within FDD, Aβ co-depositing has also been found mainly in a perivascular postion (Vidal *et al.*, 2000b).

Because FDD combines severe vascular amyloid, perivascular and parenchymal plaques, as well as NFT formation, the study of the disease may provide useful information leading to the understanding of the relationship between cerebrovascular amyloidogenesis and neurodegeneration. After the identification of ADan the production of a specific antibody (Ab5282) raised to C-terminal amino acids of the ADan protein (CFNLFNSQEKHY) was produced (Vidal *et al.*, 2000b).

With this anti-ADan antibody available, it would now be possible to study the distribution of ADan and the correlation between protein deposition and the conformational state of the protein.

Tau immunoreactive structures were found to be numerous within the hippocampus where ANs mostly around amyloid affected blood vessels, NFTs and NTs were seen in large numbers (Vidal *et al.*, 2000b). A study of their correlation to the ADan peptide could also be undertaken.

The purpose of this study was to investigate the distribution and patterns of ADan deposition using immunohistochemistry with the antibody Ab5282. Using antibody Ab5282 the visualisation of both conformational states of ADan, amyloid and pre-amyloid, could be undertaken using immunohistochemistry in combination with thioflavine-S or Congo red. The distribution and relationship of NFTs, NTs and ANs to ADan deposits was investigated using the AT8 antibody.

The astrocytic response to ADan deposits was studied using GFAP immunohistochemistry and the microglial response was addressed using CD68 and CR3/43 antibodies. Ultrastructural characteristics of amyloid and diffuse deposits as well as NFTs were studied by EM and iEM.

4.2 Material and Methods

4.2.1 Tissue

Brain and spinal cord samples from 3 cases of FDD, 5 sporadic AD cases, diagnosed by using standard criteria (Mirra *et al.*, 1991), and 3 normal control cases were collected at post mortem (table 15). For routine stains and immunohistochemistry tissue samples were fixed in 10% formalin in PBS. For EM, selected tissue samples from the hippocampal formation from case 1 were fixed in 3% buffered glutaraldehyde after fixation in 10% formalin.

Case	Age	Sex	Cause of Death	Diagnosis
1	43	M	Bronchopneumonia	FDD
2	60	F	Bronchopneumonia	FDD
3	58	M	Not recorded	FDD
4	69	F	Acute tracheobronchitis	AD
5	92	F	Pneumonia	AD
6	88	M	Bronchopneumonia	AD
7	89	F	AD	AD
8	85	F	Acute tracheobronchitis	AD
9	56	M	Cardiac failure	Control
10	33	M	Acute bronchopneumonia	Control
11	75	F	Head injury	Control

***Table 15**: Cases used in FDD pathological study*

4.2.2 Antibodies

The antibodies used for this study are listed in table 16. Immunohistochemical analysis was carried out at the light microscopy level using standard protocols (section 2.2). To determine the conformational state of the protein deposits sections were double stained with Ab5282 and thioflavine-S as described in section 2.6.2 and with Ab5282 and Congo red as described in section 2.5.1. Tissue sections from the hippocampal formation, amygdala, and cerebellum including the dentate nucleus, cerebral cortex and

white matter were used for double staining with Ab338 and either GFAP or CD68 (section 2.7.2).

Antibody	Source	Species	Pretreatment	Dilution
5282	Dr J Ghiso	Polyclonal	Formic acid	1:2000
5282 Abs	Dr J Ghiso	Polyclonal	Formic acid	1:2000
5282 PI	Dr J Ghiso	Polyclonal	Formic acid	1:2000
AT8	Autogen Bioclear	Monoclonal	Microwave	1:600
GFAP	Dako	Polyclonal	Tyrpsin	1:1000
CD68	Dako	Monoclonal	Trypsin	1:200
CR3/43	Dako	Monoclonal	Pressure cook	1:200

***Table 16**: Antibodies used for pathological study of FDDAbs: Antibody preabsorbed with synthetic peptide used for immunisation, PI: Pre-immune*

4.2.3 Immunnoelectron microscopy

Ultrathin sections were prepared from case 1 as described in section 2.8.1. The sections were then immunostained as described in section 2.8.3 and viewed under a JOEL 1200EX electron microscope.

4.2.4 Semi-quantitation of CAA

The presence and frequency of Ab5282 positive plaques and CAA were evaluated in different anatomical regions using a semi-quantitative approach as used for the evaluation in FBD (section 2.9.1).

4.2.5 Semi-quantitation of parenchymal deposits

For the quantitation of Ab5282 positive parenchymal deposits amyloid plaques were defined as Ab5282-, Congo red-, and thioflavine-S positive structures with or without an associated blood vessel, whereas diffuse deposits were often ill-defined, Ab5282 positive, but Congo red negative structures, which were only weakly stained, if at all, with thioflavine-S. The semi-quantitative approach was used as described in section 2.9.2 for FBD.

4.2.6 Semi-quantitation of tau pathology

The severity of NFT, NT and AN pathologies was evaluated separately in a semi-quantitative manner as described in section 2.9.3.

4.3 Results

4.3.1 Macroscopic description

The brain weights of cases 1 and 2 were 1,438g and 1,220g respectively; the weight of case 3 was not recorded. The leptomeninges were thick and opaque and the degree of atheroma in the blood vessels at the base of the brain varied from absent in case 3, mild in case 1 to severe in case 2. On slicing, the lateral ventricles were found to dilated and there was thinning of the cortical ribbon and reduction in the white matter bulk. In addition, case 1 showed focal perivascular gray translucent areas in the white matter. The hippocampi were reduced in bulk. The brainstem and cerebellum were atrophic and the cranial nerve roots of case 3 were noted to be thin. The spinal cord was examined in cases 1 and 2 and found to narrowed in the antero-posterior dimension and on slicing showed yellow discolouration. The spinal nerve roots were thin and firm.

4.3.2 Histological examination

All cases showed similar features and, although the severity of the disease varied, will be described together. The histological examination revealed widespread vascular pathology affecting small arteries, arterioles and capillaries in the parenchyma and leptomeninges throughout the CNS. The blood vessels affected had thickened, eosinophilic walls with fine spicules of eosinophilic material radiating into the parenchyma surrounding the blood vessels. This finding was common in the hippocampal CA1 region, subiculum and the cerebellar cortex where the lumina of

capillaries were often occluded. Congo red staining with apple green birefringence in polarized light and thioflavine-S positivity confirmed that ADan was in an amyloid conformational state (figure 4.1C-J). This congophilic material was also present in the parenchyma but the majority was associated with affected blood vessels (figure 4.1C-F) and perivascular plaques (figure 4.1G and 4.1H). These were found to be most common in the CA1 region of the hippocampus as well as the subiculum, entorhinal cortex and neocortex. Whereas they were relatively uncommon in the cerebellar cortex despite the amount of vascular pathology seen in this region.

In addition to vascular pathology, the CA1 sub-region of the hippocampus and the subiculum showed marked abnormalities with neuronal loss, NFTs and extracellular ghost tangles. Silver staining revealed the presence of NFTs and fine NTs predominantly in limbic structures (figure 4.1A and 4.1B). Bulbous ANs were found around amyloid bearing blood vessels most frequently in the CA1 sub-region of the hippocampus and the subiculum, but neuritic plaques were not a feature. Extracellular NFTs (ghost tangles) were confirmed in the hippocampal CA1 region and subiculum.

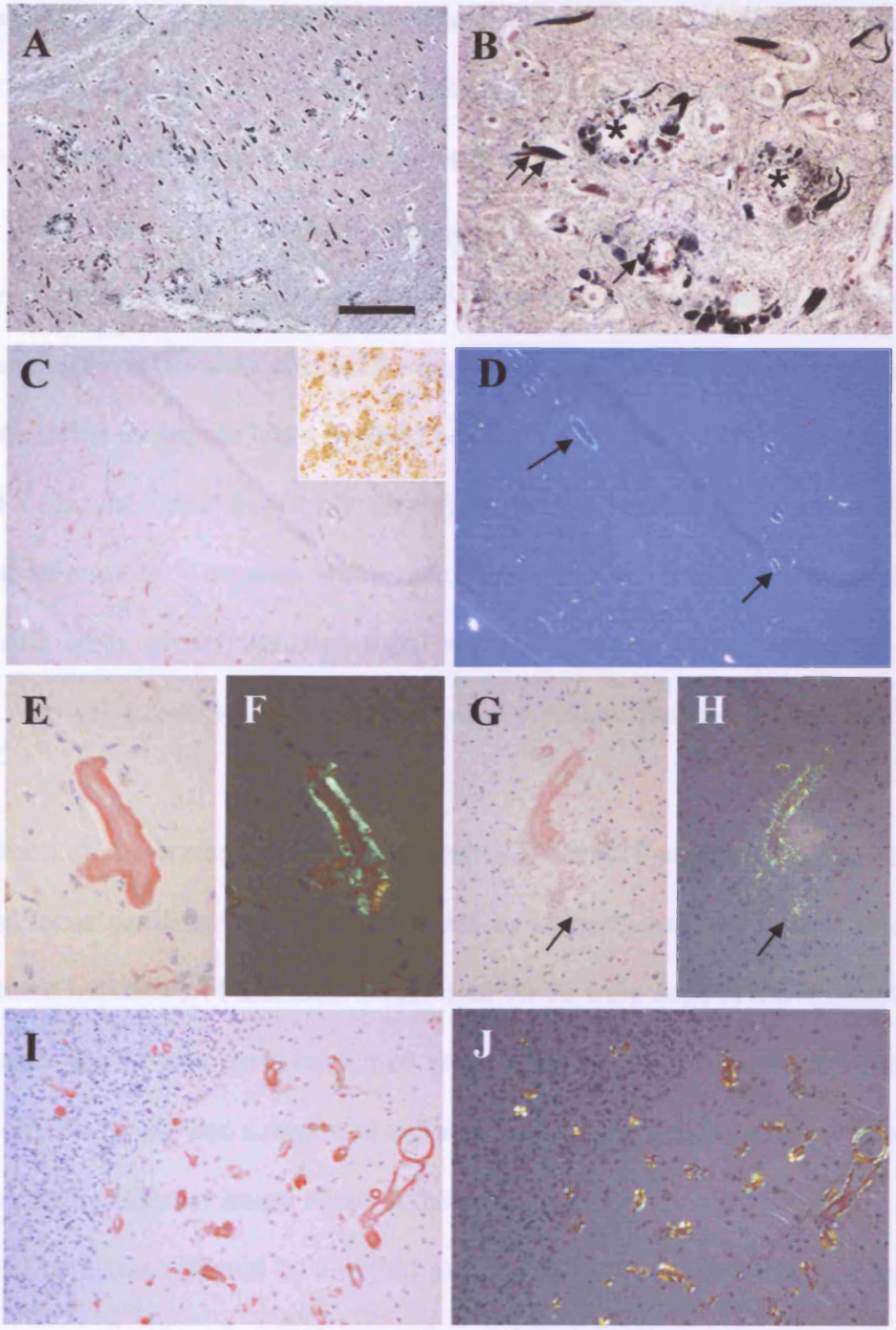

Figure 4.1: Pathological findings in FDD. A: Numerous NFTs shown on the Bielschowsky's silver stain in the CA1 subregion of the hippocampus. No argyrophilic plaques are present. **B:** Abnormal neurites (arrows) cluster around amyloid-laden blood vessels (asterisks). **C & D:** Congo red staining of the hippocampal formation showing amyloid deposition within the blood vessels (arrows) but on Congo red reactivity observed corresponding to the severe ADan parenchymal deposition (C, inset). **E & F:** Hippocampal blood vessel with amyloid deposition. **G & H:** Some vessels are surrounded by loose perivascular amyloid deposits. **I & J:** Congo red positivity mainly restricted to blood vessels in the cerebellum. Bar in panel A represents 500μm in A; 1000 μm in C and D; 250μm in B; 100μm in G,H,I and J represents 100μm and 45μm in E and F.

The neocortex showed no spongiosis and only mild neuronal loss. The hemispheric and deep cerebellar white matter was rarified with patchy myelin pallor and axonal loss with occasional axonal retraction balls, and the perivascular spaces were frequently enlarged. Several small areas of infarction of varying age were found in the hemispheric white matter in addition to other regions such as the deep gray nuclei, cerebellum and pons.

The cerebellum was severely affected by amyloid angiopathy and was atrophic with loss of volume in the molecular layer, granule cell depletion, and marked loss of basket and Purkinje cells, the latter frequently displaying axonal torpedoes. Bergman glia were increased in number. The deep white matter showed similar changes to those of the hemispheric white matter, although folial white matter was less affected. The dentate nucleus was well preserved although mild neurofibrillary pathology was found in one case.

Examination of the brainstem showed widespread amyloid angiopathy. The substantia nigra and locus ceruleus were well populated by neurons with only small amounts of free pigment indicative of cell loss. Occasional NFTs were seen in the substantia nigra in one case. The pontine base contained small areas of old infarction in 2 cases. The inferior olive in case 2 had a region of cell loss and gliosis, which was most likely to be secondary to the vascular lesion noted in the pons.

The spinal cord was affected by amyloid angiopathy in all areas throughout its length. Silver impregnation demonstrated circumferential peripheral axonal loss. Anterior horn cells were well preserved and the nerve roots available for examination showed no significant pathology.

4.3.3 Ab5282 immunohistochemistry, Congo red and thioflavine-S staining of blood vessels.

All three cases showed widespread vascular pathology. Many small arteries, arterioles and capillaries in the leptomeninges (figure 4.2G, inset), gray and white matter throughout the CNS had thickened, eosinophilic walls frequently with fine spicules of eosinophilic material radiating into the parenchyma surrounding capillaries. Small arteries with a diameter of up to 1mm were labelled by Ab5282 (figure 4.2I), although the majority of the blood vessels were smaller than 300 μm. Some of the small arteries and arterioles showed an accentuation of Ab5282 labelling in the outer perimeter, while in severely affected blood vessels Ab5282 was seen throughout the full thickness of the blood vessel wall (figure 4.2G, inset). The glia limitans and the perivascular parenchyma around some of the affected blood vessels were also labelled with Ab5282 (figure 4.2I).

Preparations double stained with Ab5282 and thioflavine-S and examined by confocal microscopy confirmed a close overlap between ADan and amyloid deposits within blood vessels (figure 4.3D-F). The severity of CAA varied considerably between anatomical areas and was entirely absent only in the globus pallidus in all three cases (tables 17 and 18). CAA was mild in the striatum, nucleus basalis of Meynert and substantia nigra and was moderate in structures such as the amygdala, entorhinal cortex, different neocortical areas, thalamus, subthalamus, red nucleus, pontine base, spinal cord, and both cerebral and cerebellar white matter. Severe CAA was observed in the hippocampus, cerebellar cortex and the retina.

4.3.4 ADan immunohistochemistry, Congo red and thioflavine-S staining of parenchymal lesions.

Semi-quantitative analysis showed that the hypothalamus, midbrain tectum and periaqueductal gray, locus ceruleus, retina and the hippocampal formation were severely affected by parenchymal ADan deposits (figure 4.2A-C), other limbic structures such as amygdala and anterior thalamus, and cerebellum (figure 4.2G and 4.2H). Other regions were less severely affected and there was no involvement of the optic nerve, cingulate gyrus, globus pallidus, nucleus basalis of Meynert, thalamus, subthalamic nucleus, substantia nigra, red nucleus and gray matter of the lumbar and sacral cord (tables 17 and 18). Congo red and thioflavine-S staining of adjacent sections demonstrated that the majority of the parenchymal lesions were negative or weakly positive and therefore largely represent protein deposition in the non-fibrillar or pre-amyloid form, for which the term of diffuse deposits was used in this study (figure 4.1C and 4.1D). This finding was confirmed by studies using double labelling with Ab5282 and thioflavine-S and confocal microscopy (figure 4.3A-C). Diffuse deposits were morphologically of 2 types: compact deposits of varying size that showed some similarity with the cotton wool plaques of variant AD with spastic paraparesis (Crook *et al.*, 1998c; Houlden *et al.*, 2000b) (figure 4.2E), and ill-defined, cloudy or loose deposits which often had a peri-neuronal disposition (figure 4.2A and 4.2B). Both types of diffuse deposits were frequent in the hippocampal formation where ghost tangles sometimes labelled with Ab5282 were found. In the parasubilculum, the parvopyramidal cell clusters were occupied by Ab5282 positive, ill-defined diffuse lesions.

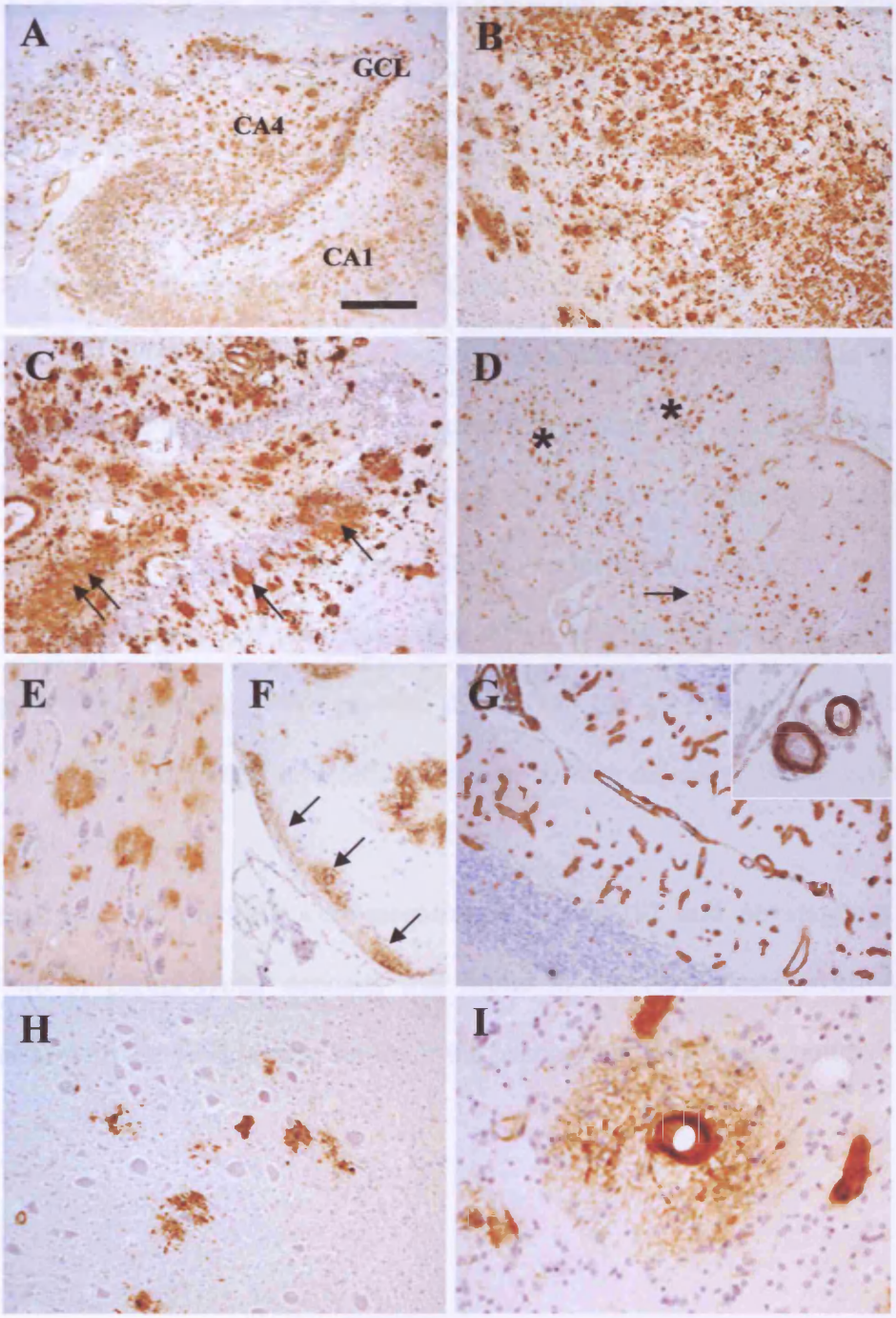

Figure 4.2: Distribution of ADan in FDD shown by Ab5282 immunohistochemistry. A: Plaque-like and ill defined parenchymal deposits outlining the anatomical regions of the hippocampus. **B:** Ill-defined deposits in the CA1 subregion. **C:** Parenchymal deposits near to the GCL are better defined (arrow), while the deposits in the CA4 are large and confluent (double arrow). **D:** The staining pattern is bilaminar in the entorhinal cortex (asterisk) and the two bands become united towards the transentorhinal cortex (arrow). **E:** Well-defined plaques are found in the subiculum. **F:** Subpial deposition of ADan (arrow) is also found in the frontal cortex. **G:** Severe CAA found in the cerebellum, inset showing leptomingeal vessels. **H:** Diffuse ADan plaques in the cerebellar dentate nucleus. **I:** A large perivascular deposit found in the frontal cortex. Bar in panel A represents 1000μm in A and D; 500 μm on C and G; 250μm on B, F and H; 100μm on E; 45μm on I and G (inset).

In the entorhinal cortex, ADan was most commonly found as compact diffuse deposits and formed a bilaminar pattern with relative sparing of the middle cortical laminae, in a manner similar to that seen in FBD (figure 4.2D). Neocortical deposits were mostly of the diffuse type and were only mild to moderate in severity. The cerebellar cortex also contained mild to moderate, loose, diffuse deposits of ADan predominantly in the granular cell layer, and there were similar deposits occasionally found in the molecular layer and white matter. Subpial deposition of ADan was also characteristic in the cerebellum. In one case (case 3) compact diffuse ADan deposits were found in the dentate nucleus (figure 4.2H). The midbrain tectum, periaqueductal gray matter and IVth nerve nucleus were variably, but often severely affected by diffuse peptide deposits, although there were no such deposits in the substania nigra. In the pons the locus ceruleus contained moderate to severe diffuse deposits. While elsewhere these were only mild.

Normal and AD controls were negative with Ab5282 and no staining of vascular amyloid or parenchymal deposits was found in the FDD cases when Ab5282 was replaced with the pre-immune serum or the primary antibody was ommitted.

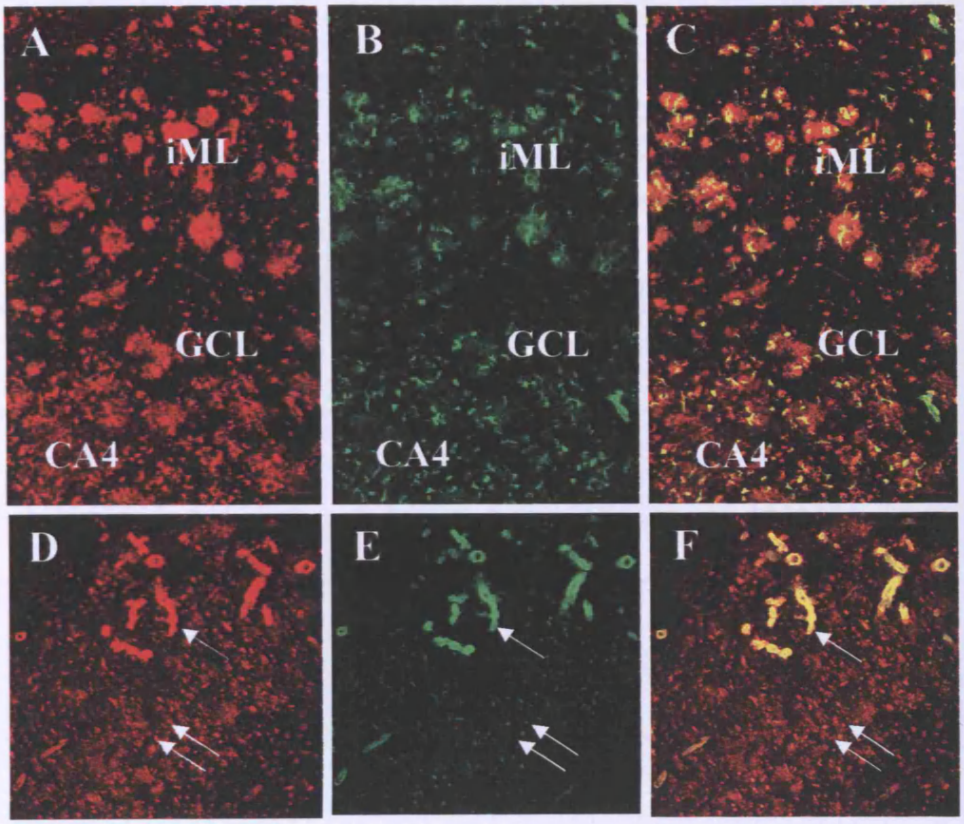

Figure 4.3: ADan and thioflavine-S double labelling for confocal microscopy (ADan: red (A & D), thioflavine-S: green (B & E), combined images C & F). A –C: The well-defined ADan deposits adjacent to the hippocampal granular cell layer are in part also thioflavine-S positive while those in the CA4 subregion are mainly thioflavine-S negative. There is a good overlap between ADan (**D**) and thioflavine-S (**E**) staining of blood vessels (arrow) in the CA4 subregion, whereas the Ab5282 positive parenchymal deposits are mainly thioflavine-S negative (double arrow) (**F**) (Obj x10).

	Type of Lesion								
	Amyloid plaques		**Diffuse deposits**		**Amyloid angiopathy**		**NFT**	**AN**	**NT**
	ADan	Aβ	ADan	Aβ	ADan	Aβ			
Retina (1)	+++	0	++	0	+++	0	0	0	0
Optic nerve (2)	0	0	0	0	++	0	0	0 - +	0
Optic tract (2)	0	0	0 - +	0	++	0	N/A	0 - +	0 - +
Hippocampus (3)	0 - +	0	+++	++ - +++	+++	++ - +++	+++	++ - +++	+++
Subiculum (3)	0	0	+++	+ - ++	++	++	+ - +++	+ - +++	++ - +++
Amygdala basal (2)	+	0	+++	0 - +++	++	0 - ++	++ - +++	++	++ - +++
Amygdala lateral (2)	0 - +	0	+	0 - +++	++	0 - ++	+ - ++	0 - ++	+ - ++
Amygdala (1)	+	0	++	++	++	++	+++	++	+++
Septum (2)	0	0	+ - +++	+	++ - +++	+	+ - ++	+	+ - ++
Uncus (2)	0	0	+ - +++	0 - +++	++	+ - ++	++ - +++	+	+++
Entorhinal cortex (3)	+ - ++	0	+ - +++	++ - +++	+ - ++	++ - +++	+ - +++	+ - +++	++ - +++
Fusiform gyrus (3)	0	0	+	+ - +++	++	+ - ++	+ - +++	+ - +++	+ - +++
1st, 2nd, 3rd temporal gyri (3)	0 - ++	0	0 - ++	+ - ++	++	++ - +++	+ - ++	+ - ++	+ - ++
Frontal cortex (3)	0 - +	0	0 - +	++ - +++	++	++	+	+ - ++	+ - ++
Cingulum (1)	0	0	0	++	++	+	+	+	+
Insular cortex (2)	0	0	0 - +	++ - +++	++	+ - ++	++ - +++	+ - +++	++ - +++
Parietal cortex (2)	0	0	+	++ - +++	++	+ - ++	+ - ++	+ - +++	+ - +++
Occipital cortex (3)	0 - ++	0	0 - ++	+ - +++	++	++	0 - +	+	0 - +
Cerebral white matter (3)	0	0	+	0 - ++	++	0 - +	N/A	++	+
Hypothalamus (2)	0	0	+ - +++	+	++	+ - ++	+ - ++	+ - ++	+ - ++
Caudate (3)	0	0	0	0 - +++	0 - +	0	0 - +	0	0 - +
Putamen (3)	0	0	0	+ - ++	0 - +	0	0	0	0 - +
Globus pallidus (3)	0	0	0	0	0	0	0	0	0
Claustrum (2)	0	0	0 - +	+	+ - ++	0 - +	+	0 - ++	+ - ++
Meynert nucleus (3)	0	0	0	0 - +++	+	0 - +	++	0 - +	++
Thalamus (2)	0	0	0	0 - ++	+ - ++	0 - ++	+ - ++	0	+
Subthalamus (2)	0	0	0	0 - +	++	0	0	0	0

Table 17: *Distribution of different ADan and Aβ lesion types and tau pathology in familial Danish dementia*
Numbers in brackets refer to the number of cases, in which this area could be examined. NFT = neurofibrillary tangle, AN = abnormal neurite, NT = neuropil thread

	Type of Lesion								
	Amyloid plaques		**Diffuse deposits**		**Amyloid angiopathy**		**NFT**	**AN**	**NT**
	ADan	Aβ	ADan	Aβ	ADan	Aβ			
Tectum (3)	0 - ++	0	+ - +++	0 - ++	++	0 - +++	0 - ++	0 - +++	0 - ++
Periaqueductal gray (2)	0 - +	0	+ - +++	0 - ++	+ - ++	0	+ - ++	0	+
Midbrain raphe (2)	0	0	+	0 - +	+	0	0 - ++	0	0 - +
Substantia nigra (3)	0	0	0	0 - +	+	0	0 - +	0	0 - +
Red nucleus (1)	0	0	0	0	++	0	0	0	0
Cerebral peduncle (2)	0	0	0 - +	0 - +	+ - ++	0 - +	N/A	0	0
Locus coeruleus (3)	0 - +	0	++ - +++	0	++ - +++	0	+ - ++	0 - +	+ - ++
Pontine raphe (2)	0	0	0 - +	0 - +	++	0	+ - ++	0 - +	+
Pontine base (3)	0 - +	0	0 - +	0 - +	++	0 - +	0	0	0
Inferior olive (3)	0 - +	0	0 - ++	0	+ - ++	0	0	0	0
Pyramid (3)	0	0	0 - +	0	0	0	N/A	0	0
Cerebellar cortex (3)	0 - +	0	+ - ++	0 - +	+++	+ - ++	0	0	0
Cerebellar white m. (3)	0	0	0 - +	0 - +	+ - ++	0	N/A	0	0
Dentate nucleus (3)	0 - +	0	0 - ++	0	++	0	0 - +	0 - +	0 - +
Cervical cord LC (2)	0	0	+	0	+ - ++	0	N/A	0 - +	0
Cervical cord PC (2)	0	0	+	0	+ - ++	0	N/A	0	0
Cervical cord VC (2)	0	0	+	0	+ - ++	0	N/A	0 - +	0
Cervical cord GM (2)	0	0	0 - +	0	+ - ++	0	0 - +	0 - +	0 - +
Thoracic LC (3)	0	0	0 - +	0	++	0	N/A	0 - ++	0
Thoracic PC (3)	0	0	0 - +	0	+ - ++	0	N/A	0	0
Thoracic VC (3)	0	0	0 - +	0	+ - ++	0	N/A	0 - +	0
Thoracic GM (3)	0	0	0 - +	0 - +	+ - ++	0	0 - +	0 - +	0 - +
Lumbar LC (2)	0	0	0 - +	0	0 - +	0	N/A	0 - +	0
Lumbar PC (2)	0	0	0 - +	0	0 - +	0	N/A	0	0
Lumbar VC (2)	0	0	0 - +	0	+	0	N/A	0 - +	0
Lumbar GM (2)	0	0	0	0	+	0	0 - +	0	0 - +
Sacral LC (1)	0	0	+	0	+	0	N/A	0	0
Sacral PC (1)	0	0	+	0	+	0	N/A	0	0
Sacral VC (1)	0	0	+	0	+	0	N/A	0	0
Sacral GM (1)	0	0	0	0	0	0	0	0	+

Table 18: *Distribution of different ADan and Aβ lesion types and tau pathology in familial Danish dementia*
Numbers in brackets refer to the number of cases, in which this area could be examined. NFT = neurofibrillary tangle, AN = abnormal neurite, NT = neuropil thread

4.3.5 Aβ immunohistochemistry of blood vessels

A proportion of the parenchymal capillaries (figure 4.4C), arterioles, leptomeningeal blood vessels (figure 4.4E) and veins were affected by Aβ deposition, although the number of blood vessels containing ADan exceeded those with Aβ deposits. Some of the blood vessels were affected with Aβ deposition alone, but in a considerable number co-localization of both Aβ and ADan was established using confocal microscopy (figure 4.5A-C, 4.5D-F). Such peptide co-localization was sometimes evident throughout the circumference of the blood vessel wall, but in other instances there were isolated foci within the blood vessels wall containing only one of the peptides. Aβ amyloid angiopathy was most severe in the hippocampal formation, where capillaries of the CA1 subregion (figure 4.4A) and subiculum were prominently affected, limbic structures, neocortex (figure 4.4B), thalamus, and cerebellum, while there was little involvement of the blood vessels by Aβ depostion in the brainstem and spinal cord (table 18).

4.3.6 Aβ immunohistochemistry of parenchymal deposits

In the CNS parenchymal subpial peptide deposits, perivascular plaques (figure 4.4C, 4.4D and 4.5G-I) and diffuse deposits were often found to contain Aβ in addition to ADan. As many subpial and perivascular deposits were congophilic it was not possible to ascertain whether only one or both of the component peptides was present in the fibrillar conformation, and parenchymal Aβ deposits have, therefore, only been classified as of diffuse type. The hippocampus, limbic structures and neocortex were most severely and consistently affected by parenchymal Aβ deposits, which took the form of mainly perivascular lesions (figure 4.4A), compact diffuse deposits and loose or cloudy diffuse deposits sometimes surrounding neurons.

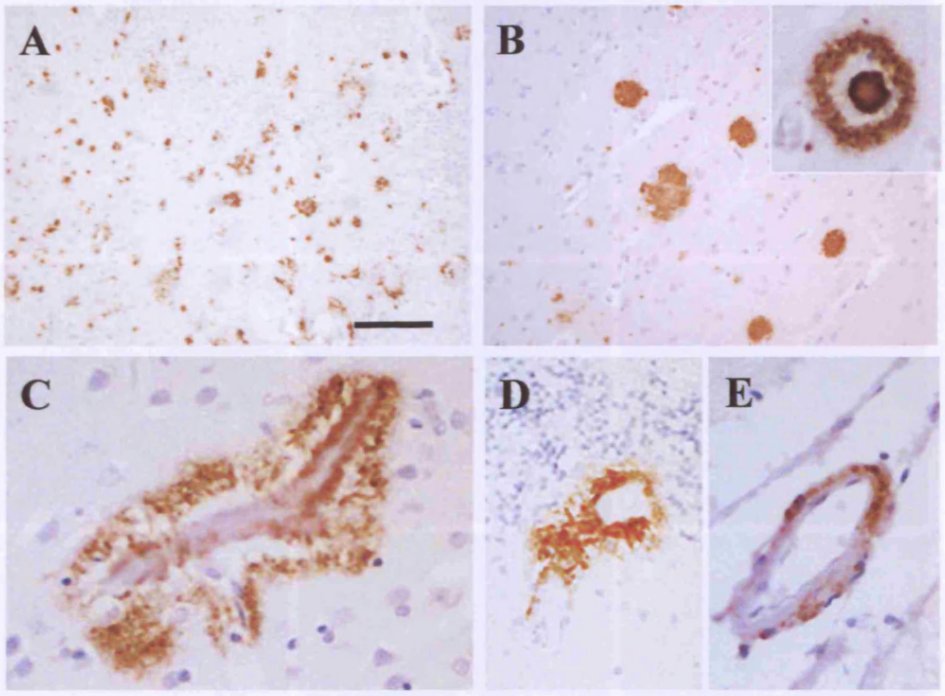

Figure 4.4: Aβ immunohistochemistry in FDD. A: Aβ distribution in the hippocampal formation. **B:** Well-defined Aβ plaques in the parietal cortex, a mature plaque with core in the parietal cortex (inset) **C:** A capillary showing vascular and perivascular Aβ deposition. **D:** A rare Aβ deposit is found in the Purkinje cell layer of the cerebellum. **E:** An occasional leptomeningeal vessel with Aβ is also found. Bar in panel A represents 250μm on panel A; 100μm on panel B; 55μm on panel D ; 28μm on panels C and E.

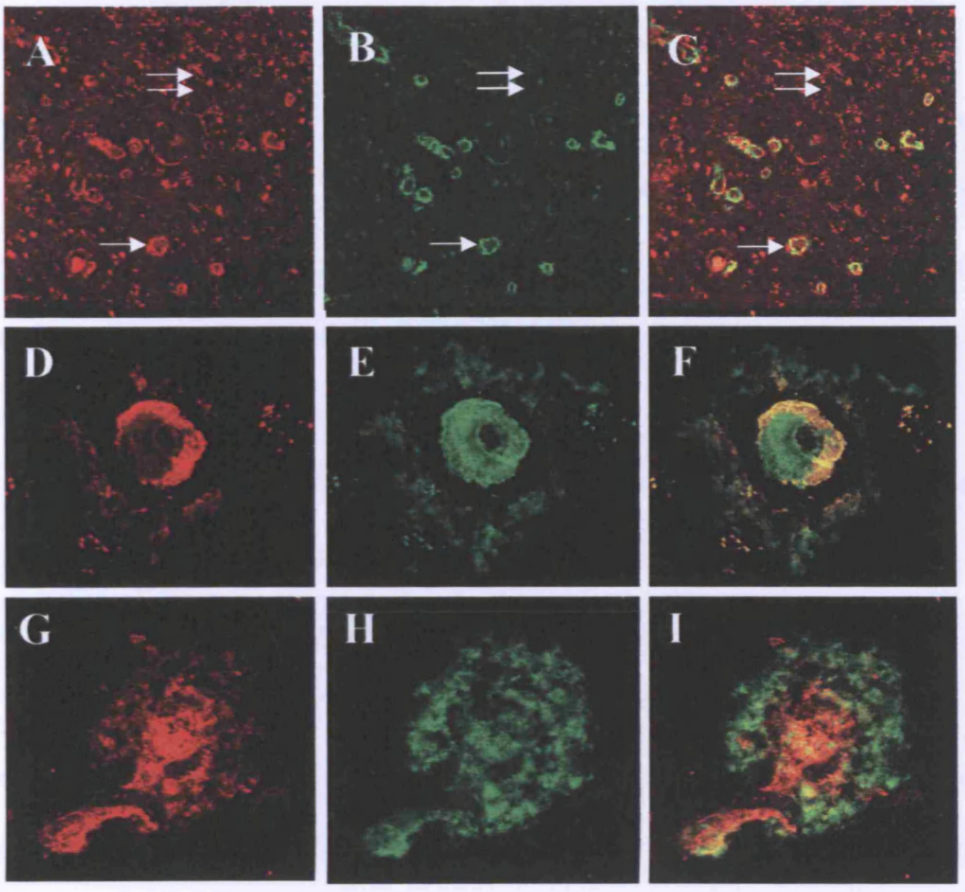

Figure 4.5: ADan and Aβ double immunohistochemistry and confocal microscopy (ADan: red (A, D and G), Aβ: green (B, E and H), combined images C, F and I). A-C: While ADan is found in both parenchyma (double arrow) and blood vessels (arrow) in the parasubiculum, Aβ is largely found in the blood vessels (arrow) (obj. x25). **D-F:** A neocortical blood vessel showing deposition of both ADan (red) and Aβ (green), but the overlap is incomplete (obj. x63). **G-I:** A further neocortical blood vessel showing ADan and Aβ co-deposition with the vessel wall primarily containing ADan (red), while the perivascular deposit is largely Aβ (green) (obj. x63).

In the parietal cortex of case 1 several lesions had the appearance of the classical cored plaques found in AD (figure 4.4B, inset), however, these were noted to be unstained by Congo red and did not contain ADan. In the hippocampus the CA1 subregion was most severely affected with diffuse and perivascular Aβ deposits. The subiculum also showed marked perivascular deposition and Aβ peptide, like ADan, was also found to be deposited on extracellular 'ghost tangles'. The pre-α neuronal clusters of the entorhinal cortex were highlighted by diffuse deposition of Aβ. In the neocortex, Aβ deposits were found predominantly in superficial cortical laminae and were often found to be more numerous than those of ADan. The occasional Aβ diffuse deposits were found in the cerebellum but these were very rare compared to the amount of ADan deposition.

Several areas of the CNS had parenchymal Aβ deposition without ADan deposits; these included the cingulum, striatum, nucleus basalis of Meynert, thalamus, and subthalamus. There were regions, notably the retina, optic nerve and tract, red nucleus, locus ceruleus, dentate nucleus and the spinal cord, with the exception of the thoracic grey matter, in which ADan was found in either blood vessels and/or parenchyma in the absence of Aβ.

4.3.7 AT8 immunohistochemistry and its correlation with ADan and Aβ deposition.

The hippocampus was consistently the region most severely affected by all three types of neurofibrillary pathology with abundant NFTs (figure 4.6A and 4.6B), including ghost tangles; bulbous ANs and fine NTs (figure 4.6B). Abnormal neurites around amyloid deposits in blood vessel walls were frequent in the CA1 subregion and in the subiculum (figure 4.6C and 4.6D).

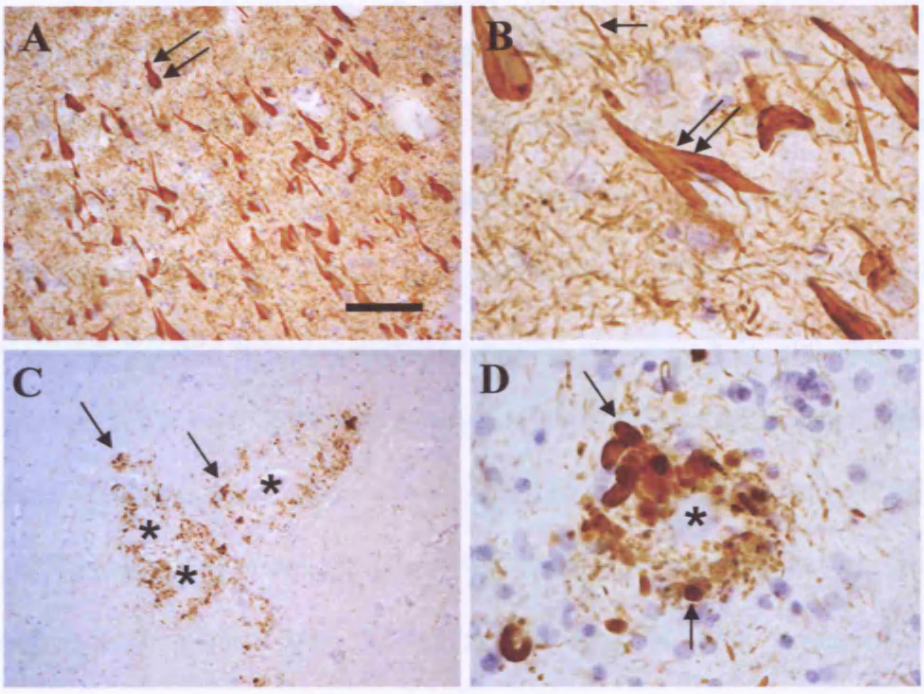

Figure 4.6: Tau (AT8) immunohistochemistry in FDD. A & B: Numerous NFTs (double arrows) and NTs (arrow) in the hippocampus. **C & D:** Abnormal neurites (arrows) are clustered around amyloid-laden blood vessels (asterisks). Bar in panel A represents 100μm in A and C; 28μm on panels D and B.

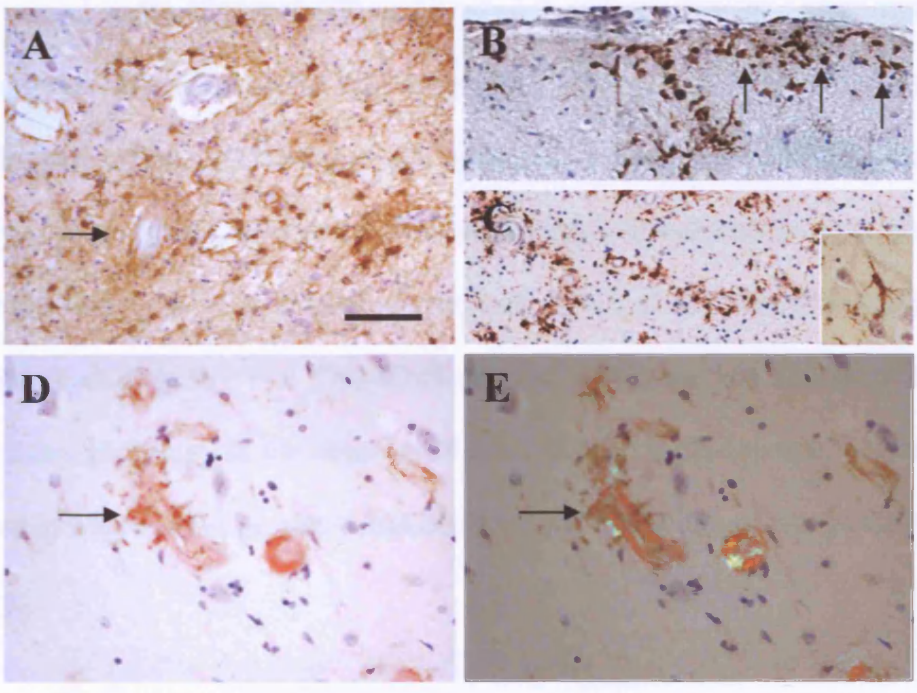

Figure 4.7: Astrocytic and microglial response in FDD demonstrated by GFAP & CR3/43 immunohistochemistry. A: Reactive astrocytes tend to cluster around amyloid laden blood vessels (arrow) **B:** Activated microglia cells tend to be orientated towards subpial amyloid deposits (arrows). **C:** Activated microglial cells are found within the cortex, inset showing an activated microglial cell in the subiculum. **D & E:** Activated microglia tend to cluster around amyloid laden vessels, as shown with a double Congo red and CR3/43 staining (arrows). Bar in panel A represents 100μm in A, B and C; 55μm on panels D and E .

Neurons showing finely granular cytoplasmic staining representing pre-tangles were also observed. Scanty NFTs were seen in the dentate fascia. Although other limbic regions were also affected by these pathological structures, their involvement showed a greater variation between cases. All neocortical regions examined showed neurofibrillary pathology with NFTs most frequent in the parietal and temporal lobes, while ANs and NTs were most commonly found in the parietal cortex. Neocortical vessel-related neurites were often more commonly seen in the superficial cortical laminae, while those related to subpial amyloid were more frequent in sulci than on the locus ceruleus both showed neurofibrillary pathology, but the substantia nigra was inconsistently involved by NFTs and NTs without ANs. Of note was the mild involvement of the dentate nucleus in 1 case by NFTs, ANs and NTs.

Abnormal neurites were only found in relation to ADan and/or Aβ deposited as amyloid in blood vessel walls (figure 4.6D) or in subpial regions, but they were not seen in association with diffuse ADan or Aβ parenchymal deposits. The regions most severely affected by parenchymal ADan deposition were also severely affected by neurofibrillary pathology. The neocortex, in which diffuse ADan deposits were never more severe than '++', but showed up to '+++' diffuse Aβ deposits, also had neurofibrillary pathology of all 3 types graded up to '+++'. No CNS regions were observed in which there was neurofibrillary pathology in the absence of either ADan or Aβ deposits, although there were areas in which either peptide could be found without accompanying neurofibrillary pathology.

4.3.8 GFAP, CD68 and CR3/43 immunohistochemistry.

The astrocytic response demonstrated by GFAP immunohistochemistry showed some variation between cases. The relationship to amyloid deposits was confirmed by double

labelling using an anti-GFAP antibody and Congo red. The hippocampus and subiculum displayed severe astrocytosis with reactive astrocytes and numerous processes distributed evenly within the parenchyma (figure 4.7A) and in increased numbers around amyloid-laden blood vessels (figure 4.7A, arrow). The neocortex was involved by mild, patchy astrocytosis, which was accentuated around amyloid containing blood vessels and in the superficial cortex in relation to subpial amyloid deposition. There was moderate to severe fibrillary astrocytosis in the subcortical white matter that was most marked in the posterior frontal and parietal lobes. The cerebellum showed prominent Bergmann gliosis and diffuse astrocytosis of the cortex and white matter with relative sparing of the dentate nucleus.

Microglial distribution was assessed by CD68 immunohistochemistry and the antibody CR3/43 recognizing MHC class II antigen was used to assess the presence of reactive, activated microglia (figure 4.7B). Double labelling with each antibody and Congo red in the hippocampus and temporal lobe was used to assess the relationship between microglia and amyloid deposits. Both antibodies showed a diffuse distribution of microglia throughout the hippocampus and subiculum with an increase in density of cells around amyloid-bearing blood vessels (figure 4.7C and 4.7D) and around perivascular plaques. The cortex and white matter showed a pattern of microglia response similar to that observed for astrocytes. In the cerebellum, activated microglia were distributed throughout although they were more frequent in the white matter.

4.3.9 Immunoelectron microscopy with Ab5282

iEM was performed on a sample from the hippocampus of case 1 using Ab5282 to localize ADan peptide. Tissue preservation enabled the identification of blood vessels, cell processes, neurons and glial cells. Several small blood vessels had deposits of

randomly orientated amyloid filaments of approximately 10nm diameter within the basement membrane and extending into the surrounding parenchyma, these amyloid fibrils were recognized by Ab5282 (figure 4.8A and 4.8B). Amyloid laden blood vessels were also found covered with the Ab5282 immunolabelling (figure 4.8A). Labelling was found in association with amorphous electron dense material in association with small numbers of 10nm filaments representing parenchymal preamyloid (figure 4.8C and 4.8D). No labelling was found when the primary antibody was omitted or the pre-immune serum was used. NFTs were confirmed to be composed of PHFs with a maximum diameter of approximately 20 to 25 nm and periodic constrictions at about 80 nm.

4.3.10 Double immunoelectron microscopy with Ab5282 and Aβ

Double labelling for iEM was performed with Ab5282 and Aβ antibodies, on a sample from the hippocampus of case 1, to determine the relationship of the two amyloidogenic peptides ADan and Aβ peptide. The two peptides were found to co-localize within the same lesions including parenchymal deposits and amyloid-laden blood vessels (figure 4.9). Ab5282 was found labelling parenchymal deposits and amyloid affected blood vessels without any Aβ positive staining, but Aβ labelling was only found in conjunction with Ab5282 labelling. No labelling was found when the primary antibody was omitted or the pre-immune serum was used.

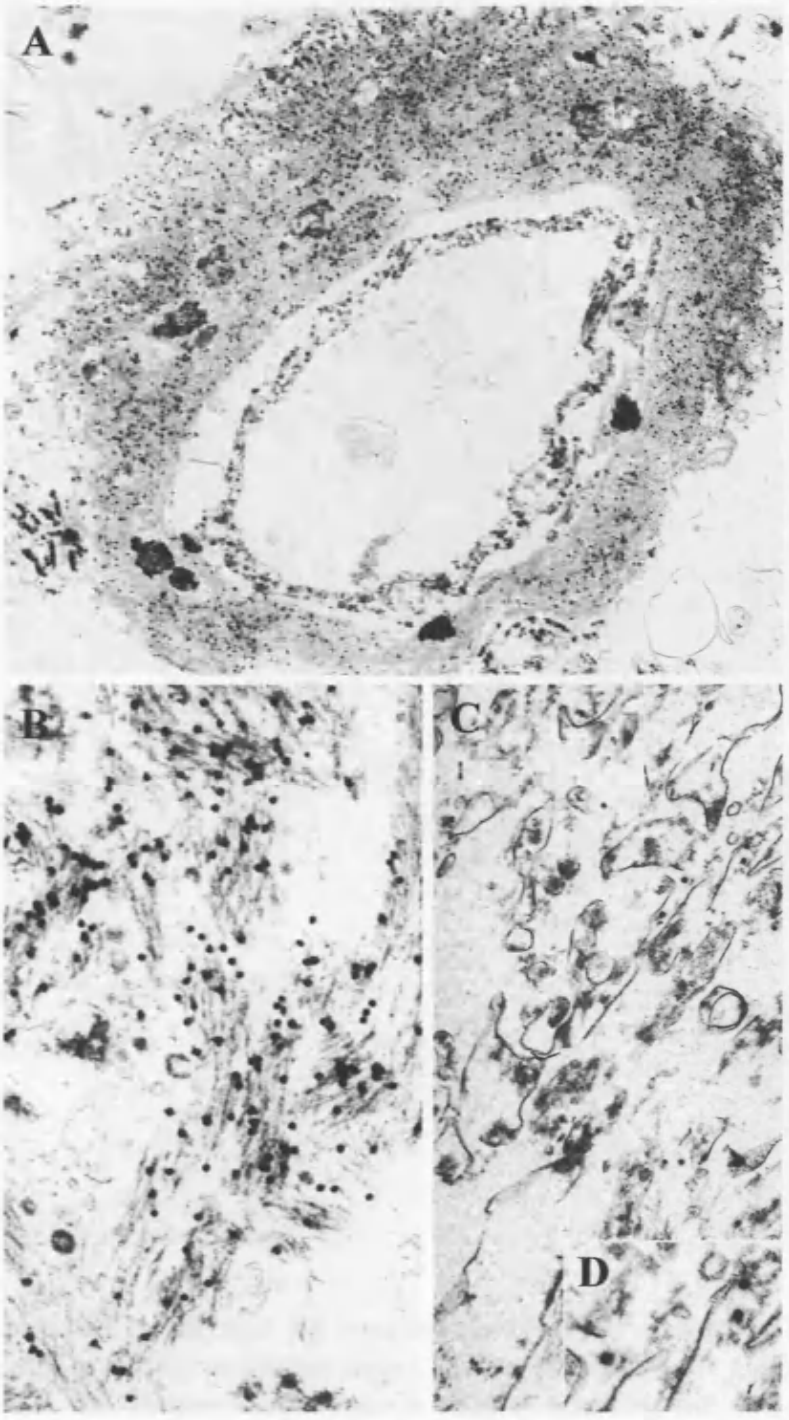

Figure 4.8: Ab5282 immunoelectron microscopy in FDD. A: A blood vessel showing expanded basal lamina labelled with antibody to ADan. **B:** The anti-ADan antibody decorates fibrillar material corresponding to amyloid in an affected vessel. **C:** The diffuse parenchymal deposits are composed of amorphous electron dense material with sparse filaments representing pre-amyloid. Gold particle size 20 nm. Original magnification in A x6,600; B and C x10,000; D x16,000.

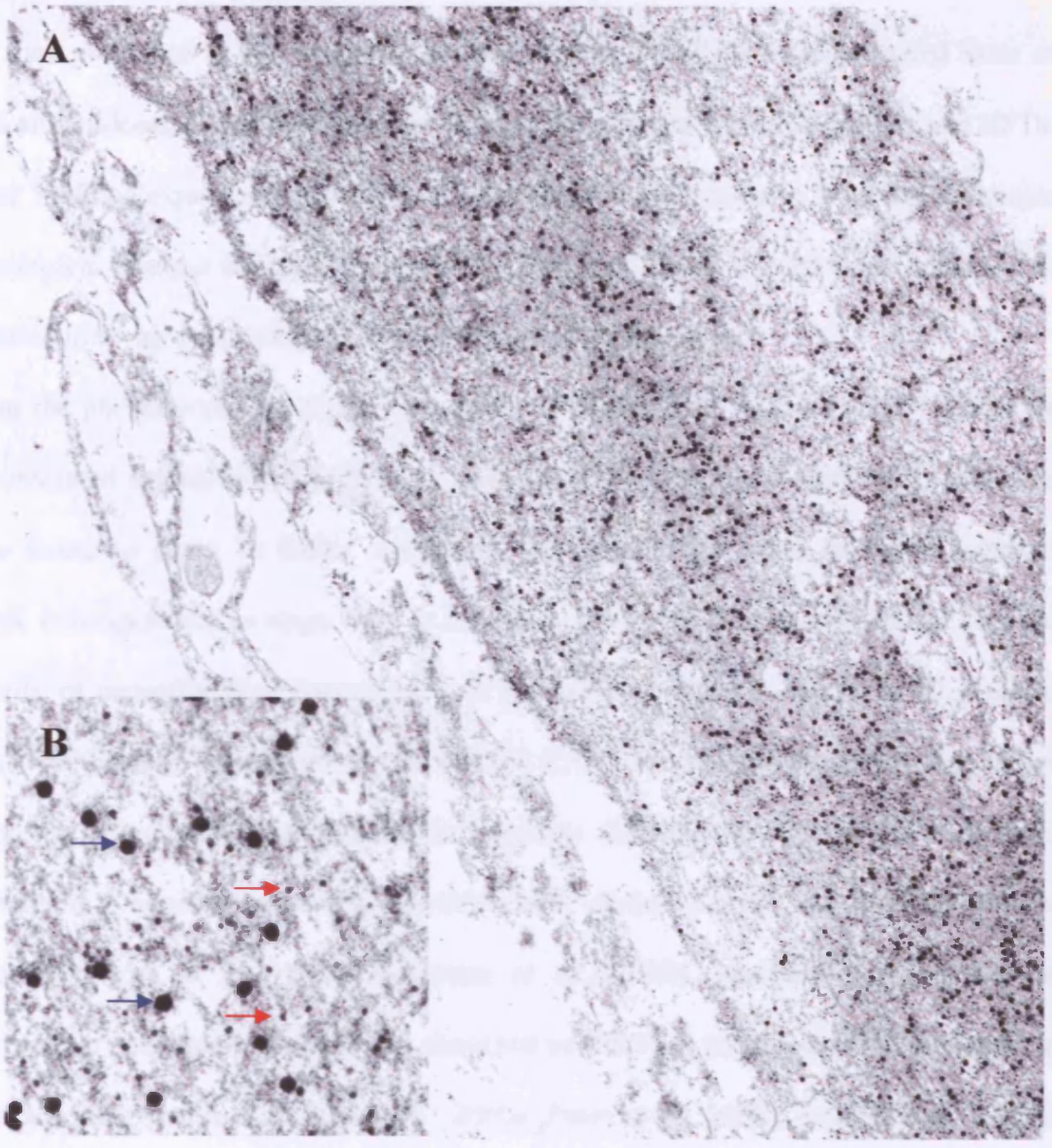

Figure 4.9: Double ADan and Aβ immunoelectron microscopy in FDD. A: A blood vessel showing expanded basal lamina labelled with antibodies to ADan and Aβ. **B:** Higher magnification of (A) showing the two amyloid peptides labelling the same amyloid deposit; ADan shown with 10nm particles (red arrows) and Aβ shown with 20nm particles (blue arrows). Original magnification in A x12,000; B x30,000.

4.4 Discussion

The data presented in this chapter illustrated that FDD, which is an inherited form of CNS amyloidosis, is characterised by widespread CAA, parenchymal lesions and NFTs. These findings expand the spectrum of neurodegenerative diseases in which the major pathological changes include neurofibrillary pathology and nerve cell death occurring in combination with deposition of extracellular protein aggregates.

Using the phosphorylation dependent anti-tau antibody AT8 (Goedert *et al.*, 1993) we demonstrated extensive tau pathology, including NFTs, NTs and ANs. NFTs and NTs were found to occur in limbic structures, neocortices, and some of the subcortical nuclei, corresponding to stage V-VI in the Braak and Braak system used for grading the severity of neurofibrillary degeneration in AD (Braak & Braak, 1991). In all 3 cases, ANs were located around blood vessels with CAA, but not in association with either ADan or Aβ parenchymal pre-amyloid lesions (defined as Congo red –negative, thioflavine-S negative or weakly positive and ultrastructurally non-fibrillar protein deposits (Verga *et al.*, 1989; Giaccone *et al.*, 1992). Perivascular clustering of argyrophilic and tau immunoreactive abnormal neurites has been described in relation to CAA associated with Aβ (Vidal *et al.*, 2000a; Peers *et al.*, 1988), prion protein (Ghetti *et al.*, 1996), and ABri deposition (Holton *et al.*, 2002; Revesz *et al.*, 1999). The presence of ANs around CAA of various origins and their absence in association with preamyloid lesions suggests a correlation between the fibrillation of amyloidogenic peptides and formation of ANs (Holton *et al.*, 2002; Vickers *et al.*, 1996).

Using Ab5282 specifically recognizing ADan, we demonstrated that this amyloidogenic peptide which is associated with the genetic defect in FDD, is a major component of both the vascular and parenchymal lesions throughout the CNS. From the pathological data presented here, however it is not possible to ascertain whether full length ADan is

the only significant species comprising the cerebral vascular amyloid and the parenchymal lesions since the residues recognized by Ab5282 (CFNLFLNSQEKHY) are not exclusive to ADan, but are also present in ADanPP and potential C-terminal fragments that may be processed from either ADanPP or ADan. (studies in Chapter 7 aim to identify the ADan deposits present in vascular amyloid and species that are present in the parenchymal lesions).

This study showed that in FDD the majority of the hippocampal and neocortical parenchymal ADan lesions often have ill-defined boundaries and show tinctorial, optical and ultrastructural features of preamyloid rather than amyloid (Verga *et al.*, 1989; Giaccone *et al.*, 1992). In contrast, in FBD (as has been demonstrated in chapter 3) the majority of the hippocampal ABri lesions are well-defined, plaque-like and of amyloid nature, although pre-amyloid lesions are predominant in some of the anatomical areas such as the entorhinal and transentorhinal cortices (Holton *et al.*, 2002; Revesz *et al.*, 1999). The combination of preamyloid lesions and neurofibrillary degeneration in FDD is analogous to that seen in variant AD with spastic paraparesis, which is also characterized by the pre-amyloid Aβ plaques of the cotton wool-type in association with neurofibrillary degeneration (Crook *et al.*, 1998; Houlden *et al.*, 2000; Steiner *et al.*, 2001; Verkkoniemi *et al.*, 2001). This observation adds further weight to the evidence that amyloid conformation per se is not a prerequisite for NFT formation. The experimental data currently available are not sufficient to explain the predominance of preamyloid lesions in FDD. One possibility is that due to the difference in the primary sequence ADan forms amyloid fibrils less efficiently than ABri does, although conversion of multiconformational proteins into predominantly β-pleated fibrils is not thought to be significantly dependent only on sequence per se (Lansbury, Jr., 1999). It is, however, possible that the difference in the amino acid sequence is sufficient to make

ADan less able to attract and/or bind to amyloid associated components such as ApoE, HSPGs, SAP or ACT, which have been shown to modulate aggregation of Aβ in vivo, which would be required, possibly in combination with other factors for efficient fibril formation.

In all 3 cases studied, we were able to demonstrate the presence of various degrees of Aβ peptide deposition either in combination with ADan or alone, in blood vessels and in brain parenchyma. The Aβ parenchymal deposition similar to that of ADan, was most severe in the limbic structures, but also occurred in neocortical areas where it was more severe than deposition of ADan. The significance of Aβ deposition cannot be clarified at present. Co-deposition of ADan and Aβ, as has been shown for Aβ and cystatin C (Levy *et al.*, 2001), is a possibility although the presence of Aβ alone in several anatomical areas makes this possibility less likely. The possibility of a second hereditary neurodegenerative disease should be considered although in the absence of neocortical neuritic plaques the diagnosis of AD could not be made on morphological grounds.

The presence of two amyloidogenic peptides has also been observed within other diseases. A study has shown in four cases of GSS the presence of Aβ deposits co-localised with PrP protein in amyloid plaques (Miyazono *et al.*, 1992). The results reported were the first evidence for colocalization of the two amyloidogenic peptides PrP and Aβ protein in the same amyloid plaques at the light and electron microscope level. Although the amyloid plaques that were purified from the youngest GSS patient (aged 45) were immunolabelled by anti-PrP, but not by anti-Aβ, suggesting that Aβ is only observed in the older GSS patients and that it is a secondary event to the deposition of PrP (Miyazono *et al.*, 1992). The Aβ deposition found in this study is unlikely to represent an aging phenomenon as the youngest patient in our series was 43 years old at

the time of death. Several studies have also shown the co-localisation of two other peptides α-synuclein and tau. The first study showed that some Lewy bodies (LBs) in the substantia nigra from diffuse Lewy body disease (DLBD), but not PD, had tau immunoreactivity with a peripheral pattern of immunostaining (Galloway *et al.*, 1988). This was followed by a study that demonstrated the presence of tau in LBs in a case of familial PD (Contursi kindred) due to mutations in α-synuclein (Duda *et al.*, 2002). More recently the observations have been extended to sporadic Lewy body disease where the location of the tau immunoreactivity was detected in the cytoplasm of neurons with LBs, at the periphery of LBs, with α-synuclein immunoreactivity in the core of the LB, or throughout the LB. Although the most common location of the tau epitopes was at the periphery of the LB, suggesting the deposition of the tau in LBs is a secondary process to α-synuclein deposition and presenting the possibility that α-synuclein might serve as a seed for tau aggregation (Ishizawa *et al.*, 2003). This is an interesting possibility that the formation of amyloid fibrils from one peptide may seed the formation of a second amyloidogenic peptide. In FDD the ADan deposits found in the blood vessels have been shown to form amyloid fibrils in this study, with occasional Aβ deposits. The parenchymal deposits on the other hand are pre-amyloid deposits therefore if a seeding process was taking place here oligomers or protofibrils would be acting as the seeding agent and not the amyloid fibrils themselves.

With the detailed pathological analysis of FBD (see chapter 3) and FDD (this chapter) completed, questions could now start to be answered. The mechanism of peptide deposition, whether other molecules are implicated in this process. For example amyloid associated proteins, are they just innocent bystanders involved in the deposition of the amyloid forming peptides or involved in converting pre-amyloid to amyloid peptides. Compelling evidence continues to accumulate for a significant role of

local inflammatory processes in the progression of neurodegenerative disorders, mechanisms which have been studied extensively in AD (Akiyama *et al.*, 2000). In particular complement activation and its proinflammatory consequences have been demonstrated to contribute extensively to disease pathogenesis (Tenner, 2001). Most of the studies have been completed on AD cases, but with activated microglia expressing major histocompatibility class II antigens characteristic of inflammatory processes and reactive astrocytes present around amyloid lesions, an investigation of complement activation was completed in both FBD and FDD.

Although ABri and ADan only differ by 12 amino acids there is a remarkable difference in the way the peptides are deposited in the CNS. ABri primarily forming amyloid lesions (see chapter 3) and ADan forming amyloid lesions in affected blood vessels but only pre-amyloid deposits are found in the parenchyma. This difference must arise from the primary sequence of the peptides forming different secondary structures and making the peptides behave in different ways. To try and understand the properties of the peptides a biochemical study was undertaken to assess the solubility of the peptides and the degree to which the peptides would oligomerise. This was taken a step further and the heterogeneity of the peptides was investigated.

With all the subsequent investigations following this chapter, work was carried out not only on the FBD and FDD cases but also sporadic AD cases and variant AD with spastic paraparesis. This was to ensure a clear comparison between the two novel amyloid peptides, ABri and ADan, with Aβ in both amyloid and pre-amyloid lesions. For a combination of preamyloid lesions and neurofibrillary degeneration in FDD is analogous to that seen in variant AD with spastic parapaesis.

Chapter 5

Amyloid associated proteins in BRI2 gene-related dementias.

Chapter 5 – Hypothesis and specific questions

In this chapter. I wished to investigate the hypothesis that AAPs play a role in ABri and ADan fibrillogenesis. The specific questions I wished to investigate were; 1) Are AAPs, which are known to co-localise with Aβ deposits in AD and some other cerebral and systemic amyloidoses, present in ABri and ADan lesions in FBD and FDD?; 2) Is the conformational state of these novel amyloidogenic peptides related to the deposition of AAPs?

As the presence of AAPs in Aβ lesions in AD has been linked to the process of Aβ fibrillogenesis, this study aimed to establish whether such proteins are also associated with ABri and ADan lesions thus raising the possibility of a more general role for these proteins in amyloid fibril formation. This question was addressed by an immunohistochemical study investigating the distribution of Apolipoprotein E (ApoE), Apolipoprotein J (ApoJ), α-1-antichymotrypsin (ACT), serum amyloid P component (SAP), cystatin C and various heparan sulphate proteoglycans (HSPGs), including agrin, perlecan, glypican-1 and syndecans. The conformational state of the amyloidogenic peptides in the different lesion types was established using thioflavine-S staining.

5.1 Introduction

Why amyloid fibrils form and the steps involved in the process of amyloid fibril formation from its precursor proteins are still not fully understood. After the identification of Aβ, as the major component of cerebrovascular amyloid and senile plaques in AD, evidence was found that a heterogenous group of proteins termed AAPs are co-deposited within the parenchymal and vascular Aβ deposits in AD and with amyloid proteins in other forms of cerebral or systemic amyloid diseases (Alexandrescu, 2005; Calero *et al.*, 2000; McLaurin *et al.*, 2000; Wisniewski *et al.*, 1995) and other disorders of protein misfolding (Ishii & Haga, 1984). While the deposition of some of these proteins may be a secondary event a series of *in vitro* data shows that several AAPs may influence the process of conversion of soluble amyloid proteins to both soluble and insoluble forms with high β-sheet content (Alexandrescu, 2005; McLaurin *et al.*, 2000). Such molecules include ApoE (introduced in section 1.10.1), which is a major apolipoprotein in the brain, produced mainly by astrocytes

(Pitas *et al.*, 1987). The ApoE gene is associated with altered risk of AD and CAA in that the possession of ApoE-ε4 is associated with an increased risk for both pathologies (Greenberg *et al.*, 1995; Nicoll *et al.*, 1997; Strittmatter & Roses, 1996) while that of ApoE-ε2 decreases the risk of AD, but increases the risk of CAA-associated vasculopathy and intercerebral haemorrhage (McCarron *et al.*, 1999). ApoE has been shown to co-localise with Aβ in CAA and senile plaques and also NFTs in AD (Namba *et al.*, 1991; Pitas *et al.*, 1987; Wisniewski & Frangione, 1992). ApoJ (clusterin or SP40-40) is a complement inhibitor, which converts the hydrophobic MAC into a hydrophilic structure thus preventing its insertion into cell membranes. ApoJ can also be classed as an AAP and has been show to associate with Aβ lesions (Lidstrom *et al.*, 1998; McGeer *et al.*, 1992).

Several proteases and protease inhibitors have been demonstrated in the amyloid lesions in AD. These include the decameric glycoprotein SAP (Coria *et al.*, 1988; Rozemuller *et al.*, 1989), a normal plasma glycoprotein synthesized exclusively in the liver (Kalaria & Grahovac, 1990) which has been suggested to be an elastase inhibitor (Li & McAdam, 1984) (see section 1.10.2). ACT, which belongs to the group of serine protease inhibitors, has also been shown to be present (Rozemuller *et al.*, 1991). ACT is an acute-phase reactant and member of the SERPIN superfamily; it is produced by hepatocytes in the liver, alveolar epithelial cells in the lung (Hood *et al.*, 1980; Potter *et al.*, 2001) and by astrocytes within the brain (Pasternack *et al.*, 1989; Rozemuller *et al.*, 1991). ACT has been shown to be associated with the Aβ protein but not with other amyloidoses (Abraham *et al.*, 1990; Rozemuller *et al.*, 1991) (see section 1.10.3). Cystatin C, the mutated form of which causes HCHWA-I, has also been shown to be associated with amyloid deposits. Cystatin C belongs to a group of potent, non-covalent, competitive inhibitors of cysteine proteinases of the papain superfamily (Bobek & Levine, 1992). The possibility that cystatin C may have a role in the pathogenesis of other amyloidoses was raised by the observation that it is present in Aβ parenchymal and vascular amyloid lesions in AD (Levy *et al.*, 2001) (see section 1.10.4).

HSPGs are another major class of AAPs which have been implicated in the pathogenesis of amyloid diseases (Snow *et al.*, 1988). They have been shown with Aβ deposits which have been shown to accumulate in both senile plaques and amyloid-laden blood vessels in AD (Perlmutter *et al.*, 1990; Snow *et al.*, 1988), DS (Snow *et al.*, 1990) and HCHWA-D (Maat-Schieman *et al.*, 2000) (the structure and function of which are introduced in section 1.10.6)

Although the presence of most of these AAPs within the amyloid lesions is unknown, it has been assumed that most are deposited because of or in response to amyloid accumulation. ApoE, on the other hand, has been shown to bind to Aβ *in vitro* forming an SDS-stable complex, with ApoE4 forming such a complex more rapidly than the ApoE3 (Strittmatter *et al.*, 1993b; Strittmatter *et al.*, 1993a). Several studies have examined the effect of ApoE on Aβ conformation, showing that lipid free ApoE increases Aβ fibril formation (Ma *et al.*, 1994; Sanan *et al.*, 1994; Soto *et al.*, 1996). In contrast other studies have shown that lipid free ApoE decreases fibrillogenesis through inhibiting Aβ seeding or nucleation (Evans *et al.*, 1995; Wood *et al.*, 1996), suggesting the ApoE influences the fibrillogenesis process in some way.

The majority of the information about AAPs available within the literature is linked with Aβ. To date there is no data available about the AAPs present in the *BRI2*-gene related dementias and whether an association with ABri and ADan is observed. In this immunohistochemical study we aimed to investigate the distribution of ApoE, ACT, SAP, cystatin C and various HSPGs that had been studied previously in AD and HCHWA-D (van Horssen *et al.*, 2001) and to establish whether they were present in both FBD and FDD amyloid and preamyloid lesions. By investigating the presence and distribution of these AAPs in the ABri lesions in FBD and ADan lesions FDD we wished to study whether their association with Aβ lesions in AD is indeed protein specific, or may contribute to the fibrillogenesis of other proteins. We also wished to establish whether the conformational state of amyloid protein deposited influences the efficency of deposition of the AAPs.

5.2 Material and methods

5.2.1 Tissue collection

Brain samples from 5 FBD, 3 FDD, 5 AD cases, including one familial case of variant AD with cotton wool plaques associated with the *PS1* ΔI83/ΔM84 mutation (Houlden *et al.*, 2000b; Steiner *et al.*, 2001) and 4 normal controls were collected at post mortem. The criteria for the neuropathological diagnosis of FBD and FDD have been previously described (Holton *et al.*, 2001c; Holton *et al.*, 2002b; Plant *et al.*, 1990; Revesz *et al.*, 1999), while for that of AD standard criteria were used (Mirra *et al.*, 1991); (The National Institute on Aging and Reagan Institute Working Group, 1997). For immunohistochemistry, carried out on paraffin-embedded tissue, 7μm serial sections were cut from the hippocampus, cerebellum and frontal cortex in all cases listed above. For immunohistochemistry, carried out on frozen tissue, 7μm serial sections were cut from the hippocampus and frontal cortex from one FBD case and three sporadic AD cases; frontal cortex from one variant AD case with cotton wool plaques.

5.2.1 Antibodies

The panel of antibodies used in this study (table 19 and table 20) to establish the pattern of deposition of the AAPs including: ApoE, ApoJ, SAP, ACT, cystatin C and various HSPGs. HSPGs included agrin, perlecan, syndecans, glypican-1 and HS GAG side chains. The antibodies recognizing amyloid proteins were as follows: polyclonal antibody 338 (Ab338), polyclonal antibody 5282 (Ab5282) and antibodies to Aβ (amino acids 17-26, Biosource International).

Antigen/ antibody	Dilution	Pretreatment	Source
Aβ (17-26)	1:4000	FA / PC	Biosource
ABri, 338 (24-34)	1:2000	Formic Acid	Dr J Ghiso
ADan, 5282 (21-34)	1:1000	Formic Acid	Dr J Ghiso
Apo J (Clusterin)	1:600	FA / PC	Santa Cruz Biotechnology Inc
Apo E	1:200	FA / PC	Autogen Bioclear
Cystatin C	1:200	FA / PC	Upstate biotechnology

***Table 19**: Antibodies used on paraffin embedded tissue in the AAPs study*

Antigen/ antibody	Dilution	Source
Amyloid P component	1:200	NovaCastra
α-1-antichymotrypsin	1:500	NovaCastra
Agrin JM72	1:500	Dr. M M Verbeek
Agrin BI31	1:750	Dr. M M Verbeek
Perlecan 1948	1:500	Dr. M M Verbeek
Pan-HSPG 3G10	1:300	Dr. M M Verbeek
Syndecan 1,3 2E9	1:100	Dr. M M Verbeek
Syndecan 2 10H4	1:300	Dr. M M Verbeek
Syndecan 1 1C7	1:300	Dr. M M Verbeek
Glypican 1 S1	1:500	Dr. M M Verbeek
Heparan sulphate side chains JM403	1:100	Dr. M M Verbeek
Heparan sulphate side chains JM13	1:50	Dr. M M Verbeek

***Table 20**: Antibodies used on frozen tissue in the AAPs study*

5.2.2 Immunohistochemistry

For this study, immunohistochemistry for paraffin sections was carried as described in section 2.2 and frozen section as described in section 2.4.

5.2.3 Semi-quantitative assessment

For each antibody the intensity and extent of the staining of amyloid plaques, vascular amyloid and parenchymal preamyloid lesions and/or cotton wool plaques were assessed and documented using a four-tiered scale. Absence of staining = -; Patchy and weak staining = +; Weak, but extensive staining = ++; Extensive and strong staining = +++.

5.3 Results

5.3.1 Deposition patterns and conformational state of amyloid proteins

Serial sections of the hippocampus, frontal cortex and cerebellum have confirmed our previous observations that in FBD Ab338 stained frequent amyloid-laden blood vessels (figure 5.1 AI and AII) and also the different amyloid plaques (figure 5.1 BI and BII) and preamyloid parenchymal deposits (Chapter 3, Holton *et al.*, 2001). In FDD, in addition to cerebral blood vessels showing CAA, Ab5282 stained hippocampal and other parenchymal ADan deposits in a manner indicative of preamyloid diffuse deposits (figure 5.1 DI and DII) (Chapter 4, Holton *et al.*, 2002). In three of the four AD cases the Aβ plaque morphology included plaques with an amyloid core as well as diffuse deposits. CAA (figure 5.1 CI and CII) due to Aβ deposition was also a feature. In the familial variant AD case and one of the sporadic AD cases Aβ-positive cotton wool plaques and CAA were prominent (figure 5.1 EI and EII).

5.3.2 Distribution of ApoE in FBD and FDD

Deposition of ApoE in FBD followed a similar pattern to that of ABri (Chapter 3, (Holton *et al.*, 2001). Both large and small hippocampal plaques (figure 5.2A) and preamyloid, diffuse deposits (figure 5.2B) were positively stained with the anti-ApoE antibody (table 21). The dense amyloid plaque core and the looser radiating fibrillar area surrounding the core stained with equal intensitiy. All blood vessels affected by CAA in the hippocampus, frontal cortex and cerebellum (table 21) (figure 5.2C & 5.2D) stained for ApoE. It was also noted, although not part of the focus of this study, that all NFTs found in all subregions of the hippocampus, previously stained with tau antibodies including the ghost tangles were also positive for ApoE (figure 5.2E).

In FDD the parenchymal diffuse deposits were stained for ApoE (figure 5.3A & 5.3B), although the staining intensity was less than that of the amyloid-laden blood vessels, which showed strong positivity (figure 5.3C & 5.3D). ApoE deposition was also found in the subpial and perivascular deposits. NFTs, which are also frequent in FDD showed strong positivity in the entorhinal cortex and the hippocampus (figure 5.3E).

In AD the staining pattern mirrored that seen within FBD and FDD with both plaque (figure 5.3F) and vascular amyloid (figure 5.3F, insert) showing strong staining with the anti-ApoE antibody. Diffuse deposits in AD and the cotton wool plaques in variant AD were also positive for ApoE in a manner similar to that seen in the preamyloid ADan lesions in FDD (figure 5.3G, double arrow). Amyloid-laden blood vessels within vAD showed an intense staining pattern with the anti-ApoE antibody (figure 5.3G, arrow). NFTs were frequently stained with the ApoE antibody in both AD and variant AD (data not shown).

Amyloid associated protein	FBD			FDD		Sporadic AD			Variant AD	
	CAA	Plaque	Diffuse	CAA	Diffuse	CAA	Plaque	Diffuse	CAA	CWP
Amyloid protein (ABri, ADan, Aβ)	+++	+++	++	+++	+++	+++	+++	+++	+++	+++
Apolipoprotein E	+++	+++	++	+++	++	+++	+++	++	+++	++
Apolipoprotein J	+++	+++	++	+++	++	+++	+++	++	+++	++
Serum amyloid P	+++	+++	+	+++	+	+++	+++	+	+++	++
α-1-antichymotrypsin	++	++	+	+++	+	+++	+++	++	+++	+++
Cystatin C	+++	+++	+	++	-	++	+	-	+	-
Agrin	+++	+++	++	+++	+	+++	+++	++	+++	+++
Perlecan	+	+	-	+	-	-	-	-	-	-
Syndecan-1, -3	+	+	-	+	+	-	+	-	+	+
Syndecan-2	++	+++	+	+++	++	+	++	+	+	+
Syndecan-3	+	++	-	++	+	++	++	++	++	++
Glypican-1	++	+++	++	+++	++	+++	+++	++	++	++
HS GAG side chains JM403	+++	+++	++	+++	+	++	++	+	++	++
HS GAG side chains JM13	++	++	+	++	-	+	++	+	+	+
Pan-HSPG 3G10	+++	+++	+	+	-	+++	++	+	++	+

Table 21: *Semi-quantitative analysis of the deposition of AAPs in CAA, amyloid plaques and diffuse deposits in FBD, FDD and AD. FBD = familial British dementia; FDD = familial Danish dementia; AD = Alzheimer's disease; CAA cerebral amyloid angiopathy; CWP = cotton wool plaque*

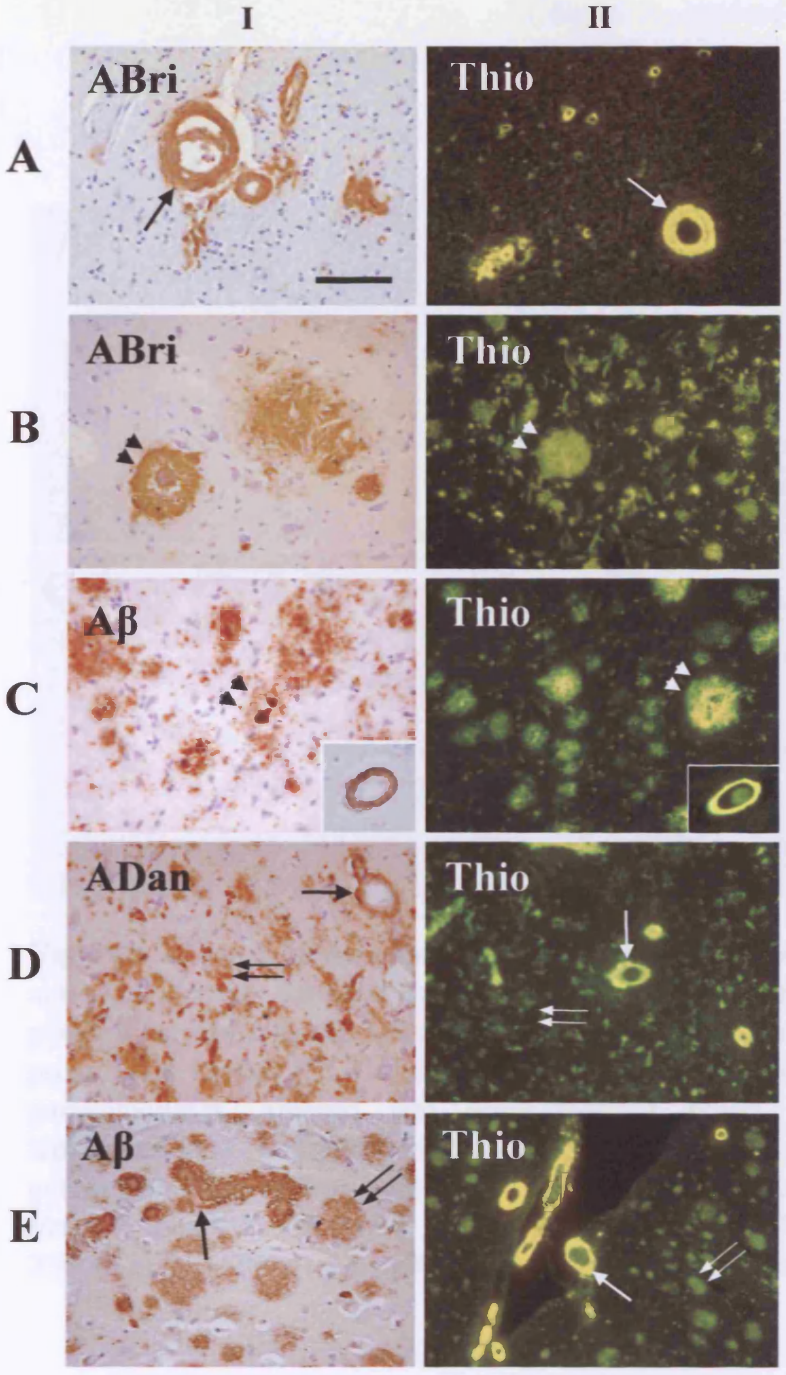

Figure 5.1: Amyloid immunohistochemistry and thioflavine-S staining in FBD, FDD, AD and variant AD with cotton wool plaques (vAD). Amyloid lesions in FBD in row A (CAA, arrow) and row B (plaques, arrowheads). In AD amyloid plaques are shown in row C (arrowheads) with amyloid-laden blood vessels demonstrated in inserts. In FDD CAA (arrow) and diffuse parenchymal deposits (double arrow) are illustrated in row D. In variant AD (vAD: row E) CAA is demonstrated by an arrow while cotton wool plaques are indicated by double arrows. FBD is compared with AD as the lesion types (amyloid plaques and CAA) are similar. Likewise, FDD and vAD have similar features with CAA and parenchymal, largely preamyloid deposits. Thioflavine-S staining demonstrating strong fluorescence in amyloid-laden blood vessels in all diseases. Amyloid plaques are strongly labelled in FBD and AD. Diffuse deposits are the main parenchymal lesion type in FDD showing weaker staining with thioflavine-S. The cotton wool plaques in variant AD show a similar weak staining pattern. Bar on panel A represents 100μm on A, B & C; 250μm on D&E. A x10 objective was used for the thioflavine-S images.

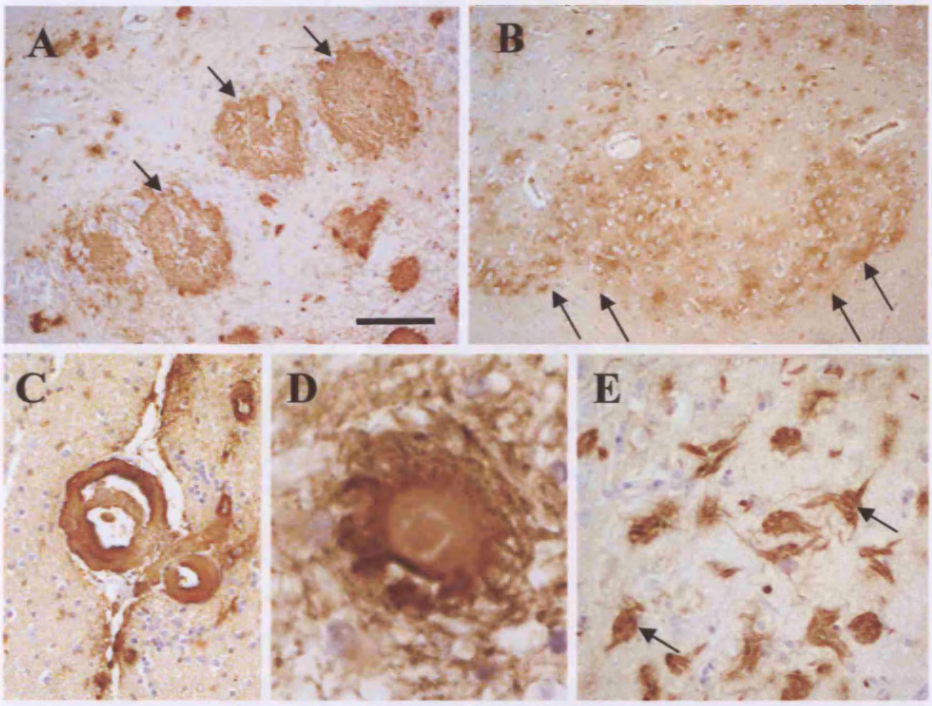

Figure 5.2: ApoE immunohistochemistry in FBD; The anti-ApoE antibody strongly labelled the amyloid plaques (A: large amyloid plaques (arrows) in the granular cell layer of the dentate fascia), preamyloid lesions (B: The parvopyramidal clusters of the pre- and parasubiculum, arrows) and amyloid-laden blood vessels (C leptomeningeal arteriole with double barrelling) and also perivascular amyloid plaques (D). E: NFTs in the hippocampus are strongly positive for ApoE (arrows). Bar on panel A represents 250μm in A; 500μm on B; 100μm on C & E and 28μm on D.

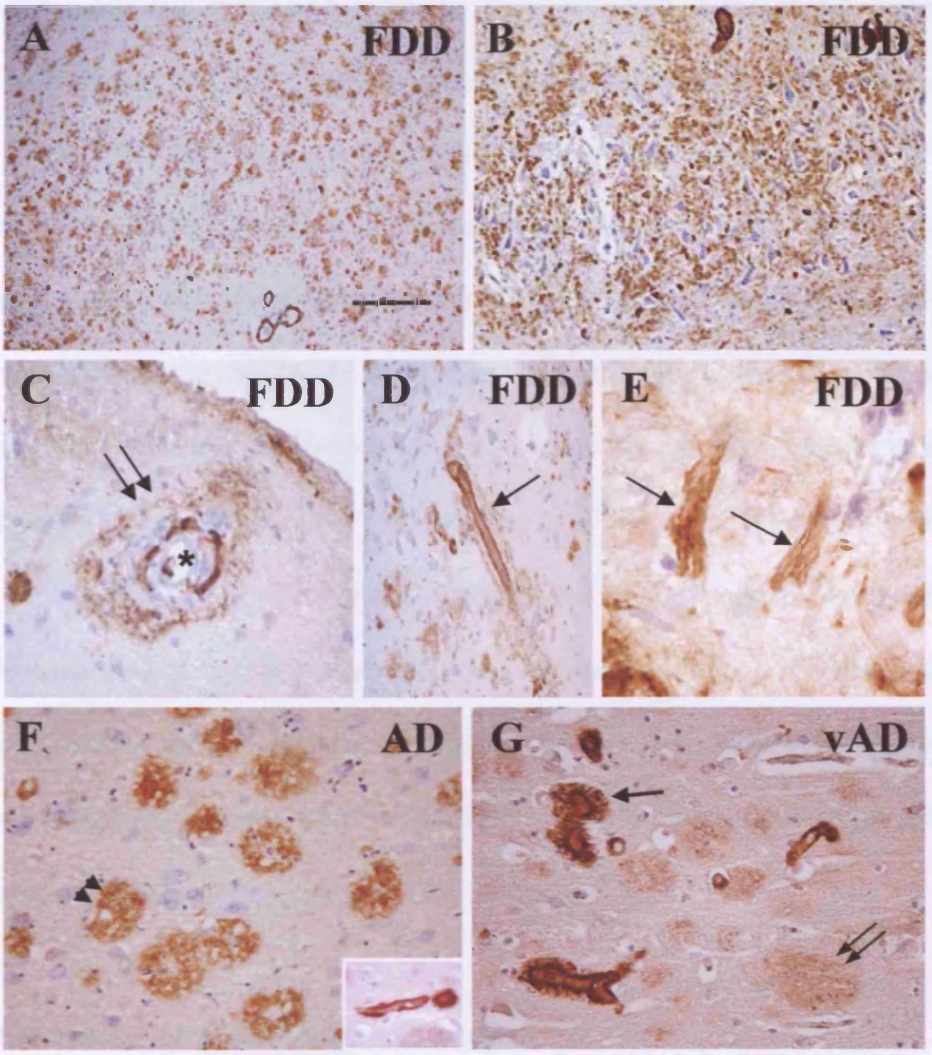

Figure 5.3: ApoE immunohistochemistry in FDD (A-E), AD (F) and vAD (G); In FDD ApoE positive diffuse parenchymal deposits in the CA4 (A) and CA1 (B) hippocampal subregions. Amyloid-laden blood vessels of all sizes, including small arteries, arterioles (C, asterisk), often with perivascular deposition (C, double arrow), and capillaries (D, arrow) were also strongly labelled. As in FBD, the majority of the hippocampal NFTs (E, arrows) were stained with the anti-ApoE antibody. In AD both amyloid plaques (F, arrowheads) and blood vessels with CAA (F, insert) were positive for ApoE. In vAD a strong intense staining pattern was observed within the amyloid-laden blood vessels (G, arrow) and a weaker staining pattern observed in the diffuse cotton wool plaques (G, double arrow). Bar in panel A represents 500μm in A; 250μm on panel B,F and G; 45μm on panels C and D; 28 μm in panel E.

5.3.3 Distribution of ApoJ in FBD and FDD

In the FBD cases the anti-ApoJ antibody strongly labelled the blood vessels with amyloid deposition, in addition to both amyloid plaques and 'diffuse' preamyloid deposits. Therefore the staining pattern seen in ApoJ immunohistochemistry closely overlapped with that seen in Ab338 immunohistochemistry. In FDD the ApoJ staining pattern also closely mimicked that seen in ADan immunohistochemistry, with both amyloid-laden blood vessels and preamyloid deposits being stained. The antibody recognizing ApoJ strongly labelled all affected amyloid-laden blood vessels of all sizes including capillaries in the AD cases, including the cotton wool plaques. In general, the staining pattern seen in ApoJ immunohistochemistry was similar to that seen in Aβ immunohistochemistry in that the anti-ApoJ antibody stained all plaques types, perivascular lesions as well as subpial deposits, irrespective of whether they were of amyloid or diffuse/preamyloid nature. Nevertheless, amyloid lesions were usually more strongly stained than the diffuse/preamyloid Aβ lesions were.

5.3.4 Distribution of SAP in FBD and FDD

In FBD, the amyloid structures that stained with Congo red and thioflavine-S were also strongly positive with the antibody to SAP. The large and small amyloid plaques were all positively stained with the anti-SAP antibody (table 21) (figure 5.5A). The intensity of the SAP immunoreactivity varied throughout the plaque, the large cored plaques found within the CA4 had intensely stained cores, but the staining was weaker towards the outer limits of the plaques (figure 5.5A insert). Within the CA1 subregion of the hippocampus, all arteries and arterioles with CAA showed positivity for SAP (figure 5.5B & 5.5C), with a small proportion of capillaries affected by amyloid deposition

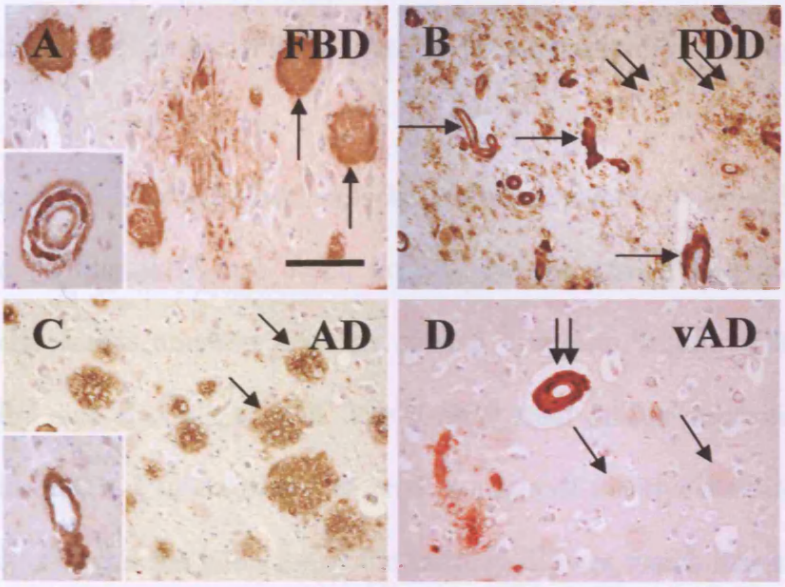

Figure 5.4: ApoJ immunohistochemistry in FBD, FDD, AD and vAD; The anti-ApoJ antibody strongly labelled the amyloid plaques and amyloid-laden blood vessels (large amyloid plaques (arrows) in CA4 of the hippocampus and arteriole, insert). In FDD ApoJ positive diffuse parenchymal deposits in the CA1 (double arrows), together with amyloid-laden blood vessels (arrows). In AD the amyloid plaques are shown labelled with the anti-ApoJ antibody (arrows) with amyloid-laden blood vessels demonstrated in the insert. In vAD the CAA showed intense labelling (double arrow) with the cotton wool plaques showing a weaker labelling intensity (arrows). Bar on panel A represents 100μm in A and D; 250μm on B & C.

were positive for SAP. The diffuse parenchymal lesions showed weak patchy positivity. The anti-SAP antibody stained the NFTs including ghost tangles in FBD, with the NFTs in the pre-α clusters of the entorhinal cortex showing a particularly strong staining (data not shown).

In FDD all amyloid affected blood vessels, including arteries (figure 5.5E, asterisk), arterioles and capillaries (figure 5.5D, arrow), showed strong immunoreactivity for SAP. The perivascular amyloid deposits around arterioles (figure 5.5E, arrow) and capillaries were also strongly stained. The parenchymal diffuse deposits were weakly positive (figure 5.5D, double arrow). A small amount of positive staining was seen in the subpial regions, but the intensity of the staining did not match that seen within the blood vessels. No NFTs were found to be SAP immuno-positive in FDD.

In AD the staining pattern mirrored that seen within FBD and FDD with all amyloid structures, both plaque (figure 5.5F) and vascular (figure 5.5F, insert), showing strong staining with the anti-SAP antibody, while diffuse deposits were weakly stained. In variant AD the amyloid-laden blood vessels showed strong staining with the anti-SAP antibody (figure 5.5G, arrow), whereas a weaker staining pattern was observed in the cotton wool plaques (figure 5.5G, double arrow). NFTs were also found to be positive in both the sporadic and variant AD cases (data not shown).

5.3.5 Distribution of ACT in FBD and FDD

In FBD amyloid plaques were positive for ACT (figure 5.6A) in both the CA1 and CA4 subregions of the hippocampus (table 21). The large plaques of CA4 were stained with equal intensity in the core and the periphery. All blood vessels affected by ABri deposition were positive for ACT (figure 5.6A, insert) (table 21). Perivascular plaques stained with ABri were positive for ACT (figure 5.6A, insert). The parenchymal diffuse

deposits were weakly and patchily labelled with the anti-ACT antibody. In FBD NFTs were also positive for ACT, with the majority being in the CA1 subregion.

In FDD all blood vessels affected by ADan deposition were positive for ACT and the perivascular plaques were also positive for ACT (figure 5.6B, arrow). The parenchymal diffuse plaques showed weak positivity (figure 5.6B, double arrow) and the hippocampal NFTs remained unstained.

In AD the staining pattern mirrored that seen within FBD and FDD with all amyloid structures, both plaque (figure 5.6C, arrowhead) and vascular (figure 5.6C, insert), showing strong staining with the anti-ACT antibody. The diffuse deposits usually showed weaker positivity for ACT, although the cotton wool plaques were more strongly labelled (figure 5.6D, double arrow). The amyloid-laden blood vessels in vAD showed strong labelling for the anti-ACT antibody (figure 5.6D, arrow). No NFTs were shown to be positive with the anti-ACT antibody within the AD cases studied.

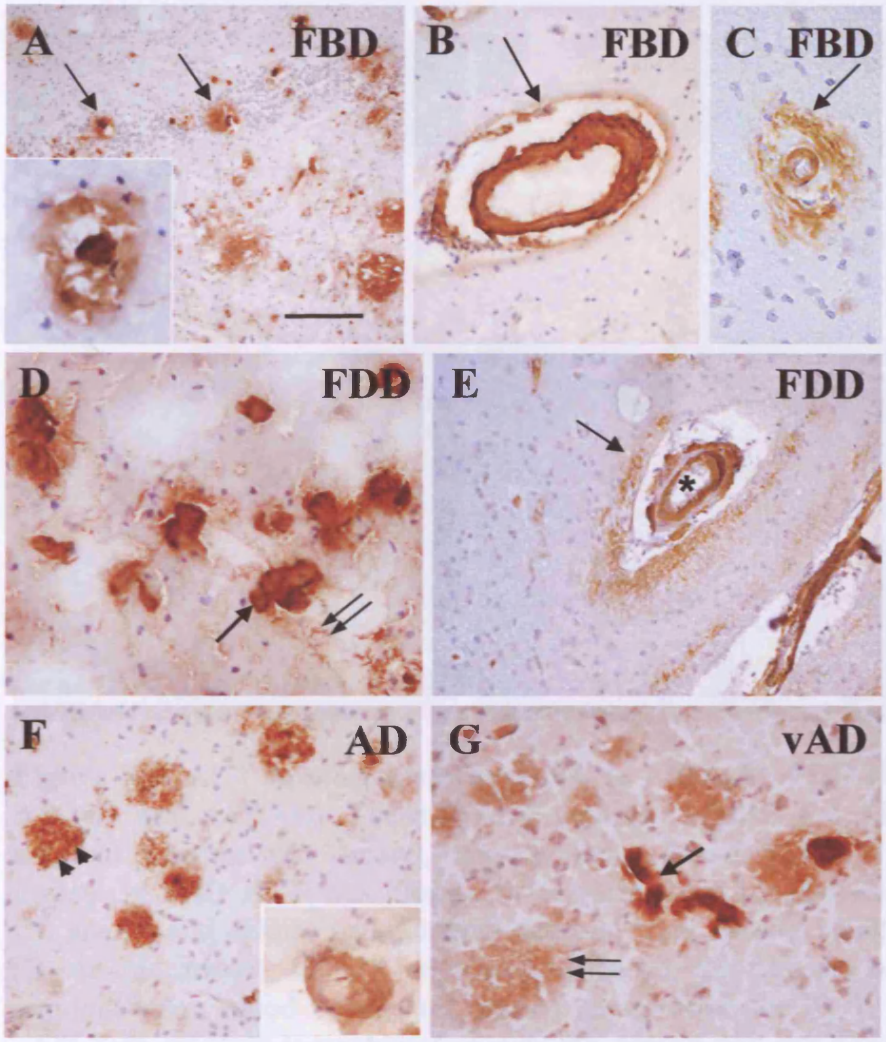

Figure 5.4: Serum amyloid P (SAP) immunohistochemistry in FBD (A-C), FDD (D & E), AD (F) and vAD (G). In FBD amyloid plaques (A, arrow and insert showing a large hippocampal plaque with higher magnification), amyloid-laden blood vessels (B, arrow) and perivascular amyloid plaques (C, arrow). In FDD positive staining was found in vascular (D, arrow) and perivascular amyloid (E, arrow). Preamyloid ADan deposits showed weak staining for SAP (D, double arrow). In AD both amyloid plaques (F, arrowheads) and amyloid-laden blood vessels (F, insert) were positive for SAP. In vAD an intense staining pattern was observed within the amyloid-laden blood vessels (G, arrow) and a weaker staining pattern observed in the diffuse cotton wool plaques (G, double arrow). Bar in panel A represent 250μm in A; 100μm in panel B, D, E and F; 45μm in panels C and G.

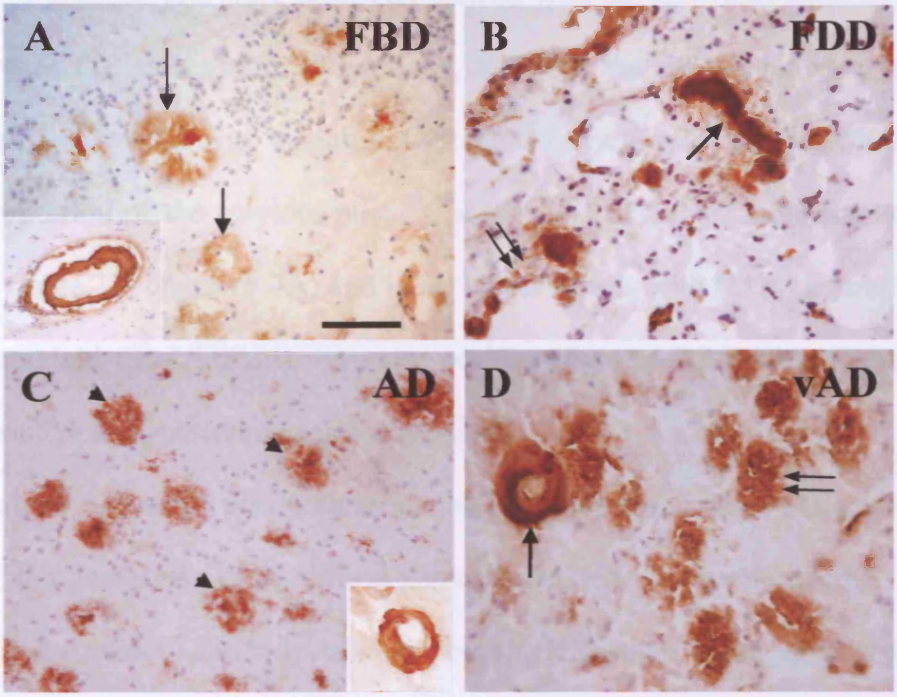

Figure 5.6: ACT immunohistochemistry in FBD (A), FDD (B), AD (C) and vAD (D). The anti-ACT antibody labelled the ABri amyloid plaques (A, arrow), amyloid-laden blood vessels (A, insert). In FDD ACT was present in amyloid-laden blood vessels (B, arrow) and diffuse parenchymal deposits were weakly labelled (B, double arrow). In AD amyloid plaques (C, arrowheads) and amyloid-laden blood vessels (C, insert) are positive for ACT. In vAD both amyloid-laden blood vessels (D, arrow) and the diffuse deposits (D, double arrow) showed an intense staining pattern for ACT. Bar in panel A represents 250μm in A and C; 100μm in panels B and D.

5.3.6 Distribution of cystatin C in FBD and FDD

All the amyloid deposits that were positively stained with the anti-ABri antibody were also stained with the anti-cystatin C antibody, although the overall intensity of the staining was slightly weaker with the latter. Cystatin C immunoreactivity was found in a significant proportion of the amyloid plaques of the CA1 and CA4 subregions of the hippocampus (table 21) (figure 5.7A) and in all blood vessels with CAA (figure 5.7C). Perivascular amyloid ABri deposits were also positive (figure 5.7C, double arrow), but the diffuse preamyloid deposits remained unstained.

In FDD cystatin C deposition was present in amyloid-laden blood vessels (figure 5.7D, double arrow) but no staining of the diffuse parenchymal deposits was detected.

In AD the anti-cystatin C antibody labelled the amyloid-laden blood vessels (figure 5.7E, insert) along with a few weakly positive plaques (figure 5.7E, arrowheads). Amyloid-laden blood vessels found in vAD showed strong labelling with the anti-cystatin C antibody (figure 5.7F, arrow) although the cotton wool plaques remained unstained (data not shown).

No NFTs were found to be positive with anti-cystatin C antibody in any of the diseases studied.

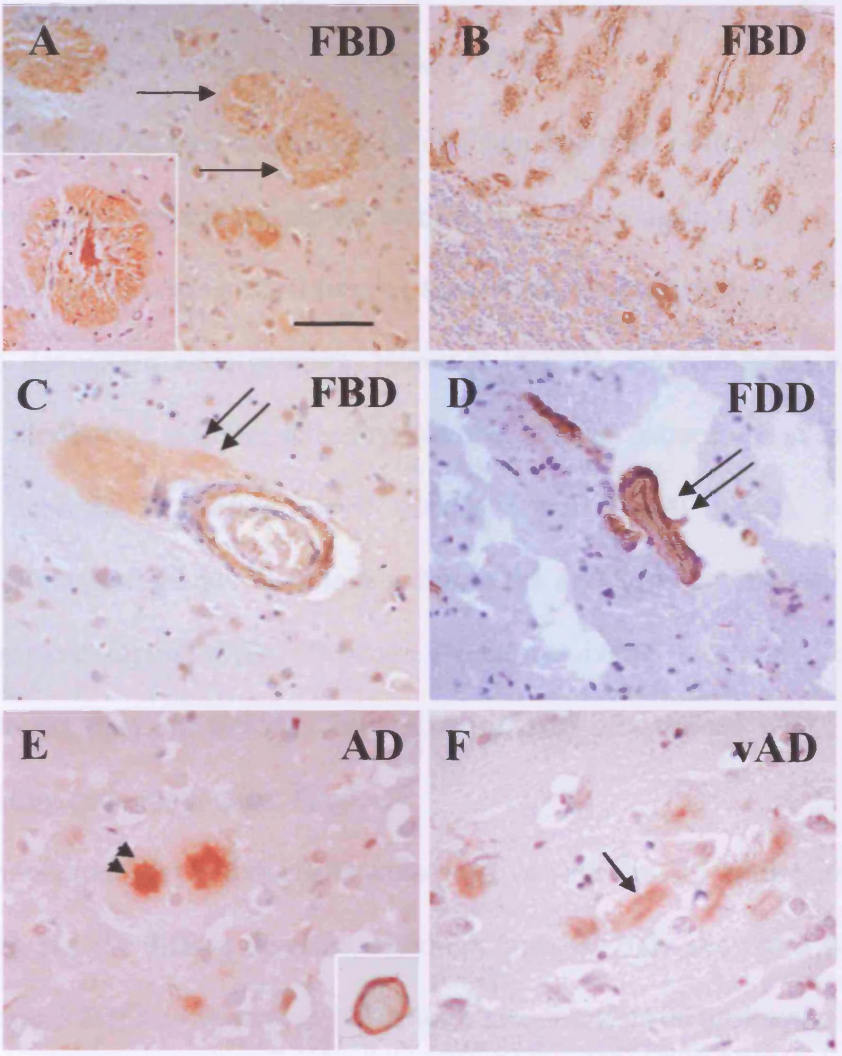

Figure 5.7: Cystatin C immunohistochemistry in FBD (A-C), FDD (D), AD (E) and vAD (F). The anti-cystatin C antibody strongly labelled the ABri amyloid plaques demonstrated in the hippocampus (A, arrows and insert), and cerebellum (B), amyloid-laden blood vessels (C), showing a perivascular deposit (C, double arrow). In FDD only blood vessels affected by ADan amyloid deposition were stained (D, double arrow). Cystatin C positive amyloid plaques (E, arrowheads) and amyloid-laden blood vessels (E, insert) in AD. In vAD blood vessels with CAA (F, arrow) showed strong staining while the diffuse deposits were negative. Bar in panel A represents 250μm in A & D; 500μm on panel B, 100μm on panels C, E and F;

5.3.7 Distribution of heperan sulphate proteoglycans in FBD and FDD

5.3.7.1 Distribution of agrin in FBD and FDD

JM-72 and BI-31, the two antibodies recognising the core protein of agrin, showed similar staining patterns and stained the same structures. As agrin is present in basement membranes all blood vessels regardless of size, whether unaffected or severely affected by amyloid deposition were positive. However in FBD, amyloid-laden blood vessels showed an increase in staining intensity and the staining pattern was clearly different from that seen in unaffected blood vessels (figure 5.8A, insert). All types of hippocampal amyloid plaque were labelled with the anti-agrin antibodies (figure 5.8A, arrow). The parenchymal diffuse deposits were extensively, but usually less intensely stained than the amyloid lesions. The anti-agrin antibody stained NFTs and NTs in FBD, including occasional ghost tangles.

In FDD the vascular amyloid deposits were positive with the anti-agrin antibody (figure 5.8B arrow), but the diffuse deposits, although positive, only showed a weak staining pattern (figure 5.8B, double arrow). NFTs were also found to be positive in FDD.

In AD including the cotton wool variants the amyloid-laden blood vessels (figure 5.8C insert, 5.8D, arrow) were strongly labelled by the anti-agrin antibodies as were the amyloid plaques (figure 5.8C double arrow) and cotton wool plaques (figure 5.8D double arrow). NFTs were found to be positive in both sporadic and variant AD.

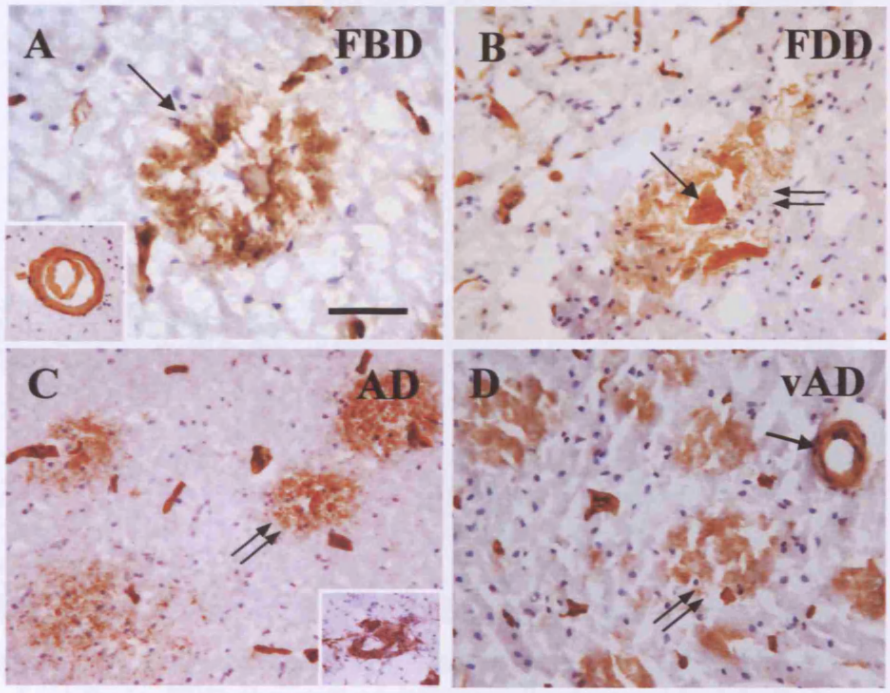

Figure 5.8: Agrin immunohistochemistry in FBD, FDD, AD and vAD. As agrin is a normal component of the basement membrane, all blood vessels are stained with the anti-agrin antibody. However, agrin is also deposited in the ABri amyloid plaques (A, arrow) and blood vessels with CAA (A, insert). In FDD blood vessels with amyloid deposition were positive for agrin (B, arrow), while only occasional diffuse deposits were positive for agrin (B, double arrow). In AD both amyloid plaques (C, double arrow) and blood vessels with CAA (C, insert) were positive for agrin. In vAD a strong intense staining pattern was observed within both the amyloid-laden blood vessels (D, arrow) and the diffuse cotton wool plaques (D, double arrow). Bar on panels A represents 45μm in panels A; 100μm on panels B and D; 250 μm on panel C.

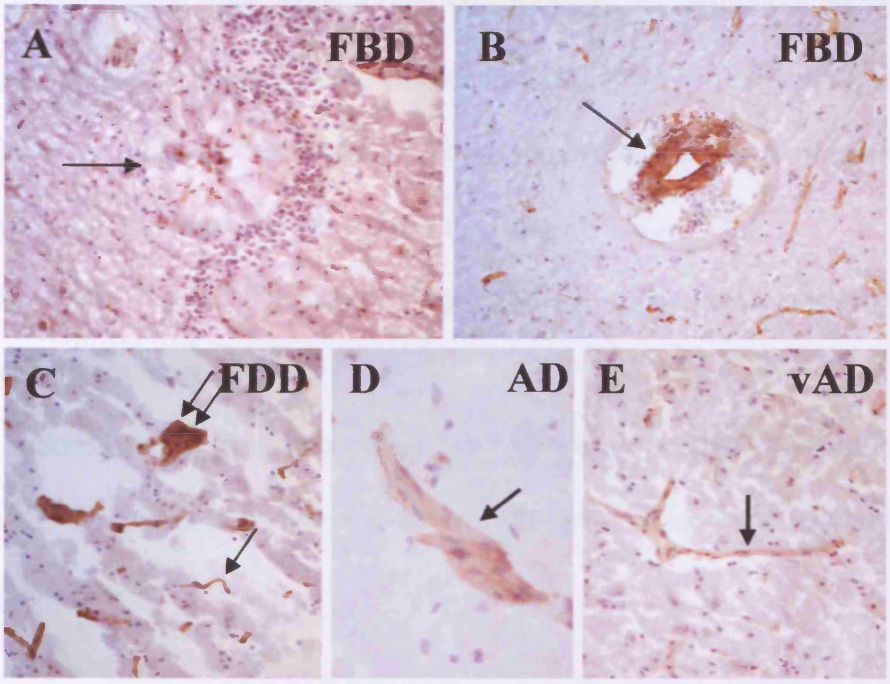

Figure 5.9: Perlecan immunohistochemistry in FBD, FDD, AD and vAD. In FBD the anti-perlecan antibody weakly labelled a proportion of ABri amyloid plaques (A, arrow) and amyloid-laden vessels of all sizes were weakly stained in FBD (B, arrow). In FDD amyloid-laden blood vessels were positive for perlecan (C: arteriole- double arrow; capillary – arrow). The parenchymal preamyloid ABri and ADan lesions were negative in both diseases. In AD amyloid plaques and amyloid-laden blood vessels were negative perlecan, but positive staining was seen in vessels with normal morphology (D, arrow) A similar pattern was seen in vAD with only blood vessels with normal morphology showing positive staining for perlecan (E, arrow). Bar on panels A represents 100μm in panels A, B C and E; 28μm on panel D.

5.3.7.2 Distribution of perlecan in FBD and FDD

Similar to agrin, perlecan is present within the basement membrane and therefore, the majority of blood vessels were stained with this antibody. In addition, a small number of ABri amyloid plaques (figure 5.9A, arrow) and larger amyloid-laden blood vessels (figure 5.9B, arrow) showed patchy, weak staining with the anti-perlecan antibody, but the parenchymal diffuse deposits were always unstained.

In FDD a few blood vessels with amyloid were labelled (figure 5.9C) and parenchymal diffuse deposits were unstained.

In the AD controls no staining was present in amyloid or preamyloid lesions (figure 5.9D and 5.9E). No NFTs were found to be positive with anti-perlecan antibody in any of the diseases studied.

5.3.7.3 Distribution of syndecans in FBD and FDD

Three antibodies directed against different members of the syndecan family, 2E9 (anti-syndecan-1, -3), 10H4 (anti-syndecan-2) and IC7 (anti-syndecan-3), were used to investigate the expression of these cell membrane associated HSPGs.

In FBD both syndecan-2 and syndecan-3 were present in amyloid-laden blood vessels (figure 5.10A, insert) and amyloid plaques (figure 5.10A, double arrow), while the parenchymal diffuse ABri deposits showed weak, patchy positivity for syndecan 2. The antibody recognizing syndecan-1, -3 showed some weak positivity in a proportion of the amyloid lesions, but did not stain the parenchymal diffuse lesions.

In FDD, in a pattern similar to that seen in FBD, syndecan-2 and syndecan-3 were present in the blood vessels with CAA (figure 5.10B, arrow). Syndecan-2 was more consistently present in the parenchymal preamyloid lesions than syndecan-3. Syndecan-

1,-3 immunohistochemistry showed mostly a similar pattern to that in FBD, but labelling of a proportion of the parenchymal diffuse deposits was also noted.

In AD the pattern of staining for syndecans was similar to that seen in FBD with syndecan-2 and syndecan-3 being present in the vascular (figure 5.10C, insert) and parenchymal amyloid lesions (figure 5.10C, arrowheads). Syndecan-3 staining was, however, also present in Aβ parenchymal diffuse deposits, but not in similar ABri lesions. The antibody to syndecan-1, -3 mostly stained amyloid plaques. In variant AD both the cotton wool plaques and blood vessels with CAA showed significant staining for syndecan-3, while they showed weaker and more patchy reactivity for syndecan-2 (figure 5.10D) and syndecan-1,-3.

5.3.7.4 Distribution of glypican-1 in FBD and FDD

Immunohistochemistry with the S1 antibody directed against the glypican-1 core protein demonstrated that a significant proportion of blood vessels affected by amyloid deposition contained glypican-1 in both FBD (figure 5.11B and 5.11B, insert) and FDD (figure 5.11C, arrow and 5.11D) as did the amyloid plaques in FBD (figure 5.11A, arrow). The diffuse parenchymal deposits were also stained in both FBD and FDD.

In AD all vascular (figure 5.11E, insert) and parenchymal amyloid lesions (figure 5.11E, arrowheads) were positive for glypican-1. The cotton wool plaques in the variant AD cases were positive for glypican-1 (figure 5.11F, double arrow) and the amyloid-laden blood vessels showed a strong staining pattern with the anti-glypican-1 antibody (figure 5.11F, arrow). A proportion of the NFTs were positive in the hippocampus the in FBD and AD cases.

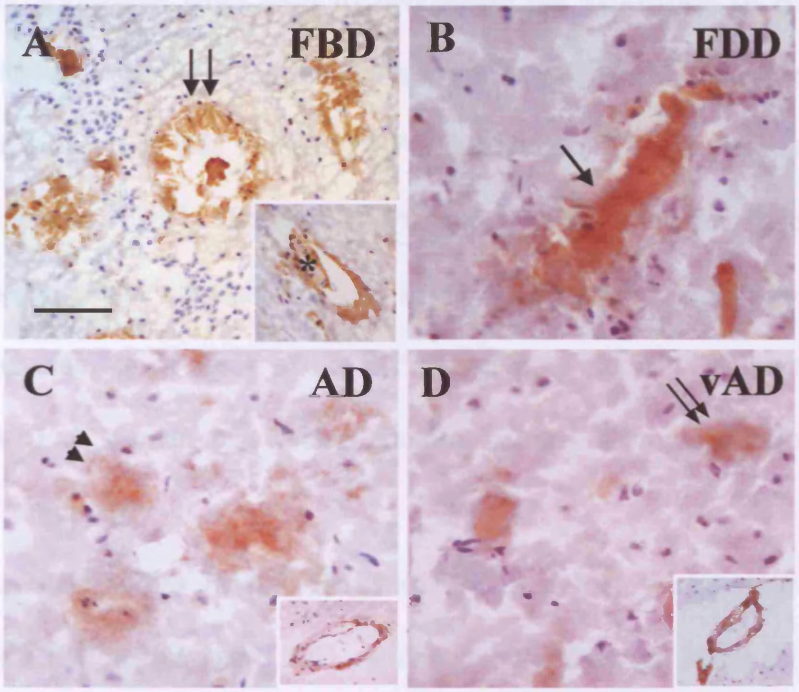

Figure 5.10: Syndecan-2 immunohistochemistry in FBD, FDD, AD and vAD. In FBD syndecan-2 stained both amyloid plaques (A, double arrow) and amyloid-laden blood vessels (A, insert asterisk), while the parenchymal diffuse ABri deposits showed weak patchy positivity (data not shown). In FDD anti-syndecan-2 antibody stained amyloid-laden blood vessels (B, arrow), but not the preamyloid parenchymal deposits (data not shown). In AD both amyloid plaques (C, arrowheads) and blood vessels with CAA (C, insert) were positive for syndecan-2. In vAD staining was observed within the amyloid-laden blood vessels (D, insert) and the diffuse cotton wool plaques (D, double arrow). Bar on panel A represents 100μm on A; 45μm on panel B,C and D.

5.3.7.5 Distribution of HS GAGs in FBD and FDD

Three different antibodies were used to investigate the expression of HS GAG side chains: the JM403 and JM13 antibodies recognizing different epitopes in the HS polysaccharide side chain and the pan-HSPG antibody 3G10 that was raised against heparitinase-digested HSPGs. The pan-HSPG and JM403 antibodies stained amyloid-laden blood vessels and amyloid plaques in FBD (figure 5.12A, arrow and 5.12B, asterisk). Weak staining of some of the diffuse, preamyloid ABri deposits was noted (data not shown). A similar, but weaker staining pattern of amyloid lesions was seen with the JM13 antibody.

In FDD all three antibodies JM403, JM13 and 3G10 stained the amyloid-laden blood vessels (figure 5.12C, arrow and 5.12D, double arrow), although 3G10 showed weaker staining of fewer blood vessels than the other two antibodies. The parenchymal diffuse deposits showed patchy weak staining for JM403 and 3G10 (figure 5.12D, double arrow).

In AD, including variant AD, all three antibodies labelled the amyloid-laden blood vessels (figure 5.12F, arrow), but the intensity of labelling with JM13 in variant AD was less. In AD amyloid plaques were labelled with variable intensity as were the diffuse Aβ deposits (figure 5.12E, arrowheads). The cotton wool plaques were labelled by all three antibodies (figure 5.12F, double arrows), although the staining seen with JM13 and 3G10 was the weakest.

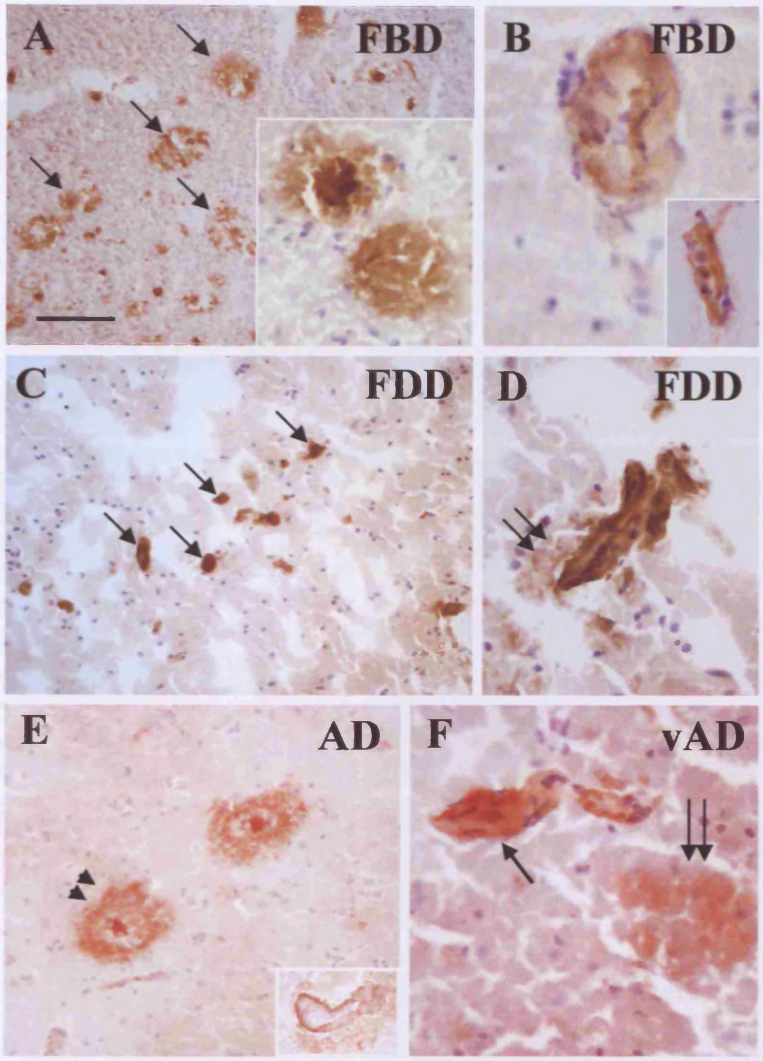

Figure 5.11: Glypican-1 immunohistochemistry in FBD (A & B), FDD (C & D), AD (E) and vAD (F). The anti-glypican antibody strongly labelled the ABri amyloid plaques (A, arrows). The amyloid-laden blood vessels of all sizes were similarly strongly stained in FBD (B) and FDD (C, arrows and D). In FDD perivascular deposits were also positive for glypican-1 (D, double arrow). In AD amyloid plaques were positive for glypican-1 (E, arrowheads) as were amyloid-laden blood vessels (E, insert). In vAD both blood vessels with CAA (F, arrow) and diffuse deposits (D, double arrow) showed equal intensity of staining. Bar in panel A represents 250μm on A; 100μm on panel C and E; 45μm on panel D and F; 28μm on panels B.

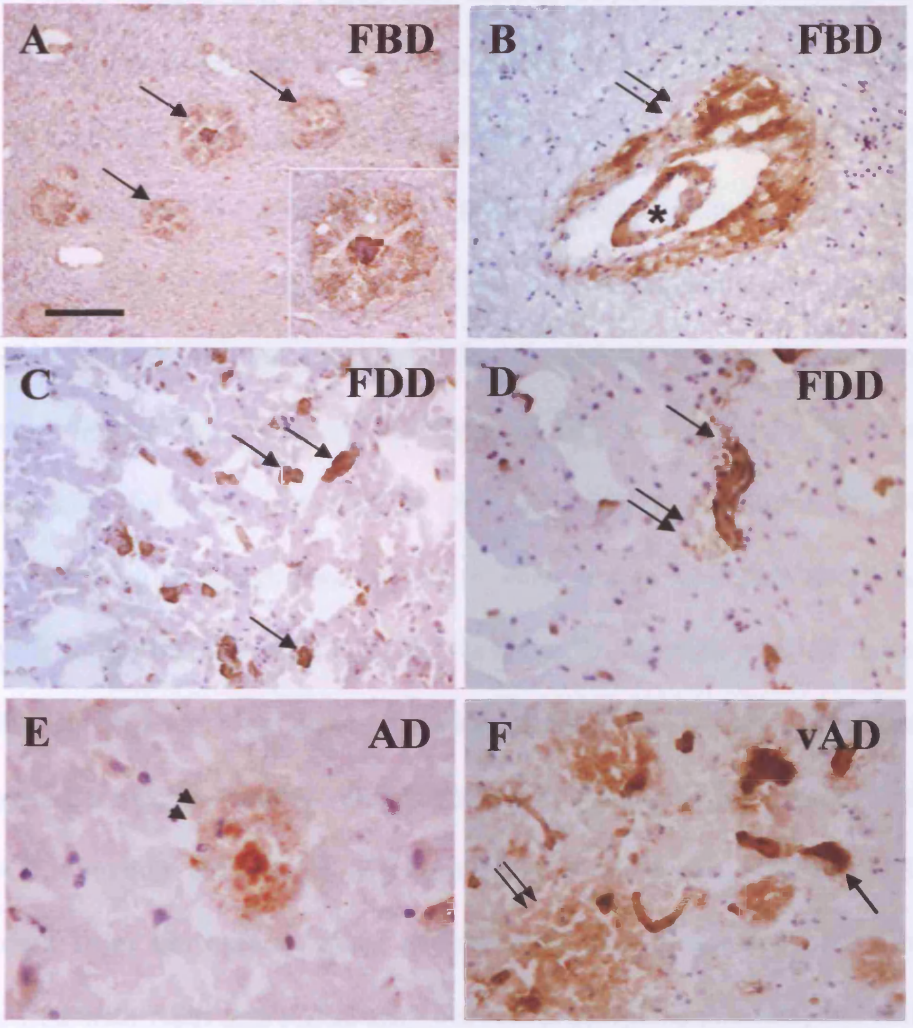

Figure 5.12: HS GAG (JM403) immunohistochemistry in FBD (A&B), FDD (C&D), AD (E) and vAD (F). In FBD positive staining for JM403 (HS side chains) was seen in amyloid plaques (A, arrows) and amyloid-laden blood vessels (B: double arrow pointing to a perivascular plaque surrounding an arteriole, asterisk). In FDD JM403 immunoreactivity was seen in amyloid-laden blood vessels (C: affected capillaries highlighted by arrows; D: faintly labelled perivascular amyloid lesion). In AD amyloid plaques were positive for HS GAG side chains (E, arrowheads). In vAD both blood vessels with CAA (F, arrow) and diffuse deposits were positive for HS GAG (JM403) (F, double arrow). Bar in panel A represents 250μm in A; 100μm in all other panels; 28 μm in panel E; 45 μm in panel F.

5.4 Discussion

It has been proposed that a significant number of AAPs or 'pathological chaperones' may have a prominent role in the pathogenesis of amyloid-linked cerebral diseases *in vivo* in that they are able to influence the process of amyloid fibril formation by stabilizing amyloid fibrils once they have formed (Alexandrescu, 2005). This, together with recent *in vitro* data suggesting that the protofibrillary intermediates rather than the amyloid fibrils are the protein species that are linked to neurodegeneration, may have important implications for our understanding of the pathogenesis of a number of cerebral amyloid conditions such as AD (Caughey & Lansbury, Jr., 2003). Of the cerebral amyloid diseases most of the *in vitro* and *in vivo* data about AAPs that are available in the literature relate to AD. In order to establish whether these findings are specific to AD or may have a wider implication for the understanding of the pathogenesis of other cerebral amyloidoses, we systematically investigated the patterns of AAP deposition in the novel *BRI2* gene-related dementias, FBD and FDD.

The data from the current study demonstrated that a number of AAPs are closely associated with ABri and ADan amyloid and preamyloid parenchymal lesions and also CAA, in FBD and FDD in a manner mostly similar to that seen in AD. A group of AAPs including ApoE, ApoJ, agrin, glypican and HS GAG side chains rather extensively co-deposited with both amyloid and preamyloid ABri and ADan lesions (figure 5.13). The remainder was predominantly seen in relation to parenchymal and vascular amyloid lesions, although most of the anti-AAP antibodies labelled at least some of the diffuse (preamyloid) ABri and ADan parenchymal lesions. The rather significant co-deposition of some of the AAPs in diffuse ABri, ADan or Aβ lesions including the cotton wool plaques seen in variant AD may be interpreted in at least two ways. Either AAP binding to parenchymal or vascular protein deposits is not entirely

dependent on amyloid conformation or, alternatively, the binding of AAPs to ABri, ADan and Aβ preamyloid lesions, including the cotton wool plaques, reflects that such lesions contain variable numbers of amyloid fibrils. The latter is supported by their weak labelling with thioflavine-S and the observation that preamyloid lesions in FBD and FDD and the cotton wool plaques in variant AD can be demonstrated by iEM to contain sparse amyloid fibrils, in addition to amorphous electron dense material (Holton *et al.*, 2001a; Holton *et al.*, 2002a).

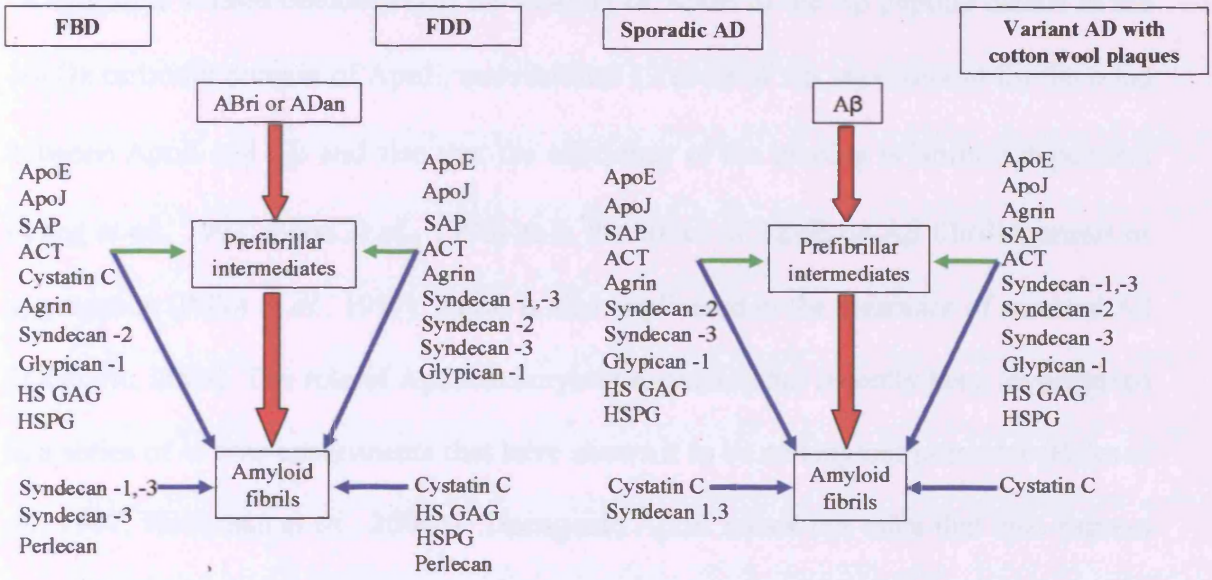

Figure 5.13: *A schematic diagram summarizing the deposition of AAPs in the BRI2-gene related dementias. The AAPs are listed for the BRI2-gene related dementias, FBD and FDD, AD and variant AD with cotton wool plaques. The diagram shows the progression from soluble peptides (ABri, ADan and Aβ) through prefibrillar intermediates to amyloid fibrils indicated with the red arrows. The AAPs co-deposited with the prefibrillar intermediates (diffuse deposits) are indicated with the green arrows. AAPs which are co-deposited with the proteins in amyloid conformation, either amyloid plaques or amyloid-laden blood vessels, are indicated with the blue arrows. In both AD and vAD perlecan not co-deposited with either prefibrillar intermediates or amyloid fibrils and is therefore not represented on the diagram.*

ApoE and ApoJ have been previously shown to be present in Aβ amyloid in AD and with other tested cerebral and systemic amyloids (Namba *et al.*, 1991; Wisniewski & Frangione, 1992). The current investigations have shown that ApoE and ApoJ (see

chapter 6) are extensively associated with ABri and ADan amyloid and pre-amyloid lesions, suggesting that the amyloid conformational state of ABri, ADan and Aβ is not a prerequisite of the co-deposition of apolipoprotein. These findings are consistent with the notion the ApoE and ApoJ may exercise an early influence on the process of ABri and ADan fibril formation. *In vitro* and *in vivo* data indicate that both apolipoproteins have a major role in Aβ fibrillogenesis in that it can interact with Aβ and facilitate the conversion of soluble into fibrillar Aβ with high β-sheet content (Holtzman, 2004). Biochemical studies demonstrated the binding of ApoE to the Aβ peptide occurs in the 10kDa carboxyl domain of ApoE, and residues 12 to 28 of Aβ are essential for the bond between ApoE and Aβ and also that the efficiency of the binding is isoform dependent (Yang *et al.*, 1997; Zhou *et al.*, 1996) as is the effect of ApoE on Aβ fibrillogenesis or aggregation (Pillot *et al.*, 1997). ApoE is also implicated in the clearance of cerebral Aβ (Zlokovic, 2004). The role of ApoE in amyloid formation has recently been investigated in a series of *in vivo* experiments that have shown it to be an amyloid promoter (Bales *et al.*, 1997; Holtzman *et al.*, 2000b). Transgenic ApoE knock out mice that also express human APP showed a variable amount and speed of amyloid deposition that was dependent on the number of copies of the ApoE gene (Bales *et al.*, 1997). Mature, fibrillar amyloid never formed in the $ApoE^{-/-}$ mice. These results suggest that mouse ApoE was influencing Aβ metabolism promoting the conversion of soluble Aβ to a species rich in β-sheet conformation. Our results correlate with these *in vivo* experiments and transgenic animal models in that we observed ApoE immunolabelling of all lesion types regardless of the conformational state of the respective amyloid protein in FBD, FDD and AD. The diffuse parenchymal deposits found in FBD and FDD were also equally and intensely stained, consistant with the hypothesis that ApoE binding is early and has a role in promoting amyloid formation. There are also data to

suggest that ApoE binding also protects the amyloid formed from proteolytic breakdown (Wisniewski *et al.*, 1994a). Studies also suggest that ApoJ is produced at similar levels to ApoE (May & Finch, 1992) and similarly acts as an Aβ chaperone, regulating the conversion of Aβ to insoluble forms (Oda *et al.*, 1995; Lambert *et al.*, 1998). An *in vivo* study has been carried out to assess the effects of ApoJ on Aβ metabolism and structure using knockout mice (DeMattos *et al.*, 2004). PDAPP mice were compared with PDAPP $ApoJ^{-/-}$ and PDAPP $ApoE^{-/-}/ApoJ^{-/-}$. The results were interesting because the single knockout mice, PDAPP $ApoJ^{-/-}$ showed significantly less thioflavine-S positive material than would be seen with the ApoJ gene present. Since both ApoE and ApoJ independently contribute to Aβ fibril formation *in vivo* (Bales *et al.*, 1997; Bales *et al.*, 1999; Holtzman *et al.*, 2000b), you might expect that there would be less fibril formation in the PDAPP $ApoE^{-/-}/ApoJ^{-/-}$ mice. However, within these mice greater levels of thioflavine-S positive deposits were found than in the normal genotypes. The magnitude of the effect of removing both molecules on Aβ levels and onset of deposition was similar in extent to that described for overexpressing presenilin mutations in APP transgenic mice (Duff *et al.*, 1996; Borchelt *et al.*, 1997; DeMattos *et al.*, 2004). This study shows that ApoE and ApoJ cooperatively suppress Aβ deposition and that ApoE is contributing to this effect via directly influencing the metabolic fate of soluble, extracellular Aβ (DeMattos *et al.*, 2004).

No similar data are available as yet about the significance of ApoE and ApoJ in the regulation of the fibrillisation process and/or clearance of ABri and ADan. For this further *in vitro* studies, and once transgenic models of FBD and FDD have become available, *in vivo* experiments are required.

As in AD (Coria *et al.*, 1988) SAP immunoreactivity was observed in all amyloid-laden blood vessels and amyloid plaques within the FBD and FDD and the diffuse

parenchymal deposits were only weakly labelled, including variant AD (*PS1* ΔI83/ΔM84) with cotton wool plaques showed positive immunoreactivity within the pre-amyloid structures. This observation is in keeping with previous investigations such as that demonstrated by using iEM that anti-SAP antibodies decorate amyloid fibrils, but are not associated with protofibrils (Holm *et al.*, 2000). Although originally SAP was thought to be produced solely by the liver, more recent data suggest that it is also synthesized in the brain, particularly by pyramidal neurons, and that its synthesis is up-regulated in AD (Yasojima *et al.*, 2000). SAP has a major role in fibrillogenesis as under experimental conditions it stabilizes and protects fibrils from phagocytic and proteolytic degradation and amyloid deposition is reduced and delayed in SAP knockout mice (Botto *et al.*, 1997). The Ca^{2+}-dependent protective effect of SAP on amyloid fibrils may be due to its ability to enhance the strength and density of local amyloid inter-fibrillar interactions thus forming compact fibril networks with increased density of fibril entanglements (MacRaild *et al.*, 2004). The presence of SAP in ABri and ADan amyloid lesions and its relative paucity in the diffuse lesions is in keeping with previous studies showing that SAP is ubiquitously associated with all types of amyloid while it has little or no affinity for amyloid proteins in their native state (Coria *et al.*, 1988; Gallo *et al.*, 1994; Hamazaki, 1995; Pepys *et al.*, 1994).

These observations would also be in keeping with previous investigations demonstrating by iEM that SAP molecules bind to and coat the surface of mature amyloid fibrils, but not that of protofibrils composed of $A\beta_{1-42}$ (Holm *et al.*, 2000). The high level of labelling obsevred in the cotton wool plaques is apparently contrary not only to these previous studies, but also to a morphological study of variant AD in which no immunoreactivity for SAP in the cotton wool plaques was seen, although that study employed formalin fixed paraffin sections (Verkkoniemi *et al.*, 2001) while we used a

different antibody on frozen sections. The relative abundance of SAP in our preparations may suggest that the rather widely dispersed amyloid fibrils in the cotton wool plaques observed using Aβ iEM (personnal observation) are capable of efficient binding of SAP.

In this study we demonstrated that the acute phase protein ACT co-deposited with vascular ABri and ADan amyloids in FBD and FDD and it was also found in CAA within the AD controls, in addition to a significant proportion of amyloid plaques in both FBD and AD. ACT was also detected in ADan diffuse deposits and significantly in the Aβ diffuse lesions and cotton wool plaques. ACT can bind directly to the Aβ peptide *in vitro* and promote polymerization and fibrillization of synthetic Aβ peptide (Ma *et al.*, 1994), perhaps by initiating or catalyzing the self-assembly process (Janciauskiene *et al.*, 1996). Several *in vivo* observations also support the association between ACT and amyloid formation in AD: both amyloid and preamyloid lesions have been shown to contain ACT (Abraham *et al.*, 1988b; Picken *et al.*, 1990; Potter *et al.*, 1992), amyloid plaques are found in brain regions in which ACT mRNA and protein are over-expressed by astrocytes in AD (Potter *et al.*, 1992) and furthermore, transgenic mice with both ACT and human APP transgenes exhibit elevated total Aβ levels and increased amounts of Aβ deposits when compared with mice with only the APP transgene (Nilsson *et al.*, 2001). Genetic support for the involvement of ACT in AD was suggested by the observation that the inheritance of ACT-A allele, in which alanine replaces threonine at position -15 in the signal peptide, correlates with an increased risk of developing AD in ApoE ε4 carriers (Kamboh & DeKosky, 1995), although this observation was not confirmed by subsequent studies (Muller *et al.*, 1996;). Our finding of ACT deposition in ABri and ADan amyloid lesions is of particular interest as previous studies have suggested a direct role for ACT in amyloid formation in AD, but

not in other amyloid diseases (Abraham *et al.*, 1988a; Potter *et al.*, 1992; Abraham *et al.*, 1988b; Potter *et al.*, 1992). Further *in vitro* studies are required to elucidate the biochemical mechanisms of ACT binding to ABri and ADan and the subsequent effects on the aggregation and fibrillization of these two amyloid peptides.

We demonstrated a variable degree of co-localization of cystatin C with both ABri and ADan vascular and parenchymal amyloid lesions. Previous studies showed that cystatin C is also present in vascular Aβ in AD and also in senile plaques (Levy *et al.*, 2001; Vinters *et al.*, 1990). Whether the association of cystatin C with Aβ plays a primary role in amyloidosis of AD or it is a late event, in which cystatin C binds to the already formed Aβ amyloid fibrils is still unknown. Since cystatin C has cysteine protease inhibitory activity, it may play a role in protecting Aβ (or ABri and ADan) deposits from proteolytic degradation or together with ACT may be present as a result of an ongoing anti-inflammatory response that is present in relation to the amyloid lesions (Akiyama *et al.*, 2000; Eikelenboom *et al.*, 1991; Rostagno *et al.*, 2002).

We have found that HSPGs also co-deposit in ABri and ADan amyloid lesions, as has been shown for other forms of cerebral and systemic amyloidosis, supporting the view that one feature of all amyloids is the presence of highly sulphated proteoglycans (van Horssen *et al.*, 2003; Ancsin, 2003) which may directly contribute to the complex structure of the amyloid fibrils (Inoue *et al.*, 1999). Our data suggest that of the major HSPGs investigated agrin, glypican-1 and syndecans are significantly associated with both ABri and ADan vascular and parenchymal amyloid lesions and variably with preamyloid lesions. Although perlecan was shown to be a potent facilitator of Aβ fibril formation *in vitro* and it was initially described as a major HSPG in AD *in vivo* (Snow *et al.*, 1988; Snow *et al.*, 1994), this latter observation was not confirmed by recent studies using a well-characterized anti-perlecan antibody (van Horssen *et al.*, 2001;

Verbeek *et al.*, 1999). Using the same anti-perlecan antibody we observed only weak staining of a relatively small proportion of ABri plaques and CAA in both FBD and FDD, but saw no immunoreactivity in the AD controls. These findings are consistent with the notion that the HSPG core protein perlecan is unlikely to play a major pathogenic role in either FBD, FDD or AD. We also demonstrated co-localization of HS GAG side chains with ABri parenchymal amyloid lesions, blood vessels with CAA due to ABri, ADan or Aβ and less consistently with preamyloid lesions. HS GAGs are ubiquitously expressed in basal laminae and cell surfaces and can modulate the functions of proteins, such as growth factors or protease inhibitors (Ancsin, 2003). HS GAG accumulation has been observed in a number of human amyloid diseases *in vivo*, including AD and prion diseases (Perlmutter *et al.*, 1990; Snow *et al.*, 1988; Snow *et al.*, 1990). Furthermore, *in vitro* studies demonstrated that HS GAGs are able to promote a shift in the structure of Aβ from a predominantly random to a β-sheet-rich secondary structure and that they enhance fibril formation of a number of other proteins implicated in neurodegenerative diseases including prion protein, α-synuclein and tau (for review see Ancsin, 2003).

As deposition of the HSPG core protein agrin has previously been described only in relation to Aβ in AD (Cotman *et al.*, 2000; van Horssen *et al.*, 2001; Verbeek *et al.*, 1999) and in experimental AA amyloidosis (Wien *et al.*, 2004), our findings indicate that this basement membrane associated HSPG may have a more generic role in the pathogenesis of cerebral and systemic amyloid diseases. It has been shown that under experimental conditions agrin is able to bind, probably through its HS GAG side chains, to the fibrillar, but not to the soluble form of Aβ and that it is also able to stabilize and protect Aβ fibrils from proteolytic degradation (Cotman *et al.*, 2000).

The presence of AAPs in amyloid lesions in different diseases suggests a general participation of these molecules in amyloid formation and it is tempting to speculate that they may play a similar role in FBD and FDD to that proposed for other amyloidoses. However, further experimental studies are required to establish how AAPs bind to ABri and ADan and what effect this binding may have on the fibrillization of these two amyloid proteins, which are capable of initiating a neurodegenerative cascade. It also remains to be investigated whether AAPs, and, in particular, those which are normally associated with cell membranes, could influence the incorporation of the amyloid subunits into cell membranes and modulate the formation of the recently described ion-channel–like structures, thus contributing to the mechanism of cell death in these diseases (Quist *et al.*, 2005).

Chapter 6

Complement activation in BRI2 gene-related dementias.

Chapter 6 – Hypothesis and specific questions

In this chapter, I wished to investigate the hypothesis that activiation of the complement pathways is implicated in the pathogenesis of both FBD and FDD. The specific questions I wished to concentrate on were: 1) Are the complement pathways (classical and alternative) fully activated in both FBD and FDD?: 2) Is there a correlation between the conformational state of ABri and ADan and complement activation?

In relation to Aβ deposition activation of the complement pathways has been documented with implications for fibrillogenesis, host response and the mechanism of neurodegeneration. This study investigates by immunohistochemistry the presence of complement components of both the classical and alternative pathways and complement inhibitors in FBD and FDD, and seeks to establish whether the binding of the recognition protein C1q to ABri and ADan is dependent on the conformational state of these amyloid proteins. For this C1q immunohistochemistry was combined with thioflavine-S stain and evaluated by confocal microscopy.

6.1 Introduction

In the epidemiologically most important neurodegenerative disease, AD, the Aβ protein forms extracellular plaques and can be deposited in blood vessels. Evidence suggests that cerebral inflammation is associated with AD pathogenesis (Akiyama *et al.*, 2000), and inflammatory mediators, immunologic factors and activation of the complement pathways have been implicated in this process (Vidal *et al.*, 2000a). The complement proteins have been shown by previous studies to be associated with Aβ amyloid plaques (Head *et al.*, 2001; Stoltzner *et al.*, 2000; Webster *et al.*, 1997), amyloid laden blood vessels (Verbeek *et al.*, 1998) and NFTs (Shen *et al.*, 2001; Schwab *et al.*, 1996a) *in vivo*.

In brief the complement pathways, classical (see section 1.9.2.1) and alternative (see section 1.9.2.2), consist of over 20 components that can be sequentially activated as an amplifying cascade. Antibody dependent and antibody independent activation of the complement system can lead to inflammation, opsonization and cytolysis. The classical pathway (C1 to C9) can be activated principally by the binding of the first component, C1q of C1, to an antibody or other activator. This triggers the proteolytic cascade culminating in the formation of the membrane attack complex (MAC or C5b-9), which

damages cells by forming transmembrane lytic pores, leading to cellular injury and the recruitment and activation of immune cells to the site of complement activation (Strohmeyer *et al.*, 2000). Aβ has been shown to bind to C1q and activate the classical pathway (Afagh *et al.*, 1996; Rogers *et al.*, 1992a). The alternative pathway provides an antibody independent route of complement activation, which has also been shown to be activated by Aβ (Strohmeyer *et al.*, 2000). The initiation of this pathway occurs through the hydrolysis of circulating C3, activated in the absence of antibodies and is therefore a mechanism of innate immunity. In addition to the proteins that compose the complement pathways there are also several regulatory proteins, of which Vn (Walker & McGeer, 1998; Schvartz *et al.*, 1999) and ApoJ (clusterin or SP40-40) (Lidstrom *et al.*, 1998; McGeer *et al.*, 1992) are complement inhibitors, which convert the hydrophobic MAC into a hydrophilic structure thus preventing its insertion into cell membranes.

As demonstrated in chapters 3 and 4 the *BRI2* gene-related dementias are also characterized pathologically by extracellular fibrillar and non-fibrillar protein deposition in combination with neurofibrillary degeneration (Stromgren *et al.*, 1970; Holton *et al.*, 2001; Holton *et al.*, 2002; Plant *et al.*, 1990; Revesz *et al.*, 1999). Chapters 3 and 4 also show that the overall patterns of deposition of ABri and ADan in the CNS of affected individuals are similar to those of Aβ in AD and that the parenchymal deposits are mostly of amyloid (fibrillar) nature in FBD, but are predominantly of the preamyloid (non-fibrillar) type in FDD.

This study aimed to investigate *in vivo* whether, as in AD, complement activation products are also implicated in the pathogenesis of FBD and FDD. To answer this question sequential tissue sections of FBD and FDD cases together with appropriate controls were used for immunohistochemistry using antibodies to the classical pathway recognition (C1q) and activation (C3d, C4d) components, an alternative pathway activation product (Bb), a proteolytic derivative (iC3b) common to both pathways, MAC representing the terminal stage of activation in either pathway, and its physiologic inhibitors ApoJ and Vn. In order to establish a correlation between the activation/deposition of complement components and inhibitors on one hand and the conformational state of ABri and ADan on the other, tissue sections were also stained with Congo red and thioflavine-S. Double immunohistochemical staining with an

antibody to either of the amyloid proteins and thioflavine-S was also carried out and the results were evaluated with confocal microscopy.

6.2 Material and Methods

6.2.1 Tissue

Brain samples from 5 FBD, 3 FDD, 5 sporadic and 2 familial AD cases, and 4 normal controls were collected at post mortem and shown in table 22. The familial AD cases included one variant AD case with cotton wool plaques due to *PS1* ΔI83/ΔM84 mutation (Houlden *et al.*, 2000; Steiner *et al.*, 2001), a case caused by *PS1* M233V mutation. The criteria for the neuropathological diagnosis of FBD and FDD have been previously described (Holton *et al.*, 2001; Holton *et al.*, 2002; Plant *et al.*, 1990; Revesz *et al.*, 1999), while for that of AD standard criteria were used (Mirra *et al.*, 1991).

For immunohistochemistry carried out on paraffin embedded tissue sections were cut from the hippocampus, cerebellum and frontal cortex in all cases listed above. Immunohistochemistry carried out on frozen tissue hippocampus and frontal cortex was used from one FBD and three sporadic AD cases; frontal cortex from one familial AD case and hippocampus from one FDD case.

Case	Case number	Sex	Age	Cause of Death	Diagnosis
1	PM 37-99	M	43	Bronchopneumonia	FDD
2	PM 38-99	F	60	Bronchopneumonia	FDD
3	PM 39-99	M	58	Not recorded	FDD
4	PM 91-99	F	68	Bronchopneumonia	FBD
5	PM 3319	F	65	Bronchopneumonia	FBD
6	PM 111-95	M	60	Cardiac failure	FBD
7	PM 6-00	N/A	N/A	N/A	FBD
8	PM 49-76	F	56	Not recorded	FBD
9	PM 100-95	F	46	Bronchopneumonia	FAD
10	PM 8-00	N/A	N/A	N/A	FAD
11	PM 69-99	F	92	Pneumonia	AD
12	PM 32-97	F	91	Pneumonia	AD
13	PM 73-98	M	86	Bronchopneumonia	AD
14	PM 25-98	F	69	Acute tracheo Bronchtis	AD
15	PM 83-98	F	84	Dementia	AD
16	C 4-00	M	81	Chronic obstructive airway disease	Control
17	C 5-00	F	88	Chronic obstructive airway disease	Control
18	PM 84-98	M	56	Cardiac failure	Control
19	PM 76-99	M	33	Acute bronchopneumonia	Control

***Table 22**: Cases used in the complement study.*

6.2.2 Antibodies

A panel of antibodies used in this study to establish the pattern of complement staining in relation to the amyloid proteins are shown in table 23.

Antibody	Antigen	Source	Species	Conc.
Ab338	ABri	Dr. Jorge Ghiso	Polyclonal	1:2000
Ab5282	ADan	Dr. Jorge Ghiso	Polyclonal	1:1000
Aβ 8-17	Aβ	Dako	Monoclonal	1:100
A201	C1q	Quidel	Monoclonal	1:50
A207	C3d	Quidel	Monoclonal	1:100
A213	C4d	Quidel	Monoclonal	1:1000
A209	IC3b	Quidel	Monoclonal	1:100
A239	Sc5b-9	Quidel	Monoclonal	1:100
A227	Factor Bb	Quidel	Monoclonal	1:50
Apolipoprotein J	Apolipoprotein J	Dr. Jorge Ghiso	Polyclonal	1:200
A237	Vitronectin	Quidel	Monoclonal	1:200
CR3/43 M0775	HLA-DR	Dako	Monoclonal	1:200
Z0334	GFAP	Dako	Polyclonal	1:1000

***Table 23**: Antibodies used for the complement study.*

6.2.3 Immunohistochemistry

For this study immunohistochemistry for paraffin sections was carried out as described in section 2.2; frozen sections as described in section 2.4; and free-floating sections as described in section 2.3. Staining for confocal microscopy was carried out as described in section 2.7.

6.3 Results

6.3.1 C1q expression in Aβ, ABri and ADan lesions.

C1q immunoreactivity was observed in all amyloid affected blood vessels in the AD controls (figure 6.6J-L) including those with cotton wool plaques (figure 6.7A-C). Blood vessels of all sizes including capillaries, affected with amyloid deposition, were labelled with the anti-C1q antibody. Strong C1q immunoreactivity was observed in the Aβ amyloid plaques, including those containing a central core (figure 6.6A-C). The thioflavine-S and Congo red-negative diffuse plaques, including those seen in the parvopyramidal clusters of the pre- and parasubiculum were negative or weakly positive for C1q compared with the amount of immunoreactivity found within the blood vessels. There was a similar pattern in variant AD in that while the strongly thioflavine S-positive blood vessels also showed a markedly positive reaction for C1q, the majority of the cotton wool Aβ plaques with weak thioflavine-S positivity, were also weakly positive for C1q (figure 6.7C). This staining pattern was mirrored in FBD with strong positivity for C1q in amyloid laden blood vessels (figure 6.1A-C) and in thioflavine-S positive plaques. The dense central core of the large hippocampal plaques were also strongly labelled with the anti-C1q antibody (figure 6.1D-F). In FDD strong C1q immunolabelling was found in association with blood vessels affected by ADan

deposition (figure 6.1G-I), but only weak or no immunolabelling was seen in relation to the diffuse parenchymal lesions that are mainly negative with thioflavine-S staining.

In FBD C1q and thioflavine-S double staining revealed a close topographical overlap between the two staining patterns, confirming that the anti-C1q antibody stained ABri lesions in β-pleated sheet conformation (figure 6.1A-F). Such preparations also showed that the Ab338-positive 'diffuse' thioflavine-S-negative or weakly positive lesions were either entirely negative or only weakly reactive for C1q (figure 6.1G-I). A similarly close correlation between C1q immunoreactivity and thioflavine-S fluorescence of the parenchymal lesions was noted in FDD in that thioflavine-S positive, subpial and perivascular ADan amyloid lesions were strongly labelled with the anti-C1q antibody, while the thioflavine-S-negative, parenchymal 'diffuse deposits' were negative or only weakly positive for C1q (data not shown).

Confocal microscopy was also undertaken to investigate the relationship between HLA-DR positive cells and amyloid conformation (thioflavine-S positive) and HLA-DR positive cells and C1q reactivity. In FBD HLA-DR positivity was found within cells closely associated with amyloid plaques (figure 6.2A-C), but were sparse in relation to preamyloid lesions. A similar association of the glial cellular response with the conformational state of the amyloid proteins was confirmed in FDD, as activated microglia and astrocytes were mainly clustered around amyloid-laden blood vessels, but were sparse in relation to the diffuse preamyloid parenchymal lesions (data not shown). Amyloid plaques and amyloid-laden blood vessels in FBD (figure 6.2D-F) and FDD (figure 6.2G-I) that are positive with C1q showed close association with HLA-DR positive cells.

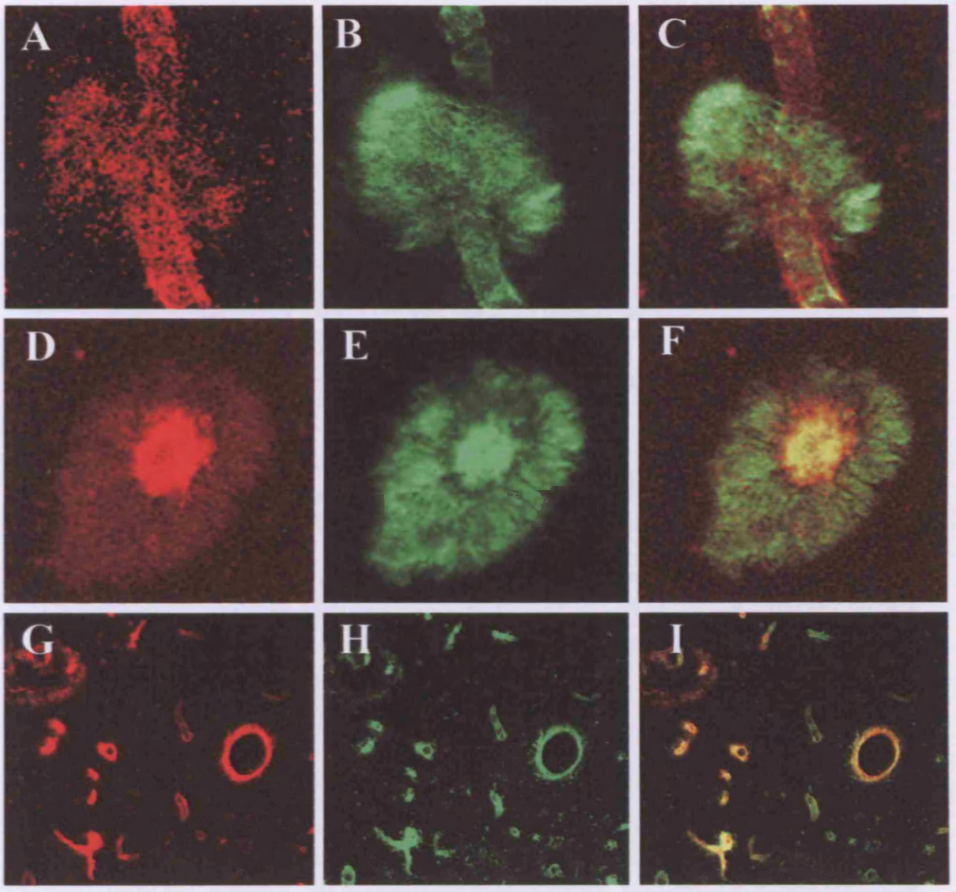

Figure 6.1: C1q deposition in FBD and FDD. (A, D and G C1q-red; B,E and H thioflavine-S- green; C, F and I combined images). C1q is deposited in amyloid-laden blood vessels (A) and amyloid plaques (E), but was not found in preamyloid lesions (not shown) in FBD. In FDD C1q was also deposited in amyloid-laden blood vessels and parenchymal preamyloid lesions were unaffected (G and H). (Confocal images; **Panels A-F**: objective 20, **Panels G-I**: objective 10).

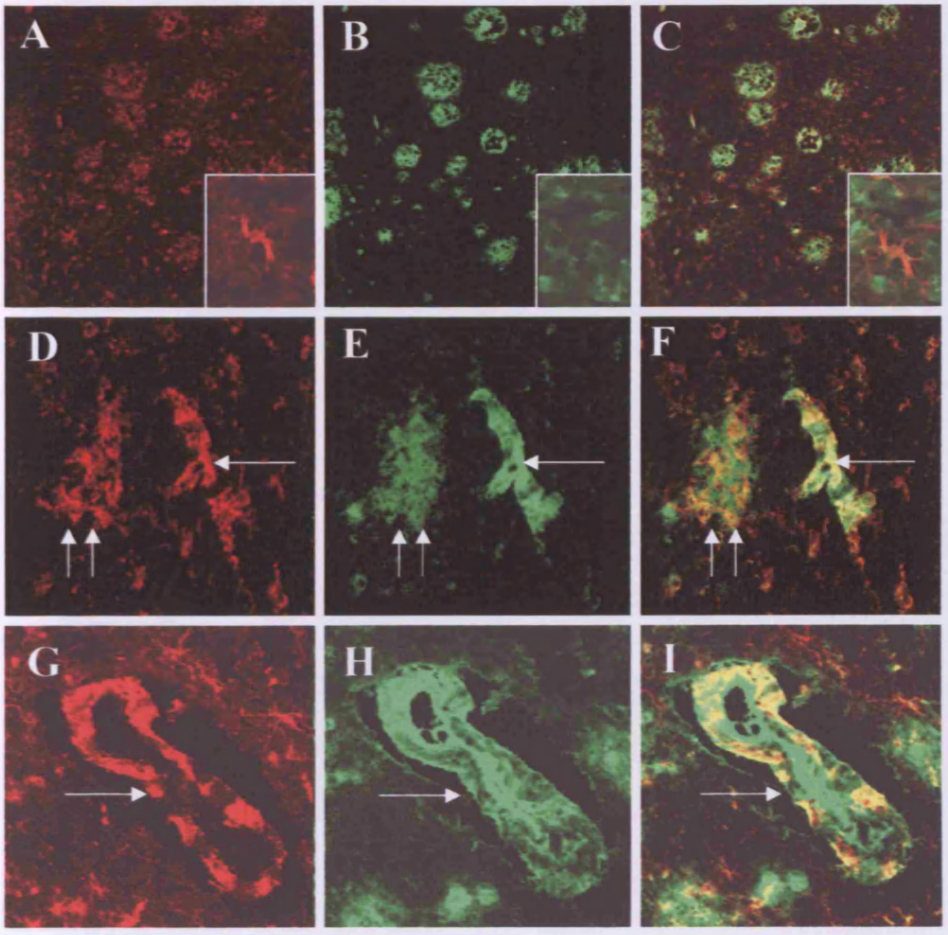

Figure 6.2: Microglial and astrocytic response in FBD and FDD. Activated microglia expressing HLA-DR (red) are closely associated with thioflavine-S positive (green) amyloid plaques in FBD (A-C). (Confocal images panels A-C: objective 10 and inset objective 40, panels d-E: objective 63). HLA-DR positivity is in close proximity of C1q containing amyloid lesions (arrow- vessel, double arrow- plaque) in both FBD (D-F) and FDD (G-I). (Confocal images **Panels G-I**: objective 40, **Panels J-L**: objective 63).

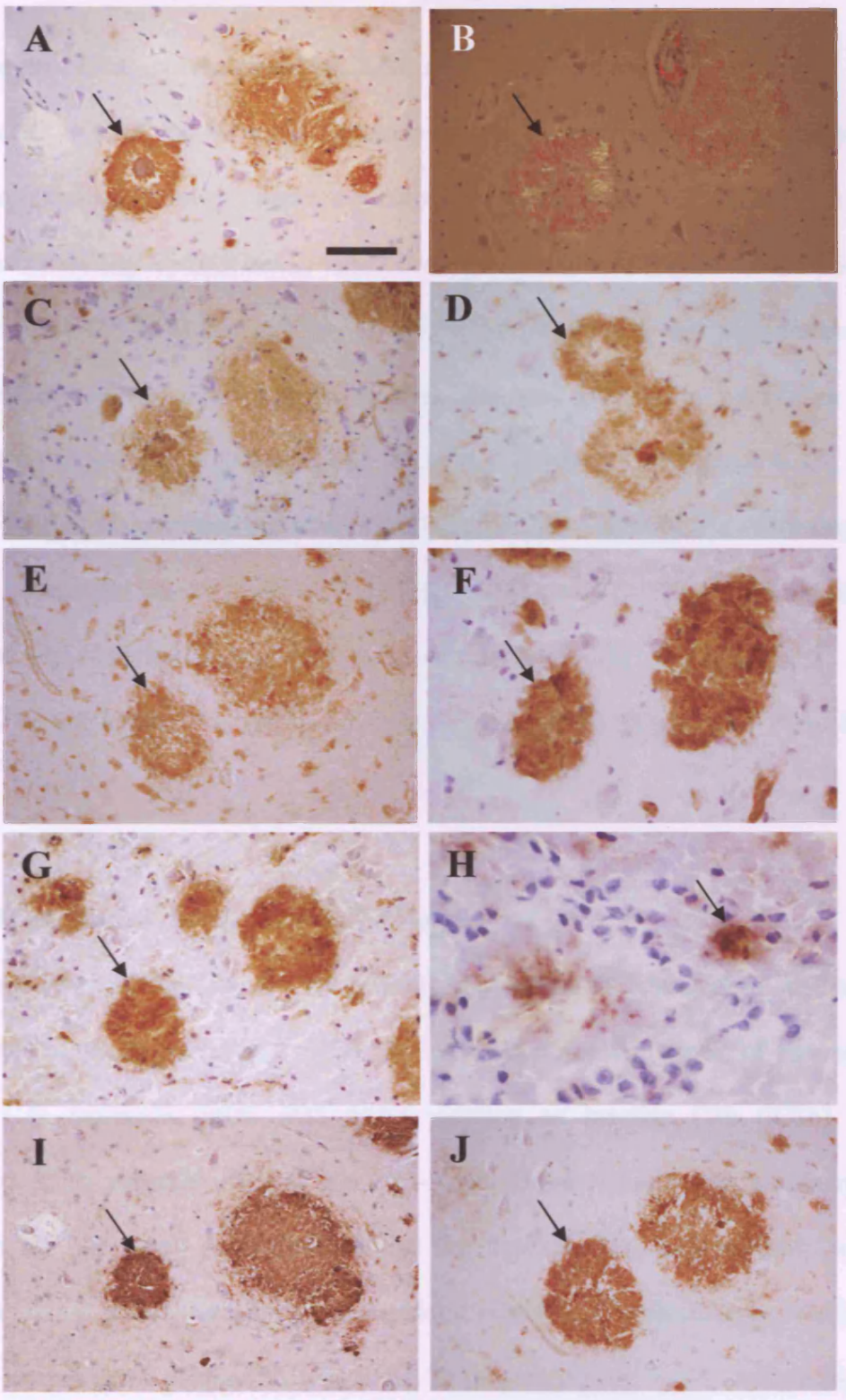

Figure 6.3: Deposition of complement components in amyloid plaques in FBD. ABri-positive amyloid plaques in the CA4 subregion of the hippocampus **(A)** are shown to be in an amyloid conformation by Congo red staining **(B)**. Amyloid plaques are also decorated by the anti-C1q **(C)**, anti-C3d **(D)**, anti-iC3b **(E)**, anti-C4d **(F)** anti-Sc5b-9 **(G)** and Bb antibodies **(H)**. Plaques were also found to be strongly positive for ApoJ **(I)** and vitronectin **(J)**. Arrows on all panels are pointing towards an amyloid plaque. Bar in panel A represents 100μm in all panels except H where it represents 45μm.

6.3.2 C3d and C4d expression in Aβ, ABri and ADan lesions

The antibodies to C3d and C4d, the presence of which indicates the activation of the classical complement pathway, showed a staining pattern similar to that seen on C1q immunohistochemistry in both blood vessels and plaques in AD (figure 6.6D-E, 6.6M-N). In both FBD and FDD strong C3d and C4d immunoreactivity was also detected in amyloid-laden blood vessels and the staining patterns with these antibodies was comparable to those seen with antibodies to ABri, ADan and C1q (figure 6.4D, 6.4F and figure 6.5E). In addition, the C3d and C4d antibodies labelled the ABri amyloid plaques of all morphological types in FBD (figure 6.3D, 6.3F). While the subpial and perivascular parenchymal amyloid lesions were also positively stained with the anti-C3d and C4d antibodies, the 'diffuse deposits' remained unstained with these latter antibodies.

6.3.3 IC3b expression in Aβ, ABri and ADan lesions

The presence of iC3b can indicate the activation of either the classical or alternative complement pathways, is formed when the unstable thioester bonds of the newly generated C3b molecule reacts with water yielding an inactive C3b (iC3b). The antibody to iC3b strongly stained amyloid-laden blood vessels and parenchymal deposits in all AD cases studied. Including the familial AD cases studied, strong staining was found within the amyloid-laden blood vessels and weak staining was found within the cotton wool plaques in which Aβ is in pre-amyloid conformation (figure 6.7E). Immunohistochemistry with an antibody to iC3b showed that in FBD there was strong immunoreactivity of both vascular and parenchymal amyloid lesions (figure 6.3E and 6.4E) while 'diffuse deposits' showed a weak positivity.

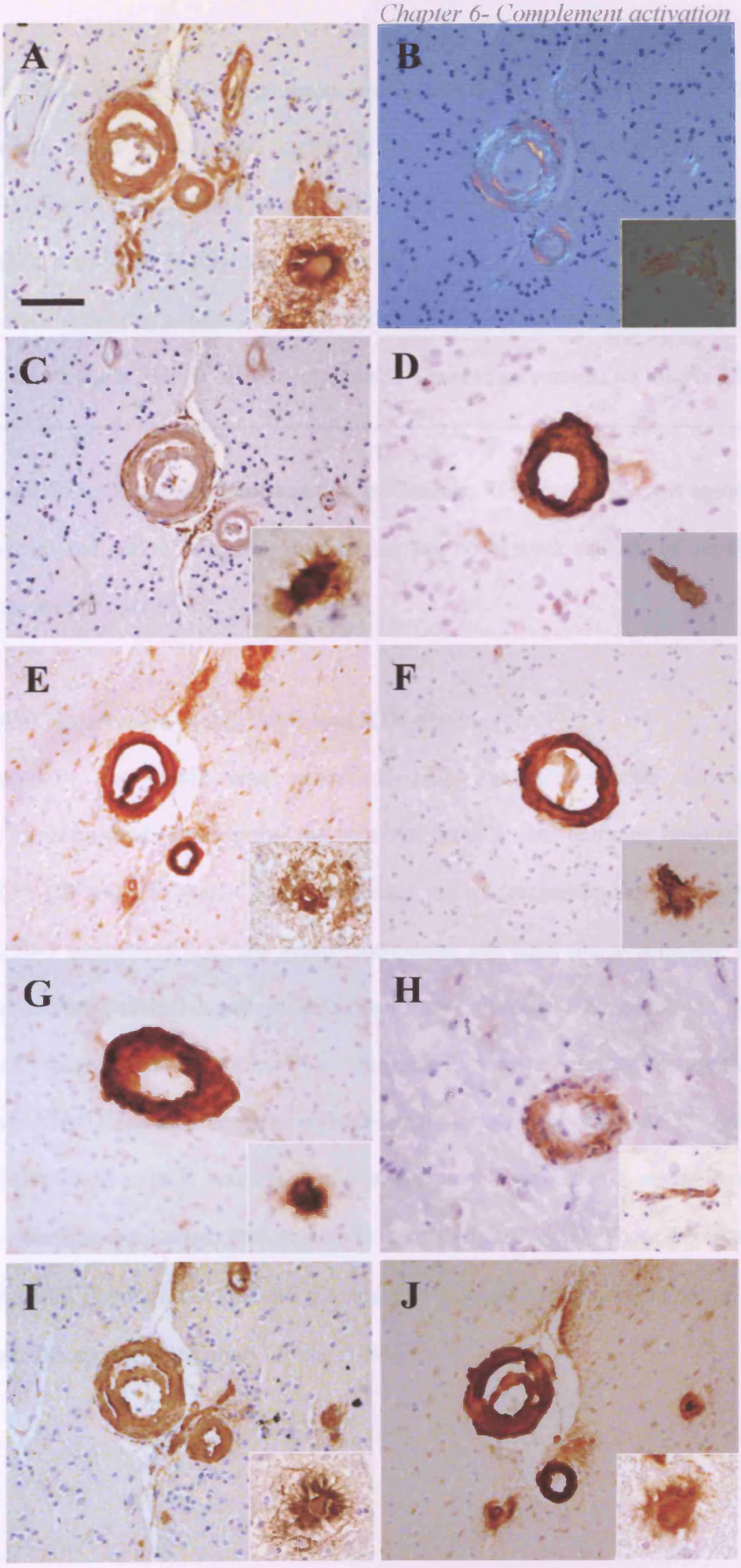
A
B
C
D
E
F
G
H
I
J

Figure 6.4: Deposition of complement components in blood vessels in FBD. Amyloid-laden blood vessels **(B)** including capillaries **(B, inserts)** due to ABri deposition **(A)** in the frontal white matter. The anti-C1q **(C)**, anti-C3d **(D)**, anti-C4d **(F)**, anti-iC3b **(E)**, anti-SC5b-9 **(G)** and anti-Bb **(H)** antibodies label blood vessels and capillaries with ABri deposition. ApoJ **(I)** and Vn **(J)** are similarly deposited in ABri containing vessel walls. Bar in panel A represents 45μm in all panels and inserts 22μm.

In FDD, in addition to the amyloid-laden blood vessels, iC3b positivity was associated with the subpial and perivascular amyloid lesions, but no or weak staining of the diffuse deposits was seen (figure 6.5E).

6.3.4 MAC expression in Aβ, ABri and ADan lesions.

Immunoreactivity for MAC was visualized using anti-C5b-9 and anti-Sc5b-9 antibodies. Both antibodies recognize the terminal complement complex consisting of C5b, C6, C7, C8 and C9. Anti-C5b-9 recognises the membrane-bound lytic complex and anti-Sc5b-9 recognises both the membrane-bound and fluid phase complex. In the current studies both antibodies gave similar results and, although the antibody to Sc5b-9 gave a more intensive labelling than C5b-9 did, the two will be described together. In the AD cases MAC deposited in both amyloid-laden blood vessels (figure 6.6O) and the staining of the blood vessels was especially strong in the variant AD cases, in which CAA, also affecting capillaries, was especially severe (figure 6.7G). There were various amounts of MAC deposition in the Aβ plaques and a weak staining of the cotton wool plaques was also apparent (figure 6.6E and 6.7G).

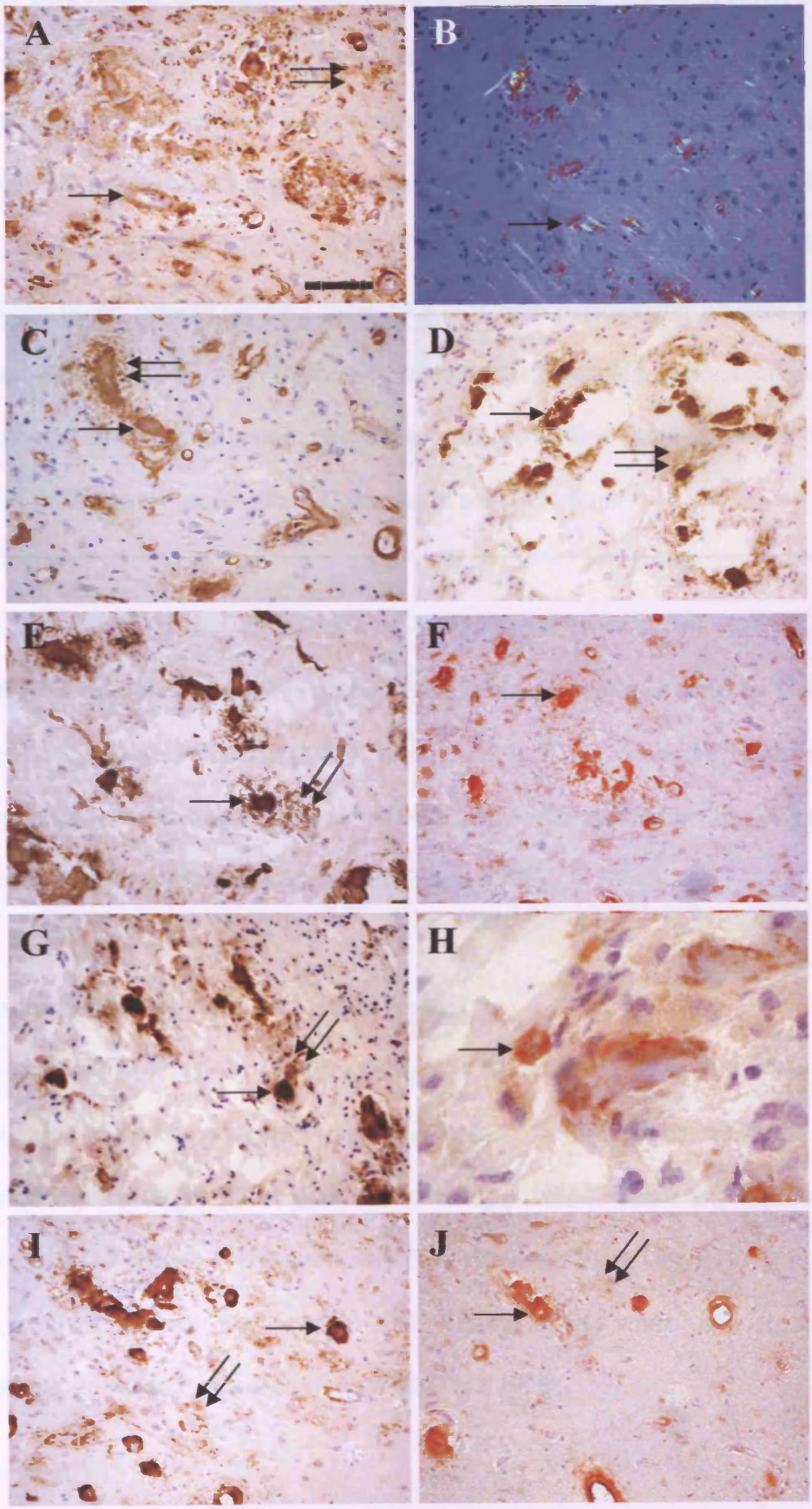
A
B
C
D
E
F
G
H
I
J

Figure 6.5: Deposition of complement components in FDD. ADan deposits in both blood vessels and parenchyma (A, vessel arrow, parenchyma double arrow), while Congo red (B, vessel arrow) mainly stains blood vessels suggesting that the parenchymal ADan lesions are mainly of preamyloid nature. Deposition of complement proteins, C1q (C), C3d (D), C4d (E), iC3b (F), Sc5b-9 (G) and Bb (H) taking place in amyloid-laden blood vessels (arrow) some of which with perivascular plaques (double arrow). Anti-ApoJ (I) and Vn (J) antibodies strongly stain vascular lesions (arrow), but the parenchymal preamyloid lesions are more weakly labelled (double arrow). Bar in panel A and in all panels represents 100μm and in panel H 28μm.

In FBD MAC immunoreactivity was present in both blood vessels affected by CAA and amyloid plaques (figure 6.3G and 6.4G). In contrast in FDD, while the blood vessels affected by CAA were strongly labelled with the anti-MAC antibodies, the majority of the parenchymal lesions remained unstained (figure 6.5G).

6.3.5 Factor Bb in Aβ, ABri and ADan lesions.

There was generally a small degree of staining of mainly the central cores of the senile plaques and also of the blood vessels with CAA in the AD cases (figure 6.6G and 6.6P). Immunoreactivity for factor Bb was seen in both larger blood vessels and capillaries in both FBD and FDD (figure 6.4H and 6.5H). Furthermore various degree of staining of the ABri amyloid plaques was seen in FBD (figure 6.3H) while the parenchymal 'diffuse lesions' remained unstained in both FBD and FDD.

6.3.6 Complement inhibitors in AD, FBD and FDD lesions

An antibody recognizing the complement inhibitor ApoJ strongly labelled all amyloid-laden lesions in FBD, FDD, AD and vAD cases. In general, the staining pattern seen in ApoJ immunohistochemistry was similar to that seen with the amyloid antibodies used in each case (see section 5.3.3 for detailed results).

Vn strongly labelled ABri or ADan lesions with amyloid conformation; parenchymal amyloid plaques and CAA in FBD (figure 6.3J and 6.4J), and mostly amyloid-laden blood vessels in FDD (figure 6.5J) and the preamyloid lesions showed a weaker reaction for this antigen.

In the AD cases studied the Vn immunoreactivity followed a pattern similar to that observed with ApoJ, although in general, the diffuse lesions showed a weaker reaction for this antigen than they did for ApoJ (figure 6.6I, 6.6R, 6.7J).

6.3.7 Labelling of neurons by complement and complement inhibitor antibodies in FBD and FDD

In AD anti-C1q labelled NFTs were found in the hippocampus, entorhinal cortex and frontal cortex (figure 6.8G). Positive staining was also found in neurons unaffected by NFTs (figure 6.8M). The presence of C3d (figure 6.8H) and C4d (figure 6.8I) immunoreactivity was also noted, but the number of labelled NFTs was fewer than that seen with C1q. IC3b immunoreactivity was found in NFTs throughout the hippocampus (figure 6.8J). ApoJ and Vn positivity was found in both NFTs and ghost tangles. However the anti-ApoJ antibody stained more NFTs than Vn did and also labelled NTs (figure 6.8L).

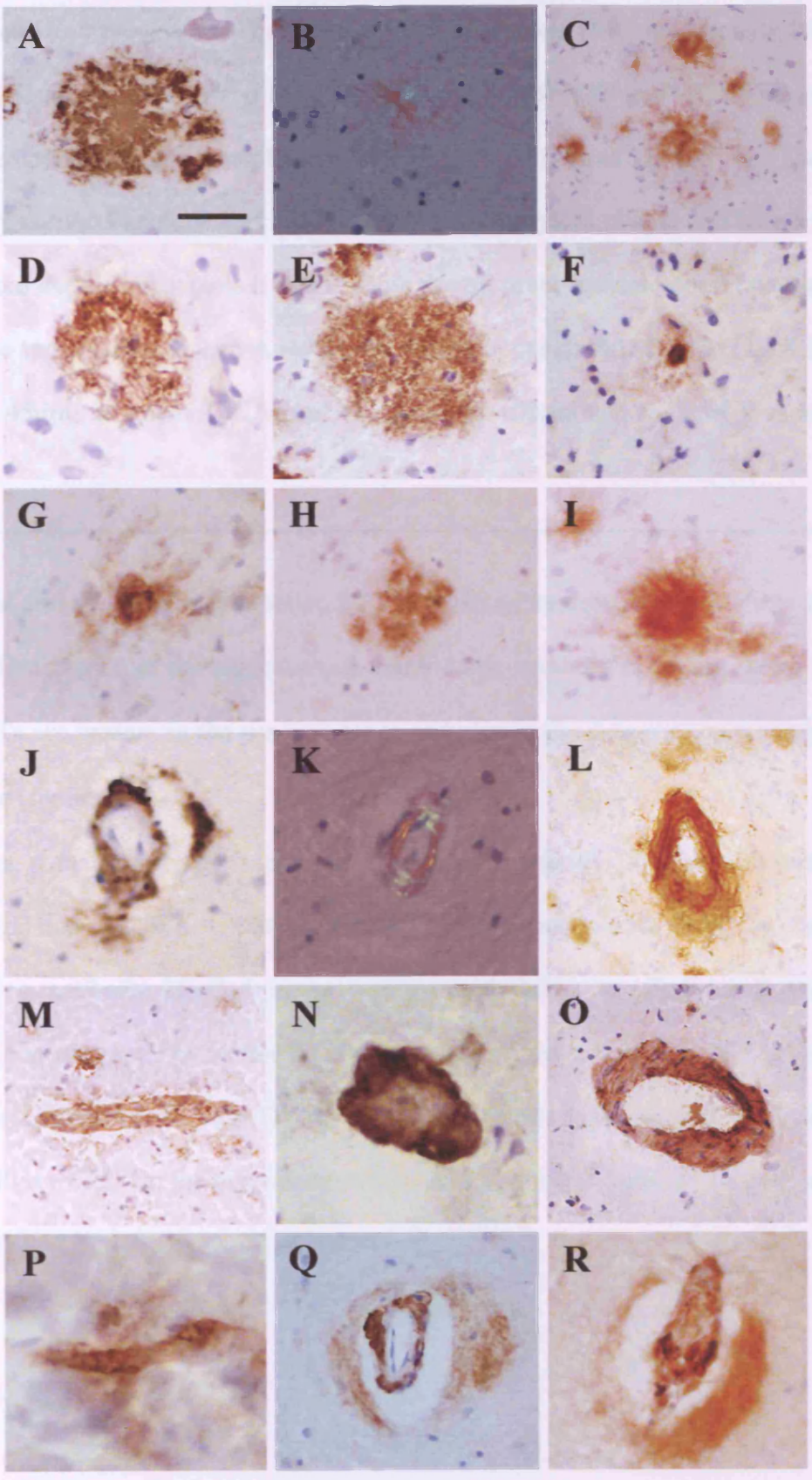
A
B
C
D
E
F
G
H
I
J
K
L
M
N
O
P
Q
R

Figure 6.6: Deposition of complement components in AD. Complement activation in AD, both amyloid plaques (A-I) and amyloid-laden vessels (J-R) are strongly labelled with C1q (C and L); C3d (D and M); C4d (E and N); Sc5b-9 (F and O); Bb (G and P). The expression of the two complement inhibitors ApoJ (H and Q) and Vn (I and R) were also positive. Panels A and J show Aβ positive amyloid plaque and blood vessel with amyloid deposition, panels B and K show the Aβ in the amyloid conformation state with Congo red staining. Bar in A represents 45μm; in panels B,D,E,F,G,H,I,J,K,N,Q,R represents 45μm; in panels C,L,M and O represents 100μm and in panel P represents 22μm.

In FBD the anti-C1q antibody labelled NFT-containing neurons and also ghost tangles in the CA1 subregion of the hippocampus and in large numbers in the entorhinal cortex where NFTs are present in the pre-α neurons and also in the deeper cortical laminae in this disease (figure 6.8A).

The tangles, some of the ghost tangle type, were also positively labelled with both C3d (figure 6.8B) and C4d (figure 6.8C) in the hippocampus and entorhinal cortex. In FDD the anti-C1q antibody labelled many neurons with NFTs or ghost tangles in the entorhinal cortex and a similar staining pattern was seen on C3d and C4d immunohistochemistry. In both FBD and FDD NFTs and ghost tangles were positive for iC3b (figure 6.8D) in the hippocampus and entorhinal cortex, and for Sc5b-9 in FBD (figure 6.8E).

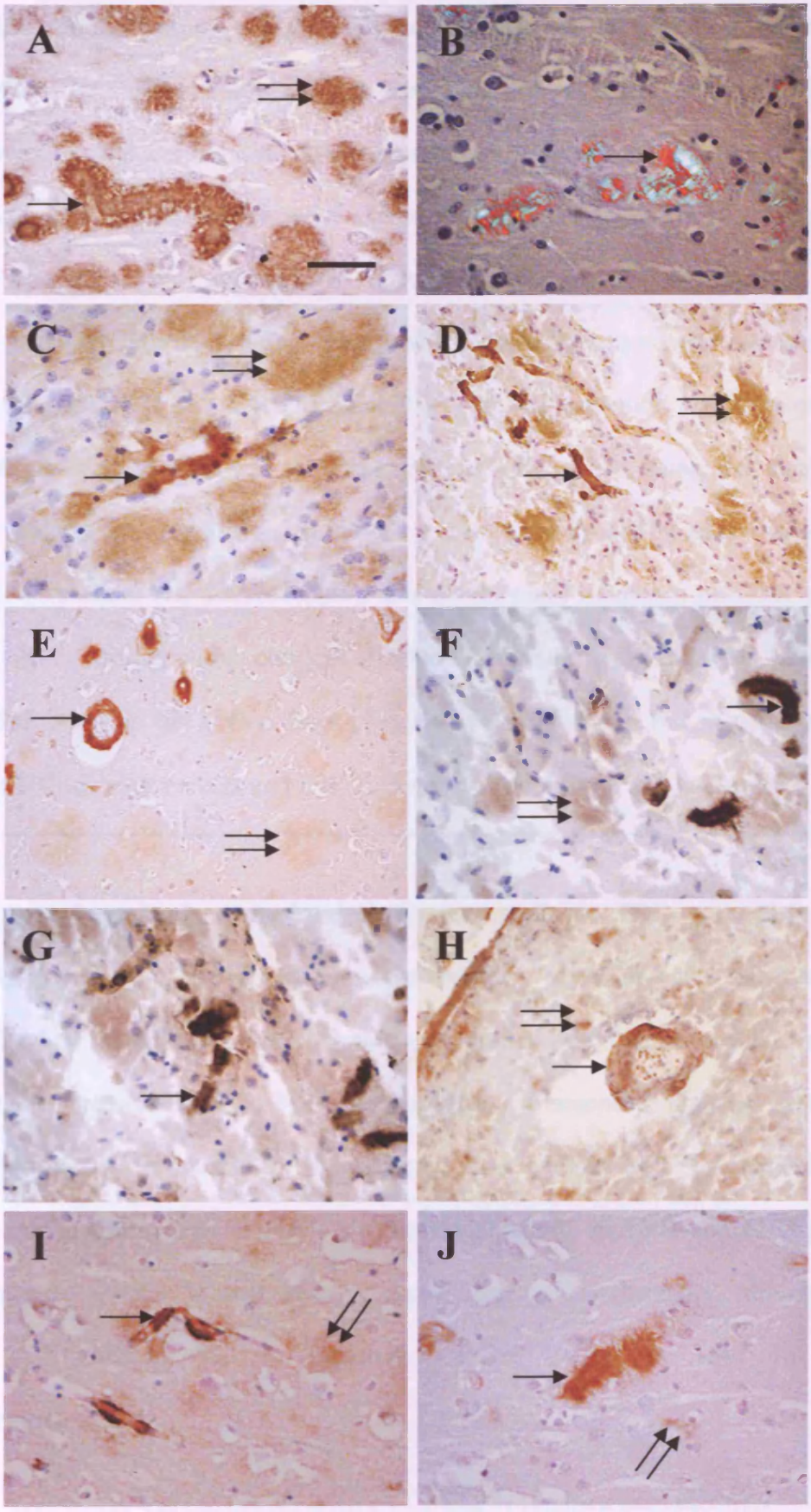
A
B
C
D
E
F
G
H
I
J

Figure 6.7: Deposition of complement components in cotton wool variant of familial AD. The pattern of complement deposition reflects the difference in amyloid load between vessels and plaques. Aβ immunolabelling was found in CAA (A, arrow) as well as the pre-amyloid 'cotton wool' plaques (A, double arrow), where as Congo red positivity was only found within CAA (arrow). Strong immunolabelling was found within all amyloid affected vessels (arrows) with all complement components including C1q (C); C3d (D); iC3b (E); C4d (F); Sc5b-9 (G), the 'cotton wool' plaques were only weakly stained (double arrows). The anti-Bb antibody, representing the alternative pathway, stained the amyloid-laden blood vessels (arrow) and weakly stained the 'cotton wool' plaques (H, double arrow). The complement inhibitors ApoJ (I) and Vn (J) positivity was found within amyloid affected vessels (arrows) of all sizes, plus weak staining found within the cotton wool plaques (double arrows). Bar in panel A, G-J represents 100μm, on panels D and E 250μm and on panels B, C and F 55μm.

The anti-Sc5b-9 antibody stained relatively few NFTs in FDD. In FBD ApoJ immunoreactivity was observed in numerous neurons, many of which possessed an NFT (figure 6.8F). While some neurons showed a granular staining pattern, the majority of the labelled neurons with an NFT demonstrated a filamentous staining pattern. A strong labelling of a proportion of the neurons, often with an NFT, by the anti-ApoJ antibody was also observed in FDD. Vn immunoreactivity in FBD and FDD gave a staining pattern similar to that seen in ApoJ immunohistochemistry, although the number of labelled neurons appeared smaller than that seen in ApoJ immunohistochemistry.

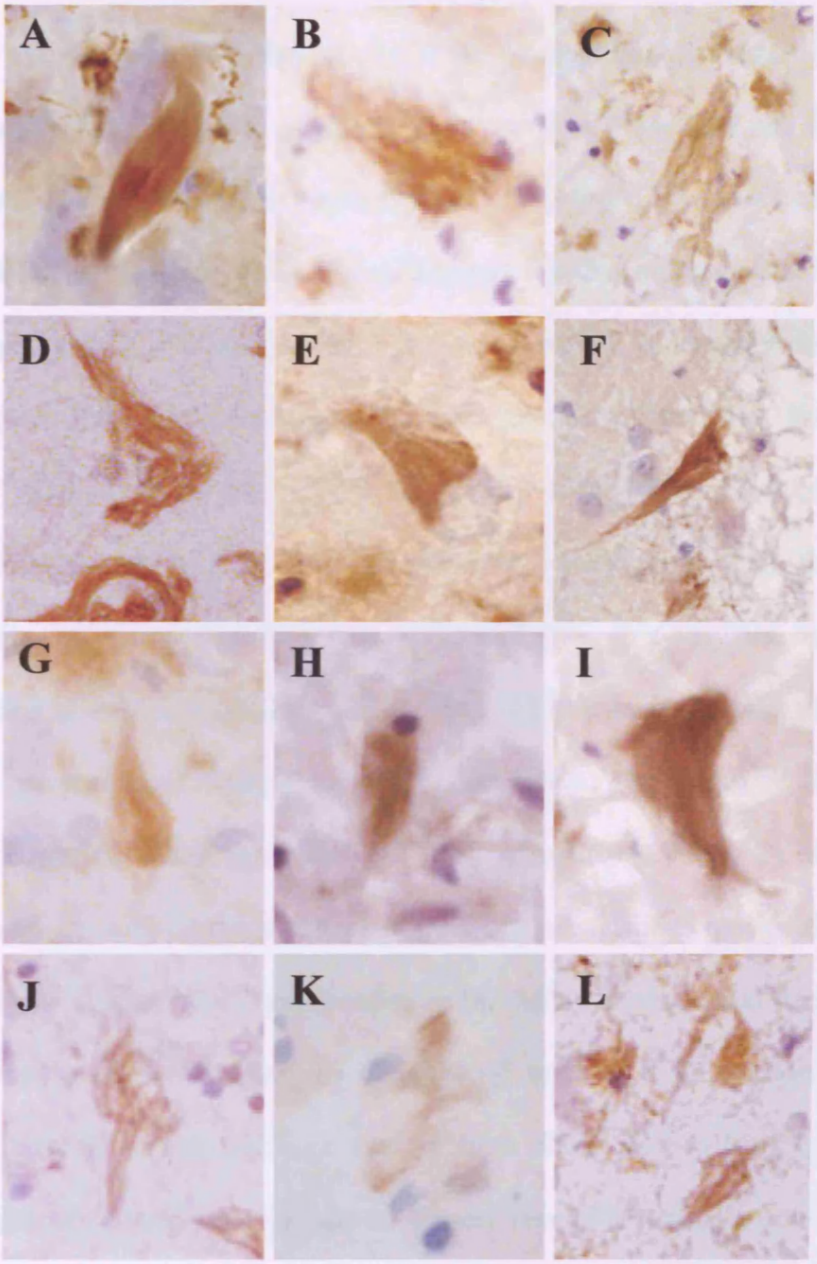

Figure 6.8: Deposition of complement components in neurons in FBD and AD. Full activation of the complement cascade was demonstrated in FBD (A-F) and AD (G-L). Panels A and G show C1q immunolabelling; panels B and H C3d; panels C and I C4d; panels D and J iC3b; panels E and K Sc5b-9 and panels F and L Apo J. All panels were taken with original objective x40.

6.4 Discussion

In this study we demonstrated that in the *BRI2* gene-related dementias complement proteins and activation fragments of the classical pathway (C1q, C3d and C4d) as well as the terminal MAC are present in parenchymal lesions and CAA, which are composed of ABri in FBD and ADan in FDD. These findings indicate not only that the classical complement pathway is activated, but also that it proceeds to its terminal stages in these diseases. Furthermore, we demonstrated that lesions, which are predominantly composed of ABri or ADan amyloid protein species in β-pleated sheet conformation, showed a stronger reaction for the complement components than those, which ultrastructurally are composed of sparse amyloid fibrils (pre-amyloid lesions). This latter correlation is well illustrated by our finding a difference in complement deposition between the parenchymal lesions of FBD and FDD. The majority of the ABri parenchymal deposits, which are mainly of amyloid nature (Chapter 3) were strongly labelled with all the anti-complement antibodies, including those recognizing MAC in FBD, while there was a weak or no reaction in the ADan parenchymal deposits, which are predominantly of the 'diffuse' or preamyloid type in FDD (Chapter 4). These observations provide strong evidence that in both *BRI2* gene-related dementias the overall patterns of complement deposition closely resemble those observed in AD, in which a similar correlation between the conformational state of Aβ and the degree of complement deposition has been demonstrated (Berkenbosch *et al.*, 1992; Eikelenboom & Stam, 1982; Ishii & Haga, 1984; McGeer *et al.*, 1989; Rogers *et al.*, 1992b; Rozemuller *et al.*, 1992; Verbeek *et al.*, 1998; Webster *et al.*, 1997) and supported by data of the current study of AD cases. Interestingly we consistently found a variable and often weak staining of the cotton wool plaques with all the anti-complement antibodies, including MAC, in the variant AD cases. These latter findings suggest that weak, but

full activation of the complement pathway also takes place in variant AD. We also observed that immunolabelling with the complement antibodies, similar to the parenchymal ADan lesions, shows a good correlation with the weak positivity of the cotton wool plaques for thioflavine-S and also the presence of sparse amyloid fibrils, which can be found with EM (data not shown). These findings at first seem to be at variance with data of a previous study, which suggested that only negligible plaque-related labelling for C1q, C3d and C9 is present in the cotton wool plaques (Crook *et al.*, 1998b). It is, however, possible that this difference in the observations can be explained by the different methodological approaches employed in the two studies. Twenty micrometer thick free floating paraffin sections were used for C1q and frozen tissue sections for downstream complement components in the current study, while 4μm paraffin sections were used in the above cited study. This latter method in our experience can underestimate the level of complement deposition in Aβ and other amyloid lesions (data not shown).

Extensive investigations have been undertaken to prove that the presence of complement proteins are harmful and that they are an important component of the AD pathogenesis. Recent studies, however, showed that increased clearance of Aβ can improve cognitive function in mouse models of AD (Janus *et al.*, 2000; Morgan *et al.*, 2000). Clearance of Aβ in these experiments was achieved by immunizing mice with synthetic Aβ, which can prevent or reduce Aβ accumulation (Schenk *et al.*, 1999). However, a recent study provides evidence for a role of complement and innate immune responses in AD-like mice and supports the concept that certain inflammatory defense mechanisms in the brain may be beneficial in neurodegenerative diseases (Wyss-Coray *et al.*, 2002). This study demonstrated that expression of a complement inhibitor increased the AD-like pathology, including amyloid deposition and neurodegeneration

in mice expressing human amyloid precursor protein (hAPP), whereas increased complement C3 production was associated with reduced Aβ deposition in hAPP/ TGF-β1 transgenic mice. These data support that complement activation products may protect against Aβ-induced toxicity and reduce the accumulation or promote the clearance of amyloid. In addition to direct neuroprotective effects (Fishelson *et al.*, 2001), complement may stimulate clearance and reduce the accumulation of Aβ and degenerating neurons via complement receptors on phagocytic microglia.

In vitro studies have shown that aggregated Aβ peptides, especially $A\beta_{1-42}$, are able to directly activate the classical complement pathway by their binding to the recognition component C1q. Several studies have shown that the C1q binding site of Aβ is located in the region of the N-terminal 1-11 amino acids and that residues Asp^7 and/or Glu^{11} are essential in this process (Velazquez *et al.*, 1997; Webster *et al.*, 1997). It is noteworthy, however, that a synthetic peptide composed of the N-terminal 1-16 amino acids of $A\beta_{1-42}$ alone, which is unable to form amyloid fibrils due to lack of the C-terminal region, is not sufficient for complement activation. This observation provides experimental support to the hypothesis that formation of the fibrillar structure, leaving the essential N-terminal region of Aβ to adopt the necessary conformation and/or to provide the appropriate charge pattern for an efficient recognition by C1q, is also an essential precondition of complement activation (Tacnet-Delorme *et al.*, 2001). A recent biochemical study has demonstrated that ABri and ADan, which form spontaneous β-pleated sheet rich structures and show very fast aggregation kinetics, are also able to form stable complexes with C1q and can fully activate the classical complement cascade *in vitro*. ABri and ADan have also been shown to be able to produce complements at levels that are comparable to those produced by $A\beta_{1-42}$

(Rostagno *et al.*, 2002). This latter study has demonstrated that the complement-activating site of ABri and ADan is localized to the N-terminal region of these amyloid peptides. However, no information is available about the precise C1q binding sites of ABri and ADan peptides as yet, and to answer these questions further experimental investigations would be required. The current study has also demonstrated *in vivo* the presence of the alternative complement pathway activation product factor Bb in association with ABri, ADan and Aβ amyloid lesions. Although previously no evidence was found for the occurrence of components of the alternative complement pathway in AD, our *in vivo* findings are supported by data of recent studies demonstrating that some activation or amplification of the alternative pathway does occur in AD (Bradt *et al.*, 1998; Strohmeyer *et al.*, 2000c). Furthermore there is also now experimental evidence showing that the alternative pathway can be activated using synthetic ABri and ADan peptides (Rostagno *et al.*, 2002).

The current investigations also demonstrated that ApoJ and Vn are present in both amyloid and preamyloid ABri and ADan lesions. The significance of these findings is that both ApoJ and Vn are inhibitors of the complement systems and the neuroprotective role attributed to ApoJ in AD may be due to this activity (Calero *et al.*, 2000). Experimental data suggest that the complement inhibitor activity of both ApoJ and Vn is related to their ability to interact with the terminal complement components. ApoJ inhibits the complement cascades by binding to the C5b-7 complex inhibiting its insertion into the cell membrane, hence inhibiting the formation of MAC with the addition of C8 and C9 (Tschopp *et al.*, 1993). This interaction between ApoJ and the terminal complement components makes the complex hydrophilic and lytically inactive (Tschopp *et al.*, 1993). Vn, acting at the stage of C5b-9 and neutralizing the lytic activity of the complex, also binds to C8 and C9. Although both ApoJ and Vn are able

to interact with C9, the former binds to the C9b while the later to the C9a fragment, therefore simultaneous binding is possible. This could more efficiently reduce the impact of complement attack (Tschopp *et al.*, 1993). ApoJ not only acts as a complement inhibitor, but can also be classified as an AAP influencing aggregation and fibrillization of amyloidogenic proteins (Calero *et al.*, 2000). ApoJ acting as an AAP is discussed in chapter 5.

In both FBD and FDD there was a significant reaction by HLA-DR-positive microglia and also astrocytes, which also occasionally expressed HLA-DR, in relation to the ABri and ADan parenchymal and vascular amyloid lesions. Such a reaction (see also chapters 3 and 4) was sparse or absent in relation to preamyloid lesions. Microglial cells and astrocytes are both known to produce inflammatory mediators, including complement proteins (McGeer & McGeer, 1995; McGeer & McGeer, 2001). Furthermore light and confocal microscopy data of this study also suggest that ABri and ADan fibrillar deposits can be in close contact with microglial cells and/or astrocytes. The widespread expression of MHC class II antigens by microglia, which is a consistent marker of activation (Tooyama *et al.*, 1990), is consistent with a phagocytic role and suggests that microglia may contribute to the clearance of cerebral ABri and ADan deposits. This is comparable to AD, in which it had also been documented that activated microglia are in close contact with Aβ plaques and also that they are able to internalize Aβ (Stalder *et al.*, 1999). In this regard complement activation may facilitate the phagocytosis of ABri and ADan amyloid fibrils in a manner similar to that suggested for Aβ fibrils (Stalder *et al.*, 1999). In order to elucidate the biological functions of microglia and astrocytes in FBD and FDD, further experimental investigations are required.

The importance of inflammation in neurodegenerative processes and, in particular in AD has become clear over recent years. Dementia has been shown to correlate with the

detection of inflammatory markers, activated microglia, reactive astrocytes and increased levels of cytokines and complement products around amyloid plaques and dystrophic neurites (Emmerling *et al.*, 2000), with the use of anti-inflammatory drugs in epidemiological studies being associated with a reduced risk of AD (Rogers *et al.*, 1996). These findings together with the *in vitro* demonstration that complement activation can lead to cell death in both rat hippocampal and neuronal cell lines (Schultz *et al.*, 1994; Shen *et al.*, 1995), point to the importance of chronic inflammation in the pathogenesis of AD and other neurodegenerative diseases.

Chapter 7

Biochemical and immunohistochemical analysis of ABri in FBD and ADan and Aβ in FDD.

Chapter 7 – Hypothesis and specific questions

In this chapter, I wished to investigate the hypothesis that biochemical heterogeneity of ABri and ADan exists in different lesion types in FBD and FDD respectively.

As correlation exists between the N- and C- terminal heterogeneity of the Aβ peptide species and different lesion types in AD, the question was addressed whether similar heterogeneity occurs in FBD and FDD. In this study, ABri and ADan species deposited in blood vessels and parenchymal lesions were isolated and biochemically characterised. In addition, the heterogeneity of the Aβ species co-deposited in the parenchyma and CAA in FDD was also studied by immunohistochemistry, utilising a panel of antibodies specific for N- and C-terminally modified Aβ species.

7.1 Introduction

The Aβ peptide is the major component found within senile plaques (Dickson, 1997) and CAA (Kalaria & Hedera, 1996) in AD. This 4kDa peptide produced by proteolytic cleavage of the APP by β-secretase (cleaving at the N-terminus) and γ-secretase (cleaving at the C-terminus) (Checler, 1995). The mechanism by which Aβ is deposited in the CNS may be affected by several factors 1) N- and C-terminal modifications of the Aβ peptide, 2) Mutations within the Aβ region of the *APP* gene, 3) Mutations in *PS1* and *PS2* genes, 4) Change in ratio between Aβx-40/ Aβx-42, 5) Clearance of Aβ from the CNS.

Biochemical and immunohistochemical analysis of the Aβ deposits demonstrated the presence of N- and C-terminally heterogeneous peptide species (Iwatsubo *et al.*, 1994b; Saido *et al.*, 1995; Saido *et al.*, 1996), in addition to the full length Aβ1-42. In sporadic AD cases Aβx-42 has been shown to be both the earliest and the most abundant peptide identified in plaques, whereas Aβx-40 predominates in blood vessels (Iwatsubo *et al.*, 1994b; Iwatsubo *et al.*, 1995; Wisniewski *et al.*, 1994b). *In vitro* truncation of the C-terminus reduces the aggregation properties and toxicity of the peptide, for example Aβ1-40 is less toxic than Aβ1-42 (Pike *et al.*, 1995). Several isoforms of Aβ42 have been found truncated at the N-terminus (Aβ4-42, Aβ8-42, Aβ12-42 and Aβ17-42) and such peptides aggregate more readily and are more toxic than the full-length Aβ1-42

(Pike *et al.*, 1995). Interestingly, N-terminally truncated isoforms of Aβx-40 (Aβ4-40, Aβ8-40, Aβ12-40) have also been found to be more toxic than the full-length peptide (Aβ1-40) (Pike *et al.*, 1995). Biochemical *in vivo* studies have demonstrated the L-aspartates present at positions 1 and 7 of Aβ, can be isomerized or stereoisomerized and the glutamates present at positions 3 and 11 can undergo intramolecular dehydration forming Aβ species that begin with pyroglutamate (pE) (Mori *et al.*, 1992; Russo *et al.*, 1997). The pyroglutamate modifications confer enhanced resistance to most aminopeptidases, therefore the abundance of Aβ3(pE)-x likely reflects a decrease in clearance. Aβ in AD plaques has been shown to stain with antibodies specific for N-terminal Aβ3(pE), and such species have been shown to be an important component of the total Aβ load in AD, as assessed by immunoblotting (Saido *et al.*, 1995). The N-terminally truncated Aβ species Aβ11-x has also been shown to be generated by transgenic rodent neurons supporting the notion that truncated species may play a role in AD pathogenesis (Gouras *et al.*, 1998). These observations raise the posibility that the different Aβ species may interact differently with the extracellular environment, making Aβ movement through the different local environments in the CNS an important determinant of cerebral amyloid pathology (Herzig *et al.*, 2004).

The potential for aggregation and toxicity of Aβ species found, can be influenced by mutations of the *APP* and *PS1* genes. Missense mutations within or in close proximity of the Aβ coding region of the *APP* gene are associated with familial forms of AD. Approximately 18 mutations of the *APP* gene have been reported, five of which, the Dutch E693Q causing HCHWA-D (Levy *et al.*, 1990a), Flemish A692G (Hendriks *et al.*, 1992), Artic E693G (Nilsberth *et al.*, 2001), Italian E693K (Miravalle *et al.*, 2000) and Iowa D694N (Van Nostrand *et al.*, 2001) are located in the mid-part of the Aβ sequence. In HCHWA-D (E693Q) the major pathological findings include extensive CAA in the leptomeningeal small arteries and cortical arterioles, but unlike in AD, parenchymal amyloid deposition is minimal and NFTs are not a feature (Maat-Schieman *et al.*, 1996). In HCHWA-D Aβ40 predominates in the leptomeningeal and cortical blood vessel walls with limited labelling in the parenchyma (Castano *et al.*,

1996). The Flemish mutation (A692G) affecting the amino acid immediately before that affected by the Dutch mutation, also has prominent CAA with predominantly Aβ40 deposits (Kumar-Singh *et al.*, 2002). APP mutations flanking the Aβ region interfere with the normal processing of APP, enhancing the formation of β-amyloid peptides ending at residue 42 (Teller *et al.*, 1996; Selkoe, 1998). For example the double Swedish mutation [KM670/671NL] affects the two residues located just before the N-terminus of Aβ, immediately preceding the β-secretase cleavage site (Johnston *et al.*, 1994; Axelman *et al.*, 1994). The pathological phenotype of the Swedish mutation is AD with Aβ plaques as well as extensive NFT pathology (Bogdanovic *et al.*, 2002). Mutations occurring around the γ-secretase cleavage site, including the London mutation (V717I) and the Florida mutation (I716V) enhance the production of Aβ42 (Hardy, 1997; Selkoe, 2001). The phenotypes of these mutations are that of classical AD including extensive NFT pathology.

Mutations, including point mutations and deletions, found in the *PS1* gene have also been shown to increase the brain burden Aβx-42, but not Aβx-40 resulting in parenchymal amyloid deposition (Citron *et al.*, 1997; Duff *et al.*, 1996). Deletions in the *PS1* gene may show a unique morphological phenotype with large 'cotton wool' plaques unlike those observed in AD (Mann *et al.*, 2001b; Houlden *et al.*, 2000; Crook *et al.*, 1998)

The ratio of Aβx-40/Aβx-42 may be a critical factor in the pathogenesis and a determinant of the morphological phenotype. Studies with transfected cell cultures have shown that cells expressing the double Swedish mutation release approximately 7 times more Aβ than their wild type counterparts (Johnston *et al.*, 1994). This mutation increases the total amount of Aβ, leaving the ratio between Aβx40/Aβx-42 unchanged. Whereas in HCHWA-D individuals enhanced deposition of Aβx-40 shifts the ratio

towards Aβx-40 and towards a more vascular pathology (Ozawa *et al.*, 2002). In an effort to understand the mechanism of Aβ deposition, transgenic mouse models have been constructed that express the genes implicated in AD: mutant *APP*, *PS1* and *ApoE*, *tau* as well as wildtype *APP*. Recent work has yielded many lines of transgenic mice that show Aβ deposition and cognitive impairment (Janus *et al.*, 2000). The effect of the overall ratio between Aβx40/Aβx-42 has been examined in transgenic mice. For example in the APPDutch mice the vast majority of Aβ is Aβx-40 with approximately 12 times more AβDutch40 than AβDutch42 (Herzig *et al.*, 2004). Furthermore, the double APPDutch-PS45 mice, produced by crossbreeding the APPDutch mice with the PS45 mice overexpressing mutant PS1 (G384A), resulted in increased Aβx-42 production with the development of parenchymal amyloid lesions (plaques) composed of AβDutch42 rather than vascular pathology (Herzig *et al.*, 2004). Thus, although AβDutch preferentially accumulates Aβ in and around cerebral blood vessels, by genetically shifting the AβDutch40/AβDutch42 ratio to favour AβDutch42 is sufficient to alter the distribution of the resulting amyloid pathology from the vasculature to the parenchyma (Herzig *et al.*, 2004).

The accumulation of Aβ in the brain is determined not only by the rate of Aβ generation but also by its clearance. Evidence suggests that both the LRP and RAGE receptors are involved in receptor mediated bidirectional flux of Aβ across the BBB (Zlokovic, 2004). While LRP appears to mediate Aβ movement from brain to periphery, RAGE has been strongly implicated in the influx of Aβ into the CNS. In addition, evidence exists to suggest that 10%-15% Aβ can enter into the CSF from the brain and onward into the blood stream (Shibata *et al.*, 2000). LRP, located at the BBB, has been shown to favour the clearance of Aβ40 over the more amyloidogenic species Aβ42 and the

mutant form of Aβ containing two *APP* gene mutations (Dutch and Iowa) (Deane *et al.*, 2004). These data suggest that the mutations not only render Aβ more prone to amyloid formation, but may also impede efflux out of the brain via the LRP receptor (Deane *et al.*, 2004). Different proteases (neprilysin, endothelin-converting enzyme, angiotensin-converting enzyme, plasmin and insulin degrading enzyme) have been implicated in proteolysis-related clearance of Aβ from the CNS (Carson & Turner, 2002; Morelli *et al.*, 2003; Morelli *et al.*, 2002; Farris *et al.*, 2004). Clearance experiments in rats showed that after infusion of radiolabelled Aβ peptides into the lateral ventricle, 40% of the injected radioactivity was present in the blood and urine and taken up by the liver and kidneys, indicating a clearance mechanism and involvement of systemic organs in the catabolism of Aβ (Ghersi-Egea *et al.*, 1996).

FBD has been previously shown to be pathologically characterised by CAA and amyloid plaques, which are composed of ABri (Holton *et al.*, 2001; Vidal *et al.*, 1999). ABri is a 4kDa peptide cleaved by a furin-like proteolysis from the C-terminus of the mutated precursor protein ABriPP (Vidal *et al.*, 1999). ABri isolated from leptomeningeal fibrillar deposits shows a high degree of polymerization and a post-translationally modified N-terminus (pyroglutamate) at position 1 (Vidal *et al.*, 1999). In contrast, soluble ABri from sera of FBD patients consistently revealed monomeric forms of ABri with no obvious N-or C-terminal heterogeneity (Ghiso *et al.*, 2001). However, little is known about the heterogeneity of the amyloidogenic peptide ABri composing the different CNS lesions and whether these ABri species differ when they deposit in in the parenchyma or blood vessels. FDD is pathologically similar to FBD, but both the vascular and parenchymal deposits are composed of ADan (see chapter 4; (Holton *et al.*, 2002; Vidal *et al.*, 2000b). The first 22 residues of ADan and ABri are identical and biochemically ADan has also been demonstrated to possess N-teminal

modifications described in relation to ABri with pyroglutamates found at position 1 (Vidal *et al.*, 2000b). An interesting finding of all FDD cases, so far examined, is the presence of widespread co-deposition of Aβ.

As a correlation exists between the N- and C- terminal heterogeneity of the Aβ peptide species and different lesion types in AD, the question addressed here was whether a similar heterogeneity of ABri, ADan and Aβ occurs in FBD and FDD respectively. To address this question ABri and ADan species deposited in blood vessels and parenchymal lesions were isolated and biochemically characterised in FBD and FDD respectively, along with the co-depositing Aβ in FDD. Several regions were taken from frozen material for the study, including the hippocampus, entorhinal cortex, occipital cortex and thalamus. The extraction strategy took advantage of the differential solubility properties of soluble peptides (soluble in PBS), pre-amyloid (insoluble in PBS but soluble in SDS) and the amyloid fractions (insoluble in PBS or SDS, but soluble in formic acid). From each extraction step several techniques were undertaken to reveal the amyloid species contained in the tissue, including mass spectrometry and western blot analysis. The availability of a panel of antibodies specific for N- and C-terminally modified Aβ species made it possible to study the heterogeneity of the Aβ species co-deposited in the parenchyma and CAA in FDD and AD using immunohistochemical techniques. The immunohistochemical investigation was used to confirm mass spectrometry results or add additional information about the heterogeneity of the Aβ species present in FDD and AD.

7.2 Material and methods

7.2.1 Tissue

Brain from two FBD cases (1&2), one FDD case (3), two sporadic AD cases (6&7), two familial AD cases, which included one case with variant AD with cotton wool plaques due to *PS1* ΔI83/ΔM84 mutation (4) (Houlden *et al.*, 2000b; Steiner *et al.*, 2001), a case caused by *PS1* M233V mutation (5) and two age-matched controls were collected at post mortem (8&9) (table 24). The pathological diagnosis of AD was made using standard criteria (Mirra *et al.*, 1991).

Case	Case number	Age	Sex	Cause of death	Diagnosis
1	PM 91-99	68	F	Bronchopneumonia	FBD
2	PM 3319	65	F	Bronchopneumonia	FBD
3	PM 37-99	43	M	Bronchopneumonia	FDD
4	PM100-95	46	F	Bronchopneumonia	FAD
5	PM132-99	N/A	N/A	N/A	FAD
6	A96/95	86	M	Bronchopneumonia	AD
7	A104/95	81	M	N/A	AD
8	C8-99	79	M	Ca.prostate	Control
9	C4-99	91	M	Bronchopneumonia	Control

***Table 24**: Cases used in biochemical analysis of amyloid and preamyloid species.*

From case 1 frontal, occipital, cerebellum including the dentate nucleus were dissected and used for biochemical analysis; from case 2 occipital and parietal lobes were available for use; from case 3 frontal, posterior frontal, temporal, thalamus, occipital, dura vessels, hippocampus, entorhinal cortex and leptomeninges were used; from cases 4, 6, 8 and 9 frontal cortex was used; from case 5 occipital cortex was used; from case 7 the hippocampus was used.

7.2.2 Protein extraction

Crude protein extraction was undertaken as described in section 2.9.1. From these crude extracts the protein was further purified as described in section 2.9.2.

7.2.2.1 Mass spectrometry

All cases and all samples of protein extract were subjected to mass spectrometry analysis as described in section 2.10.

7.2.2.2 Immunoblotting

Aliquots from the samples extracted were subjected to western blot analysis using antibodies specific to ABri, ADan and Aβ as described in section 2.12. Antibodies used for western blot analyses are listed in table 25.

Antibody	Source	Species	Dilution
Aβ 1-17	Biosource	Monoclonal	1:4000
Aβ 17-26	Biosource	Monoclonal	1:4000
Ab338	Gift Dr J Ghiso	Polyclonal	1:3000
Ab5282	Gift Dr J Ghiso	Polyclonal	1:3000

***Table 25**: Antibodies used for western blot analysis of non-fibriallar and fibrillar ADan, ABri and Aβ species in FDD, FBD and AD.*

7.2.2.3 Immunoprecipitation

Samples from the FDD case (case 3) underwent immuoprecipitation to extract only the ADan or Aβ species from the samples before analysis with MS. Experimental procedures are described in section 2.12.

7.2.3 Immunohistochemistry

7.2.3.1 Tissue

Brain from three cases of FDD (1-3), six sporadic AD cases (7-12) and three familial AD cases (4-6) were collected at post mortem (table 26). The pathological diagnosis of AD was made using standard criteria (Mirra *et al.*, 1991). For immunohistochemical analysis the hippocampus, frontal cortex and cerebellum were used from cases 1-4 and

7-12. From case 6 only hippocampus and frontal cortex were available and from case 5 only frontal cortex was available for immunohistochemical analysis.

Case	Case number	Age	Sex	Cause of death	Diagnosis
1	PM37-99	43	M	Bronchopneumonia	FDD
2	PM38-99	60	F	Bronchopneumonia	FDD
3	PM39-99	58	M	Not recorded	FDD
4	PM100-95	46	F	Bronchopneumonia	FAD
5	PM8-00	N/A	N/A	N/A	FAD
6	PM 3385	35	F	FAD	FAD
7	PM69-99	92	F	Pneumonia	AD
8	PM32-97	91	F	Pneumonia	AD
9	PM93-99	76	F	AD	AD
10	PM73-98	86	M	Bronchopneumonia	AD
11	PM25-98	69	F	Acute tracheobronchitis	AD
12	PM83-98	84	F	Dementia	AD

***Table 26:** FDD, familial AD and sporadic AD cases used in N-terminal Aβ immunohistochmeical study.*

7.2.3.2 Antibodies

Immunohistochemical analysis was carried out at light microscopy level using the standard protocol (section 2.2) and the antibodies listed in table 27.

Antibody	Source	Species	Pretreatment	Dilution
Aβ 1-17	Biosource	Monoclonal	FA + PC	1:4000
Aβ 17-26	Biosource	Monoclonal	FA + PC	1:4000
Aβ 8-15	Dako	Monoclonal	FA + PC	1:100
Aβ x-40	Biosource	Polyclonal	FA + PC	1:100
Aβ x-42	Biosource	Polyclonal	FA + PC	1:100
Aβ 1(rD)	Gift from Dr T Saido	Polyclonal	FA + PC	1:1000
Aβ 1(D)	Gift from Dr T Saido	Polyclonal	FA + PC	1:500
Aβ 3(pE)	Gift from Dr T Saido	Polyclonal	FA + PC	1:100
Aβ 11(pE)	Gift from Dr T Saido	Polyclonal	FA + PC	1:1000

***Table 27:** Antibodies used for N-terminal immunohistochemical Aβ study in FDD and AD. FA; Formic Acid, PC; Pressure Cook.*

7.3 Results

7.3.1 Biochemical analysis

7.3.1.1 Direct western blot analysis of FBD

Western blot analysis was carried out on the PBS-soluble; SDS-soluble; formic acid fractions for ABri using the anti-Ab338 antibody. A summary of the results are shown in table 28, showing the monomeric, dimeric and trimeric ABri species present in each analysed fraction.

Case	Region	Subregion	PBS-soluble fraction			SDS-soluble fraction			Formic acid fraction		
			ABri			ABri			ABri		
			M	D	T	M	D	T	M	D	T
1	Frontal cortex	Gray matter	+	+	+	+	+	-	+	+	+
1	Frontal cortex	White matter	+	+	+	+	+	-	+	+	-
1	Frontal cortex	Blood vessels	+	+	-	+	+	+	+	+	+
1	Occipital cortex	Gray matter	+	+	+	+	-	-	+	+	+
1	Occipital cortex	White matter	+	+	+	+	-	-	+	-	-
1	Occipital cortex	Blood vessels	+	+	-	+	+	-	+	+	+
1	Cerebellum	Blood vessels	+	+	-	+	+	+	+	+	+
1	Cerebellum	-	+	+	-	+	-	-	+	-	-
1	Cerebellum	Dentate nucleus	-	-	-	+	-	-	+	+	-
2	Occipital cortex	Gray matter	+	-	-	+	+	-	+	+	-
2	Occipital cortex	White matter	+	-	-	+	+	-	+	+	-
2	Occipital cortex	Blood vessels	+	-	-	+	+	-	+	+	+
2	Parietal cortex	Gray matter	+	+	-	+	+	-	+	+	-
2	Parietal cortex	White matter	+	+	-	+	+	-	+	+	-
2	Parietal cortex	Blood vessels	+	+	-	+	+	-	+	+	+

Table 28: *Direct western blot analysis of non-fibrillar and fibrillar ABri species in FBD. Identified in PBS-soluble, SDS-soluble and formic acid fractions from case 1 and case 2 showing monomeric (M), dimeric (D) and trimeric (T) species present.*

Samples from case 1 are shown in figure 7.1 with bands clearly visible that represent the monomeric (3.4 kDa), dimeric (6.8 kDa) and trimeric (10.2 kDa) forms of ABri. The monomeric form of ABri was present in all PBS-soluble fractions obtained apart from the dentate nucleus. In case 2 the monomeric form was found in all areas investigated (table 28).

The dimeric form of ABri was present in the PBS-soluble fractions of all FBD tissue apart from the occipital cortex from case 2. The trimeric form was only present in the PBS-soluble fraction in the white and gray matter of the frontal and occipital cortices from case 1 (figure 7.1). The blood vessels extracted from the same regions did not show any ABri trimers.

The fraction collected after re-suspension in SDS was investigated for the presence of pre-amyloid/SDS-soluble peptides. All samples studied had visible monomeric bands in the pre-amyloid (SDS-soluble fraction). As summarised in table 28 and shown in figure 7.1 for case 1. Dimeric species were found in the frontal (gray and white matter, and blood vessels) cortex of case 1 (figure 7.1) and occipital and parietal cortices from case 2 (table 28), along with the blood vessels found in the cerebellum. Trimers were found in the blood vessels extracted from the frontal and occipital cortices from case 1 (figure 7.1B lanes 6&7), but not the parenchyma.

The amyloid fraction, the fraction remaining after extraction by PBS and SDS and treated with formic acid, showed a greater amount of ABri than the previous fractions. Especially in the blood vessels extracted from all regions from case 1 (figure 7.1C lanes 5-7) and the blood vessels from the occipital and parietal cortices from case 2 (table 28). A similar pattern was observed in the parenchymal extracts with the white matter from all the cortices only producing a monomeric band (figure 7.1C lanes 2&4), while in the gray matter monomeric, dimeric and trimeric bands were observed (figure 7.1C lanes 1&3).

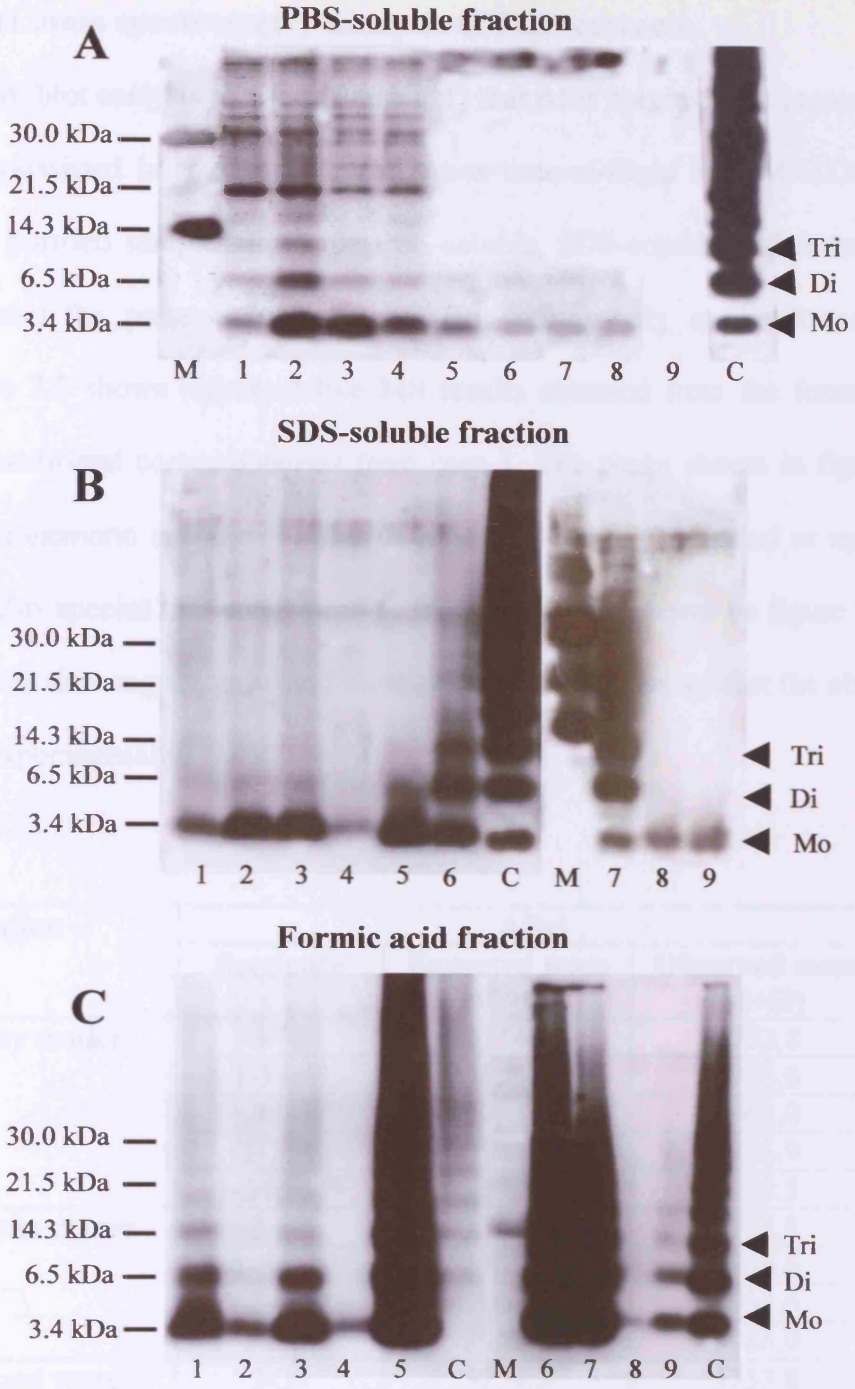

Figure 7.1: Direct western blot analysis of ABri in FBD (Case 1). Western blot analysis of PBS-soluble, SDS-soluble and formic acid extracted fractions from different regions of FBD (case 1), showing monomeric (Mo), dimeric (Di) and trimeric (Tri) ABri species. In the PBS-soluble fraction the majority of ABri species present was monomeric in all samples with a faint band shown in the dimeric region. In the SDS-soluble fraction stronger bands were seen in the monomeric bands, along with stronger bands in the dimeric region in the frontal and cerebellum blood vessels. In the formic acid fraction monomeric bands were visible in all regions and strong dimeric bands were seen in all blood vessel samples and gray matter samples, whereas white matter samples did not appear to contain any dimeric species. Lane **1** frontal (gray matter), lane **2** frontal (white matter), lane **3** occipital (gray matter), lane **4** occipital (white matter), lane **5** occipital (blood vessels), lane **6** frontal (blood vessels), lane **7** cerebellum blood vessels, lane **8** cerebellum, lane **9** dentate nucleus (M-marker and C- synthetic control).

7.3.1.2 Direct mass spectrometry analysis of FBD extracts

Although western blot analysis showed (figure 7.1) that ABri species were present in all fractions Matrix-assisted laser desorption ionisation-time-of-flight MS (MALDI-TOF) analysis of the purified samples from the PBS-soluble, SDS-soluble and formic acid fractions indicated the presence of various ABri species only in the formic acid fractions. Figure 7.2 shows representative MS results obtained from the formic acid fraction from the frontal cortex obtained from case 1. The peaks shown in figure 7.2 correspond to monomeric species of ABri in either full length, truncated or modified peptides. The ABri species that correspond to the major peaks shown on figure 7.2 are shown in table 29, showing the expected mass of the ABri species against the observed mass obtained experimentally.

Region	ABri		
	Sequence	Expected mass [M+H]	Observed mass [M+H]
Frontal gray matter	3-34	3754.3	3753.8
	1-34pE	3936.5	3936.6
	1-34pE*	3964.5	3962.0
	1-34*	3982.5	3986.9
	1-34pE**	3992.5	3988.5
Frontal white matter	3-34	3754.3	3753.8
	1-34pE	3937.5	3936.6
	1-34pE*	3964.5	3964.6
	1-34*	3983.5	3986.9
Frontal blood vessels	3-34	3754.3	3753.8
	3-34*	3782.3	3782.4
	3-34**	3810.3	3810.8
	1-34pE	3936.5	3936.8
	1-34pE*	3964.5	3964.6
	1-34pE**	3992.5	3992.6

Table 29: *Direct mass spectrometry analysis of fibrillar ABri. Theoretical average and observed ABri molecular masses bearing a single disulphide-bond between cysteine residues 5 and 22, are shown in the table from the frontal gray matter, white matter and extracted blood vessels (case 1). Formylated species are indicated by * and species containing a pyroglutamate are indicated with pE. M+H; protonated molecular ions.*

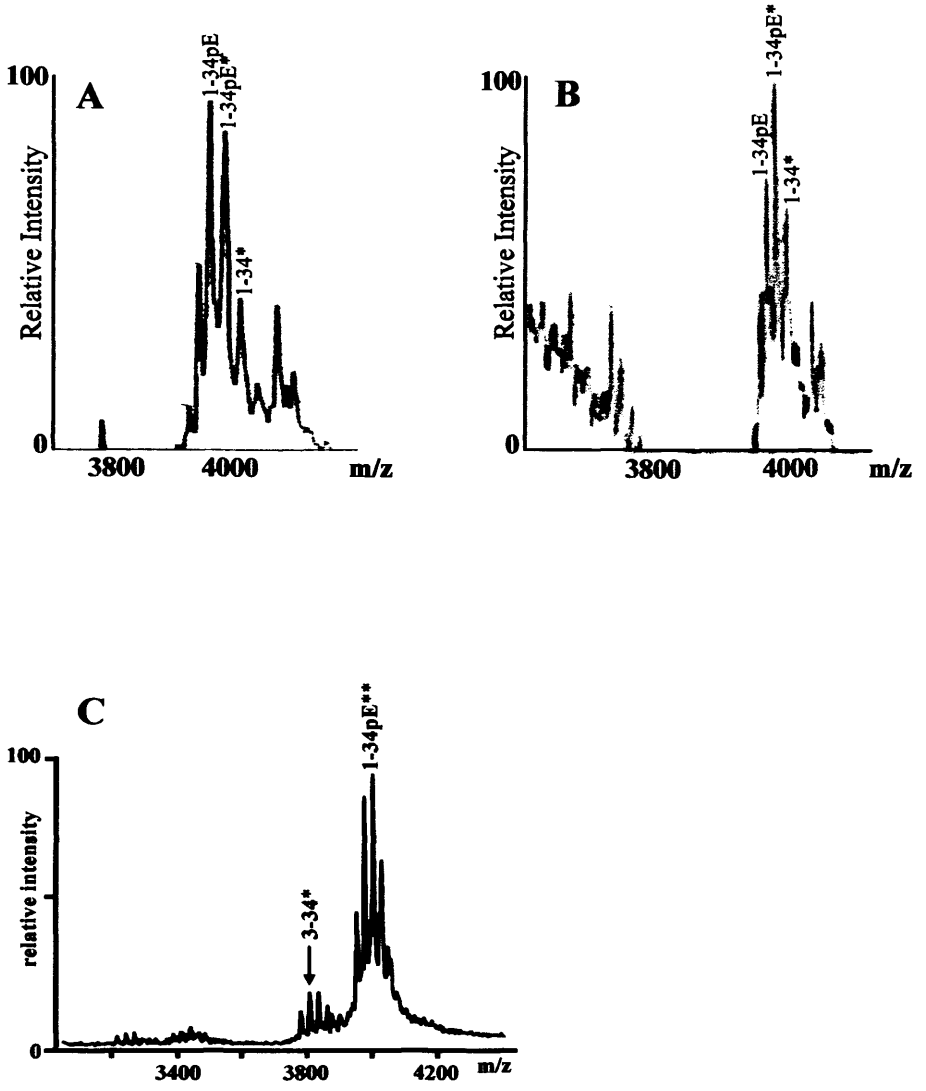

Figure 7.2: Direct mass spectrometry analysis of fibrillar ABri. For MALDI-TOF analysis, ABri molecules were desalted by ZipTip micro-reverse phase column, eluted with 90% (v/v) acetonitrile-0.1% trifluroacetic acid in water, as described in the material and methods. *Panel A:* Frontal gray matter FA-extracts from microvessel-depleted cortex after PBS and SDS extractions. *Panel B:* Frontal white matter FA extracts and *Panel C:* Blood vessel extracts from frontal cortex in FA-isolated vessels after PBS and SDS extractions. See table 29 for detailed listing of ABri species present. m/z; used to denote the dimensionless quantity formed by dividing the mass number of an ion by its charge number [mass to charge ratio].

7.3.1.3 Analysis of non-fibrillar ABri species in FBD extracts after immunoprecipitation.

Although ABri species were seen on the western blot anaylsis from the PBS and SDS extraction without immunoprecipitation no species were found when MS analysis was undertaken. Therefore the additional immunoprecipitation step was introduced to obtain a concentrated ABri sample for MS analysis.

Western blot analysis was carried out on the FBD samples after immunoprecipitation, although the blots obtained without immunoprecipitation showed the presence of monomeric and multimeric species (figure 7.1). Western blots were repeated to confirm their presence after the immunoprecipitation step (figure 7.3). The PBS-soluble and SDS-soluble fractions clearly showed the monomer, dimeric and trimeric ABri species (figure 7.3).

MALDI-TOF MS analysis was carried out after immunoprecipitation. The PBS-soluble fractions were composed of a mixture of two ABri full length species (ABri 1-34) differing in 18 mass units, a difference equivalent to the mass of one molecule of water, corresponding to a pyroglutamate N-terminal modification. The SDS-extracted fractions contained the same two ABri species when analysed with MS to those found in the PBS-soluble fractions. The experimental masses found for ABri 1-34 and ABri 1-34pE were in good agreement with the expected masses of the post-translationally modified species, with a single disulphide bond between cysteine residues 5 and 22 (table 30, figure 7.3).

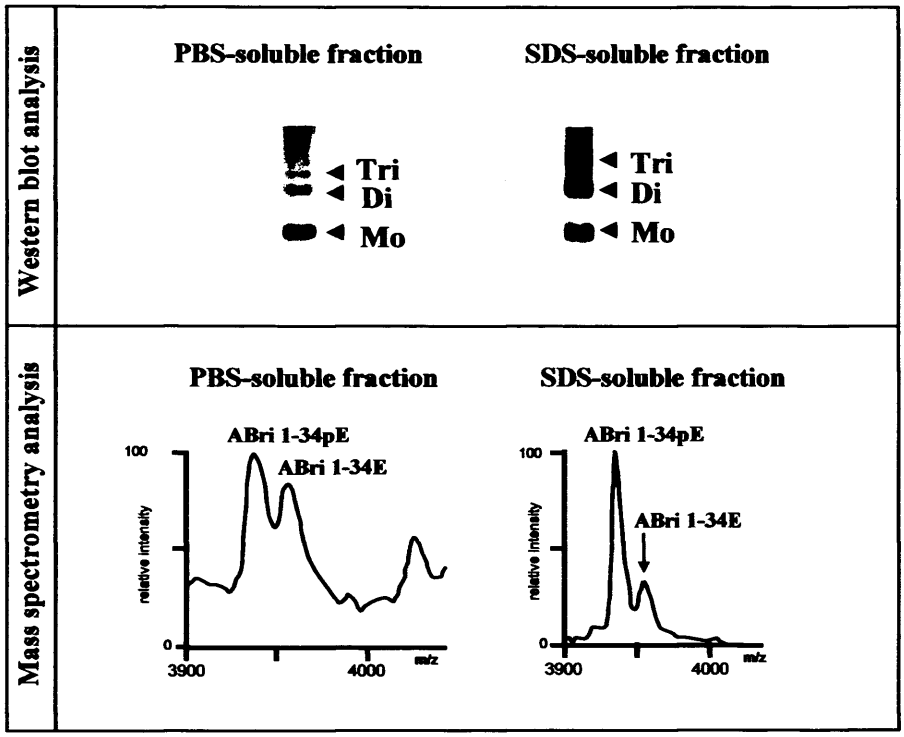

Figure 7.3: Western blot and MALDI-TOF MS analysis of PBS-soluble and SDS-extracted fraction from FBD after immunoprecipitation. ABri species were immunoprecipitated with Dynabeads coated with Ab338. Bound peptides were eluted and analysed either by western blot using Ab338 or by MALDI-TOF MS. Theoretical average masses and experimental ABri molecular masses are shown in table 30. Mo, monomers; Di, dimers; Tri, trimers.

ABri Species	Observed Mass [M+H]		Expected mass [M+H]
	PBS	SDS	
1-34pE	3935.6	3936.5	3936.5
1-34	3951.5	3953.8	3954.5

Table 30: *Mass spectrometry analysis of non-fibrillar ABri deposits after immunoprecipitation. ABri molecules were immunoprecipitated using Dynabeads coated with Ab338 and subsequently eluted in Tris-Tricine sample buffer. MS analysis via MALDI-TOF revealed full-length ABri (1-34) and full-length ABri with pyroglutamate (pE) modification in both PBS and SDS soluble fractions. M+H; protonated molecular ions.*

7.3.1.4 Direct western blot analysis of FDD

Samples were analysed from the PBS-soluble, SDS-soluble/pre-amyloid and formic acid/ amyloid fractions. Western blots were run for each fraction and blotted using both Ab5282 to recognise ADan peptides and a cocktail of Ab4G8 and Ab6E10 antibodies to recognise Aβ peptide species. A summary of the findings from all regions are shown in table 31.

Blood vessels extracted from the leptomeninges showed a monomeric band (~3.4 kDa) corresponding to ADan in the PBS-soluble fraction, but no band corresponding to Aβ was present (figure 7.4, lane 3). No other bands in any other region studied showed any positivity in the PBS-soluble fractions for either ADan or Aβ (table 31). The SDS-soluble fractions analysed yielded a monomeric and dimeric forms of ADan from the blood vessels extracted from the leptomeninges, but no Aβ was found (figure 7.4, lane 3).

All formic acid fractions from all regions studied (table 31) showed the monomeric form of ADan, although the intensity of the staining varied between samples. For example, the amount of monomeric ADan seen in the thalamus (figure 7.5, lane 15) was substantially less than that observed in the blood vessels separated from the temporal lobe (figure 7.5, lane 25). All samples showed a dimeric form of ADan, apart from the

thalamus, third temporal gyrus gray matter (figure 7.5, lane 11) and entorhinal cortex (figure 7.4, lane 2). The trimeric form of ADan was found in a limited number of samples where the amount of ADan was greatly increased. These included the blood vessels extracted from the leptomeninges, blood vessels that underwent only formic acid extraction (those blood vessels not previously undergone PBS and SDS extractions), first temporal gyrus gray matter and blood vessels extracted from this region.

	PBS-soluble fraction						**SDS-soluble fraction**						**Formic acid fraction**					
	ADan			**Aβ**			**ADan**			**Aβ**			**ADan**			**Aβ**		
Region	**M**	**D**	**T**	**M**	**D**	**T**	**M**	**D**	**T**	**M**	**D**	**T**	**M**	**D**	**T**	**M**	**D**	**T**
Posterior frontal gray matter	-	-	-	-	-	-	-	-	-	-	-	-	+	+	+	+	+	-
Posterior frontal white matter	-	-	-	-	-	-	-	-	-	-	-	-	+	+	-	+	+	-
Posterior frontal blood vessels	-	-	-	-	-	-	-	-	-	-	-	-	+	+	-	+	+	-
Second frontal gyrus gray matter	-	-	-	-	-	-	-	-	-	-	-	-	+	+	-	+	+	-
Second frontal gyrus white matter	-	-	-	-	-	-	-	-	-	-	-	-	+	+	-	+	+	-
Second frontal gyrus blood vessels	-	-	-	-	-	-	-	-	-	-	-	-	+	+	-	+	+	-
Third temporal gyrus gray matter	-	-	-	-	-	-	-	-	-	-	-	-	+	+	-	-	+	-
Third temporal gyrus white matter	-	-	-	-	-	-	-	-	-	-	-	-	+	+	-	+	+	-
Third temporal gyrus blood vessels	-	-	-	-	-	-	-	-	-	-	-	-	+	+	-	+	+	-
Second temporal gyrus gray matter	-	-	-	-	-	-	-	-	-	-	-	-	+	+	-	-	-	-
Second temporal gyrus white matter	-	-	-	-	-	-	-	-	-	-	-	-	+	+	-	+	+	-
Second temporal gyrus blood vessels	-	-	-	-	-	-	-	-	-	-	-	-	+	+	-	+	+	-
Occipital gray matter	-	-	-	-	-	-	-	-	-	-	-	-	+	+	+	-	-	-
Occipital white matter	-	-	-	-	-	-	-	-	-	-	-	-	+	+	-	-	-	-
Occipital blood vessels	-	-	-	-	-	-	-	-	-	-	-	-	+	+	-	-	-	-
First temporal gyrus gray matter	-	-	-	-	-	-	-	-	-	-	-	-	+	+	+	+	+	-
First temporal gyrus white matter	-	-	-	-	-	-	-	-	-	-	-	-	+	+	-	-	+	-
First temporal gyrus blood vessels	-	-	-	-	-	-	-	-	-	-	-	-	+	+	+	+	+	-
Thalamus	-	-	-	-	-	-	-	-	-	-	-	-	+	+	-	-	-	-
Thalamus blood vessels	-	-	-	-	-	-	-	-	-	-	-	-	+	+	-	-	-	-
Dura blood vessels	+	+	-	-	+	-	+	+	-	-	-	-	+	+	+	+	+	-
Hippocampus	-	-	-	-	-	-	-	-	-	-	-	-	+	+	-	+	+	-
Entorhinal	-	-	-	-	-	-	-	-	-	-	-	-	+	-	-	-	-	-
Leptomeninges blood vessels	+	-	-	-	-	+	+	-	-	-	-	-	+	+	+	+	+	-

Table 31: *Direct western blot analysis of non-fibrillar and fibrillar ADan and Aβ species in FDD. Identified in PBS-soluble, SDS-soluble and formic acid fractions from case 3, showing monomeric (M), dimeric (D) and trimeric (T) species.*

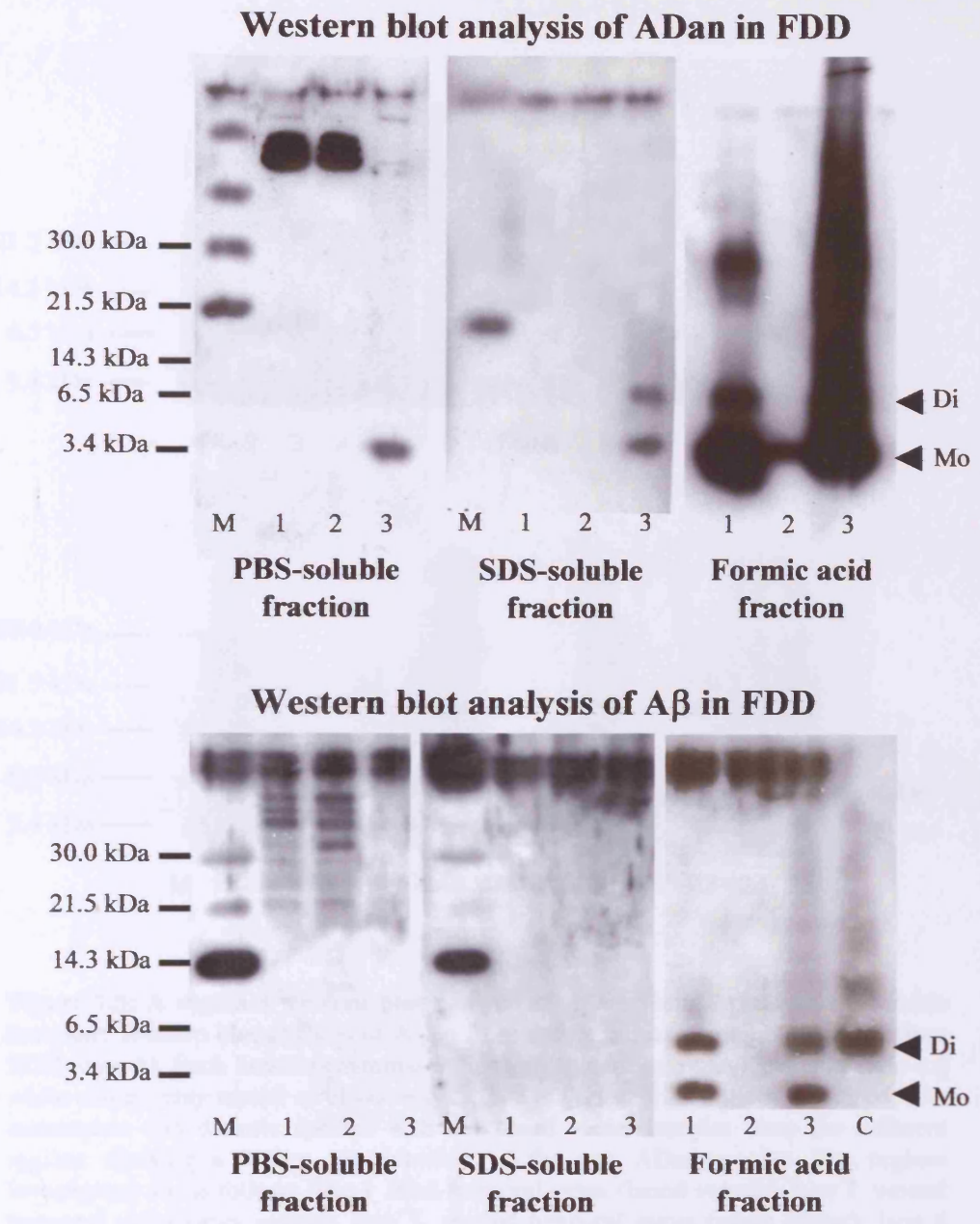

Figure 7.4: Direct western blot analysis of ADan and Aβ from hippocampus, entorhinal cortex and leptomeningeal blood vessels. Western blot analysis ADan (detected with Ab5282) and Aβ (detected with Ab4G8 and Ab6E10) from the PBS-soluble, SDS-soluble and formic acid extracted fractions from hippocampus (lane 1), entorhinal cortex (lane 2) and blood vessels extracted from the leptomeninges (lane 3) of FDD, showing monomeric (Mo) and dimeric (Di) ADan and Aβ species. Monomeric ADan species were found in the leptomeningeal blood vessels in the PBS-soluble fraction, whereas monomeric and dimeric species were found in the SDS-soluble and formic acid fraction. With a greater amount found in the formic acid fraction. The hippocampal sample showed only monomeric and dimeric species in the formic acid insoluble fraction, whereas only a monomeric band was found from the entorhinal cortex sample. Aβ monomeric and dimeric species were only found in the formic acid insoluble fraction in the hippocampal and leptomeningeal blood vessels. The absence of ADan and Aβ from the PBS and SDS fractions were the main reason for introducing the immunoprecipitation step necessary to visualize soluble ADan and Aβ. (M-marker and C-synthetic control).

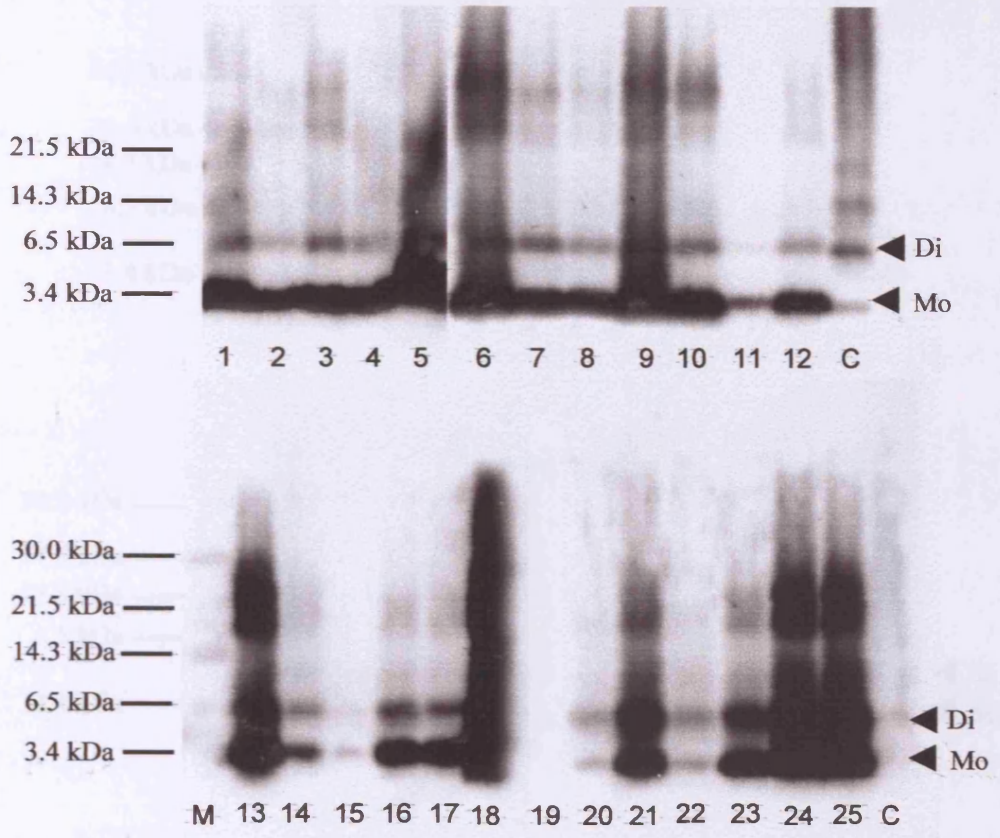

Figure 7.5: A regional western blot analysis of ADan from formic acid insoluble fraction: Western blot analysis of ADan from the formic acid insoluble fraction from FDD (case 3). Each lane representing a different anatomical region and subregion e.g white matter, gray matter or blood vessels. The majority of the regions contained both monomeric and dimeric species with the blood vessel samples from the different regions showing a higher concentration of the two ADan species. The regions investigated are as follows lane **1** third temporal gyrus (blood vessels), lane **2** second temporal gyrus (gray matter), lane **3** second temporal gyrus (white matter), lane **4** second temporal gyrus (blood vessels), lane **5** posterior frontal (blood vessels), lane **6** posterior frontal (gray matter), lane **7** posterior frontal (white matter), lane **8** second frontal gyrus (gray matter), lane **9** second frontal gyrus (white matter), lane **10** second frontal gyrus (blood vessels), lane **11** third temporal gyrus (gray matter), lane **12** third temporal gyrus (white matter), lane **13** dura blood vessels, lane **14** thalamus blood vessels, lane **15** thalamus, lane **16** occipital (gray matter), lane **17** first temporal gyrus (white matter), lane **18** formic acid vessels, lane **19** thalamus, lane **20** occipital (white matter), lane **21** occipital (gray matter), lane **22** occipital (blood vessels), lane **23** first temporal gyrus (white matter), lane **24** first temporal gyrus (gray matter), lane **25** first temporal gyrus (blood vessels), **C** control, **M** marker.

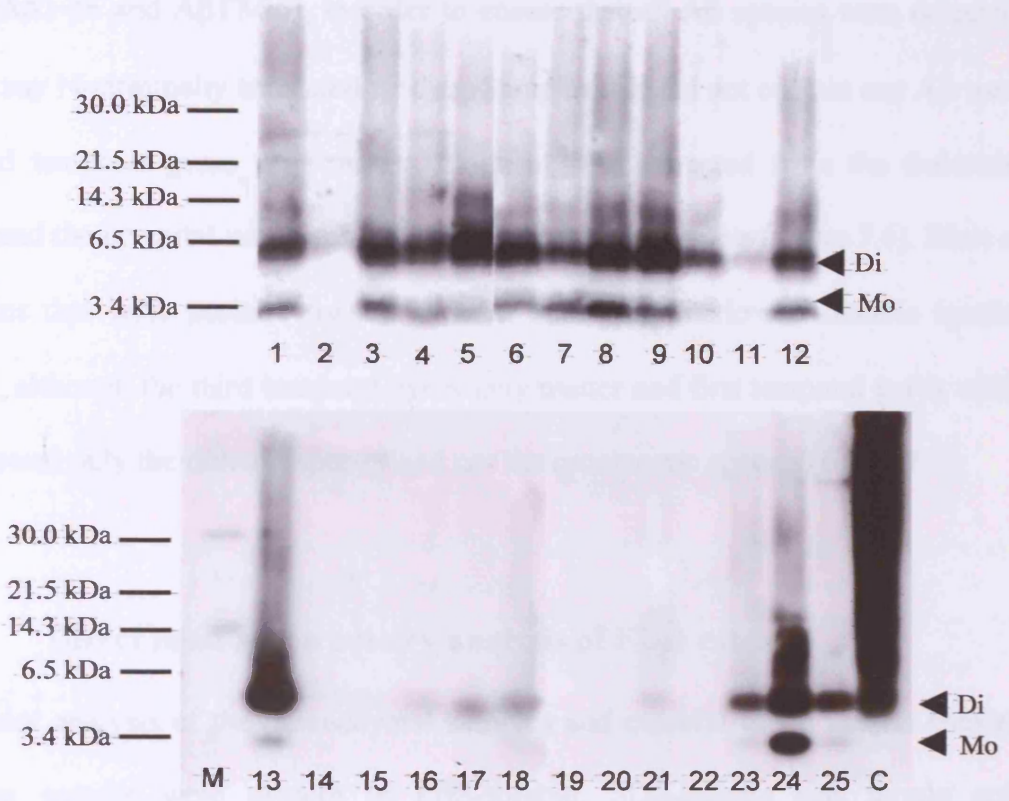

Figure 7.6: A regional western blot analysis of Aβ from formic acid insoluble fraction: Western blot analysis of Aβ (detected using Ab4G8 and Ab6E10) from the formic acid insoluble fraction from FDD (case 3). Each lane representing a different anatomical region and subregion e.g white matter, gray matter or blood vessels. Monomeric (Mo) and dimeric (Di) species were found within the temporal and frontal regions and dura vessels. The regions investigated are as follows lane **1** third temporal gyrus (blood vessels), lane **2** second temporal gyrus (gray matter), lane **3** second temporal gyrus (white matter), lane **4** second temporal gyrus (blood vessels), lane **5** posterior frontal (blood vessels), lane **6** posterior frontal (gray matter), lane **7** posterior frontal (white matter), lane **8** second frontal gyrus (gray matter), lane **9** second frontal gyrus (white matter), lane **10** second frontal gyrus (blood vessels), lane **11** third temporal gyrus (gray matter), lane **12** third temporal gyrus (white matter), lane **13** dura blood vessels, lane **14** thalamus blood vessels, lane **15** thalamus, lane **16** occipital (gray matter), lane **17** first temporal gyrus (white matter), lane **18** formic acid vessels, lane **19** thalamus, lane **20** occipital (white matter), lane **21** occipital (gray matter), lane **22** occipital (blood vessels), lane **23** first temporal gyrus (white matter), lane **24** first temporal gyrus (gray matter), lane **25** first temporal gyrus (blood vessels), **C** control, **M** marker.

The formic acid fractions were also investigated using two Aβ antibodies combined together (Aβ1-16 and Aβ17-26), in order to ensure that all Aβ species were detected, including any N-terminally truncated species. Samples that did not contain any Aβ were the second temporal gyrus gray matter, blood vessels extracted from the thalamus, thalamus and the occipital white and gray matter and blood vessels (figure 7.6). Most of the samples that were positive for Aβ showed both monomeric and dimeric species (table 31), although the third temporal gyrus gray matter and first temporal gyrus white matter showed only the dimeric species and not the monomeric species (figure 7.6).

7.3.1.5 Direct mass spectrometry analysis of FDD extracts

Western blot analysis of the parenchymal samples and cerebral blood vessels showed that ADan species were present in PBS-soluble, SDS-soluble and formic acid sequentially extracted fractions. As, expected the majority of ADan was recovered from the amyloid extracts and it was not possible to evaluate the direct MS results for the PBS and SDS samples as no peaks corresponded to any ADan species.

Analysis of the formic acid fractions revealed complexity in terms of composition of ADan species. The interpretation of the MS analysis was challenging due to the additional presence of mono-, di-, and tri-formylated species likely on the lysine and/or serine residues (Duewel & Honek, 1998) artificially generated due to the extraction procedure (additional mass of 28 for each formylation). Both parenchymal and vascular lesions were composed of a heterogenous mixture of post-translationally modified and N- and C-terminally truncated ADan species. The predominant species were ADan1-33pE, ADan1-28pE and ADan1-34pE although the presence of ADan3-28, ADan1-27pE, ADan1-30pE, ADan3-33, ADan3-34, ADan1-33 and ADan1-34 were consistently demonstrated (table 32, figure 7.7).

ADan species	Expected Mass [M+H]	Observed mass in parenchyma	Observed mass in vessels
3-28	3090.6	3091.5	3091.3
1-27pE	3158.7	3158.8	3159.1
1-28pE	3272.8	3272.9	3272.7
1-30pE	3488.0	3489.2	3489.3
3-33	3700.2	3700.7	3701.3
3-34	3863.4	3863.7	3864.8
1-33pE	3882.4	3883.3	3883.4
1-33	3900.4	3903.2	3900.4
1-34pE	4045.6	4045.6	4046.5
1-34	4063.6	4063.6	4063.7

Table 32: *Direct mass spectrometry analysis of fibrillar ADan. Mass spectrometry analysis via MALDI-TOF revealed full-length ADan (1-34), C- and N-terminally truncated species along with N-terminally modified species with pyroglutamate (pE). Peaks were also found corresponding to formylated species as shown in figure 7.7. M+H; protonated molecular species.*

7.3.1.6 Analysis of ADan species in FDD extracts after immunoprecipitation

An immunoprecipitation step was carried out on the samples for the same reason as the FBD samples. When analysed previously without prior immunoprecipitation, gray and white matter were separated from each other and the blood vessels. Because the results obtained from the gray and white matter were similar for the immunoprecipitation experiments parenchyma was separated from the blood vessels. Using a combination of immunoprecipitation and western blot/ mass spectrometry it was possible to detect ADan species in the PBS and SDS soluble fractions. There were noticeable differences in terms of degree of aggregation, in the PBS-soluble fraction ADan species were mainly monomeric, with some dimers barely visible in both parenchymal and vascular fractions (figure 7.8).

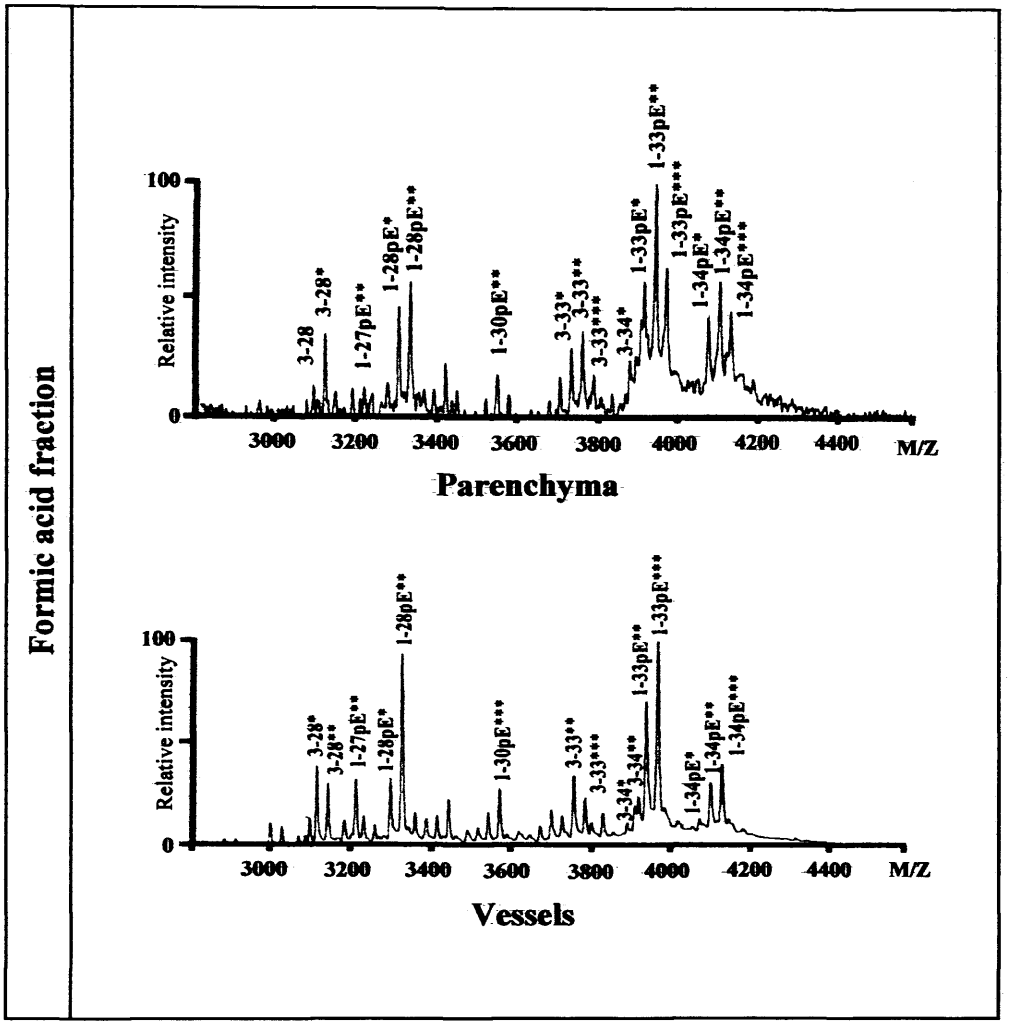

Figure 7.7: Direct mass spectrometry analysis of fibrillar ADan deposits. Formic acid fractions from blood vessel depleted frontal cortex and leptomeningeal blood vessels after PBS and SDS extractions contain various ADan species. Both C- and N-terminally truncated species were found with and without modifications. The theoretical average masses and experimental ADan molecular masses are shown in table 34. Peaks corresponding in mass to formylated species are indicated by asterisks (*, single formylation: **, double formylation: ***, triple formylation: pE pyroglutamate modification)

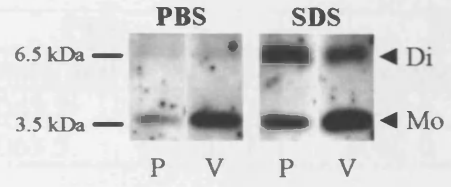

***Figure 7.8**: Western blot analysis of ADan species extracted from PBS and SDS fractions after immunoprecipitation. ADan molecules were immunoprecipitated using Dynabeads with anti-ADan Ab5282 and subsequently eluted in Tris-Tricine sample buffer for Western blot analysis. Mo, monomers; Di, Dimers; P, parenchyma; V, vessels.*

Whereas the SDS-soluble fractions showed a higher tendency to aggregate. The presence of dimeric ADan species in the parenchymal extracts showed an equal intensity to the monomeric species, although the vascular samples still showed a higher monomeric content (figure 7.8).

MALDI-TOF MS was carried out after immunoprecipitation showing the PBS-soluble fractions were composed of a mixture of two ADan species differing in 18 mass units 4045.2 for parenchyma / 4045.3 for blood vessels (expected 4045.2) and 4063.5 for parenchyma / 4062.7 for blood vessels (expected 4063.6), a difference equivalent to the mass of one molecule of water and likely corresponding to ADan-pE and ADan species (table 33, figure 7.9). The SDS-extracted fractions contained the same two ADan species when analysed with MS to those found in the PBS-soluble fractions. The experimental masses 4043.6 for parenchymal /4045.6 for blood vessels and 4062.0 for parenchymal /4063.6 for blood vessels were in good agreement with the expected masses of the post-translationally modified ADan-pE (4045.6) and the wild-type ADan (4063.6), with a single disulphide-bond between cysteine residues 5 and 22 (table 33, figure 7.9).

ADan species	PBS		SDS		Expected mass [M+H]
	Parenchymal	Vessel	Parenchymal	Vessel	
1-34pE	4045.2	4045.3	4043.6	4045.6	4045.6
1-34	4063.5	4062.7	4062.0	4063.6	4063.6

Table 33: *Mass spectrometry analysis of non-fibrillar ADan deposits after immunoprecipitation. ADan molecules were immunoprecipitated using Dynabeads coated with anti-ADan Ab5282 and subsequently eluted with a 4:4:1 mixture of isopropyl alcohol/water/formic acid. Mass spectrometry analysis via MALDI-TOF revealed full-length ADan (1-34) and full-length ADan with pyroglutamate modification (pE) in both the PBS-soluble and SDS-soluble fractions. M+H; protonated molecular species.*

7.3.1.7 Direct analysis of Aβ species in FDD extracts

The western blot analysis of the PBS-soluble, SDS-soluble and formic acid fractions from the leptominenges, hippocampus and entorhinal cortex showed that Aβ species were only present in detectable amounts in the formic acid fraction. However, the direct MS results from the formic acid fraction showed no Aβ species to be present. The MS readings showed an array of peaks none of which corresponded to any known Aβ species (data not shown). Further analysis using immunoprecipitation was carried out to identify the Aβ species found present on the western blot analysis.

7.3.1.8 Analysis of Aβ species in FDD after immunoprecipitation.

Using a combination of immunoprecipitation and western blot/ mass spectrometry it was possible to detect Aβ species in the PBS and SDS soluble fractions. There were noticeable differences in terms of degree of aggregation, in the PBS-soluble Aβ species were mainly dimeric, with some monomers barely visible in both parenchymal and vascular fractions (figure 7.10). The SDS-soluble fractions also showed a high tendency to aggregate, with dimeric Aβ species in the parenchymal and vascular extracts showing a greater intensity than the monomeric species (figure 7.10).

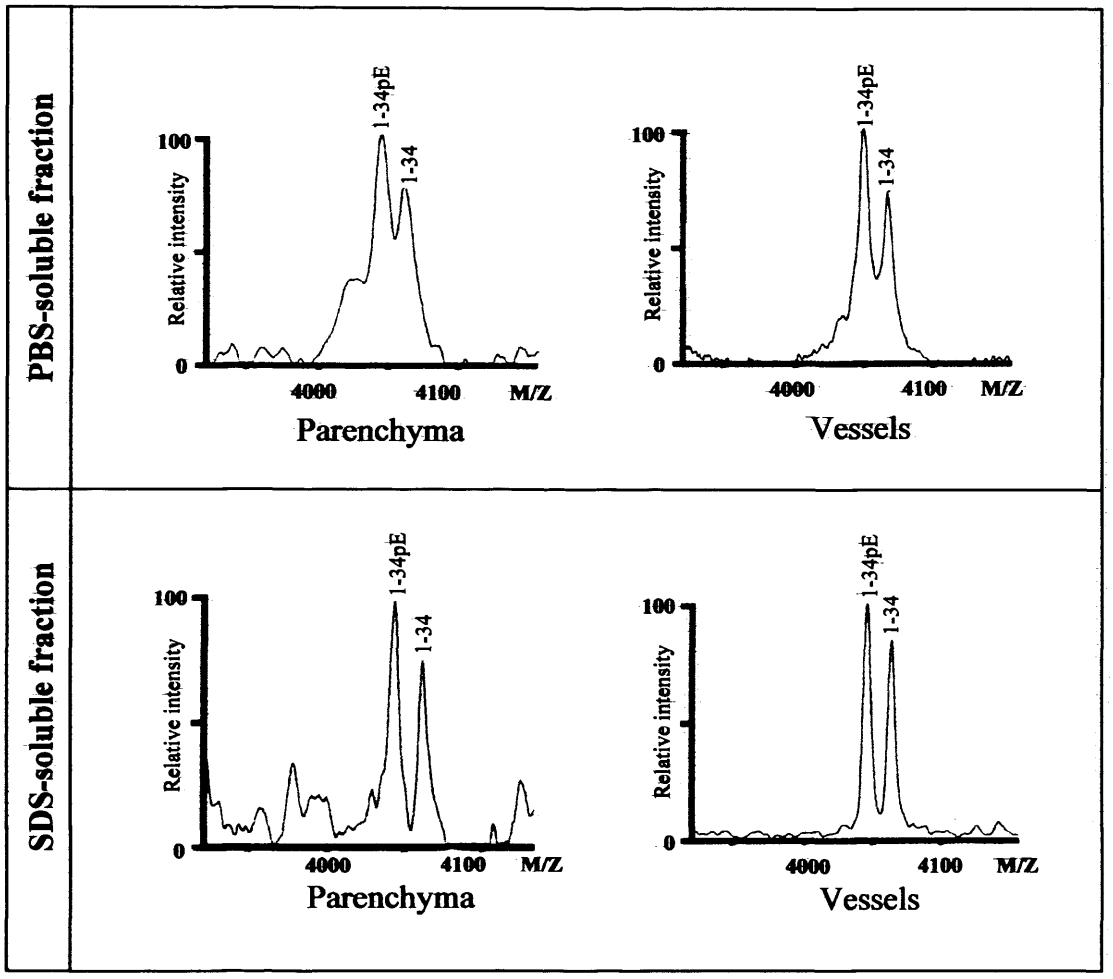

Figure 7.9: Mass spectrometry analysis of non-fibrillar ADan deposits after immunoprecipitation. ADan molecules were immunoprecipitated using Dynabeads coated with anti-ADan Ab5282 and subsequently eluted in water/isopropyl alcohol/formic acid (4:4:1) for mass spectrometry via MALDI-TOF. PBS-soluble fractions from blood vessel depleted frontal cortex and leptomeningeal blood vessels are shown to contain both the full length ADan species (1-34) and the full length with a pyroglutamate modification at the N-terminus. SDS-soluble fractions from the same regions showed the same ADan species present. The theoretical average masses and experimental ADan molecular masses are shown in table 33.

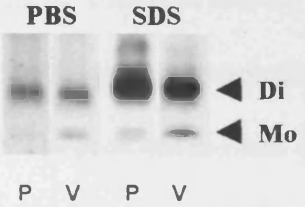

Figure 7.10: *Western blot analysis of Aβ species extracted from PBS and SDS fractions after immunoprecipitation. Aβ molecules were immunoprecipitated using Dynabeads with anti-Aβ antibody 4G8 and subsequently eluted in Tris-Tricine sample buffer for Western blot analysis. Mo, monomers; Di, Dimers; P, parenchyma; V, vessels.*

In parenchymal extracts MALDI-TOF MS analysis after immunoprecipitation revealed a small peak that corresponded to the Aβ4-34 fragment (experimental 3473.5; expected 3472.9) no other peaks corresponded to any other Aβ species (table 34, figure 7.11). Vascular extracts, on the other hand, showed major peaks corresponding to Aβ1-42, Aβ4-42 and Aβ1-40, the latter being a minor component (table 34, figure 7.11).

When the SDS-extracts were analysed by the same procedures, MS indicated that the parenchymal and blood vessel extracts mainly contained Aβ1-42 and its N-terminally truncated derivative Aβ4-42 whereas Aβ1-40 was a minor component (table 34, figure 7.11). The double peak obtained in this sample is due to the presence of Aβ peptides bearing oxidized Met35 (Met Sulpoxide +16 mass units) most probable a technical artefact due to the use of formic acid to process this sample for MS.

Aβ species	PBS soluble fraction		SDS soluble fraction		Expected mass
	Parenchymal	Vessels	Parenchymal	Vessels	[M+H]
4-34	3473.5	-	-	-	3472.9
4-42	-	4199.4	4200.0	4198.1	4199.8
1-40	-	4329.3	4331.1	4331.1	4330.9
1-42	-	4513.9	4514.9	4515.6	4515.1

Table 34: *Mass spectrometry analysis of non-fibrillar Aβ in FDD after immunoprecipitation. Aβ species were immunoprecipitated with Dynabeads coated with a mixture of anti-Aβ1-17 and anti- Aβ17-26 antibodies. Bound peptides were eluted and analysed by MS. PBS-soluble and SDS-soluble fractions of the frontal cortex and leptomeningeal blood vessels were analysed.*

When the formic acid extracts were analysed by MS for both parenchymal and vascular samples the most prominent signal corresponded to an experimental mass of 4200.0, consistent with the theoretical protonated mass of 4199.8 for Aβ4-42. Both Aβ1-42 and Aβ1-40 were also present in the sample, although Aβ1-40 was a minor contributor to the formic acid extract. Two additional peaks differing in +16 and +28 mass units with Aβ4-42 were also observed. Both experimental masses matched the expected values for Aβ4-42 (Met Sulphoxide) and Aβ4-42 (formylated) (table 35, figure 7.11).

Since samples were exposed to formic acid during the extraction procedure and prior to the MS analysis, these Aβ derivatives may well represent undesirable secondary products of the specimen treatment rather then actual post-translationally modified components present in the lesions. Alternatively, these oxidised Aβ42 species may represent existent *in vivo* neurotoxic subproducts of oxidative stress, as previously proposed (Butterfield, 2002).

Aβ species	Parenchymal	Vessels	Expected mass [M+H]
4-42	4200.0	4200.2	4199.8
4-42 OX	4215.9	4216.3	4215.8
4-42*	4228.1	4228.4	4227.8
1-40	4330.0	4330.3	4330.9
1-42	4514.9	4515.9	4515.1

Table 35: *Mass spectrometry analysis of fibrillar Aβ in FDD. MS analysis of parenchymal FA-extracts from micro-vessel depleted frontal cortex after PBS and SDS extractions. Along with FA fractions from leptomenigeal blood vessels. M+H; protonated molecular ions.*

It is interesting to note that the Aβ1-40 species was found to be a minor species in FDD when the pathological eveidence of AD suggests the major species of Aβ found in vascular structures is Aβ1-40. Further immunohistochemical investigations have been carried out to confirm this finding (section 7.3.2).

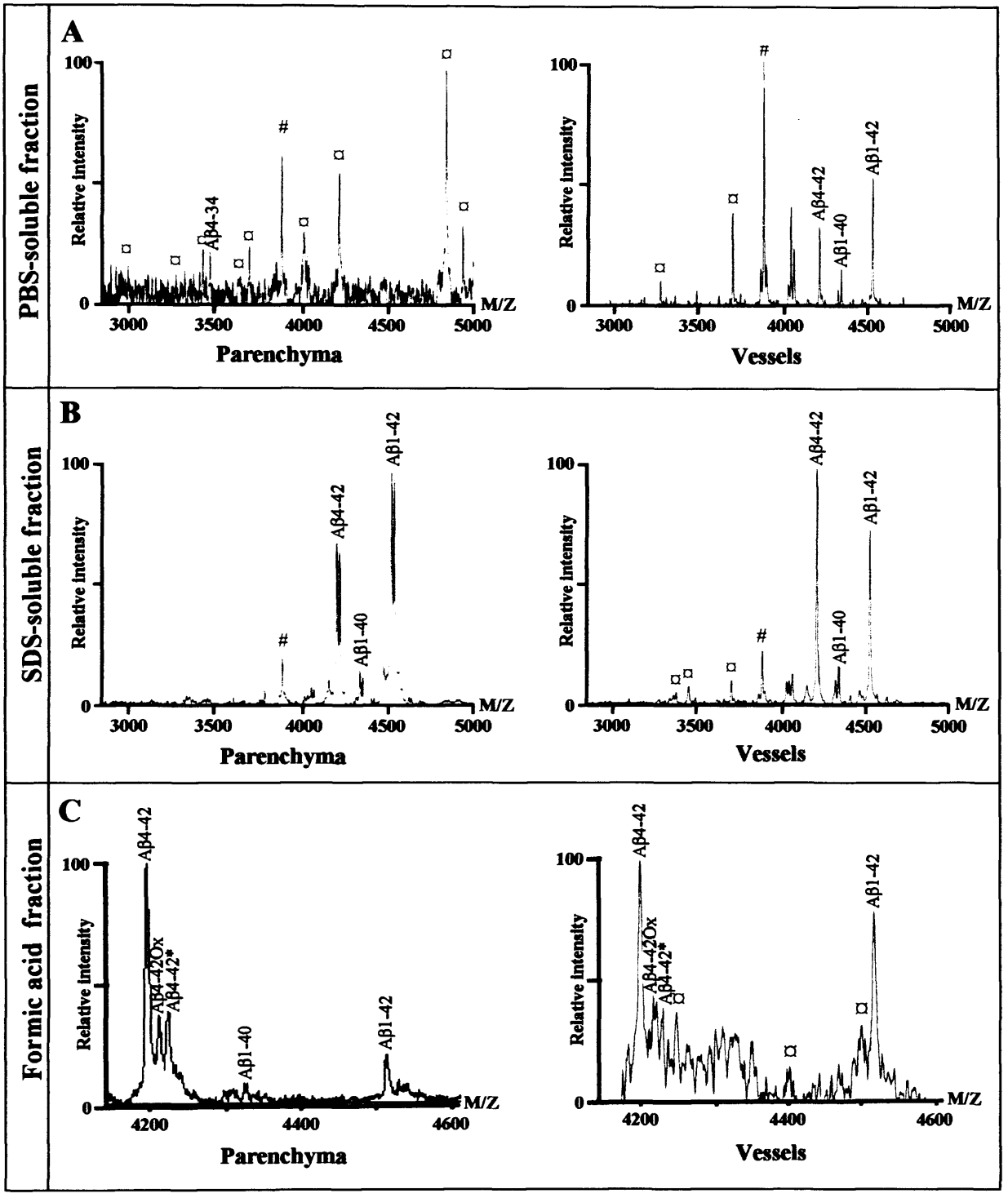

Figure 7.11: Mass spectrometry analysis of Aβ in FDD after immunoprecipitation. Aβ species were immunoprecipitated with Dynabeads coated with a mixture of Aβ1-17 and Aβ17-26. Bound peptides were eluted and analysed by MALDI-TOF MS as described in material and methods. PBS extracted fractions of microvessel-depleted frontal cortex (parenchyma) and isolated microvessels from frontal cortex (vessels) (panel A), SDS-extracted fractions (panel B) and formic acid extracted fraction (panel C). Theoretical average masses and experimental Aβ molecular masses are shown in tables 36 & 37. Peaks of MS indicated by # were present in the negative controls (without brain extracts) and considered to be non-specific. Peaks notated by ¤ were also obtained in negative controls (using brain extracts but uncoated Dynabeads) and considered non-specific.

7.3.1.9 Western blot analysis of sporadic AD, FAD and normal controls

In the PBS-soluble fractions, no monomeric Aβ species were found in any region studied. Aβ dimers were found in the frontal gray matter of FAD (case 4) and the frontal blood vessels of sporadic AD (case 6) (table 36). No Aβ species were detected in the SDS-soluble fractions in any AD, FAD or normal control cases. The formic acid extraction samples showed an abundance of Aβ in both monomeric and dimeric forms in both sporadic AD and FAD (table 36). Of the two normal controls used, one (case 8) showed no Aβ species which was predictable, but the other control used (case 9) showed both monomeric and dimeric species of Aβ. This may be due to the age of the control case (91 years) (table 36).

Case	Diagnosis	Region	Subregion	PBS-soluble fraction			SDS-soluble fraction			Formic acid fraction		
				Aβ			Aβ			Aβ		
				M	D	T	M	D	T	M	D	T
4	FAD	Frontal cortex	White matter	-	-	-	-	-	-	+	+	-
4	FAD	Frontal cortex	Gray matter	-	+	-	-	-	-	+	+	-
4	FAD	Frontal cortex	Blood vessels	-	-	-	-	-	-	+	+	-
5	FAD	Occipital cortex	White matter	-	-	-	-	-	-	+	+	-
5	FAD	Occipital cortex	Gray matter	-	-	-	-	-	-	+	+	-
5	FAD	Occipital cortex	Blood vessels	-	-	-	-	-	-	+	+	-
6	AD	Frontal cortex	White matter	-	-	-	-	-	-	+	+	-
6	AD	Frontal cortex	Gray matter	-	-	-	-	-	-	+	+	-
6	AD	Frontal cortex	Blood vessels	-	+	-	-	-	-	+	+	-
7	AD	Hippocampus	-	-	-	-	-	-	-	-	-	-
8	Control	Frontal cortex	White matter	-	-	-	-	-	-	-	-	-
8	Control	Frontal cortex	Gray matter	-	-	-	-	-	-	-	-	-
8	Control	Frontal cortex	Blood vessels	-	-	-	-	-	-	-	-	-
9	Control	Frontal cortex	White matter	-	-	-	-	-	-	+	+	-
9	Control	Frontal cortex	Gray matter	-	-	-	-	-	-	+	+	-
9	Control	Frontal cortex	Blood vessels	-	-	-	-	-	-	+	+	-

Table 36: *Western blot analysis of non-fibrillar and fibrillar Aβ species in sporadic AD, FAD and normal controls. Distribution of Aβ species in extracted supernatants from cases 4 and 5 (familial AD), cases 6 and 7 (sporadic AD) and cases 8 and 9 normal controls. Showing monomeric (M), dimeric (D) and trimeric (T) Aβ species.*

7.3.1.10 Mass spectrometry analysis of Aβ species in sporadic AD, FAD and normal controls

Mass spectrometry analysis was carried out on PBS-soluble, SDS-soluble and formic acid fractions collected from the sporadic AD, FAD and normal control cases. In sporadic AD and FAD major Aβ species in both the gray and white was both Aβ1-42 and Aβ1-40. Whereas in the blood vessels Aβ1-40 species without any modifications were dominant (data not shown).

7.3.2 Immunohistochemical study of Aβ species in FDD, AD and FAD

7.3.2.1 Aβ immunohistochemistry in FDD

Antibodies to Aβ1-16, Aβ17-26 and Aβ8-15 gave a similar staining pattern and will therefore be described together and referred to as Aβ (figure 7.12). Aβ immunohistochemistry revealed that a large number of blood vessels including capillaries and arterioles (figure 7.12F) were positive in the CA1 subregion of the hippocampus and subiculum (figure 7.12C). The majority of the labelling in this region was vascular, but an occasional perivascular Aβ deposit (figure 7.12B) was found. In addition, sparse diffuse deposits were weakly stained. In the CA4 subregion of the hippocampus no vascular Aβ was found, but diffuse deposits were present in the parenchyma (figure 7.12E, 7.12H). A similar pattern of diffuse staining was present in the CA2 and CA3 subregions. In the parahippocampus, entorhinal and transentorhinal cortices Aβ deposits were seen in capillaries and arterioles. In addition, prominent perivascular deposits were detected. Such deposits were found around blood vessels that were affected by Aβ deposition and also around blood vessels that were negative for Aβ, but were obviously affected by amyloid deposition, therefore by ADan deposition (figure 7.12B). The fusiform gyrus showed prominent vascular and perivascular

deposits, but an increase in the number of compact parenchymal diffuse plaques was observed (figure 7.12H). Affected blood vessels tended to be more frequent in the superficial laminae and parenchymal deposits in the deeper laminae. Dense staining was also found the subpial region of the fusiform gyrus (figure 7.12A). The neocortical regions showed a similar staining pattern to that observed in the fusiform gyrus showing an increase in the number a compact Aβ positive ill-defined plaques and the occasional leptomeningeal blood vessel affected by the deposition of the peptide was seen.

7.3.2.2 Heterogeneity of Aβ species in FDD

The three FDD cases (cases 1-3) studied showed varying degrees of staining intensity with the different N- and C-terminal Aβ antibodies. Although the intensity varied the structures stained by each antibody were the same, so will be described together. Immunohistochemistry was carried out using antibodies recognising different N-terminal amino acids N1(D), N1(rD), N3(pE) and N11(pE) (Saido TC et al 1995). N1(D), N1(rD) and N3(pE) stained Aβ affected blood vessels throughout the hippocampus and subiculum (figure 7.13 C-E), although the diffuse parenchymal plaques stained weakly. The staining pattern found in the fusiform gyrus and neocortices was similar to that seen with Aβ. N11(pE) on the other hand stained all structures shown to be positive with Aβ, including capillaries, arterioles, diffuse deposits, compact plaques, perivascular plaques and subpial deposits but the overall staining intensity was weaker than that observed with the other N-terminal antibodies (figure 7.13F).

C-terminal heterogeneity of the Aβ species were also investigated using Aβx-40 and Aβx-42 end specific antibodies. Aβx-42 showed strong immunolabelling of all structures labelled with Aβ deposition (figure 7.13H). The anti-Aβx-40 antibody

showed a staining pattern with scanty immunolabelling present in capillaries and arterioles, including leptomeningeal vessels (figure 7.13G). Weak staining was found in a few perivascular plaques and there was some diffuse deposits stained, but the number Aβ deposits stained was considerably lower than that seen with anti-Aβx-42 antibody. These findings confirmed the observations seen using mass spectrometry, although differing from what one would expect from the data relating to Aβ, Aβ1-42 was found to be the major Aβ species over Aβ1-40 using immunohistochemistry.

7.3.2.3 Aβ immunohistochemisty in FAD

As in FDD, the staining pattern for the Aβ antibodies Aβ1-16, Aβ17-26 and Aβ8-15 was very similar so will all be described together and referred to as Aβ. In the superficial cortical layers cotton wool plaques were found in the subpial region (figure 7.14B, arrow), which was followed by a layer of diffuse deposits (figure 7.14B, double arrow). Cotton wool plaques were found throughout the deeper cortical layers (figure 7.14A). In the hippocampus all cotton wool plaques were found to be positive with Aβ. Blood vessels, including capillaries and arterioles were positive in the hippocampus but reduced in number compared to that seen in the cortical regions. Diffuse deposits with no definite structures were found in the parvopyramidal clusters (figure 7.14C). In the entorhinal cortex all lesion types were stained including diffuse deposits (figure 7.14D, arrow), cotton wool plaques (figure 7.14G, 7.14H) and blood vessels (figure 7.14E arrow, 7.14I), but here the positive staining in the capillaries became prominent. Positive staining was also found in the white matter in the blood vessels and a small amount of diffuse staining, along with a large amount of subpial staining (figure 7.14F).

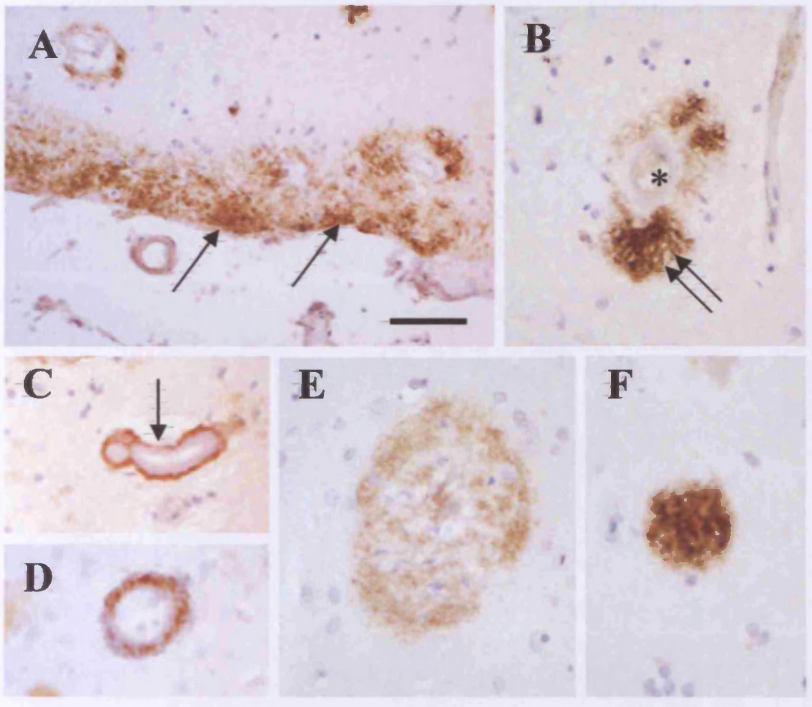

Figure 7.12: Immunohistochemical study of Aβ deposition in FDD. Panels A-F are immunostained with Aβ 1-16 antibody (Biosource International). Subpial deposits stained with Aβ (A, arrows). Perivascular staining (B, double arrow) was seen around blood vessels affected with ADan amyloid (B, asterisk). Vascular Aβ staining was observed in the periphery of ADan amyloid-laden capillaries (C, arrow), along with arterioles showing patchy Aβ deposition (D, arrow). Plaques positively stained with Aβ were found throughout the parenchyma in various forms including diffuse deposits (E) and compact ill-defined plaques (F). Bar in panel A represents 100μm on panel A; 55μm on panel B,F; 28μm on panels C, D and E

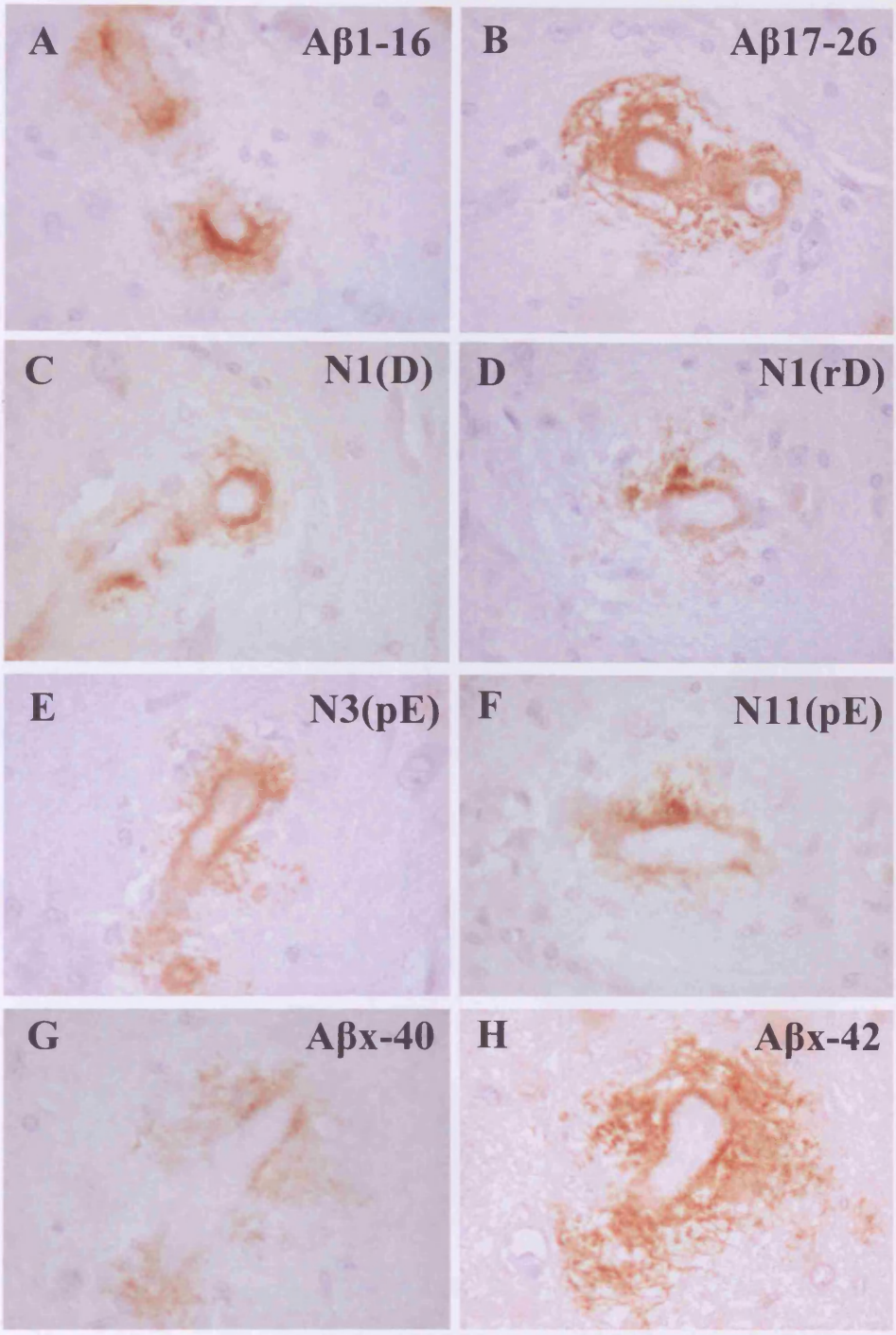

Figure 7.13: N-terminal Aβ immunohistochemistry in FDD blood vessels. In FDD positive Aβ staining was found in all types of blood vessels from small capillaries, to arterioles and arteries. Serial sections were used and the pathological lesions recognised using Aβ1-16 (A), Aβ17-26 (B), N1(D) (C), N1(rD) (D), N3(pE) (E), N11(pE) (F), Aβx-40 (G), Aβx-42 (H). Bar in panels A-H represents 55μm.

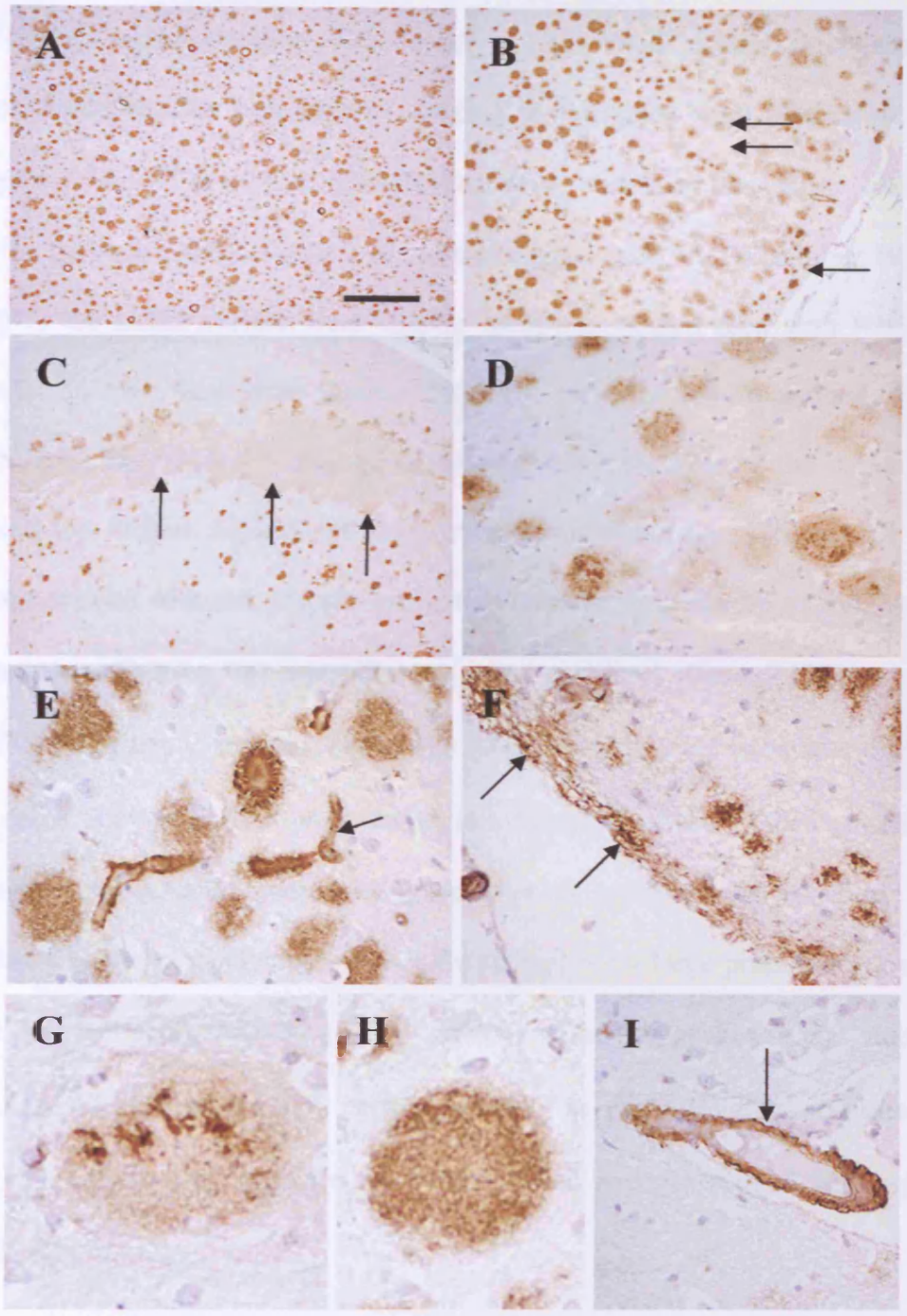

Figure 7.14: Aβ deposition in FAD. Aβ17-26 immunohistochemistry in FAD showing the pathological lesions stained. The dense staining of the cotton wool plaques in the deep cortical layers is shown in A. The different types of diffuse plaques are shown the cortical layers in B, with traditional cotton wool plaques found towards the subpial (arrow), and more diffuse cloudy deposits found in the cortical layers below (double arrow). The diffuse deposit of the parvopyrmaidal clusters of the entorhinal cortex are shown in C, arrows. Panel D shows the looseness of the diffuse deposits compared to the cotton wool plaques. Panel E (arrow) shows the intensity of the vascular staining in the capillaries. Panel F (arrows) shows the amount of Aβ deposited in the subpial. Panels G and H show two plaques at higher magnification. Panel I (arrow) shows a large arteriole positively stained with Aβ. Bar in panel A represents 250 μm in A-D; 55 μm in panels E,F and I; 28 μm in panels G and H.

7.3.2.4 Heterogeneity of Aβ species in FAD

Strong N1(D) immunolabelling was found in the blood vessels throughout the hippocampus whereas the parenchymal staining in the cotton wool plaques was very weak (figure 7.15C). The diffuse Aβ structures with no defined boundaries, like those found in the parvopyramidal clusters, remained negative with N1(D) staining. Whereas with N1(rD) the blood vessels were equally as strong as that seen with N1(D) the parenchymal staining was more intense than seen with the N1(D) antibody (figure 7.15D). N3(pE) and N11(pE) antibodies showed weak staining of the cotton wool plaques and the diffuse deposits of the parvopyramidal clusters. Whereas all blood vessels were stained with anti-N3(pE) and anti-N11(pE) antibodies the staining was not as prominent as with Aβ or the antibodies starting at position 1 (figure 7.15E).

The distribution of two C-terminal antibodies Aβx-40 and Aβx-42 were investigated in the FAD cases. Aβx-40 gave strong staining in all amyloid affected blood vessels with the occasional perivascular plaque being positive. A small portion of cotton wool plaques found in the parenchyma was weakly stained but a large proportion remained unstained (figure 7.15G). Aβx-42 gave a contrasting staining pattern to that seen with Aβx-40. Aβx-42 gave occasional positive staining in the capillaries and arterioles (figure 7.15H, inset). The cotton wool plaques were strongly stained with Aβx-42 (figure 7.15H).

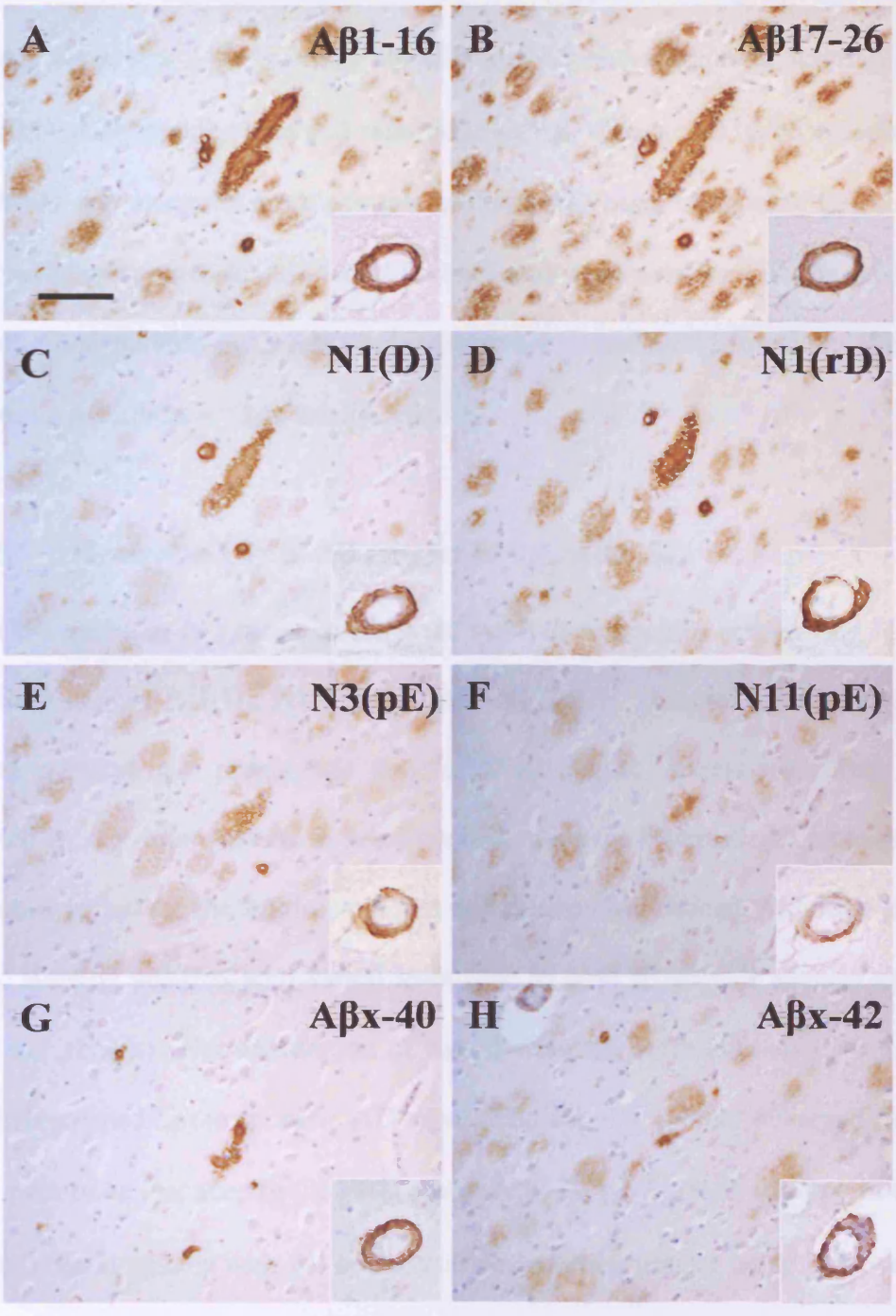

Figure 7.15: Distribution of Aβ staining in FAD. Parenchymal cotton wool plaques and an amyloid-laden capillary immunolabelled with a panel of Aβ antibodies. Serial sections that were stained with Aβ1-16 (A), Aβ17-26 (B), N1(D) (C), N1(rD) (D), N3(pE) (E), N11(pE) (F), Aβx-40 (G), Aβx-42 (H). Inset shows a cortical arteriole immunostained with the same panel of Aβ antibodies. Bar in panel A represents 100μm in panels B-H. In insets bar represents 45 μm.

7.3.2.5 Aβ immunohistochemistry in sporadic AD

The Aβ antibodies Aβ1-16, Aβ17-26 and Aβ8-15 showed similar staining patterns so will all be described together and referred to as Aβ. Occasional blood vessels, including capillaries and arterioles were positive in those AD cases containing CAA. Cored and compact plaques were found in all AD cases and were positive with the Aβ antibodies. Diffuse deposits with no definite structures were occasionally found and were positive with the Aβ antibodies (data not shown).

7.3.2.6 Heterogeneity of Aβ species in sporadic AD

In all the sporadic AD cases investigated the four antibodies recognising N-terminally truncated species (N1(D); N1(rD); N3(pE); N11(pE)) all showed positive reactivity in all the amyloid and preamyloid structures. All blood vessels regardless of size, if affected by amyloid deposition, were positive with the N-terminally truncated species. The same is true for the amyloid plaques and preamyloid lesions. Although the intensity of the staining patterns seen varied from case to case all peptide species were present (data not shown). The distribution of two C-terminal antibodies Aβx-40 and Aβx-42 was investigated in the sporadic AD cases. The staining pattern observed followed the same pattern as that seen in the FAD cases. Aβx-40 gave strong staining in all amyloid affected blood vessels with the occasional perivascular plaque being positive and Aβx-42 gave occasional positive staining in the capillaries and arterioles with plaques being strongly stained with Aβx-42 (data not shown).

7.4 Discussion

The data from this study showed that in both FBD and FDD the complexity of the extracted peptides (ABri and ADan) increased as the solubility of the deposits diminished, as reflected in the degree of oligomerisation, predominant amyloid subunits, extent of post-translational modifications and magnitude of N- and C- terminal proteolytic degradations. In general terms, non-fibrillar deposits appeared less complex than the fibrillar counterparts, perhaps reflecting the presence of early intermediate states of the fibrillisation process (table 37).

	Analysis	Fraction								
		PBS-soluble			SDS-soluble			Formic Acid		
F	Western Blot	M	D	T	M	D	T	M	D	T
B	Mass Spectrometry	1-34pE*			1-34pE*			3-34*		
D		1-34			1-34			1-34pE		
								1-34		
F	Western Blot	M	D	-	M	D	-	M	D	T
D	Mass Spectrometry	1-34pE*			1-34pE*			1-34pE*		
D		1-34			1-34			1-34		
								1-33pE		
								1-33		
								3-34		
								3-33		
								1-30pE		
								1-28pE		

***Table 37**: Summary of findings in FBD and FDD for the peptides ABri and ADan.* The table summarises the peptide species observed with western blot analysis in the PBS-soluble, SDS-soluble and formic acid fractions. The mass spectrometry results show the major species present in the three fractions in order from the species with the major peak (*) to the speices with the smallest peak being less abundant in the sample analysed. M; monomer, D; dimer, T; trimer.

The Aβ species with a more restricted pattern of heterogeneity were also retrieved in all the FDD extracts but not from FBD tissue. This study confirmed previous studies, in FAD and sporadic AD, in that Aβx-40 was found to be the principal component of Aβ vascular deposits whereas Aβx-42 the main component of parenchymal lesions. This was confirmed with both mass spectrometry and immunohistochemical studies.

Suprisingly in FDD the principal component found in vascular and parenchymal deposits, with mass spectrometry and confirmed by the immuohistochemical studies, was Aβx-42, alongside its N-terminal degradation derivative Aβ4-42. This latter finding could not be confirmed with immunohistochemical analysis for no antibodies recognising peptide species starting at position 4 are available at present. Interestingly the N-terminally truncated Aβ4-42 has been shown to aggregate more readily and be more toxic than the full length Aβ1-42 (Pike *et al.*, 1995).

	Analysis	**Fraction**			**Immuno.**
		PBS-soluble	**SDS-soluble**	**Formic Acid**	
F	Western Blot	- D -	M D -	M D -	
D	Mass	4-34*	4-42*	4-42*	1-42**
D	Spectrometry	4-42	1-42	1-42	N1(D)
		1-42	1-40	1-40	N1(rD)
		1-40			N3(pE)
					N11(pE)
					1-40
F	Western Blot	- D -	- - -	M D -	
A	Mass	1-40*	1-40*	1-40*	1-40**
D	Spectrometry	1-42	1-42	1-42	1-42
					N1(D)
					N1(rD)
					N3(pE)
					N11(pE)
A	Western Blot	- D -	- - -	M D -	
D	Mass	1-40*	1-40*	1-40*	1-40**
	Spectrometry	1-42	1-42	1-42	1-42
					N1(D)
					N1(rD)
					N3(pE)
					N11(pE)

Table 38: *Summary of findings of the Aβ peptide in FDD, FAD and AD.* The table summarises the Aβ species observed with western blot analysis in the PBS-soluble, SDS-soluble and formic acid fractions. The mass spectrometry results show the major species present in the three fractions in order from the species with the major peak (*) to the speices with the smallest peak being less abundant in the sample analysed. Immunohistochemical results show the N- and C-terminal truncated species present in the three diseases in order of staining intensity - ** representing the most abundant species. M; monomer, D; dimer, T; trimer.

Interestingly using both mass spectrometry and immunohistochemistry the Aβx-40 species were found to be negligible in FDD (table 38). It is also informative to note that the immunohistochemical studies showed the presence of several Aβ species that were not revealed by mass spectrometry analysis (N1(D); N1(rD); N3(pE); N11(pE)). This may be explained by the methodologies used in the mass spectrometry procedures, where the tissue is processed and the N-terminally truncated species may be diluted out to an undetectable amount, while with immunohistochemistry the peptides are detected in-situ. One possible way around this would be to immunoprecipitate with the N-terminal antibodies followed by mass spectrometry to investigate the presence of the peptide with this methodology.

The non-fibrillar deposits extracted from PBS-soluble and SDS-soluble fractions in the FBD cases showed that the ABri isolated formed mainly monomeric species, but ABri oligomeric species were present in smaller amounts. Both C- and N-terminally truncated ABri species were found. However, if no truncation was present at the N-terminus of ABri a pyroglutamate modification was likely to be present. Cyclic pyroglutamate has been previously found in truncated forms of the Aβ peptide in AD (Mori *et al.*, 1992; Saido *et al.*, 1996; Tekirian *et al.*, 1998), along with early observations in FBD (Vidal *et al.*, 1999). Pyroglutamate modification has also been found in some hormones and neuropeptides including neurotensin, thyrotropin and gonadotropin-releasing hormones in which their biological activities largely depend on the existence of the N-terminal pyroglutamate (Sykes *et al.*, 1999). Although the final pyroglutamate product is the same, neuropeptides and amyloids differ in the amino acid that serves as a substrate for the post-translational modification. In the neuropeptides and peptide hormones the post-translational modification occurs at a glutamine residue and cyclization involves the nucleophilic attack of the α-amino group on the aminidated

carboxyl group and the release of NH_3 catalyzed by glutaminyl cyclase at neutral pH (Busby, Jr. *et al.*, 1987; Fischer & Spiess, 1987). Few examples are known of the post-translational modification from glutamic acid to pyroglutamate, involving a dehydration reaction losing a molecule of water instead of a deamination reaction. Examples of this post-translational modification are bovine and ovine β-lipotropin and joining peptide derived from the proteolytic processing of their common precursor pro-opiomelanocortin (Bateman *et al.*, 1990; Yamashiro & Li, 1976), Aβ N-terminal truncated derivatives Aβ3pE and Aβ11pE in AD (Mori *et al.*, 1992; Saido *et al.*, 1996), along with the recently identified ABri and ADan (Tomidokoro *et al.*, 2005; Vidal *et al.*, 1999). Whether the same glutaminyl cyclase is responsible for the dehydration process in all these cases remains to be investigated. Since this N-terminal modification was not detected in the soluble circulating ABri and ADan species, it is conceivable that cyclization occurs at the sites of ABri and ADan deposition.

ABri species extracted with formic acid (amyloid fraction) showed a range of species from the monomeric form to species with a high degree of oligomerization. Interestingly the gray matter from the different cortical regions showed a high degree of oligomerization along with the blood vessels from the different regions. Whereas the white matter regions only showed monomeric species. The monomeric ABri species were found to be full length and heavily modified at the N-terminus with a pyroglutamate modification.

The non-fibrillar deposits extracted from PBS-soluble and SDS-soluble fractions from the FDD case appeared less complex than the fibrillar counterparts found in the formic acid extract, perhaps reflecting the early intermediate states of the fibrillization process. The degree of oligomerization was limited only to the dimeric forms and the degree of heterogeneity was highly restricted in the soluble fractions. After immunoprecipitation

ADan species were found in small quantities within the soluble fractions and consisted of full-length species with the occasional N-terminal pyroglutamate modification.

Analysis of the PBS and SDS soluble fractions for Aβ deposits without prior immunoprecipitation showed no Aβ deposits when western blot analysis was used. However, with the incorporation of the immunoprecipitation step N- and C-terminal truncated species were found in the soluble fractions. Aβ1-42 and N-terminally truncated Aβ4-42 were the major species whereas Aβ1-40 and Aβ derivatives ending at position 34 were minor components. Although the predominant species ending at position 42 were expected in the parenchymal extracts, their abundance in vascular components was suprising. Limited studies indicate that Aβ-related parenchymal pre-amyloid lesions are enriched in species ending at position 42. The α-secretase fragment Aβ17-42, in particular, was previously identified as the main component of pre-amyloid lesions in AD (Gowing *et al.*, 1994), DS (Lalowski *et al.*, 1996) and aged dogs (Wisniewski *et al.*, 1996) with Aβ1-42 an Aβ4-42 being minor components in the last two cases. In FDD extracts Aβ17-42 was not detected in any fraction, whereas Aβ4-42 was the major species of the pre-amyloid lesions.

ADan and Aβ species extracted with formic acid from amyloid deposits were more heterogenous. ADan was fully post-translationally modified at the N-terminus (pyroglutamate), partially N- and C-terminally degraded at positions 3, 28 and 33 and heavily oligomerized. These findings have been confirmed by a recent N-terminal sequence anaylsis in both parenchymal and vascular extracts. The minor sequences retrieved, SNXFAIR and EASNXF correspond to ADan starting at positions 3 and 1 respectively, in 3:1 ratio (Tomidokoro *et al.*, 2005). Aβ, on the other hand, was composed of Aβ1-42 and Aβ4-42 (with negligible Aβ1-40), showed higher degree of oligomerization. Whether, extensive proteolytic degradation and heavier

oligomerization reflect critical necessary steps in the process of ADan amyloid formation or simply a futile cellular effort to end and clear the formation of fibrillar deposits in still under investigation. In the case of Aβ, the N-terminal degraded Aβ4-42 is known to have a faster aggregation kinetics than the intact Aβ1-42 (Pike *et al.*, 1995). As well as analysing the Aβ species present in FDD, sporadic AD and familial AD cases were examined. Using western blot analysis of the Aβ species showed that the formic acid fraction contained the majority of the Aβ peptides. The samples from the familial AD cases showed both monomeric and dimeric Aβ species, whereas the sporadic AD case showed a predominance of the dimeric Aβ species. The MS results revealed that the major species in both the familial and sporadic AD cases were both N- and C-terminally truncated Aβ species modified with a pyroglutamate at the N-terminus. Whereas the samples obtained from the blood vessels contained more of the full-length species and less modified with the pyroglutamate residue. This finding is in contrast to the Aβ species found within FDD where no species were found with MS to contain the pyroglutamate species.

The existence of other Aβ species was also previously identified in pre-amyloid lesions based on classical immunohistochemical stainings and their reactivity with specific antibodies. Aβ1-42 and Aβ3-42pE were reported to be major components in AD, Downs syndrome and normal aging preamyloid lesions whereas antibodies recognizing position 17 were only weakly positive (Iwatsubo *et al.*, 1996). Anti-Aβ immunoreactivity was found prevalent in parenchymal pre-amyloid deposits in the Dutch variant of familial AD (Castano *et al.*, 1996). Aβ immunohistochemistry in FDD, with antibodies raised against different residues of the Aβ peptide, confirmed MS analysis results showing the presence of Aβ42 in the amyloid lesions, with little Aβ40

positivity found in the amyloid lesions. For comparison immunohistochemistry using anti-Aβ antibodies was also carried out on sporadic AD and familial AD cases. All Aβ antibodies showed positive staining in both sporadic AD and familial AD. Both N3(pE) and N11(pE) stained all structures as observed in FDD. Although this study did not find the presence of N11(pE) species in sporadic AD using MS, a study has shown the presence of both Aβ peptides beginning at position 3 and 11 as prominent bands in familial AD carrying presenilin 1 mutations (Russo *et al.*, 2000). N- and C-terminal Aβ isoforms are consistently present in AD (Harigaya *et al.*, 2000), but were found to a lesser extent in normal aging (Piccini *et al.*, 2005).

From looking at three different amyloid peptides a pattern emerged suggesting that the full length species could be produced either locally or systemically and modified in transit or at the site of cerebral deposition. The formation of a pyroglutamate residue heightens the state of degradation resistance, presumably rendering cells in and surrounding a plaque unable to clear the amyloid peptide, as they are resistant to major aminopeptidases and have a higher β-sheet to α-helical stability compared to unmodified Aβ peptides (He & Barrow, 1999). Pyroglutamate containing N-terminal truncated peptides form β-sheet structure and aggregate more readily than the full length forms. It has also been shown that pyroglutamate modified Aβ peptides remain in the β-sheet conformation at all pH values.

Analysis of the Aβ peptide in both AD and ADan showed that the modified peptides were found in all pathological lesions, suggesting that extracellular components influence the formation of the different lesions. More information could be obtained about ABri and ADan with the introduction of antibodies raised against the N-terminus of these peptides and the modified N-terminus.

In sporadic and familial AD as well as in other Aβ related disorders, amyloid deposits in cerebral blood vessels are primarily constituted of fibrillar forms of Aβ40 although the presence of Aβ42 in detectable amounts is considered a common finding in these lesions (Ghiso & Frangione, 2002). Similarly Aβ40 is the main component of vascular deposits (Van Dorpe *et al.*, 2000a; Kuo *et al.*, 2001), including the recently published APP-Dutch mouse (Herzig *et al.*, 2004). The fact that the main Aβ components of the vascular FDD lesions are Aβ42 species was an unexpected finding of unknown connotations for the disease pathogenesis. It is also not known at present whether the colocalization of ADan and Aβ reflects important aspects of the mechanism of amyloidogenesis or simply a conformational mimicry. However it is important to note that Aβ was not detected in parenchymal or vascular ABri lesions in FBD (Ghiso *et al.*, 1995; Revesz *et al.*, 1999) in spite of sharing the first 22 amino acid residues with ADan. If amyloid is indeed necessary for the development, of dementia it is certainly not exclusive for Aβ nor dependent on the presence of compact plaques. Therefore, we can propose that these disorders, FBD and FDD, are suitable models to study early steps in peptide fibrillization and the role of pre-amyloid and vascular amyloid in the process of neurodegenration.

Footnote: The immunoprecipitation steps described in this chapter were completed by Yasushi Tomidokoro after I had left New York Universtiy due to time constraints. The work however was carried out on the samples I had already prepared.

Chapter 8

Expression of BRI2 mRNA, BRI precursor protein and furin in normal human brain and FBD

Chapter 8 – Hypothesis and specific questions.

In this chapter I wished to investigate the hypothesis that cellular components of the CNS are a major source of ABri and ADan deposited in the CNS in FBD and FDD, respectively.

Understanding the origin of the ABri and ADan peptide could provide further information about the evolution of the parenchymal and vascular lesions. To test the above hypothesis that the brain is a major source of these amyloid peptides a study was undertaken to establish the cerebral distribution of BriPP and the enzyme (furin) implicated in its processing. For this study *in-situ* hybridisation, immunohistochemistry and biochemical methods were used.

8.1 Introduction

The function of the *BRI2* gene is mainly unknown, although it has become recognised that it belongs to a family of genes, which also includes the *BRI1* and *BRI3* genes, encoding integral transmembrane proteins (Deleersnijder *et al.*, 1996; Pittois *et al.*, 1998). The mechanism of cleavage of the wild type and mutated BRI precursor proteins has been investigated using *in vitro* studies. These have shown that the ubiquitous prohormone convertase (PCo) furin is able to cleave wild type BriPP between Arg243 and Glu244 to generate an N-terminal 243-amino-acid-long and a C-terminal 23-amino-acid-long fragment. The mutated precursor proteins ABriPP and ADanPP can also be cleaved at the same site producing the amyloidogenic peptides ABri and ADan. Cleavage of the mutated precursor proteins was found to be more efficient than that of the wild type and furin was more effective in producing this cleavage than other PCos expressed in brain (Kim *et al.*, 1999; Kim *et al.*, 2002). Furin is a member of the family of subtilisin-like calcium-dependent serine proteases, a group of enzymes, which function as proprotein and prohormone convertases generating a wide range of bioactive molecules. Furin is a type 1 transmembrane protein, which is synthesized as profurin and, during progression from the ER to the *trans*-Golgi network, undergoes activation by two sequential autoproteolytic cleavages, the second of which permits dissociation of the propeptide providing the final step in enzyme activation (Nakayama, 1997; Thomas, 2002). A secreted form of furin has also been described in experimental models, in which cells are transfected with furin and also in cell lines derived from malignant

glioma (Denault *et al.*, 2002; Leitlein *et al.*, 2001; Vey *et al.*, 1994; Vidricaire *et al.*, 1993).

The origin and mechanism of deposition of ABri in plaques and blood vessel walls is not known. One of the hypotheses is that ABri is produced by cellular components of the CNS. In support of this possibility are the morphological investigations demonstrating a perineuronal distribution of ABri. The association of neuronal cells with Aβ production in AD has been shown previously, therefore the possibility that neurons may be one of the cell types involved in cerebral ABri production can be raised. Such a hypothesis is further supported by previous Northern blot studies, demonstrating that BRI2 mRNA is expressed throughout the human brain and is expressed at high levels in a number of areas, which include the hippocampus, amygdala, and cerebellum (Vidal *et al.*, 1999).

Only limited information is available about the cellular origin and potential furin processing of ABri in the human brain. Both BriPP protein and furin have been demonstrated in neurons and furin was also localised in both reactive astrocytes and in ABri parenchymal amyloid lesions in FBD (Akiyama *et al.*, 2004; Schwab *et al.*, 2003). In this study we wished to investigate these issues further by analysing the distribution of BRI2 mRNA using non-radioactive *in-situ* hybridisation in parallel with immunohistochemical studies of the protein localisation and to compare these with the distribution of furin. We explored these in control brain tissue and in both FBD and AD to determine whether there was any relationship between parenchymal amyloid and pre-amyloid lesions and either BriPP or furin expression.

8.2 Material and Methods

8.2.1 Tissue

Samples of brain tissue which had been flash frozen and stored at -80^{0}C following brain removal at autopsy were obtained from four normal controls, one case of FBD, four AD cases and one case of variant AD with cotton wool plaques (table 39).

Number	Age	Sex	Diagnosis	Post mortem delay
1	43	M	Heart attack	15 hrs
2	63	M	Congestive heart disease	42 hrs
3	75	M	Pulmonary embolism	64 hrs
4	81	M	Chronic obstructive airway disease	40 hrs
5	68	F	FBD	6.5 hrs
6	79	M	AD	27 hrs
7	73	F	AD	18 hrs
8	78	M	AD	38 hrs
9	43	F	AD	75 hrs
10	46	F	Variant AD with cotton wool plaques	26 hrs

***Table 39**: Cases used for immunohistochemistry; western blotting and in situ hybridisation.*

For western blot analysis, the cerebellum was used from the control cases and frontal lobe from the FBD and four AD cases (cases 6-9). To study the distribution of furin and BriPP in the normal brain using immunohistochemistry and *in-situ* hybridisation sections were cut from the frontal cortex, basal ganglia, hippocampus and cerebellum in all control cases; temporal and occipital cortices in two of the cases and thalamus and pons in one of the cases. The hippocampus and frontal cortex were available from the FBD case. Temporal cortex was available in all AD cases.

8.2.2 Immunohistochemical staining

Antibody	Source	Dilution for IB	Dilution for IH
Ab338	Dr J Ghiso	1:2000	1:2000
Furin convertase	Affinity Bioreagents	1:1000	1:50
Ab340	Dr J Ghiso	1:500	1:500
GFAP	Chemicon	-	1:1000
NeuN	Chemicon	-	1:1000
Prohormone convertase 1	Affintiy Bioreagents	1:500	-
Prohormone convertase 2	Affinity Bioreagents	1:2500	-
Ab340 Pre-immune (Pi)	Dr J Ghiso	1:500	1:500
Ab340 Blocked	Dr J Ghiso	1:500	1:500

***Table 40**: Antibodies used for expression of BriPP study.*
IB- Immunoblotting and IH- immunohistochemistry.

Sections from the above regions were cut from flash frozen tissue and immunostained as described in section 2.4. The antibodies used in this study are listed in table 40.

Ab340, which recognises the wild type and mutant precursor proteins, was raised against the CHDKETYKLQR sequence of BriPP that is 10 residues N-terminal of the furin cleavage site. For negative controls the pre-immune rabbit serum (Ab340 Pi) or immuno-absorbed Ab340 (Ab340 Abs - see section 8.2.3) were used. Experiments in which the primary antibodies were omitted were also carried out.

8.2.3 Immuno-absorption of Ab340

Immuno-absorption of Ab340 was carried out using full length immunizing synthetic peptide (100μg of peptide per 50μl of antibody). Incubation was carried out for 1 hour at 37^{0}C and 16 hour at 4^{0}C, followed by centrifugation at 14,000g for 5 mins.

8.2.4 Double immunohistochemical staining for furin/GFAP and furin/NeuN

For the double immunohistochemical staining with light microscopy, the protocol was followed as described in section 2.2.2. Using the glucose oxidase method as the chromogen for furin (section 2.14.7) and Novored (Vector) as the chromogen for GFAP and NeuN.

8.2.5 Double immunohistochemical staining for BriPP/GFAP and BriPP/NeuN

For double immunohistochemistry with BriPP and GFAP or NeuN, the protocol was followed as described in section 2.2. Using the glucose oxidase method as the chromogen for furin (section 2.14.7) and Novored (Vector) as the chromogen for GFAP and NeuN.

8.2.6 Western blot analysis

Frozen cerebellum from four control cases and frontal cortex from the FBD case were used in the western blot analysis, and the protocol was followed as described in section 2.15.

8.2.7 Northern blot analysis

Northern blot analysis was carried out on a normal control case and the FBD case primarily to check the integrity of the RNA in the samples. The protocol followed is given in detail in section 2.13.

8.2.7 BRI2 mRNA *in-situ* hybridisation

In-situ hybridisation was carried out in the control cases, FBD and AD cases as described above and the protocol followed is described in section 2.15. The negative controls used for this study were a 1:100 dilution of the labelled probe and omitting the labelled probe completely. Three oligonucleotide probes were used in this study which are listed in table 15 in section 2.15.2. Although in a pilot experiment all three probes labelled the same structures, probe 1 labelled the structures more intensely and was, therefore, chosen for this study.

8.3 Results

8.3.1 Northern blot analysis

Northern blot analysis of mRNA showed good preservation of mRNA with hybridisation of the probe for the control housekeeping gene GAPDH producing a strong 1.4Kb band. A 2.0Kb species representing BriPP mRNA was identified using the BriPP probe (figure 8.1). The integrity of RNA, used in the northern blot analysis, was assessed by visualizing 28S and 18S ribosomal RNA bands on a denaturing agarose gel (figure 8.2). The integrity of the RNA was good as two bands were clearly visible. The upper 28S band appeared stronger than the lower 18S band and there was no smearing that would indicate degradation.

8.3.2 Western blot analysis

Immunoblotting from four controls and one FBD case with Ab340 showed a strong band at 34kDa (figure 8.3), which was absent when the pre-immune serum or the Ab340 absorbed with immunising peptide, were used (figure 8.4). The presence of furin

was confirmed in three control cases (1-3) using three different commercially available antibodies (figure 8.5). All of the antibodies demonstrated bands at 90kDa and 96kDa corresponding with the zymogen form and the cleaved lower molecular weight active form of furin, but two of the antibodies also showed multiple bands at lower molecular weights (figure 8.5). Therefore the antibody furin convertase (Affinity Bioreagents) was chosen to demonstrate the presence of furin in the four control cases (1-4), the FBD case (5) using western blot analysis (figure 8.6) before proceeding onto the immunohistochemical analysis.

8.3.3 Distribution of BRI2 mRNA assessed by *in-situ* hybridisation

A summary of the cases used in this study are given in table 41 and the major findings of the study are summarized in table 41.

			BRI2 mRNA	BriPP	Furin
Control Brain	Neurons		+	+	+
	Glia		+	-	+
	Vessels		-	-	+
FBD	Neurons		+	+	+
	Glia		+	-	+
	Normal vessels		-	-	+
	Preamyloid lesions		-	-	-
	Amyloid lesions	V	+	+	+
		P	+	+	+
AD	Neurons		+	+	+
	Glia		+	-	+
	Normal vessels		-	-	+
	Preamyloid lesions		-	-	-
	Amyloid lesions	V	+	-	-
		P	-	-	-

***Table 41**: Summary of the findings normal controls, FBD and AD.*

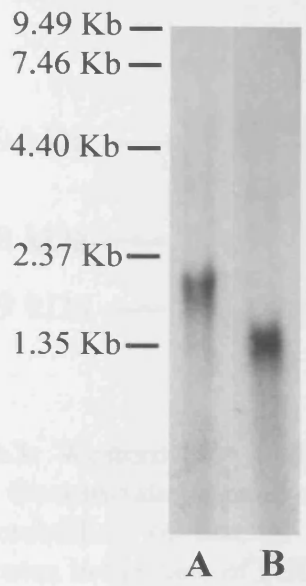

Figure 8.1: Northern blot analysis of RNA extracted from the cerebellum of a normal control showing a 2.0kB band corresponding to BriPP (A) and a 1.4Kb band corresponding to GAPDH (B).

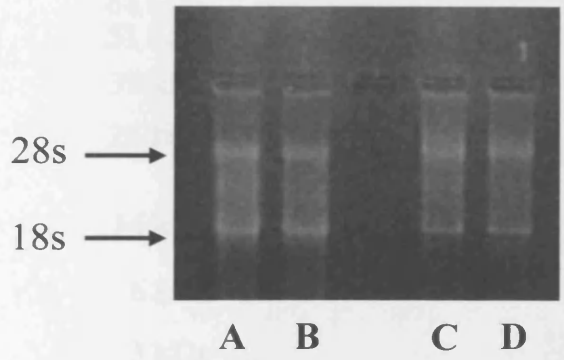

Figure 8.2: A denaturing gel showing the quality of the RNA used for the northern blot analysis. Two clear 28s and 18s rRNA bands can be seen in all four samples, A and C extracted from control cerebellum; B and D extracted from control frontal cortex. The ratio of approximately 2:1 (28s:18s) is a good indication that the RNA is intact. Partially degraded RNA would have a smeared appearance and would lack sharp rRNA bands.

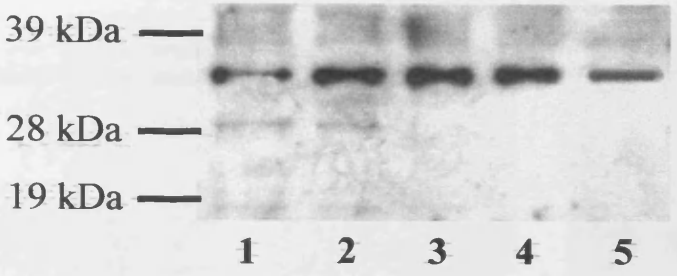

Figure 8.3: Western blot analysis for BriPP, using the Ab340 antibody demonstrates a band of 34kDa corresponding to BriPP in the cerebellum of normal controls (cases 1-4) and in the frontal cortex in the case of FBD (case 5).

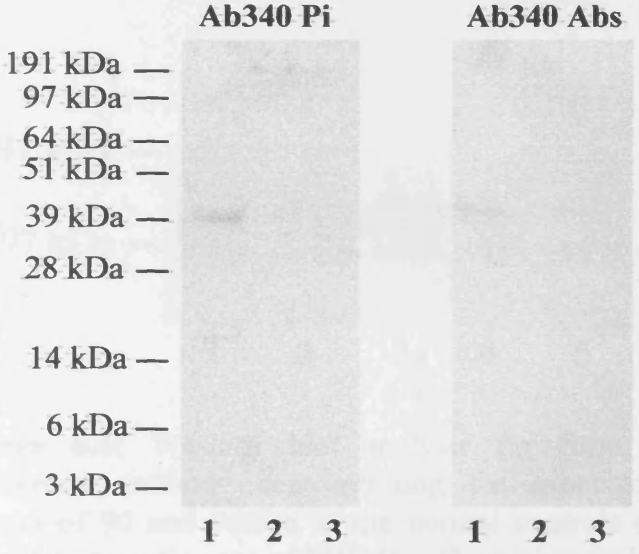

Figure 8.4: Western blot analysis using Ab340 pre-immune serum (Ab340 Pi) and immunoabsorbed Ab340 (Ab340 Abs) in the cerebellum of three control cases (1-3) demonstrating that the 34kDa band corresponding to BriPP is abolised.

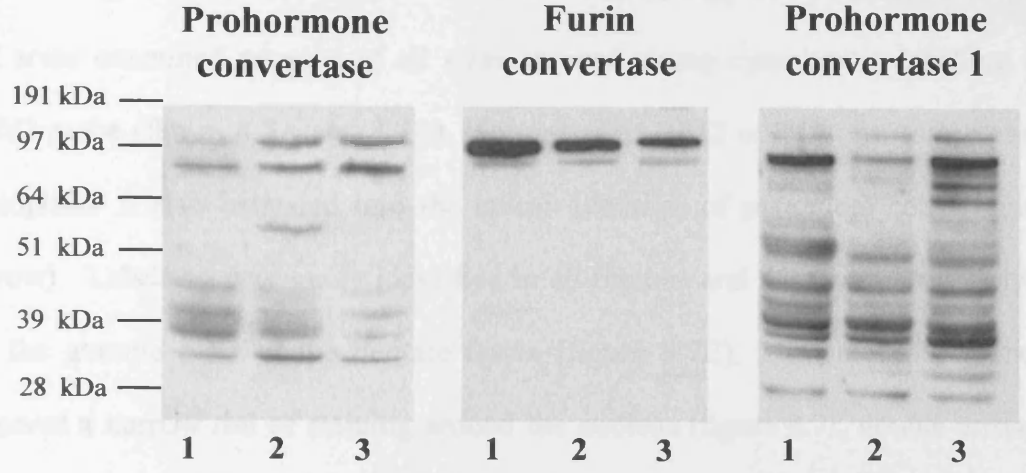

Figure 8.5: Western blot analysis with three different anti-furin antibodies, in three normal controls (1-3). All three antibodies show two bands at 96kDa and 90kDa corresponding to the zymogen form and the cleaved lower molecular weight active form of furin. All three antibodies were purchased from Affinity Bioreagents.

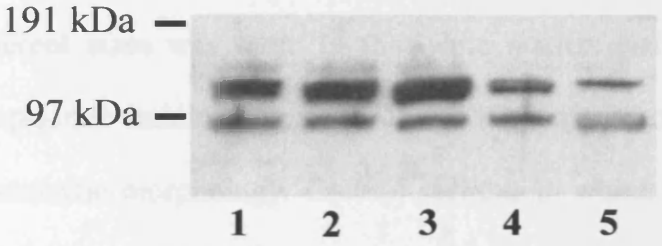

Figure 8.6: Western blot analysis for furin, using furin convertase antibody demonstrating the expected two bands around of 90 and 96kDa in the normal controls (1-4) and the frontal cortex of a case of FBD (5). The higher molecular weight bands represent the zymogen form of furin, while the lower molecular weight species corresponds to the active form of furin.

The findings were similar in all the control brains so they will be described together. In all areas examined neurons of all sizes showed strong cytoplasmic labelling with the *BRI2* probe (figure 8.7A and 8.7B). Not only was BRI2 mRNA expression seen in the cytoplasm it also extended into the apical dendrites of pyramidal cells (figure 8.7C, arrow). Labelling was easily identified in all regions and this was particularly marked in the granule cells of the dentate fascia (figure 8.7E). The cerebellar granule cells showed a narrow rim of staining around the nucleus (figure 8.7I, double arrow), while the Purkinje cells expressed BRI2 mRNA in proportion to the volume of their cytoplasm (figure 8.7H and 8.7I). Positive staining was shown to be present in the neurons of the cerebellar dentate nucleus (figure 8.7G). The neurons of the substantia nigra (figure 8.7F) were similarly strongly labelled, which despite the neuromelanin pigment (brown) could be unequivocally established (figure 8.7F). No labelling of vascular smooth muscle or endothelial cells (figure 8.7A, arrow and 8.7D) of blood vessels of different sizes was seen. In the white matter glial cells showed a small amount of cytoplasmic staining (figure 8.7J) and the majority of the positively stained cells had an astrocytic morphology. Control sections in which the labelled probe was diluted 100-fold with unlabelled probe or when the probe was ommitted from the experiment showed no positive ISH staining (data not shown).

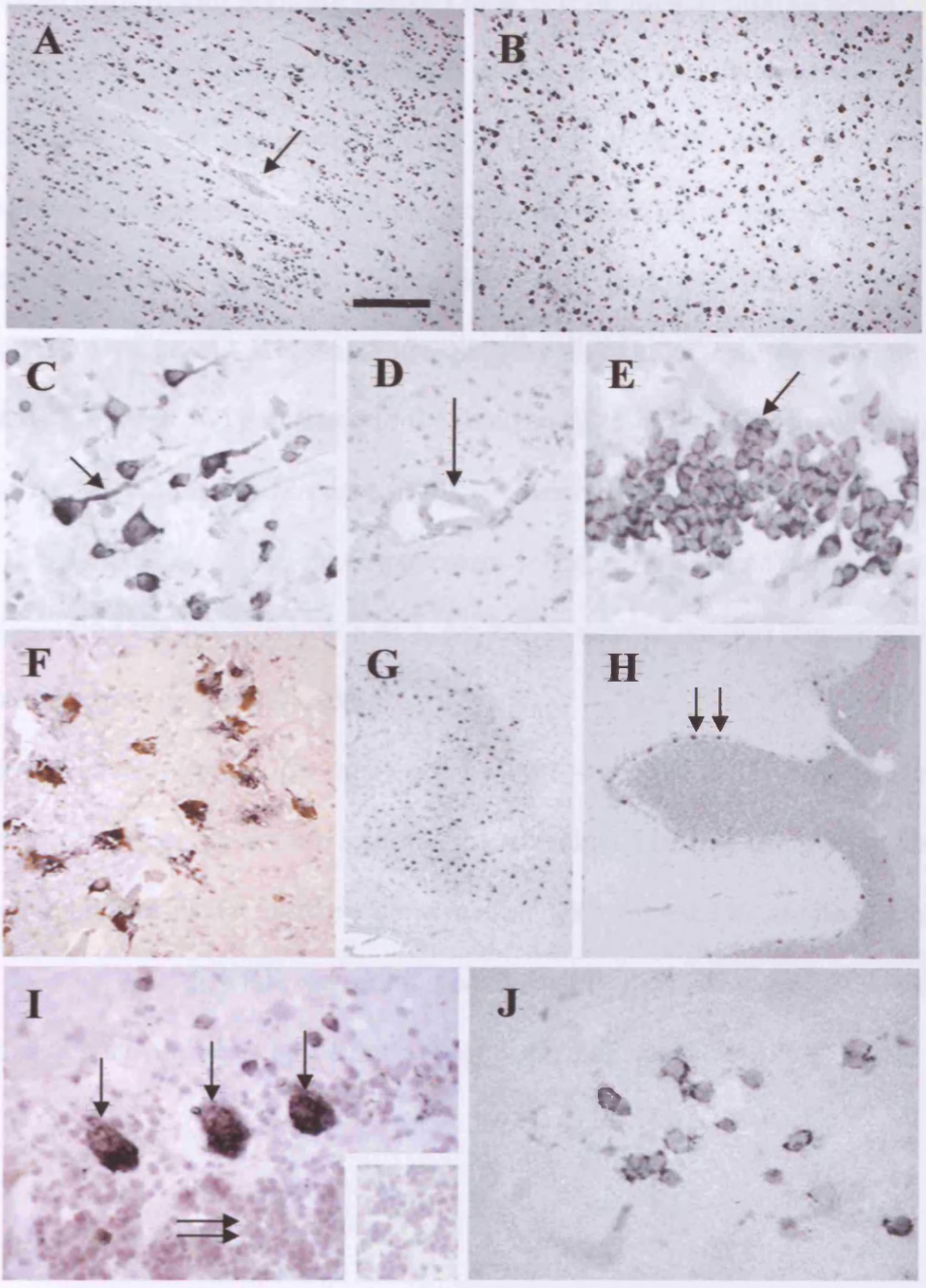

Figure 8.7: *BRI2 in-situ* hybridisation in normal human brain. *In-situ* hybridisation for BRI2 mRNA demonstrated strong expression in neurons in all areas of the normal brain as shown in the occipital cortex (A) and frontal cortex (B). Neurons of all types expressed the mRNA, this included an extension into the apical dendrite of the pyramidal cells (C, arrow). Arterioles found in the cortex remained negative (D, arrow). The granule cells of the hippocampal dentate fascia strongly express BRI2 mRNA (E, arrow), as a narrow rim around the nuclei is clearly visible. The neurons in the substania nigra were also positive (F) as were the neurons in the dentate nucleus (G). In the cerebellum the Purkinje cells were strongly stained (H and I, arrow), while the granule cells showed a narrow rim of staining around the nucleus (I, double arrow). For comparison the granule cells from a negative control stained by omitting the probe is also shown (I, inset). Glial mRNA expression was demonstrated in the cerebellar white matter (J). Bar in A and B represents 250μm; on G and H represents 500μm; on D and F represents 100μm; on C, E, I and K represents 45μm; J represents 20μm.

8.3.4 Distribution and staining pattern of BriPP in normal human brain

The distribution of the full-length precursor protein BriPP was demonstrated using the antibody Ab340, which was raised against a region of BriPP proximal to the furin cleavage site. This showed strong diffuse cytoplasmic labelling in neurons of all sizes in all regions of the brain examined (figure 8.8A and inset). The Purkinje cells of the cerebellum showed strong labelling reflecting the amount of cytoplasm (figure 8.8E double arrow, 8.8F arrow) compared to the thin rim of staining seen around the granule cells (figure 8.8F and insert). Strong staining was visible in the cytoplasm of the granule cells of the dentate fascia of the hippocampus (figure 8.8B) and all other regions studied, including the pons (figure 8.8C), cerebellar dentate nucleus (figure 8.8D) and the substantia nigra (figure 8.8D, inset).

Blood vessels were consistently unstained by Ab340 (figure 8.8E, arrow). Neuronal staining was confirmed by double immunohistochemical labelling using an antibody to the neuronal marker NeuN used in combination with the Ab340 antibody (data not shown). It was not possible to demonstrate BriPP expression in glial cells by immunohistochemical means in the normal controls (data not shown).

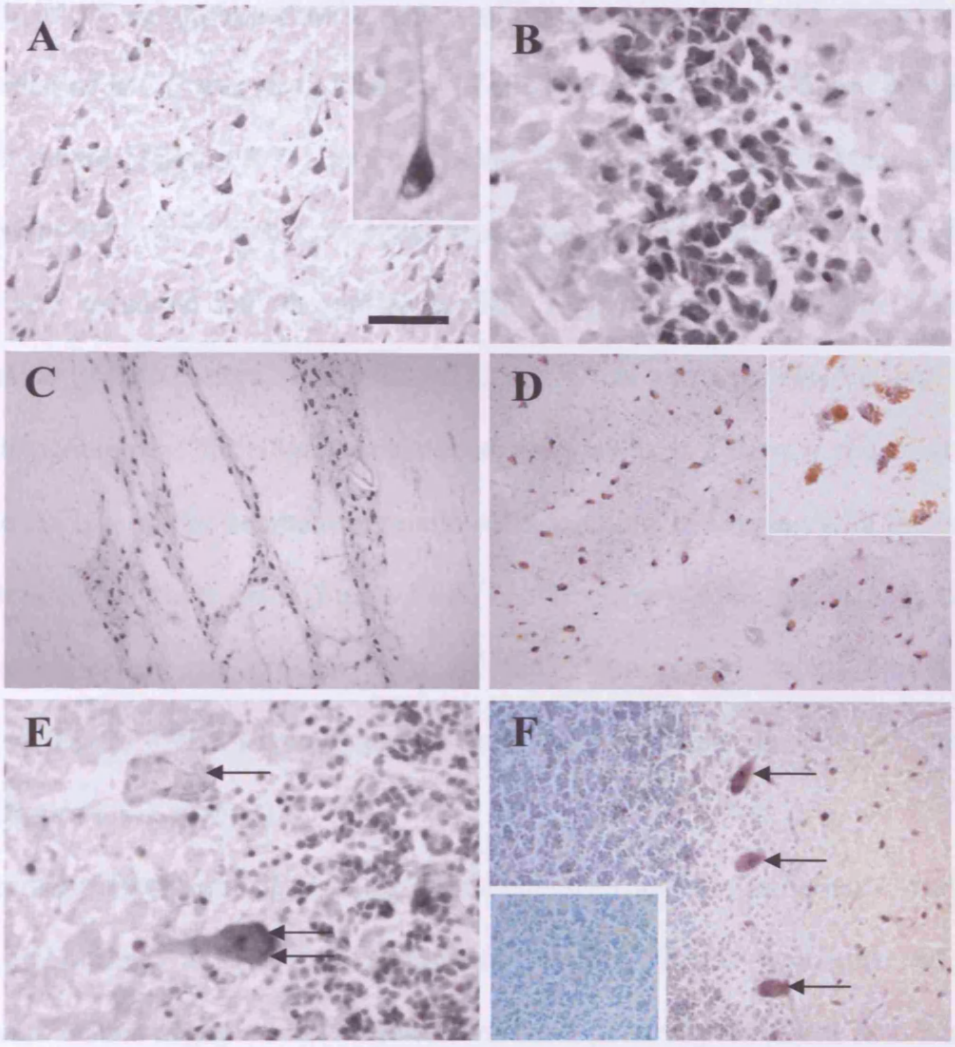

Figure 8.8: BriPP immunohistochemistry in normal human brain. BriPP expression was observed in all neuronal types demonstrated in cerebral cortex (A), with expression extended into the apical dendrites (A, inset), granule cells of the hippocampal dentate fascia (B), pons (C), cerebellar dentate nucleus (D) and the substantia nigra (D, insert). The cerebellar Purkinje cells show abundant cytoplasmic staining (E) and there is a narrow band of staining around the nucleus in the granule cells (F): Inset on F shows a negative control in which the primary antibody was omitted. Blood vessels were found to be negative (E, arrow). Bar in A represents 100μm; on panels C and D represents 250μm; on panels D (inset), F and F (inset) represents 100μm; on panels A (inset), B and E represents 30μm.

8.3.5 Distribution and staining pattern of furin in normal human brain

In all of the brain regions examined a pattern of immunohistochemical staining for furin similar to that of BriPP was seen. Neurons of all sizes in all cortical (figure 8.9A), sub-cortical, brainstem (figure 8.9F) and cerebellar (figure 8.9E) regions examined were strongly positive for furin with a punctate cytoplasmic staining pattern. The cytoplasmic positivity also extended into the apical dendrite of pyramidal cells (figure 8.9A and inset). Similar to the pattern seen with BRI2 mRNA *in situ* hybridisation and BriPP immunohistochemistry, furin immunohistochemistry showed a narrow rim of staining around the nucleus of the cerebellar granule cells, which is in keeping with the volume of the cytoplasm of these cells (figure 8.9E, double arrow). A similar staining pattern was observed when the granule cells of the hippocampal dentate fascia were investigated (figure 8.9B). Leptomeningeal vascular smooth muscle cells were positive for furin (figure 8.9G, arrows).

Double immunohistochemical staining with antibodies to furin and NeuN confirmed neuronal cytoplasmic furin expression but also showed that in both grey and white matter small NeuN negative cells showed variable positivity for furin and therefore represent glia (figure 8.9H, arrows). Using double labelling with GFAP to identify astrocytes it was not possible to demonstrate that such positively labelled cells were astrocytes.

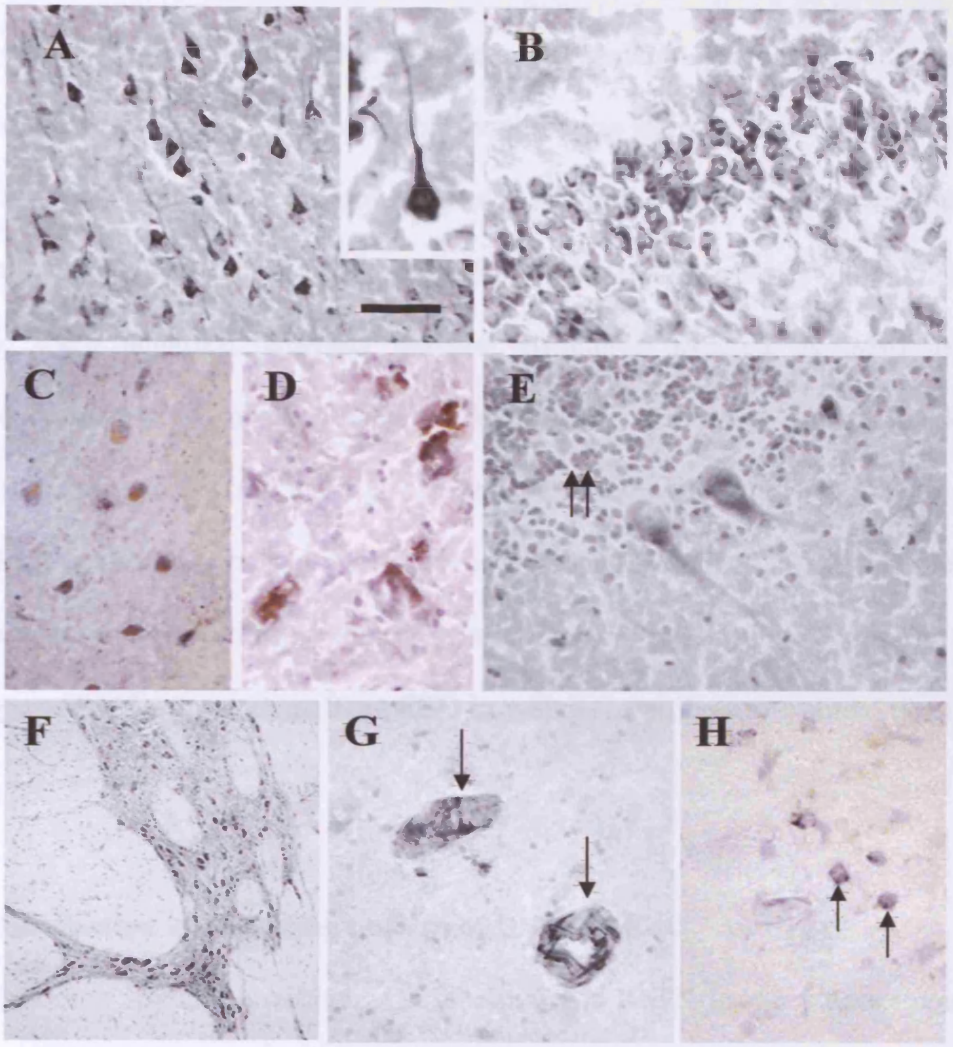

Figure 8.9: Furin immunohistochemistry in normal human brains. Furin expression could be demonstrated in all neuronal types in different regions including the frontal cortex (A) granule cells of the hippocampal dentate fascia (B), dentate nucleus (C), substantia nigra (D), cerebellar Purkinje cells and granule cells (E) and pontine neurons (F). Blood vessels were also positive (G). Glial cells were also labelled in white matter (H). Bar in A, C represents 100μm; on panel F represents 500μm; on panels B, E, D, G and H represents 45μm.

8.3.6 Distribution of BRI2 mRNA assessed by *in-situ* hybridisation in FBD

In a case of FBD *in-situ* hybridisation showed a BRI2 mRNA expression pattern similar to that observed in the normal human brain with strong staining in neurons throughout the cortical layers of the frontal cortex (figure 8.10A and insert), the hippocampal CA1 subregion and the dentate fascia (figure 8.10B). Normal blood vessels without amyloid deposition were negative, whereas vascular structures affected by ABri amyloid deposition showed strong positive staining (figure 8.10A arrow and 8.10C). In addition, parenchymal amyloid lesions were also found to contain BRI2 mRNA (figure 8.10D and 8.10E), but the pre-amyloid ABri lesions remained unstained. Positive staining of glial cells with an astrocytic morphology was found in the white matter of the frontal cortex (figure 8.10F). In sections from FBD in which the probe was omitted no staining was seen.

8.3.7 Distribution and staining pattern of BriPP in FBD

In the FBD case immunohistochemical labelling for BriPP in the hippocampus and frontal cortex showed the same staining pattern as described in the normal human brain. Neurons throughout the cortical layers of the frontal cortex (figure 8.11A) and the hippocampal subregions were strongly stained. Strong staining was also visible in the dentate fascia of the hippocampus (figure 8.11B). ABri amyloid plaques and blood vessels with amyloid deposition were also positively labelled (figure 8.11E). Large hippocampal plaques that had distinct central cores (figure 8.11C) were stained with equal intensity, along with the plaques that were less well defined in appearance and lacked the central core, but were still classed as amyloid plaques (figure 8.11D).

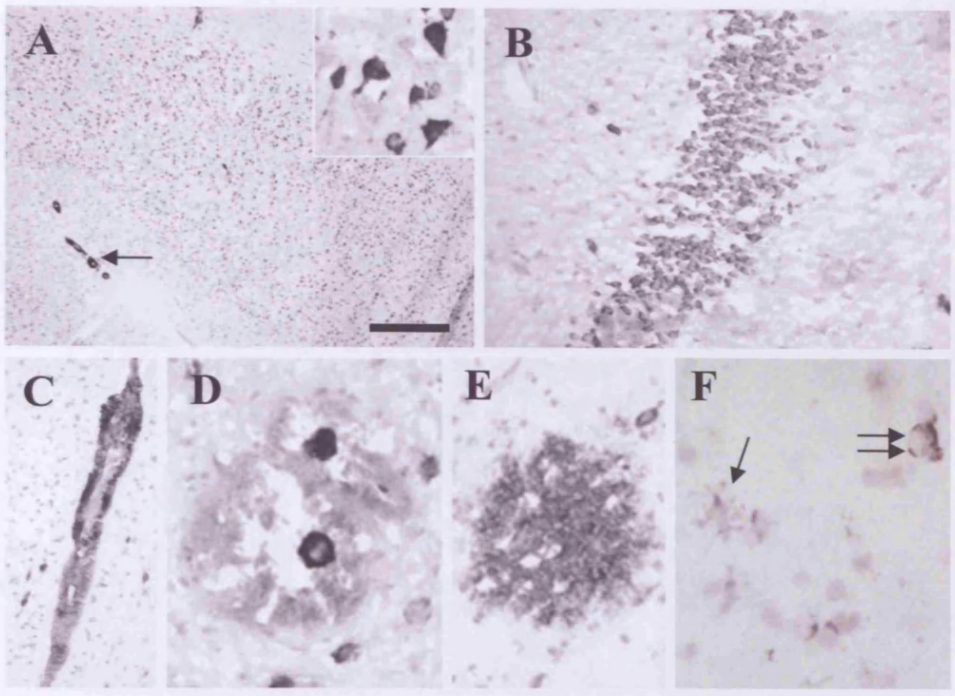

Figure 8.10: *BRI2 in-situ* hybridisation studies in FBD. BRI2 mRNA expression demonstrated in the frontal cortex (A), and at higher magnification (A, insert) The granule cells of the hippocampal dentate fascia strongly express BRI2 mRNA (B). Positive staining was also seen in all amyloid structures in FBD including amyloid-laden blood vessels (A, arrow and C), cored plaques (D) and less well defined plaques (E). Glial mRNA expression was demonstrated in the white matter of the frontal cortex (F, arrow), the majority of which had astrocytic morphological appearance. Bar in A represents 500μm; on panels B and C represents 100μm; on panels D - F represents 55μm.

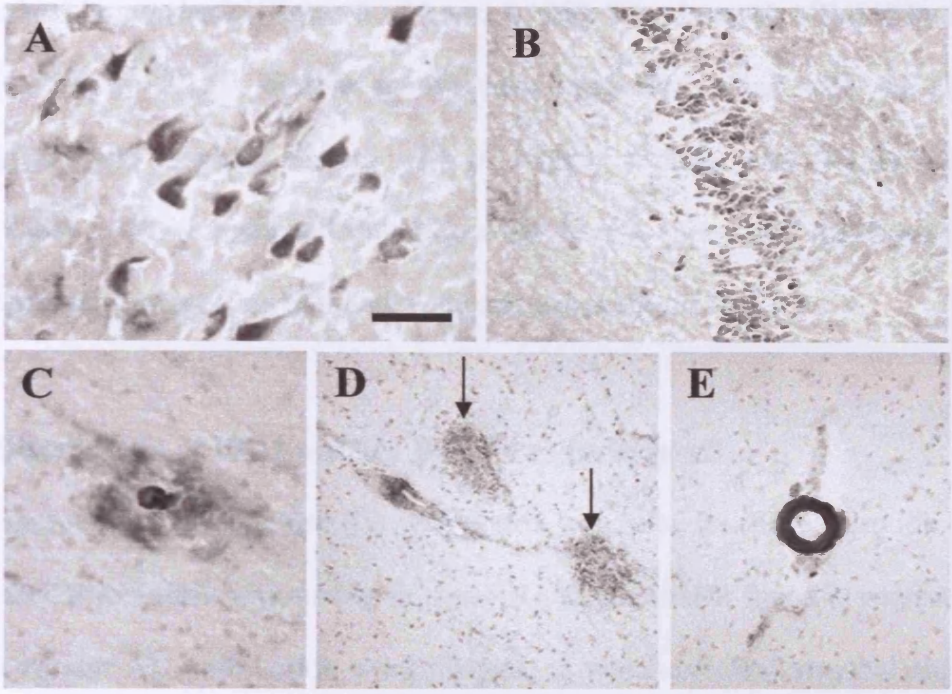

Figure 8.11: BriPP immunohistochemistry in an FBD case. Immunohistochemical staining using the Ab340 which recognises the full length wild-type BriPP and N-terminal fragments of both wild-type and mutant precursor proteins produced by furin-like cleavage. All neurons were positive in the frontal cortex (A) and throughout the hippocampus, including the dentate fascia (B). Positive staining was also seen in all structures containing amyloid, including cored plaques found in the CA4 (C), ill defined white matter ABri deposits (D, arrow) and amyloid-laden blood vessels (E). Bar in panel A and C represents 45μm: on panels B, D and E represents 100μm.

8.3.8 Distribution and staining pattern of furin in FBD

Immunohistochemical staining for furin showed similar staining patterns to those found in the normal human brain (figure 8.12A and 8.12B). Blood vessels affected by amyloid deposition (figure 8.12E, double arrow) were intensely stained with the anti-furin antibody, as were amyloid plaques with or without a dense core (figure 8.12C and 8.12D). Glial cells were stained throughout the frontal cortex and hippocampus with their morphology suggesting that they were astrocytes (figure 8.12F).

8.3.9 Distribution of BRI2 mRNA, BriPP and furin in AD

In both sporadic AD and variant AD with cotton wool plaques the distribution of BRI2 mRNA, BriPP and furin was similar in neurons and glia to that found in controls and in FBD. In variant AD with cotton wool plaques, in which cerebral amyloid angiopathy (CAA) is a prominent feature, BRI2 mRNA was found in the walls of amyloid laden blood vessels although the cotton wool plaques, which are largely composed of Aβ in preamyloid conformation, did not contain the mRNA. In sporadic AD the amyloid plaques and amyloid laden blood vessels did not contain BRI2 mRNA although CAA was sparse in the cases available for study (results not shown). No deposition of BriPP or furin was found in either amyloid or preamyloid lesions in sporadic or variant AD.

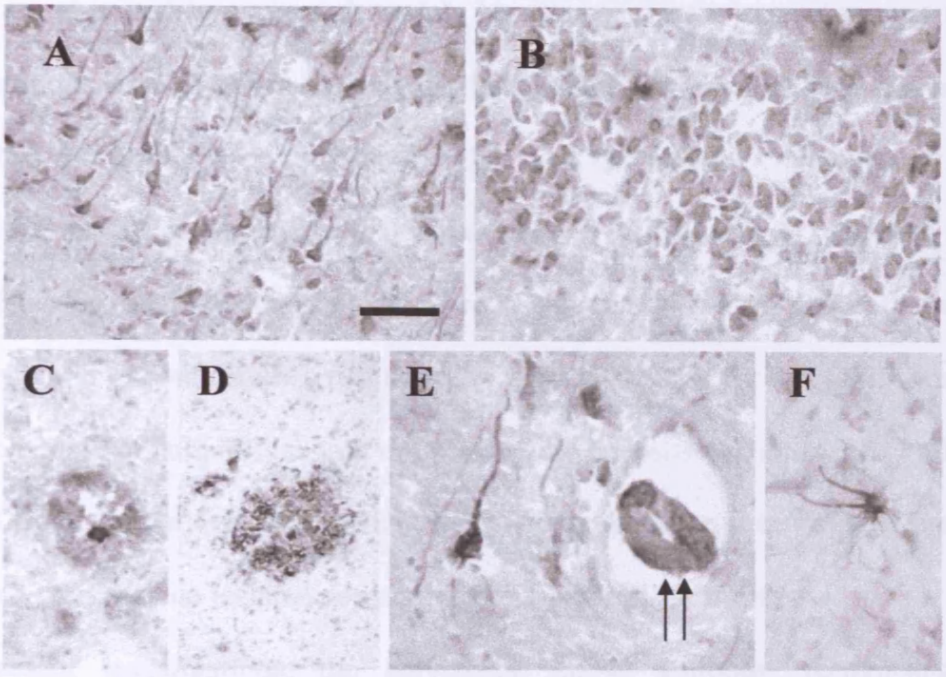

Figure 8.12: Furin immunohistochemistry in an FBD case. Immunohistochemical staining for furin was used to determine the distribution of protein expression. Expression was seen in all neuronal cells throughout the hippocampus CA1 (A) and the granule cells of the dentate fascia (B). ABri plaques with (C) or without a core (D) were also positive with furin. Panel E shows the expression of furin in an arteriole alongside a neuron with expression spreading down the apical dendrite. Glial cells with clear astrocytic morphology are also shown to be positive with furin immunohistochemistry. Bar in A represents 100μm; on D and C represents 100μm; on B, E and F represents 45μm.

8.4 Discussion

This study demonstrated that BRI2 mRNA is widely expressed by neurons and also by glial cells throughout the normal brain. Immunohistochemistry showed that both BriPP and furin are also widely expressed, mainly by neurons, in the normal human brain. Vascular smooth muscle cells were found to have detectable levels of furin but neither BRI2 mRNA nor BriPP were identified in this site. The cellular expression of BRI2 mRNA, BriPP and furin was similar to controls in cases of FBD and AD although in the former glial cells with the morphology of reactive microglia were found to express BRI2 mRNA and in both diseases reactive astrocytes contained furin. In FBD vascular and parenchymal amyloid lesions, but not preamyloid deposits contained BRI2 mRNA, BriPP and furin. In contrast in AD BRI2 mRNA was found only in vascular amyloid deposits and there was no lesional deposition of either BriPP or furin.

In the present investigations, the polyclonal Ab340 antibody, recognising the CHDKETYKLQR amino acid sequence that is present in both the wild type BriPP and the mutated precursor protein was used to demonstrate BriPP and ABriPP in both the immunohistochemical and in immunoblotting studies. The antibody was characterised by immunoblotting and was found to recognise a band with an expected molecular weight for BriPP of approximately 34kDa which was absent when the preimmune serum or the antibody absorbed with synthetic peptide was used for immunoblotting. Furthermore, no staining was observed in control tissue sections when the same, absorbed antibody was used for immunohistochemistry. From the data presented here it can be established that BriPP is expressed by all neuronal cell types throughout the normal human brain and in both FBD and AD, but no unequivocal staining of glial cells was established despite the presence of BRI2 mRNA in the latter. The amino acid sequence recognized by Ab340 is 10 residues upstream of the furin cleavage site (Kim

et al., 1999; Vidal *et al.*, 1999; Vidal *et al.*, 2000b). Therefore this antibody is expected to recognise not only the full-length, but also the 243-amino-acid-long N-terminal fragment generated by furin-like processing of both the wild type BriPP and mutated precursor protein ABriPP making it possible that the presence of both of these fragments have contributed to the positive immunohistochemical results (Kim *et al.*, 1999; Vidal *et al.*, 1999; Vidal *et al.*, 2000b). Using three commercially available antibodies for furin immunoblotting in the control brains and the FBD case which were used for BriPP and ABriPP immunoblotting, we demonstrated two bands at 90 and 96kDa, corresponding to the zymogen form of the enzyme (Denault & Leduc, 1996). Using the furin convertase antibody for furin immunohistochemistry we were able to show that both neurons and glial cells are involved in furin expression and this can widely be observed in the normal human brain.

The findings of BriPP immunoblot and immunohistochemical studies are supported by the current *in-situ* hybridisation investigations for BRI2 mRNA, which confirmed a widespread mRNA expression with strong labelling of the hippocampal/dentate fascia neurons and cerebellar Purkinje cells. We were able demonstrate BRI2 mRNA expression by glial cells in the white matter, although no protein expression was detected immunohistochemically. There may be several reasons for the absence of immunohistochemically detectable BriPP in glial cells; 1) the mRNA is not translated into protein; 2) the protein has a rapid turnover; 3) that the precursor protein may be present in such small amounts that it is not detectable with the immunohistochemical method used in the current study. Further studies are required to clarify these issues.

A study using *in-situ* hybridisation and immunoblotting for the demonstration of mouse BRI2 mRNA and BriPP, has also suggested that both mRNA and protein are widely expressed in both grey and white matter of the mouse brain with greatest expression in

the cerebellum, granular layer of the hippocampus, and olfactory bulb (Pickford *et al.*, 2003). This latter study also emphasised that structures with a high level of mRNA expression are among those in which neurogenesis takes place in adult mammalian brain (Taupin & Gage, 2002), which is interesting in view of the role of the *BRI2* homologue *BRI1* gene in differentiation (Deleersnijder *et al.*, 1996; Pickford *et al.*, 2003).

Previous studies have suggested that the hippocampus and cerebellum are among the structures with a high level of *BRI2* mRNA expression (Pickford *et al.*, 2003; Vidal *et al.*, 1999). Corresponding protein expression may help to explain an especially high degree of ABri or ADan deposition with subsequent neurodegeneration in these structures in FBD and FDD (Chapters 3 and 4, Holton *et al.*, 2001a; Plant *et al.*, 1990; Revesz *et al.*, 1999; Holton *et al.*, 2002a). That mRNA and protein expression alone may not be the sole factor that determines the development of pathological, preamyloid and amyloid lesions in different cerebral anatomical areas may be supported by the current observation showing strong positivity in both BRI2 mRNA *in-situ* hybridisation and BriPP immunohistochemical studies in structures such as the striatum and the substantia nigra, which are not, or only mildly, affected in FBD (Holton *et al.*, 2001a; Holton *et al.*, 2002a).

This study has also shown that in FBD both the vascular and parenchymal amyloid lesions contain furin, BRI2 mRNA and BriPP. Furin, which has been suggested to be involved in the processing of BriPP (Kim *et al.*, 1999a), has also been implicated in the proteolytic processing of the precursors of several molecules associated with cerebral amyloid deposition. These include BACE, which mediates cleavage of βAPP to produce the N-terminus of the Aβ peptide in AD; ADAM10 and ADAM17 (Lopez-Perez *et al.*, 2001), which have been implicated in α-secretase activity leading to cleavage within the

Aβ sequence of βAPP; gelsolin, the precursor protein for the amyloidogenic peptide AGel, deposition of which results in a form of familial cerebral amyloid angiopathy and the recently described protein, CLAC, which co-localises to amyloid plaques in AD (Benjannet *et al.*, 2001; Bennett *et al.*, 2000; Chen *et al.*, 2001; Creemers *et al.*, 2001; Hashimoto *et al.*, 2002).

The findings of this current study show that furin and BriPP (and/or ABriPP) are present in the amyloid lesions of FBD. This points to the possibility that proteolytic processing may occur in lesions. Furin and BriPP deposition in ABri amyloid lesions is unlikely to be due to non-specific binding to amyloid peptides as neither were identified in Aβ amyloid lesions in AD. This could be supported by those *in vitro* data demonstrating that furin, which is a membrane bound protein and localised in the Golgi apparatus, also has a secreted form, which having been released via post-translational modifications of the membrane associated form, maintains enzymatic properties that are similar to those of the wild-type enzyme (Vidricaire *et al.*, 1993). Our *in-situ* hybridisation studies showed BRI2 mRNA is also present in vascular and parenchymal amyloid deposits in FBD and in vascular amyloid in AD. Previous studies analysing the non-proteinaceous components of senile plaques have identified about 50 different mRNA species, including AβPP, tau and furin and it has been suggested that both normal and degenerating neurons and their processes, which are in close contact with the amyloid plaques in AD, are a source of the mRNAs in the amyloid lesions (Ginsberg *et al.*, 1998; Marcinkiewicz, 2002). The current findings that BRI2 mRNA deposition takes place in ABri amyloid lesions, which as Aβ neuritic plaques in AD, are surrounded with abnormal neurites in FBD, but is absent in the non-neuritic preamyloid lesions of FBD and cotton wool plaques in variant AD are also in keeping with a dendritic origin of deposited BRI2 mRNA. The significance of previous and our current

observation of association of mRNA in amyloid lesions is not clear. However, recent *in vitro* studies demonstrated that conversion of cellular prion protein (PrP^{c}) to the pathological, protease-resistant form (PrP^{Sc}) is stimulated by the presence of RNA (Deleault *et al.*, 2003). It remains to be investigated whether RNA is a cofactor in the conversion of other soluble, native proteins to forms with high β-sheet content.

This study shows that, although there is local furin protein expression, there is no significant BRI2 mRNA and BriPP protein expression *in vivo* by the cellular elements, including smooth muscle cells of the walls of cerebral arteries and arterioles, which have been implicated in the pathogenesis of CAA related to Aβ deposition (Frackowiak *et al.*, 1994). The importance of this current observation is at least twofold: 1.) it could provide evidence that CAA may not be due to local production of ABri by cerebrovascular smooth muscle or other vascular cells in FBD and 2.) it may lend indirect support to the drainage hypothesis of CAA pathogenesis put forward by Weller et al. (1998). According to this proposal Aβ produced primarily by CNS cellular elements, is drained along the perivascular spaces of the brain parenchyma and leptomeninges and CAA occurs due to deposition of the amyloid proteins along these drainage pathways. It remains possible that a small amount of BRI2 mRNA and BriPP at levels below the threshold of the methods used in this study could be expressed by vascular components. Should this be the case it seems likely that this would represent a minor contribution to the deposition of protein in CAA. Theoretically it is also possible that in FBD the mutated precursor protein is drained along the drainage pathways and processed by furin produced by cerebrovascular smooth muscle cells and released in the extracellular space. This possible mechanism, even if future experimental studies supported its feasibility, would not explain amyloid deposition in capillaries, which do not possess smooth muscle cells, and also that, similar to AD, larger arteries are less

affected by CAA than small arteries and arterioles in FBD. It is also of note that in FBD the amyloid peptides ABri has been shown to be present in the plasma at levels 20 times higher than that of Aβ and, in at least FBD, amyloid deposition in systemic organs has also been documented (Ghiso *et al.*, 2001). It remains, however, to be investigated, perhaps with the help of future transgenic animal models and other experimental approaches, how efficient the separation of the central and peripheral pools of ABri and ADan is by the blood brain barrier, and thus determine the role systemically produced ABri species may play in the pathogenesis of cerebral amyloid lesions in FBD.

In conclusion this study has presented evidence that BRI2 mRNA is produced by neurons and glia in normal human brain. The presence of furin in neurons and glia suggests that cleavage of the wild type and mutated precursor proteins can take place in these cells, resulting in the generation of C-terminal fragments, including ABri. These findings confirm previous suggestions for a cerebral, neuronal and possibly glial origin of these amyloid peptides. The absence of BRI2 mRNA in cerebrovascular cells suggests that local production of ABri by vessels is unlikely to represent a significant source of these peptides and gives indirect support to the drainage hypothesis of CAA.

Chapter 9

Conclusions

9 Conclusions

9.1 Comparisons between FBD and FDD

FBD and FDD, collectively referred to as the *BRI2* gene-related or chromosome 13 dementias, constitute alternative models for studying the role of amyloid deposition in neurodegeneration. The studies presented in this thesis have shown that the novel ABri and ADan amyloid peptides extensively deposit in the brain parenchyma in FBD and FDD, respectively. Both diseases also demonstrate severe CAA with perivascular plaque formation occurring throughout the CNS. Despite the complete homology of the first 22 amino acids of ABri and ADan, significant differences were demonstrated in the morphological manifestation of the two diseases. In FBD the majority of the parenchymal ABri lesions are well-defined, plaque-like and of amyloid nature, although pre-amyloid lesions are also present. In contrast, in FDD the majority of the parenchymal ADan lesions have ill-defined boundaries and show features of preamyloid rather than amyloid conformation. In FDD, but not in FBD, Aβ deposition either in combination with ADan or alone was also demonstrated in blood vessel walls and in brain parenchyma, the significance of which remains to be investigated.

Importantly despite these differences in ABri and ADan parenchymal lesion types, both diseases have a common end point - severe neurofibrillary pathology. Whether the pre-amyloid lesions represent the oligomeric assemblies, which have recently emerged as a major pathogenic factor in a number of neurodegenerative diseases characterised by protein misfolding (Klein *et al.*, 2001), remains to be determined.

As previously shown in AD, this study demonstrated a close association between the conformational state of ABri and ADan and the degree of astrocytic and microglial response (el Hachimi *et al.*, 1991; Pike *et al.*, 1995; Selkoe, 1999).

9.2 Amyloid associated proteins, including complement components in FBD and FDD.

This study established that AAPs and complement proteins, that have been shown to be associated with Aβ deposits in AD, are also present in ABri and ADan lesions thus supporting the notion that these proteins may have a general role in amyloid fibril formation. In general, AAPs co-deposited with both amyloid and preamyloid ABri and ADan lesions; ApoE, ApoJ, agrin, glypican-1 and HS GAG side chains were extensively associated with both lesion types whereas syndecans, HSPGs, ACT and SAP were predominantly seen in relation to amyloid lesions. It was hypothesised that binding of some AAPs to proteins in preamyloid conformation is due to the presence of variable numbers of amyloid fibrils that can be found in these lesions. The experimental data currently available are not sufficient to explain the predominance of preamyloid lesions in FDD. One possibility is that due to the difference in the primary amino acid sequence ADan forms amyloid fibrils less efficiently than ABri does, although conversion of multiconformational proteins into predominantly β-pleated fibrils is not thought to be significantly dependent only on sequence (Lansbury, Jr., 1999). However, the difference in the amino acid sequence could be sufficient to make ADan less able to attract and/or bind to AAPs such as ApoE, ApoJ, proteoglycans, SAP or ACT. These have been shown to modulate aggregation of Aβ *in vivo* and would be required, possibly in combination with other factors for efficient fibril formation. To test this hypothesis further biochemical investigations are required.

The importance of inflammation in neurodegenerative processes has become clear over recent years. Amyloid fibrils are believed to result from a change in the native conformation of amyloidogenic peptides resulting in insoluble structures, which accumulate in the form of either intra- or extracellular aggregates. In turn, these deposits trigger a complex set of inter-linking pathways usually associated with the local release

of inflammatory mediators, complement activation, cell toxicity and alterations in membrane permeability.

This study demonstrated *in vivo* that both the classical and alternative complement pathways are fully activated in FBD and FDD and that complement inhibitors are also present in the ABri and ADan lesions. This activation was dependant on the conformational state of these amyloid peptides as C1q, the recognition components of the classical pathway, was shown to co-localise strongly with vascular and parenchymal ABri and mainly with vascular ADan amyloid lesions while no, or only weak, staining of the preamyloid lesions was found. This observation also explains the different levels of activation of downstream components of the classical pathway that was demonstrated in this study in relation to amyloid and preamyloid parenchymal lesions. As it has been suggested for AD (Eikelenboom P et al 1982), activation of complement pathways may be a factor in the neurodegenerative process in both FBD and FDD.

Microglial cells and astrocytes are both known to produce inflammatory mediators, including complement proteins (McGeer and McGeer 1995, 2001). Complement deposition was also associated with significant activated microglial response in FBD and FDD. Co-localization of reactive astrocytes and microglial cells with ABri in β-conformation is strikingly similar to the findings in AD, in which a relationship between the presence of these cell types and the neurodegenerative events has been suggested (el Hachimi *et al.*, 1991; Pike *et al.*, 1995; Selkoe, 1999)

9.3 Comparison between ABri and ADan

The complexity and heterogeneity of FBD and FDD tissue deposits was assessed using biochemical and immunohistochemical approaches. For biochemical analysis a differential solubility strategy was used; water-based buffers for the extraction of

soluble peptides, detergent for the removal of non-fibrillar pre-amyloid deposits and strong acid to solubilise fibrillar amyloid deposits. In both diseases, the complexity of the extracted material increased as the solubility of the deposits decreased, as reflected in the degree of peptide oligomerisation, predominant amyloid subunits, and extent of post-translational modifications and magnitude of N- and C-terminal proteolytic degradations. In general, non-fibrillar deposits appeared less complex in the degree of polymerisation and the extent of post-translational modifications than their fibrillar counterparts. The post-translational modification of the N-terminus from glutamate to the cyclic pyroglutamate observed in both ABri and ADan is interesting and mechanistically informative, since the formation of pyroglutamate is chemically stable and poorly reversible. The presence of the N-terminal pyroglutamate, previously also found in other CNS amyloids is thought to increase the β-sheet content of the ABri and ADan peptides as well as their tendency to aggregate and polymerise and may offer protection against *in vivo* proteolysis by amino peptidases (Saido et al 1995).

Using the same biochemical approaches the major Aβ amyloid deposits were found to be Aβ4-42 and Aβ1-42 in FDD, whereas those ending at position 40 were found in negligible amounts. Immunohistochemical studies confirmed the findings observed with MS, that Aβx-42 is a major Aβ species with Aβx-40 shown in negligible amounts. The immunohistochemical studies also showed the presence of additional, including N-terminally modified Aβ species [N1, N1(rD), N3(pE) and N11(pE)] that were present in all lesion types. The predominance of the Aβx-42 in blood vessels is in striking contrast to previous studies, also confirmed by the current investigations, showing that Aβx-40 peptides isolated from blood vessels in sporadic AD and FAD are the predominant peptide species in CAA (Alonzo NC et al 1998). Whether the predominance of Aβ4-42 in FDD, which has been shown to be more toxic than the Aβ1-40 species (Pike et al

1995), represents an event that could have a major implication on the pathogenesis of this disease or reflects specific conformational mimicry requires further studies.

9.4 The BRI2 protein (BriPP) and the brain with implications on the understanding of the origin of ABri and ADan.

To determine the cell types implicated in the cerebral production of BriPP control human and FBD brain tissue was probed by *in-situ* hybridisation, immunohistochemistry and biochemical methods. The presence and distribution of furin, which has been implicated in the processing of the BriPP, was studied by immunohistochemistry. BRI2 mRNA was detected in neurons and glial cells but not in cerebrovascular smooth muscle cells or other blood vessel cellular components. BriPP was expressed by neurons, but not significantly by glia or cerebrovascular smooth muscle cells. Furin was found in both neurons and glia and, in contrast to BriPP, also in smooth muscle cells. In FBD both the vascular and parenchymal amyloid lesions contained BRI2 mRNA, BriPP and furin. These studies have confirmed that the cellular elements of the CNS are a major source of BRI2 mRNA, BriPP and furin and that the preconditions for processing the precursor protein are present.

The finding of this study that neurons are a major source of BriPP and also produce furin, together with the observation that BRI2 mRNA or BriPP is not detectable in cerebrovascular smooth muscle cells, could have an implication on our understanding the pathomechanism of CAA. These findings lend indirect evidence for the support of the drainage hypothesis which has been proposed as a major mechanism of CAA production in AD (Weller et al 1998). The findings of this study do not exclude, however that circulating, systemically produced ABri and ADan could also be a source of the cerebral amyloid lesions in FBD and FDD.

9.5 Future investigations

1) The co-existence of BriPP and furin in neurons, as demonstrated in this thesis, indicated that these cells are a likely source of ABri and ADan amyloid. However this study was unable to detect intracellular ABri and ADan in these cases. Further investigations into the potential intracellular accumulation of ABri and ADan in nerve cells would be important to further our understanding of neurodegeneration. Immunofluorescence experiments using thioflavine S, anti-oligomer specific antibodies in conjunction with ABri, ADan and NeuN would allow identification of neurons containing ABri and ADan species. If such neurons are found, additional immunohistochemistry using commercially available antibodies to various organelle markers could be used to assess the subcellular localisation.

2) Genetically modified laboratory animals that recapitulate the degenerative disorders of FBD and FDD could provide an invaluable tool to investigate the molecular mechanisms of neurodegeneration and may result in a better understanding of the link between amyloid deposition and neurodegeneration.

Animal models which have been shown to have circulating ABri and ADan may soon be available, but to date there is no information about the deposition of ABri and ADan in the CNS of such animals (J Ghiso, unpublished data). The morphological evolution of the cerebral lesions would be explored and correlated with biochemical analysis by a time course study. The impact of ABri, ADan cerebral amyloidosis on tau aggregation could be studied by crossing these animals with those having mutated or wild-type human tau.

3) The role of microglia and astrocytic involvement in the pathogenesis of FBD and FDD, has been shown to be similar to that observed in AD. Numerous studies in AD

have described how microglial lineage cells secrete neurotoxic factors upon stimulation with Aβ peptides, including soluble, oligomeric and ADDLs. It would therefore be interesting to investigate the effects of the different forms of the ABri and ADan peptides on cultured microglia and astrocytic cell lines. Whether the activation of the glial cells would result in the production neurotoxic factors that kill primary cultures neurons would be interesting and informative as to the neurotoxic species in these two diseases.

4) In FDD, but not in FBD, Aβ deposition either in combination with ADan or alone was also demonstrated immunohistochemically in blood vessel walls and in brain parenchyma. The biochemical analysis carried out in this study demonstrated the presence of Aβ4-42 in FDD, which has been shown to be more toxic than the Aβ1-40 species (Pike et al 1995). Further studies to refine the extraction techniques using laser-capture microdissection method to extract blood vessels and parenchymal deposits containing amyloid species in FDD and subject them to similar biochemical techniques carried out in this thesis. Further double immunoelectron microscopy would be carried out on more regions to validate the interaction between the two amyloidogenic peptides.

5) Recent studies support that CAA is likely to be a cofactor of dementia in AD. The effect of CAA on brain parenchyma would be studied by determining synaptic loss in relation to amyloid laden blood vessels in brain areas less affected by amyloid plaque formation. For this synaptophysin immunohistochemistry would be used and the density of the synaptic staining pattern measured with density measurements and compared between regions around the glial limitans.

In parallel the effect of ABri and ADan/Aβ on vascular smooth muscle and endothelial cells will be determined by assessing blood vessel cell lining integrity using confocal microscopy with anti-CD31 and anti-smooth muscle actin in conjuction with the corresponding anti-amyloid antibody. Results can then be correlated with the severity of CAA.

9.6 Concluding remarks

FBD and FDD are two cerebral amyloid diseases and without ABri and ADan sharing any structural identity with Aβ, show important similarities in their neuropathological features to AD. These include widespread CAA, perivascular plaques, neuritic and non-neuritic parenchymal plaques and NFTs with the classical paired helical filaments. The parenchymal plaques in FDD are primarily of the preamyloid type and co-deposition of Aβ also takes place in this disease. In both FBD and FDD the patterns of co-deposition of AAPs, complement components and inhibitors is similar to that seen in AD. The N- and C-terminal heterogeneity, post-translational modifications and oligomerisation of ABri and ADan increase as the solubility decreases. ABri and ADan may derive from several sources, but it is likely that cerebral cellular elements, primarily neurons play an important or crucial role in the production of these two amyloid peptides. Previous data and those described in this thesis, support the notion that different amyloid peptides, irrespective of their primary structure, can trigger similar pathological pathways resulting in neurodegeneration. FBD and FDD are proposed to be valuable alternative models for the study of the mechanisms of cerebral protein aggregation/amyloid formation and neurodegeneration, and it is anticipated that future studies of these diseases will be able to provide further important insight into the pathogenesis of a wide range neurodegenerative diseases.

Appendix

A1 Reagents for immunohistochemistry

A1.1 0.05M Phosphate buffered saline (PBS)

To 20 litres of distilled H_2O add 142.4g di-sodium hydrogen orthophosphate (Na_2HPO_4, BDH), 27.6g sodium dihydrogen orthophosphate dehydrate (NaH_2Po_4, BDH) and 180g NaCl (BDH). Adjust pH to 7.4.

A1.2 Citrate buffer x5

To 2 litres of distilled water, add 29.4g tri-sodium citrate (BDH) and 2.25g citric acid (BDH). Adjust pH to 6.0.

A2 Reagents used for RNA extraction

A2.1 DEPC water

Add 0.5ml of diethyl pyrocarbonate (Sigma D5758) to 500ml water, leave overnight in a fume hood and then autoclave.

A2.2 10% (w/v) Sarcosyl

Dissolve 10g of N-lauroylsarcosine (Sigma L5125) in 100ml water; treat with 0.1% (v/v) DEPC and autoclave.

A2.3 Sodium citrate (0.75 M; pH7.0)

Dissolve 22.06g citric acid tri-sodium (Sigma C8532) in 80ml water pH7 with HCL and make volume to 100ml. Treat with 0.1% (v/v) DEPC and autoclave.

A2.4 Denaturing solution (solution D)

(4M guanidium thiocyanate, 25mM sodium citrate, pH7, 0.5% sarcosyl and 0.1M 2-mercaptoethanol). To 250g guanidium thiocyanate (Sigma G6639) add 293ml DEPC treated water, 17.6 ml 0.75M sodium citrate pH7 and 26.4ml 10% sarcosyl. Dissolve at 65^0C. Store at room temperature for upto 3 months. Prepare working solution by addition of 0.36ml 2-mercaptoethanol (Sigma M3148) per 50ml stock solution – stable for 1 month at RT.

A2.5 Sodium acetate (2M; pH 4.0)

14.04ml acetic acid made up to 80ml with water then pH to 4.0 with NaOH and make up to 100ml. Treat with DEPC and autoclave.

A2.6 Chloroform:isoamyl alcohol (49:1)

To 2ml isoamyl alcohol (Sigma I1885) add 98ml chloroform (BDH)

A2.7 SDS (0.5%)

Dissolve 0.5g SDS (Lauryl sulphate, sodium salt) in 90ml water. Add 0.1 ml DEPC and make volume to 100ml with water. Leave overnight in the fume cupboard then autoclave.

A3 Reagents for Northern blot analysis

A3.1 EDTA (0.5%)

Add 18.6g EDTA (Sigma) to 80ml water. Adjust the pH to 8 with 10M NaOH, make to 100ml with water after addition of 0.1ml DEPC. Leave overnight in the fume hood then autoclave.

A3.2 MOPS-acetate-EDTA buffer

(5x MAE: 0.1M MOS, 40mM NA^+ acetate, 5mM EDTA, pH 7-7.5). Dissolve 20.6g 3-(N-morpholino) propanesulphonic acid (MOPS) (Sigma) and 3.28g sodium acetate (Sigma) in 800ml DEPC water. Adjust the pH to 7 with 2M NaOH. Add 10ml 0.5 M EDTA and make to 1 litre with DEPC water.

A3.3 Sample Mix

To 66µl 10X MOPS (Sigma, pH 7.0) add 232µl formaldehyde, 666µl formamide – care suspected carcinogen make up in the fume hood.

A3.4 Gel loading solution

(0.25% (w/v) Bromophenol blue, 0.25% (w/v) Xylene cyanole FF, 40% (w/v) sucrose in water) (Sigma).

A4 Reagents for Northern transfer

A4.1 Blotting buffer: Saline-sodium phosphate-EDTA buffer (SSPE)

20X concentrate (0.2M phosphate buffer, pH 7.4, containing 2.98 M NaCL and 0.02 M EDTA). To 174.15g NaCL (Sigma), 24g sodium phosphate (monobasic, anhydrous; Sigma) and 7.44g EDTA (Sigma) add 800ml water. Adjust the pH to 7.4 with 10M NaOH to dissolve. After addition of 1ml DEPC make the volume up to 1 litre with water. Leave overnight and autoclave.

A5 Solutions used for Protein Extraction:

A5.1 TBS:10x stock (Tris 20mM/ 150mM NaCl pH 7.5)

Add 24.2g trizma base (BDH) and 87.66g NaCl to 1000ml distilled water. Adjust to pH 7.5 with HCL. Dilute 1:10 with distilled water to use.

A5.2 Collagenase Buffer (50mM Tris, 10mM $CaCl_2$, 3mM NaN_3, pH7.5)

Add 5ml 1M Tris pH7.5 to 150mg $CaCl_2.2H_20$ and 20ng of NaN_3 and make up to 100ml with distilled water. Adjust the pH to 7.5.

A5.3 SDS Buffer (20mM Tris pH7.5, 2% SDS)
Add 24.2g trizma base (BDH) and 20g SDS (BDH) to 1000ml of distilled water.

A5.4 Coomasie Blue Staining (0.05% Coomasie Blue, 52% Methanol, 47.3% H_2O, 0.1% HAc)
Add 500mg Coomasie Blue to 520ml Methanol, 473ml distilled water and 1ml HAc.

A5.5 Coomasie Blue Destaining (52% Methanol, 47.3% H_2O, 0.1% HAc)
Add 520ml methanol to 473ml distilled water and 1ml HAc.

A5.6 Anode Buffer (x10; 2M Tris-HCL)
Add 242g trizma base to 1000ml of distilled water adjust with HCL to pH 8.9

A5.7 Cathode Buffer (x10; 1M Tris-HCL, 1M Tricine, 1% SDS)
Add 121g trizma base to 179g tricine and 10g SDS, dissolve in 1 litre of distilled water and adjust pH to 8.25.

A5.8 Gel Buffer (3M Tris-HCL, 0.3% SDS)
Add 363.5g trizma base to 3g SDS and make up to 1 litre with distilled water. Adjust pH to 8.45.

A5.9 Acrylamide Stock
40% Acrylamide/ Bis 29:1 (3.3%C) (Biorad # 161-0146)

A5.10 Composition of Gels
For slab gels Hoefer/ Pharmacia (12 x 10 x 1.5mm) – 16.5 % gels

4 Gels	Stacking Gel	Running Gel
Acrylamide/Bis (ml) (40%T,3.3%C)	2.5ml	20ml
Gel Buffer	6.2ml	20ml
Glycerol	---	6.4ml
Water	16.8ml	13.6ml
15% APS	148µl	300µl
TEMED	12.8µl	30µl
Total volume	25.66ml	60.33ml

Run at 25V for 1 hour and 90V for 5 hours or overnight at 20V for 12-14 hours.

A5.11 Rainbow Marker (amersham pharmacia biotech)
Low molecular weight range (2500-45000)
Supplied in 50% glycerol containing the following

Ovalbumin	MW 45000	Yellow
Carbonic anhydrase	MW 30000	Orange
Trypsin inhibitor	MW 20100	Blue
Lysozyme	MW 14300	Magenta
Aprotinin	MW 6500	Blue Black
Insulin (b) chain	MW 3500	Blue
Insulin (a) chain	MW 2500	Blue

A6 Reagents for EM

A6.1 Sodium Cacodylate Buffer
Dissolve 42.8g sodium cacodylate (BDH) in 1 litre of distilled water. Add 15ml NaCl to give a pH between 7.2 – 7.4. Store in a stopped bottle at 4°C.

A6.2 25% Uranyl Acetate
Dissolve 25g uranyl acetate (BDH) in 100ml methanol. This is a saturated solution and will take time to dissolve. During preparation the solution must be protected from the light, as uranyl acetate is light sensitive.

A6.3 Lead citrate
Dissolve 1.33g lead nitrate (BDH), 1.76g sodium citrate (BDH) in 30ml distilled water. Shake vigorously for one minute. Leave to stand for 30 minutes shaking occasionally. Add 8ml NaOH solution and make up to 50ml with distilled water. Store in a stoppered bottle at 4°C.

A6.4 Sodium ethoxide
Add 30.5g sodium hydroxide pellets (BDH) to 400ml absolute alcohol. Dissolve the pellets in the alcohol overnight.

A6.5 Sodium periodate solution
Add 4.7g sodium periodate (BDH) to 100ml distilled water, mix until dissolved.

A6.6 Tris-buffered saline (TBS) (0.5M)
Dissolve 60.57g tris (BDH) and 8.77g NaCl (BDH) in 800ml distilled water. Adjust pH to 7.0-7.4 with HCL, make up to 1L with distilled water.

A7 Glucose oxidase nickel DAB method.
Ref: Shu *et al* 1988 Neurosci Lett Feb29; 85(2) 169-71

A7.1 0.1M acetate buffer (pH 6.0)
A: 0.1M glacial acetic acid 200ml [1.2ml AA + 200ml dH_2O]
B: 0.1M sodium acetate 3800ml [51.68g $CH3COONa(H_2O)_3$ +3800ml dH_2O]
Mix A and B, 2000ml kept for acetate buffer and 2000ml used to make reaction solution.

A7.2 Reaction buffer (pH 6.0)
To 2000ml acetate buffer (section A7.2) add 50g nickel ammonium sulfate and 0.8g ammonium chloride.

A7.3 Reaction solution (pH 6.0)
To 100ml of reaction buffer (section A7.3) add 150mg of β-D-glucose, 50mg DAB and 10µl of glucose oxidase (add the enzyme just before you are ready to start the reaction). The reaction should take a minimum of 6 minutes.

Bibliography

Abraham CR. 2001. Reactive astrocytes and alpha1-antichymotrypsin in Alzheimer's disease. *Neurobiol.Aging* **22:** 931-936.

Abraham CR, Selkoe DJ, Potter H. 1988a. Immunochemical identification of the serine protease inhibitor alpha 1- antichymotrypsin in the brain amyloid deposits of Alzheimer's disease. *Curr Opin.Genet Dev* **52:** 487-501.

Abraham CR, Selkoe DJ, Potter H. 1988b. Immunochemical identification of the serine protease inhibitor alpha 1-antichymotrypsin in the brain amyloid deposits of Alzheimer's disease. *Cell* **52:** 487-501.

Abraham CR, Shirahama T, Potter H. 1990. Alpha 1-antichymotrypsin is associated solely with amyloid deposits containing the beta-protein. Amyloid and cell localization of alpha 1-antichymotrypsin. *Neurobiol.Aging* **11:** 123-129.

Abrahamson M, Islam MQ, Szpirer J, Szpirer C, Levan G. 1989. The human cystatin C gene (CST3), mutated in hereditary cystatin C amyloid angiopathy, is located on chromosome 20. *Hum.Genet.* **82:** 223-226.

Afagh A, Cummings BJ, Cribbs DH, Cotman CW, Tenner AJ. 1996a. Localization and cell association of C1q in Alzheimer's disease brain. *Exp.Neurol.* **138:** 22-32.

Aikawa H, Suzuki K, Iwasaki Y, Iizuka R. Atypical Alzheimer's disease with spastic paresis and ataxia.

Akiyama H, Barger S, Barnum S, Bradt B, Bauer J, Cole GM, Cooper NR, Eikelenboom P, Emmerling M, Fiebich BL, Finch CE, Frautschy S, Griffin WS, Hampel H, Hull M, Landreth G, Lue L, Mrak R, Mackenzie IR, McGeer PL, O'Banion MK, Pachter J, Pasinetti G, Plata-Salaman C, Rogers J, Rydel R, Shen Y, Streit W, Strohmeyer R, Tooyoma I, Van Muiswinkel FL, Veerhuis R, Walker D, Webster S, Wegrzyniak B, Wenk G, Wyss-Coray T. 2000. Inflammation and Alzheimer's disease. *Neurobiol.Aging* **21:** 383-421.

Akiyama H, Kondo H, Arai T, Ikeda K, Kato M, Iseki E, Schwab C, McGeer PL. 2004. Expression of BRI, the normal precursor of the amyloid protein of familial British dementia, in human brain. *Acta Neuropathol.(Berl)* **107:** 53-58.

Alexandrescu AT. 2005. Amyloid accomplices and enforcers. *Protein Sci.* **14:** 1-12.

Alonso AC, Grundke-Iqbal I, Iqbal K. 1996. Alzheimer's disease hyperphosphorylated tau sequesters normal tau into tangles of filaments and disassembles microtubules. *Nat.Med.* **2:** 783-787.

Alonzo NC, Hyman BT, Rebeck GW, Greenberg SM. 1998. Progression of cerebral amyloid angiopathy: accumulation of amyloid- beta40 in affected vessels. *J.Neuropathol.Exp.Neurol.* **57:** 353-359.

Ancsin JB. 2003. Amyloidogenesis: historical and modern observations point to heparan sulfate proteoglycans as a major culprit. *Amyloid.* **10:** 67-79.

Armstrong RA. 1998. Beta-amyloid plaques: stages in life history or independent origin? *Dement.Geriatr.Cogn Disord.* **9:** 227-238.

Aronow BJ, Lund SD, Brown TL, Harmony JA, Witte DP. 1993. Apolipoprotein J expression at fluid-tissue interfaces: potential role in barrier cytoprotection. *Proc.Natl.Acad.Sci.U.S.A* **90:** 725-729.

Axelman K, Basun H, Winblad B, Lannfelt L. 1994. A large Swedish family with Alzheimer's disease with a codon 670/671 amyloid precursor protein mutation. A clinical and genealogical investigation. *Arch.Neurol.* **51:** 1193-1197.

Bales KR, Verina T, Cummins DJ, Du Y, Dodel RC, Saura J, Fishman CE, DeLong CA, Piccardo P, Petegnief V, Ghetti B, Paul SM. 1999. Apolipoprotein E is essential for amyloid deposition in the APP(V717F) transgenic mouse model of Alzheimer's disease. *Proc.Natl.Acad.Sci.U.S.A* **96:** 15233-15238.

Bales KR, Verina T, Dodel RC, Du Y, Altstiel L, Bender M, Hyslop P, Johnstone EM, Little SP, Cummins DJ, Piccardo P, Ghetti B, Paul SM. 1997. Lack of apolipoprotein E dramatically reduces amyloid beta-peptide deposition. *Nat.Genet.* **17:** 263-264.

Bancher C, Brunner C, Lassmann H, Budka H, Jellinger K, Seitelberger F, Grundke-Iqbal I, Iqbal K, Wisniewski HM. 1989. Tau and ubiquitin immunoreactivity at different stages of formation of Alzheimer neurofibrillary tangles. *Prog.Clin.Biol.Res.* **317:** 837-848.

Bancher C, Lassmann H, Budka H, Grundke-Iqbal I, Iqbal K, Wiche G, Seitelberger F, Wisniewski HM. 1987. Neurofibrillary tangles in Alzheimer's disease and progressive supranuclear palsy: antigenic similarities and differences. Microtubule-associated protein tau antigenicity is prominent in all types of tangles. *Acta Neuropathol.(Berl)* **74:** 39-46.

Baraitser M. 1990. In: Oxford Medical Publications, 93,129,284.

Bateman A, Solomon S, Bennett HP. 1990. Post-translational modification of bovine pro-opiomelanocortin. Tyrosine sulfation and pyroglutamate formation, a mass spectrometric study. *J Biol.Chem.* **265:** 22130-22136.

Beisiegel U, Weber W, Ihrke G, Herz J, Stanley KK. 1989. The LDL-receptor-related protein, LRP, is an apolipoprotein E-binding protein. *Nature* **341:** 162-164.

Bek T. 2000. Ocular changes in heredo-oto-ophthalmo-encephalopathy. *Br.J.Ophthalmol.* **84:** 1298-1302.

Benedikz E, Blondal H, Gudmundsson G. 1990. Skin deposits in hereditary cystatin C amyloidosis. *Virchows Arch.A Pathol.Anat.Histopathol.* **417:** 325-331.

Benjannet S, Elagoz A, Wickham L, Mamarbachi M, Munzer JS, Basak A, Lazure C, Cromlish JA, Sisodia S, Checler F, Chretien M, Seidah NG. 2001. Post-

translational processing of beta-secretase (beta-amyloid- converting enzyme) and its ectodomain shedding. The pro- and transmembrane/cytosolic domains affect its cellular activity and amyloid-beta production. *J.Biol.Chem.* **276:** 10879-10887.

Bennett BD, Babu-Khan S, Loeloff R, Louis JC, Curran E, Citron M, Vassar R. 2000. Expression analysis of BACE2 in brain and peripheral tissues. *J.Biol.Chem.* **275:** 20647-20651.

Benson MD. 1996. Leptomeningeal amyloid and variant transthyretins. *Am.J.Pathol.* **148:** 351-354.

Berg L, McKeel DW, Jr., Miller JP, Storandt M, Rubin EH, Morris JC, Baty J, Coats M, Norton J, Goate AM, Price JL, Gearing M, Mirra SS, Saunders AM. 1998. Clinicopathologic studies in cognitively healthy aging and Alzheimer's disease: relation of histologic markers to dementia severity, age, sex, and apolipoprotein E genotype. *Arch.Neurol.* **55:** 326-335.

Bergeron C, Ranalli PJ, Miceli PN. 1987. Amyloid angiopathy in Alzheimer's disease. *Can.J.Neurol.Sci.* **14:** 564-569.

Berkenbosch F, Biewenga J, Brouns M, Rozemuller JM, Strijbos P, Van Dam AM. 1992. Cytokines and inflammatory proteins in Alzheimer's disease. *Res.Immunol.* **143:** 657-663.

Bjarnadottir M, Nilsson C, Lindstrom V, Westman A, Davidsson P, Thormodsson F, Blondal H, Gudmundsson G, Grubb A. 2001. The cerebral hemorrhage-producing cystatin C variant (L68Q) in extracellular fluids. *Amyloid.* **8:** 1-10.

Blaschuk O, Burdzy K, Fritz IB. 1983. Purification and characterization of a cell-aggregating factor (clusterin), the major glycoprotein in ram rete testis fluid. *J.Biol.Chem.* **258:** 7714-7720.

Bobek LA, Levine MJ. 1992. Cystatins--inhibitors of cysteine proteinases. *Crit Rev.Oral Biol.Med.* **3:** 307-332.

Bogdanovic N, Corder E, Lannfelt L, Winblad B. 2002. APOE polymorphism and clinical duration determine regional neuropathology in Swedish APP(670, 671) mutation carriers: implications for late-onset Alzheimer's disease. *J.Cell Mol.Med.* **6:** 199-214.

Borchelt DR, Ratovitski T, van Lare J, Lee MK, Gonzales V, Jenkins NA, Copeland NG, Price DL, Sisodia SS. 1997. Accelerated amyloid deposition in the brains of transgenic mice coexpressing mutant presenilin 1 and amyloid precursor proteins. *Neuron* **19:** 939-945.

Bornebroek M, Westendorp RG, Haan J, Bakker E, Timmers WF, Van Broeckhoven C, Roos RA. Mortality from hereditary cerebral haemorrhage with amyloidosis--Dutch type. The impact of sex, parental transmission and year of birth.

Botto M, Hawkins PN, Bickerstaff MC, Herbert J, Bygrave AE, McBride A, Hutchinson WL, Tennent GA, Walport MJ, Pepys MB. 1997. Amyloid deposition is

delayed in mice with targeted deletion of the serum amyloid P component gene. *Nat.Med.* **3:** 855-859.

Boyles JK, Pitas RE, Wilson E, Mahley RW, Taylor JM. 1985. Apolipoprotein E associated with astrocytic glia of the central nervous system and with nonmyelinating glia of the peripheral nervous system. *J Clin.Invest* **76:** 1501-1513.

Braak E, Braak H, Mandelkow EM. 1994. A sequence of cytoskeleton changes related to the formation of neurofibrillary tangles and neuropil threads. *Acta Neuropathol.(Berl)* **87:** 554-567.

Braak H, Braak E. 1988. Neuropil threads occur in dendrites of tangle-bearing nerve cells. *Neuropathol.Appl.Neurobiol.* **14:** 39-44.

Braak H, Braak E. 1991. Neuropathological stageing of Alzheimer-related changes. *Acta Neuropathol.(Berl)* **82:** 239-259.

Bradt BM, Kolb WP, Cooper NR. 1998. Complement-dependent proinflammatory properties of the Alzheimer's disease beta-peptide. *J.Exp.Med.* **188:** 431-438.

Buee L, Ding W, Anderson JP, Narindrasorasak S, Kisilevsky R, Boyle NJ, Robakis NK, Delacourte A, Greenberg B, Fillit HM. 1993. Binding of vascular heparan sulfate proteoglycan to Alzheimer's amyloid precursor protein is mediated in part by the N-terminal region of A4 peptide. *Brain Res.* **627:** 199-204.

Busby WH, Jr., Quackenbush GE, Humm J, Youngblood WW, Kizer JS. 1987. An enzyme(s) that converts glutaminyl-peptides into pyroglutamyl-peptides. Presence in pituitary, brain, adrenal medulla, and lymphocytes. *J Biol.Chem.* **262:** 8532-8536.

Butterfield DA. 2002. Amyloid beta-peptide (1-42)-induced oxidative stress and neurotoxicity: implications for neurodegeneration in Alzheimer's disease brain. A review. *Free Radic.Res.* **36:** 1307-1313.

Buttyan R, Olsson CA, Pintar J, Chang C, Bandyk M, Ng PY, Sawczuk IS. 1989. Induction of the TRPM-2 gene in cells undergoing programmed death. *Mol.Cell Biol.* **9:** 3473-3481.

Buxbaum JD, Choi EK, Luo Y, Lilliehook C, Crowley AC, Merriam DE, Wasco W. 1998. Calsenilin: a calcium-binding protein that interacts with the presenilins and regulates the levels of a presenilin fragment. *Nat.Med.* **4:** 1177-1181.

Cadavid D, Mena H, Koeller K, Frommelt RA. 2000. Cerebral beta amyloid angiopathy is a risk factor for cerebral ischemic infarction. A case control study in human brain biopsies. *J.Neuropathol.Exp.Neurol.* **59:** 768-773.

Calero M, Pawlik M, Soto C, Castano EM, Sigurdsson EM, Kumar A, Gallo G, Frangione B, Levy E. 2001. Distinct properties of wild-type and the amyloidogenic human cystatin C variant of hereditary cerebral hemorrhage with amyloidosis, Icelandic type. *J.Neurochem.* **77:** 628-637.

Calero M, Rostagno A, Matsubara E, Zlokovic B, Frangione B, Ghiso J. 2000. Apolipoprotein J (clusterin) and Alzheimer's disease. *Microsc.Res.Tech.* **50:** 305-315.

Carson JA, Turner AJ. 2002. Beta-amyloid catabolism: roles for neprilysin (NEP) and other metallopeptidases? *J Neurochem.* **81:** 1-8.

Caserta MT, Caccioppo D, Lapin GD, Ragin A, Groothuis DR. 1998. Blood-brain barrier integrity in Alzheimer's disease patients and elderly control subjects. *J.Neuropsychiatry Clin.Neurosci.* **10:** 78-84.

Castano EM, Prelli F, Soto C, Beavis R, Matsubara E, Shoji M, Frangione B. 1996. The length of amyloid-beta in hereditary cerebral hemorrhage with amyloidosis, Dutch type. Implications for the role of amyloid-beta. *J.Biol.Chem.* **271:** 32185-32191.

Castillo GM, Lukito W, Wight TN, Snow AD. 1999. The sulfate moieties of glycosaminoglycans are critical for the enhancement of beta-amyloid protein fibril formation. *J Neurochem.* **72:** 1681-1687.

Caughey B, Lansbury PT, Jr. 2003. Protofibrils, Pores, Fibrils, and Neurodegeneration: Separating the Responsible Protein Aggregates from the Innocent Bystanders. *Annu.Rev.Neurosci.*

Checler F. 1995. Processing of the beta-amyloid precursor protein and its regulation in Alzheimer's disease. *J Neurochem.* **65:** 1431-1444.

Chen CD, Huff ME, Matteson J, Page L, Phillips R, Kelly JW, Balch WE. 2001. Furin initiates gelsolin familial amyloidosis in the Golgi through a defect in Ca(2+) stabilization. *EMBO J.* **20:** 6277-6287.

Choi SC, Kim J, Kim TH, Cho SY, Park SS, Kim KD, Lee SH. 2001. Cloning and characterization of a type II integral transmembrane protein gene, Itm2c, that is highly expressed in the mouse brain. *Mol.Cells* **12:** 391-397.

Chomczynski P, Sacchi N. 1987. Single-step method of RNA isolation by acid guanidinium thiocyanate- phenol-chloroform extraction. *Anal.Biochem.* **162:** 156-159.

Chromy BA, Nowak RJ, Lambert MP, Viola KL, Chang L, Velasco PT, Jones BW, Fernandez SJ, Lacor PN, Horowitz P, Finch CE, Krafft GA, Klein WL. 2003. Self-assembly of Abeta(1-42) into globular neurotoxins. *Biochemistry* **42:** 12749-12760.

Citron M, Westaway D, Xia W, Carlson G, Diehl T, Levesque G, Johnson-Wood K, Lee M, Seubert P, Davis A, Kholodenko D, Motter R, Sherrington R, Perry B, Yao H, Strome R, Lieberburg I, Rommens J, Kim S, Schenk D, Fraser P, St George HP, Selkoe DJ. 1997. Mutant presenilins of Alzheimer's disease increase production of 42-residue amyloid beta-protein in both transfected cells and transgenic mice. *Nat.Med.* **3:** 67-72.

Cochran EJ, Fox JH, Mufson EJ. 1994. Severe panencephalic Pick's disease with Alzheimer's disease-like neuropil threads and synaptophysin immunoreactivity. *Acta Neuropathol.(Berl)* **88:** 479-484.

Cole GJ, Halfter W. 1996. Agrin: an extracellular matrix heparan sulfate proteoglycan involved in cell interactions and synaptogenesis. *Perspect.Dev.Neurobiol.* **3:** 359-371.

Collard MW, Griswold MD. 1987. Biosynthesis and molecular cloning of sulfated glycoprotein 2 secreted by rat Sertoli cells. *Biochemistry* **26:** 3297-3303.

Corder EH, Saunders AM, Strittmatter WJ, Schmechel DE, Gaskell PC, Small GW, Roses AD, Haines JL, Pericak-Vance MA. 1993. Gene dose of apolipoprotein E type 4 allele and the risk of Alzheimer's disease in late onset families. *Science* **261:** 921-923.

Coria F, Castano E, Prelli F, Larrondo-Lillo M, van Duinen S, Shelanski ML, Frangione B. 1988. Isolation and characterization of amyloid P component from Alzheimer's disease and other types of cerebral amyloidosis. *Lab Invest* **58:** 454-458.

Costell M, Mann K, Yamada Y, Timpl R. 1997. Characterization of recombinant perlecan domain I and its substitution by glycosaminoglycans and oligosaccharides. *Eur.J.Biochem.* **243:** 115-121.

Cotman SL, Halfter W, Cole GJ. 2000. Agrin binds to beta-amyloid (Abeta), accelerates abeta fibril formation, and is localized to Abeta deposits in Alzheimer's disease brain. *Mol.Cell Neurosci.* **15:** 183-198.

Coulson EJ, Paliga K, Beyreuther K, Masters CL. 2000. What the evolution of the amyloid protein precursor supergene family tells us about its function. *Neurochem.Int.* **36:** 175-184.

Crawford FC, Freeman MJ, Schinka JA, Abdullah LI, Gold M, Hartman R, Krivian K, Morris MD, Richards D, Duara R, Anand R, Mullan MJ. 2000. A polymorphism in the cystatin C gene is a novel risk factor for late-onset Alzheimer's disease. *Neurology* **55:** 763-768.

Creemers JW, Ines DD, Plets E, Serneels L, Taylor NA, Multhaup G, Craessaerts K, Annaert W, De Strooper B. 2001. Processing of beta-secretase by furin and other members of the proprotein convertase family. *J.Biol.Chem.* **276:** 4211-4217.

Crook R, Verkkoniemi A, Perez-Tur J, Mehta N, Baker M, Houlden H, Farrer M, Hutton M, Lincoln S, Hardy J, Gwinn K, Somer M, Paetau A, Kalimo H, Ylikoski R, Poyhonen M, Kucera S, Haltia M. 1998. A variant of Alzheimer's disease with spastic paraparesis and unusual plaques due to deletion of exon 9 of presenilin 1. *Nat.Med.* **4:** 452-455.

Cullinan WE, Day NC, Schafer MK, Day R, Seidah NG, Chretien M, Akil H, Watson SJ. 1991. Neuroanatomical and functional studies of peptide precursor-processing enzymes. *Enzyme* **45:** 285-300.

Danik M, Chabot JG, Hassan-Gonzalez D, Suh M, Quirion R. 1993. Localization of sulfated glycoprotein-2/clusterin mRNA in the rat brain by in situ hybridization. *J.Comp Neurol.* **334:** 209-227.

Day R, Schafer MK, Cullinan WE, Watson SJ, Chretien M, Seidah NG. 1993. Region specific expression of furin mRNA in the rat brain. *Neurosci.Lett.* **149:** 27-30.

de Court, Mandybur TI. 1987. Atypical Gerstmann-Straussler syndrome or familial spinocerebellar ataxia and Alzheimer's disease? *Neurology* **37:** 269-275.

de la CA, Tolvanen R, Boysen G, Santavy J, Bleeker-Wagemakers L, Maury CP, Kere J. 1992. Gelsolin-derived familial amyloidosis caused by asparagine or tyrosine substitution for aspartic acid at residue 187. *Nat.Genet.* **2:** 157-160.

de Silva HV, Harmony JA, Stuart WD, Gil CM, Robbins J. 1990a. Apolipoprotein J: structure and tissue distribution. *Biochemistry* **29:** 5380-5389.

de Silva HV, Stuart WD, Duvic CR, Wetterau JR, Ray MJ, Ferguson DG, Albers HW, Smith WR, Harmony JA. 1990b. A 70-kDa apolipoprotein designated ApoJ is a marker for subclasses of human plasma high density lipoproteins. *J.Biol.Chem.* **265:** 13240-13247.

Deane R, Wu Z, Sagare A, Davis J, Du YS, Hamm K, Xu F, Parisi M, LaRue B, Hu HW, Spijkers P, Guo H, Song X, Lenting PJ, Van Nostrand WE, Zlokovic BV. 2004. LRP/amyloid beta-peptide interaction mediates differential brain efflux of Abeta isoforms. *Neuron* **43:** 333-344.

Delacourte A, Buee L. 1997. Normal and pathological Tau proteins as factors for microtubule assembly. *Int.Rev.Cytol.* **171:** 167-224.

Delacourte A, Sergeant N, Wattez A, Gauvreau D, Robitaille Y. 1998. Vulnerable neuronal subsets in Alzheimer's and Pick's disease are distinguished by their tau isoform distribution and phosphorylation. *Ann.Neurol.* **43:** 193-204.

Deleault NR, Lucassen RW, Supattapone S. 2003. RNA molecules stimulate prion protein conversion. *Nature* **425:** 717-720.

Deleersnijder W, Hong G, Cortvrindt R, Poirier C, Tylzanowski P, Pittois K, Van Marck E, Merregaert J. 1996. Isolation of markers for chondro-osteogenic differentiation using cDNA library subtraction. Molecular cloning and characterization of a gene belonging to a novel multigene family of integral membrane proteins. *J.Biol.Chem.* **271:** 19475-19482.

DeMattos RB, Cirrito JR, Parsadanian M, May PC, O'dell MA, Taylor JW, Harmony JA, Aronow BJ, Bales KR, Paul SM, Holtzman DM. 2004. ApoE and Clusterin Cooperatively Suppress Abeta Levels and Deposition. Evidence that ApoE Regulates Extracellular Abeta Metabolism In Vivo. *Neuron* **41:** 193-202.

Denault J, Bissonnette L, Longpre J, Charest G, Lavigne P, Leduc R. 2002. Ectodomain shedding of furin: kinetics and role of the cysteine-rich region. *FEBS Lett.* **527:** 309-314.

Denault JB, Leduc R. 1996. Furin/PACE/SPC1: a convertase involved in exocytic and endocytic processing of precursor proteins. *FEBS Lett.* **379:** 113-116.

Dickson DW. 1997. The pathogenesis of senile plaques. *J.Neuropathol.Exp.Neurol.* **56:** 321-339.

Dickson DW, Farlo J, Davies P, Crystal H, Fuld P, Yen SH. 1988. Alzheimer's disease. A double-labeling immunohistochemical study of senile plaques. *Am.J.Pathol.* **132:** 86-101.

Dickson DW, Lee SC, Mattiace LA, Yen SH, Brosnan C. 1993. Microglia and cytokines in neurological disease, with special reference to AIDS and Alzheimer's disease. *Glia* **7:** 75-83.

Dong W, Seidel B, Marcinkiewicz M, Chretien M, Seidah NG, Day R. 1997. Cellular localization of the prohormone convertases in the hypothalamic paraventricular and supraoptic nuclei: selective regulation of PC1 in corticotrophin-releasing hormone parvocellular neurons mediated by glucocorticoids. *J.Neurosci.* **17:** 563-575.

Duda JE, Giasson BI, Mabon ME, Miller DC, Golbe LI, Lee VM, Trojanowski JQ. 2002. Concurrence of alpha-synuclein and tau brain pathology in the Contursi kindred. *Acta Neuropathol.(Berl)* **104:** 7-11.

Duewel HS, Honek JF. 1998. CNBr/formic acid reactions of methionine- and trifluoromethionine-containing lambda lysozyme: probing chemical and positional reactivity and formylation side reactions by mass spectrometry. *J Protein Chem.* **17:** 337-350.

Duff K, Eckman C, Zehr C, Yu X, Prada CM, Perez-Tur J, Hutton M, Buee L, Harigaya Y, Yager D, Morgan D, Gordon MN, Holcomb L, Refolo L, Zenk B, Hardy J, Younkin S. 1996. Increased amyloid-beta42(43) in brains of mice expressing mutant presenilin 1. *Nature* **383:** 710-713.

Duguid JR, Bohmont CW, Liu NG, Tourtellotte WW. 1989. Changes in brain gene expression shared by scrapie and Alzheimer disease. *Proc.Natl.Acad.Sci.U.S.A* **86:** 7260-7264.

Eikelenboom P, Rozemuller JM, Kraal G, Stam FC, McBride PA, Bruce ME, Fraser H. 1991. Cerebral amyloid plaques in Alzheimer's disease but not in scrapie-affected mice are closely associated with a local inflammatory process. *Virchows Arch.B Cell Pathol.Incl.Mol.Pathol.* **60:** 329-336.

Eikelenboom P, Stam FC. 1982. Immunoglobulins and complement factors in senile plaques. An immunoperoxidase study. *Acta Neuropathol.(Berl)* **57:** 239-242.

El Agnaf OM, Nagala S, Patel BP, Austen BM. 2001. Non-fibrillar oligomeric species of the amyloid ABri peptide, implicated in familial British dementia, are more potent at inducing apoptotic cell death than protofibrils or mature fibrils. *J.Mol.Biol.* **310:** 157-168.

el Hachimi KH, Verga L, Giaccone G, Tagliavini F, Frangione B, Bugiani O, Foncin JF. 1991. Relationship between non-fibrillary amyloid precursors and cell processes in the cortical neuropil of Alzheimer patients. *Neurosci.Lett.* **129:** 119-122.

Ellis RJ, Olichney JM, Thal LJ, Mirra SS, Morris JC, Beekly D, Heyman A. 1996. Cerebral amyloid angiopathy in the brains of patients with Alzheimer's disease: the CERAD experience, Part XV. *Neurology* **46:** 1592-1596.

Emi M, Wu LL, Robertson MA, Myers RL, Hegele RA, Williams RR, White R, Lalouel JM. 1988. Genotyping and sequence analysis of apolipoprotein E isoforms. *Genomics* **3:** 373-379.

Emmerling MR, Watson MD, Raby CA, Spiegel K. 2000. The role of complement in Alzheimer's disease pathology. *Biochim.Biophys.Acta* **1502:** 158-171.

Esiri MM, Wilcock GK. 1986. Cerebral amyloid angiopathy in dementia and old age. *J.Neurol.Neurosurg.Psychiatry* **49:** 1221-1226.

Evans KC, Berger EP, Cho CG, Weisgraber KH, Lansbury PT, Jr. 1995. Apolipoprotein E is a kinetic but not a thermodynamic inhibitor of amyloid formation: implications for the pathogenesis and treatment of Alzheimer disease. *Proc.Natl.Acad.Sci.U.S.A* **92:** 763-767.

Fagan AM, Bu G, Sun Y, Daugherty A, Holtzman DM. 1996. Apolipoprotein E-containing high density lipoprotein promotes neurite outgrowth and is a ligand for the low density lipoprotein receptor-related protein. *J.Biol.Chem.* **271:** 30121-30125.

Farris W, Mansourian S, Leissring MA, Eckman EA, Bertram L, Eckman CB, Tanzi RE, Selkoe DJ. 2004. Partial loss-of-function mutations in insulin-degrading enzyme that induce diabetes also impair degradation of amyloid beta-protein. *Am.J Pathol.* **164:** 1425-1434.

Farzan M, Schnitzler CE, Vasilieva N, Leung D, Choe H. 2000. BACE2, a beta - secretase homolog, cleaves at the beta site and within the amyloid-beta region of the amyloid-beta precursor protein. *Proc.Natl.Acad.Sci.U.S.A* **97:** 9712-9717.

Finckh U, von der KH, Velden J, Michel T, Andresen B, Deng A, Zhang J, Muller-Thomsen T, Zuchowski K, Menzer G, Mann U, Papassotiropoulos A, Heun R, Zurdel J, Holst F, Benussi L, Stoppe G, Reiss J, Miserez AR, Staehelin HB, Rebeck GW, Hyman BT, Binetti G, Hock C, Growdon JH, Nitsch RM. 2000. Genetic association of a cystatin C gene polymorphism with late-onset Alzheimer disease. *Arch.Neurol.* **57:** 1579-1583.

Fischer WH, Spiess J. 1987. Identification of a mammalian glutaminyl cyclase converting glutaminyl into pyroglutamyl peptides. *Proc.Natl.Acad.Sci.U.S.A* **84:** 3628-3632.

Fishelson Z, Attali G, Mevorach D. 2001. Complement and apoptosis. *Mol.Immunol.* **38:** 207-219.

Frackowiak J, Zoltowska A, Wisniewski HM. 1994. Non-fibrillar beta-amyloid protein is associated with smooth muscle cells of vessel walls in Alzheimer disease. *J.Neuropathol.Exp.Neurol.* **53:** 637-645.

Frangione B, Revesz T, Vidal R, Holton J, Lashley T, Houlden H, Wood N, Rostagno A, Plant G, Ghiso J. 2001. Familial cerebral amyloid angiopathy related to stroke and dementia. *Amyloid.* **8 Suppl 1:** 36-42.

Fraser PE, Nguyen JT, Chin DT, Kirschner DA. 1992. Effects of sulfate ions on Alzheimer beta/A4 peptide assemblies: implications for amyloid fibril-proteoglycan interactions. *J.Neurochem.* **59:** 1531-1540.

French LE, Chonn A, Ducrest D, Baumann B, Belin D, Wohlwend A, Kiss JZ, Sappino AP, Tschopp J, Schifferli JA. 1993. Murine clusterin: molecular cloning and

mRNA localization of a gene associated with epithelial differentiation processes during embryogenesis. *J.Cell Biol.* **122:** 1119-1130.

Fritz IB, Burdzy K, Setchell B, Blaschuk O. 1983. Ram rete testis fluid contains a protein (clusterin) which influences cell-cell interactions in vitro. *Biol.Reprod.* **28:** 1173-1188.

Gabay C, Kushner I. 1999. Acute-phase proteins and other systemic responses to inflammation. *N.Engl.J.Med.* **340:** 448-454.

Gallo G, Wisniewski T, Choi-Miura NH, Ghiso J, Frangione B. 1994. Potential role of apolipoprotein-E in fibrillogenesis. *Am.J.Pathol.* **145:** 526-530.

Galloway PG, Grundke-Iqbal I, Iqbal K, Perry G. 1988. Lewy bodies contain epitopes both shared and distinct from Alzheimer neurofibrillary tangles. *J Neuropathol.Exp.Neurol.* **47:** 654-663.

Gardella JE, Gorgone GA, Newman P, Frangione B, Gorevic PD. 1992. Characterization of Alzheimer amyloid precursor protein transcripts in platelets and megakarocytes. *Neurosci.Lett.* **138:** 229-232.

Garzuly F, Vidal R, Wisniewski T, Brittig F, Budka H. 1996. Familial meningocerebrovascular amyloidosis, Hungarian type, with mutant transthyretin (TTR Asp18Gly). *Neurology* **47:** 1562-1567.

Ghersi-Egea JF, Gorevic PD, Ghiso J, Frangione B, Patlak CS, Fenstermacher JD. 1996. Fate of cerebrospinal fluid-borne amyloid beta-peptide: rapid clearance into blood and appreciable accumulation by cerebral arteries. *J Neurochem.* **67:** 880-883.

Ghetti B, Piccardo P, Spillantini MG, Ichimiya Y, Porro M, Perini F, Kitamoto T, Tateishi J, Seiler C, Frangione B, Bugiani O, Giaccone G, Prelli F, Goedert M, Dlouhy SR, Tagliavini F. 1996. Vascular variant of prion protein cerebral amyloidosis with tau-positive neurofibrillary tangles: the phenotype of the stop codon 145 mutation in PRNP. *Proc.Natl.Acad.Sci.U.S.A* **93:** 744-748.

Ghiso J, Frangione B. 2002. Amyloidosis and Alzheimer's disease. *Adv.Drug Deliv.Rev.* **54:** 1539-1551.

Ghiso J, Haltia M, Prelli F, Novello J, Frangione B. 1990. Gelsolin variant (Asn-187) in familial amyloidosis, Finnish type. *Biochem.J.* **272:** 827-830.

Ghiso J, Plant GT, Revesz T, Wisniewski T, Frangione B. 1995. Familial cerebral amyloid angiopathy (British type) with nonneuritic amyloid plaque formation may be due to a novel amyloid protein [letter]. *J.Neurol.Sci.* **129:** 74-75.

Ghiso J, Pons-Estel B, Frangione B. 1986. Hereditary cerebral amyloid angiopathy: the amyloid fibrils contain a protein which is a variant of cystatin C, an inhibitor of lysosomal cysteine proteases. *Biochem.Biophys.Res.Commun.* **136:** 548-554.

Ghiso J, Wisniewski T, Frangione B. 1994. Unifying features of systemic and cerebral amyloidosis. *Mol.Neurobiol.* **8:** 49-64.

Ghiso JA, Holton J, Miravalle L, Calero M, Lashley T, Vidal R, Houlden H, Wood N, Neubert TA, Rostagno A, Plant G, Revesz T, Frangione B. 2001. Systemic amyloid deposits in familial British dementia. *J.Biol.Chem.* **276:** 43909-43914.

Giaccone G, Verga L, Bugiani O, Frangione B, Serban D, Prusiner SB, Farlow MR, Ghetti B, Tagliavini F. 1992. Prion protein preamyloid and amyloid deposits in Gerstmann-Straussler-Scheinker disease, Indiana kindred. *Proc.Natl.Acad.Sci.U.S.A* **89:** 9349-9353.

Giannakopoulos P, Kovari E, French LE, Viard I, Hof PR, Bouras C. 1998. Possible neuroprotective role of clusterin in Alzheimer's disease: a quantitative immunocytochemical study. *Acta Neuropathol.(Berl)* **95:** 387-394.

Ginsberg SD, Galvin JE, Chiu TS, Lee VM, Masliah E, Trojanowski JQ. 1998. RNA sequestration to pathological lesions of neurodegenerative diseases. *Acta Neuropathol.(Berl)* **96:** 487-494.

Glenner GG, Henry JH, Fujihara S. 1981. Congophilic angiopathy in the pathogenesis of Alzheimer's degeneration. *Ann.Pathol.* **1:** 120-129.

Goedert M, Jakes R, Crowther RA, Six J, Lubke U, Vandermeeren M, Cras P, Trojanowski JQ, Lee VM. 1993. The abnormal phosphorylation of tau protein at Ser-202 in Alzheimer disease recapitulates phosphorylation during development. *Proc.Natl.Acad.Sci.U.S.A* **90:** 5066-5070.

Gouras GK, Xu H, Jovanovic JN, Buxbaum JD, Wang R, Greengard P, Relkin NR, Gandy S. 1998. Generation and regulation of beta-amyloid peptide variants by neurons. *J.Neurochem.* **71:** 1920-1925.

Gowing E, Roher AE, Woods AS, Cotter RJ, Chaney M, Little SP, Ball MJ. 1994. Chemical characterization of A beta 17-42 peptide, a component of diffuse amyloid deposits of Alzheimer disease. *J Biol.Chem.* **269:** 10987-10990.

Grabowski TJ, Cho HS, Vonsattel JP, Rebeck GW, Greenberg SM. 2001. Novel amyloid precursor protein mutation in an Iowa family with dementia and severe cerebral amyloid angiopathy. *Ann.Neurol.* **49:** 697-705.

Greenberg SM, Cho HS, O'Donnell HC, Rosand J, Segal AZ, Younkin LH, Younkin SG, Rebeck GW. 2000. Plasma beta-amyloid peptide, transforming growth factor-beta 1, and risk for cerebral amyloid angiopathy. *Ann.N.Y.Acad.Sci.* **903:** 144-149.

Greenberg SM, Rebeck GW, Vonsattel JP, Gomez-Isla T, Hyman BT. 1995. Apolipoprotein E epsilon 4 and cerebral hemorrhage associated with amyloid angiopathy. *Ann.Neurol.* **38:** 254-259.

Griffiths RA, Mortimer TF, Oppenheimer DR, Spalding JM. 1982. Congophilic angiopathy of the brain: a clinical and pathological report on two siblings. *J.Neurol.Neurosurg.Psychiatry* **45:** 396-408.

Grubb A, Lofberg H. 1982. Human gamma-trace, a basic microprotein: amino acid sequence and presence in the adenohypophysis. *Proc.Natl.Acad.Sci.U.S.A* **79:** 3024-3027.

Grundke-Iqbal I, Iqbal K, Quinlan M, Tung YC, Zaidi MS, Wisniewski HM. 1986. Microtubule-associated protein tau. A component of Alzheimer paired helical filaments. *J.Biol.Chem.* **261:** 6084-6089.

Gudmundsson G, Hallgrimsson J, Jonasson TA, Bjarnason O. 1972. Hereditary cerebral haemorrhage with amyloidosis. *Brain* **95:** 387-404.

Haltia M, Prelli F, Ghiso J, Kiuru S, Somer H, Palo J, Frangione B. 1990. Amyloid protein in familial amyloidosis (Finnish type) is homologous to gelsolin, an actin-binding protein. *Biochem.Biophys.Res.Commun.* **167:** 927-932.

Hamazaki H. 1995. Amyloid P component promotes aggregation of Alzheimer's beta-amyloid peptide. *Biochem.Biophys.Res.Commun.* **211:** 349-353.

Harada A, Oguchi K, Okabe S, Kuno J, Terada S, Ohshima T, Sato-Yoshitake R, Takei Y, Noda T, Hirokawa N. 1994. Altered microtubule organization in small-calibre axons of mice lacking tau protein. *Nature* **369:** 488-491.

Hardy J. 1997. Amyloid, the presenilins and Alzheimer's disease. *Trends Neurosci* **20:** 154-159.

Hardy J, Selkoe DJ. 2002. The amyloid hypothesis of Alzheimer's disease: progress and problems on the road to therapeutics. *Science* **297:** 353-356.

Harigaya Y, Saido TC, Eckman CB, Prada CM, Shoji M, Younkin SG. 2000. Amyloid beta protein starting pyroglutamate at position 3 is a major component of the amyloid deposits in the Alzheimer's disease brain. *Biochem.Biophys.Res.Commun.* **276:** 422-427.

Harper JD, Lieber CM, Lansbury PT, Jr. 1997. Atomic force microscopic imaging of seeded fibril formation and fibril branching by the Alzheimer's disease amyloid-beta protein. *Chem.Biol.* **4:** 951-959.

Hartley DM, Walsh DM, Ye CP, Diehl T, Vasquez S, Vassilev PM, Teplow DB, Selkoe DJ. 1999. Protofibrillar intermediates of amyloid beta-protein induce acute electrophysiological changes and progressive neurotoxicity in cortical neurons. *J.Neurosci.* **19:** 8876-8884.

Hashimoto T, Wakabayashi T, Watanabe A, Kowa H, Hosoda R, Nakamura A, Kanazawa I, Arai T, Takio K, Mann DM, Iwatsubo T. 2002. CLAC: a novel Alzheimer amyloid plaque component derived from a transmembrane precursor, CLAC-P/collagen type XXV. *EMBO J.* **21:** 1524-1534.

Hatsuzawa K, Hosaka M, Nakagawa T, Nagase M, Shoda A, Murakami K, Nakayama K. 1990. Structure and expression of mouse furin, a yeast Kex2-related protease. Lack of processing of coexpressed prorenin in GH4C1 cells. *J.Biol.Chem.* **265:** 22075-22078.

He W, Barrow CJ. 1999. The A beta 3-pyroglutamyl and 11-pyroglutamyl peptides found in senile plaque have greater beta-sheet forming and aggregation propensities in vitro than full-length A beta. *Biochemistry* **38:** 10871-10877.

Head E, Azizeh BY, Lott IT, Tenner AJ, Cotman CW, Cribbs DH. 2001. Complement association with neurons and beta-amyloid deposition in the brains of aged individuals with Down Syndrome. *Neurobiol.Dis.* **8:** 252-265.

Hendriks L, van Duijn CM, Cras P, Cruts M, Van Hul W, van Harskamp F, Warren A, McInnis MG, Antonarakis SE, Martin JJ, . 1992. Presenile dementia and cerebral haemorrhage linked to a mutation at codon 692 of the beta-amyloid precursor protein gene. *Nat.Genet.* **1:** 218-221.

Hermo L, Barin K, Oko R. 1994. Developmental expression of sulfated glycoprotein-2 in the epididymis of the rat. *Anat.Rec.* **240:** 327-344.

Herndon ME, Lander AD. 1990. A diverse set of developmentally regulated proteoglycans is expressed in the rat central nervous system. *Neuron* **4:** 949-961.

Herzig MC, Winkler DT, Burgermeister P, Pfeifer M, Kohler E, Schmidt SD, Danner S, Abramowski D, Sturchler-Pierrat C, Burki K, van Duinen SG, Maat-Schieman ML, Staufenbiel M, Mathews PM, Jucker M. 2004. Abeta is targeted to the vasculature in a mouse model of hereditary cerebral hemorrhage with amyloidosis. *Nat.Neurosci.* **7:** 954-960.

Hicks PS, Saunero-Nava L, Du Clos TW, Mold C. 1992. Serum amyloid P component binds to histones and activates the classical complement pathway. *J.Immunol.* **149:** 3689-3694.

Higgins LS, Catalano R, Quon D, Cordell B. 1993. Transgenic mice expressing human beta-APP751, but not mice expressing beta-APP695, display early Alzheimer's disease-like histopathology. *Ann.N.Y.Acad.Sci.* **695:** 224-227.

Holm NE, Nybo M, Junker K, Toftedal HP, Rasmussen IM, Svehag SE. 2000. Localization of human serum amyloid P component and heparan sulfate proteoglycan in in vitro-formed Abeta fibrils. *Scand.J.Immunol.* **52:** 110-112.

Holton JL, Ghiso J, Lashley T, Rostagno A, Guerin CJ, Gibb G, Houlden H, Ayling H, Martinian L, Anderton BH, Wood NW, Vidal R, Plant G, Frangione B, Revesz T. 2001. Regional distribution of amyloid-Bri deposition and its association with neurofibrillary degeneration in familial British dementia. *Am.J.Pathol.* **158:** 515-526.

Holton JL, Lashley T, Ghiso J, Braendgaard H, Vidal R, Guerin CJ, Gibb G, Hanger DP, Rostagno A, Anderton BH, Strand C, Ayling H, Plant G, Frangione B, Bojsen-Moller M, Revesz T. 2002. Familial Danish dementia: a novel form of cerebral amyloidosis associated with deposition of both amyloid-Dan and amyloid-beta. *J.Neuropathol.Exp.Neurol.* **61:** 254-267.

Holtzman DM. 2004. In vivo effects of ApoE and clusterin on amyloid-beta metabolism and neuropathology. *J.Mol.Neurosci.* **23:** 247-254.

Holtzman DM, Bales KR, Tenkova T, Fagan AM, Parsadanian M, Sartorius LJ, Mackey B, Olney J, McKeel D, Wozniak D, Paul SM. 2000a. Apolipoprotein E isoform-dependent amyloid deposition and neuritic degeneration in a mouse model of Alzheimer's disease. *Proc.Natl.Acad.Sci.U.S.A* **97:** 2892-2897.

Holtzman DM, Epstein CJ. 1992. The molecular genetics of Down syndrome. *Mol.Genet.Med.* **2:** 105-120.

Holtzman DM, Fagan AM, Mackey B, Tenkova T, Sartorius L, Paul SM, Bales K, Ashe KH, Irizarry MC, Hyman BT. 2000b. Apolipoprotein E facilitates neuritic and cerebrovascular plaque formation in an Alzheimer's disease model. *Ann.Neurol.* **47:** 739-747.

Hood JM, Koep LJ, Peters RL, Schroter GP, Weil R, III, Redeker AG, Starzl TE. 1980. Liver transplantation for advanced liver disease with alpha-1-antitrypsin deficiency. *N.Engl.J Med.* **302:** 272-275.

Houlden H, Baker M, McGowan E, Lewis P, Hutton M, Crook R, Wood NW, Kumar-Singh S, Geddes J, Swash M, Scaravilli F, Holton JL, Lashley T, Tomita T, Hashimoto T, Verkkoniemi A, Kalimo H, Somer M, Paetau A, Martin JJ, Van Broeckhoven C, Golde T, Hardy J, Haltia M, Revesz T. 2000. Variant Alzheimer's disease with spastic paraparesis and cotton wool plaques is caused by PS-1 mutations that lead to exceptionally high amyloid-beta concentrations. *Ann.Neurol.* **48:** 806-808.

Hyman BT. 1992. Down syndrome and Alzheimer disease. *Prog.Clin.Biol.Res.* **379:** 123-142.

Ikeda S, Allsop D, Glenner GG. 1989. Morphology and distribution of plaque and related deposits in the brains of Alzheimer's disease and control cases. An immunohistochemical study using amyloid beta-protein antibody. *Lab Invest* **60:** 113-122.

Inoue S, Kuroiwa M, Kisilevsky R. 1999. Basement membranes, microfibrils and beta amyloid fibrillogenesis in Alzheimer's disease: high resolution ultrastructural findings. *Brain Res.Brain Res.Rev.* **29:** 218-231.

Ishii T, Haga S. 1984. Immuno-electron-microscopic localization of complements in amyloid fibrils of senile plaques. *Acta Neuropathol.(Berl)* **63:** 296-300.

Ishizawa K, Komori T, Shimazu T, Yamamoto T, Kitamoto T, Shimazu K, Hirose T. 2002. Hyperphosphorylated tau deposition parallels prion protein burden in a case of Gerstmann-Straussler-Scheinker syndrome P102L mutation complicated with dementia. *Acta Neuropathol.(Berl)* **104:** 342-350.

Ishizawa T, Mattila P, Davies P, Wang D, Dickson DW. 2003. Colocalization of tau and alpha-synuclein epitopes in Lewy bodies. *J Neuropathol.Exp.Neurol.* **62:** 389-397.

Iwatsubo T, Hasegawa M, Ihara Y. 1994a. Neuronal and glial tau positive inclusions in diverse neurologic diseases share common phosphorylation characteristics. *Acta Neuropathol* **88:** 129-136.

Iwatsubo T, Mann DM, Odaka A, Suzuki N, Ihara Y. 1995. Amyloid beta protein (A beta) deposition: A beta 42(43) precedes A beta 40 in Down syndrome. *Ann.Neurol.* **37:** 294-299.

Iwatsubo T, Odaka A, Suzuki N, Mizusawa H, Nukina N, Ihara Y. 1994b. Visualization of A beta 42(43) and A beta 40 in senile plaques with end-specific A beta monoclonals: evidence that an initially deposited species is A beta 42(43). *Neuron* **13:** 45-53.

Iwatsubo T, Saido TC, Mann DM, Lee VM, Trojanowski JQ. 1996. Full-length amyloid-beta (1-42(43)) and amino-terminally modified and truncated amyloid-beta 42(43) deposit in diffuse plaques. *Am.J.Pathol.* **149:** 1823-1830.

Janciauskiene S, Eriksson S, Wright HT. 1996. A specific structural interaction of Alzheimer's peptide A beta 1-42 with alpha 1-antichymotrypsin. *Nat.Struct.Biol.* **3:** 668-671.

Janus C, Chishti MA, Westaway D. 2000. Transgenic mouse models of Alzheimer's disease. *Biochim.Biophys.Acta* **1502:** 63-75.

Jenne DE, Tschopp J. 1989. Molecular structure and functional characterization of a human complement cytolysis inhibitor found in blood and seminal plasma: identity to sulfated glycoprotein 2, a constituent of rat testis fluid. *Proc.Natl.Acad.Sci.U.S.A* **86:** 7123-7127.

Jensson O, Palsdottir A, Thorsteinsson L, Arnason A. 1989. The saga of cystatin C gene mutation causing amyloid angiopathy and brain hemorrhage--clinical genetics in Iceland. *Clin.Genet.* **36:** 368-377.

Jin G, Howe PH. 1997. Regulation of clusterin gene expression by transforming growth factor beta. *J.Biol.Chem.* **272:** 26620-26626.

Johnston J, O'Neill C, Lannfelt L, Winblad B, Cowburn RF. 1994. The significance of the Swedish APP670/671 mutation for the development of Alzheimer's disease amyloidosis. *Neurochem.Int.* **25:** 73-80.

Kalaria RN, Golde TE, Cohen ML, Younkin SG. 1991. Serum amyloid P in Alzheimer's disease. Implications for dysfunction of the blood-brain barrier. *Ann.N.Y.Acad.Sci.* **640:** 145-148.

Kalaria RN, Grahovac I. 1990. Serum amyloid P immunoreactivity in hippocampal tangles, plaques and vessels: implications for leakage across the blood-brain barrier in Alzheimer's disease. *Brain Res.* **516:** 349-353.

Kalaria RN, Hedera P. 1996. beta-Amyloid vasoactivity in Alzheimer's disease. *Lancet* **347:** 1492-1493.

Kamboh MI, DeKosky ST. 1995. Apolipoprotein E genotyping in the diagnosis of Alzheimer's disease. *Ann.Neurol.* **38:** 967-970.

Kang J, Lemaire HG, Unterbeck A, Salbaum JM, Masters CL, Grzeschik KH, Multhaup G, Beyreuther K, Muller-Hill B. 1987. The precursor of Alzheimer's disease amyloid A4 protein resembles a cell-surface receptor. *Nature* **325:** 733-736.

Kawai M, Kalaria RN, Cras P, Siedlak SL, Velasco ME, Shelton ER, Chan HW, Greenberg BD, Perry G. 1993. Degeneration of vascular muscle cells in cerebral amyloid angiopathy of Alzheimer disease. *Brain Res.* **623:** 142-146.

Kawas CH, Brookmeyer R. 2001. Aging and the public health effects of dementia. *N.Engl.J.Med.* **344:** 1160-1161.

Keohane C, Peatfield R, Duchen LW. Subacute spongiform encephalopathy (Creutzfeldt-Jakob disease) with amyloid angiopathy.

Kidd M. 1964. Alzheimer's disease - an electron microscopical study. *Brain* **87:** 307-320.

Kim SH, Creemers JW, Chu S, Thinakaran G, Sisodia SS. 2002. Proteolytic processing of familial British dementia-associated BRI variants: evidence for enhanced intracellular accumulation of amyloidogenic peptides. *J.Biol.Chem.* **277:** 1872-1877.

Kim SH, Wang R, Gordon DJ, Bass J, Steiner DF, Lynn D, Thinakaran G, Meredith SC, Sisodia SS. 1999. Furin mediates enhanced production of fibrillogenic ABri peptides in familial British dementia. *Nat Neurosci* **2:** 984-988.

Kirchner J, Bevan MJ. 1999. ITM2A is induced during thymocyte selection and T cell activation and causes downregulation of CD8 when overexpressed in CD4(+)CD8(+) double positive thymocytes. *J Exp.Med.* **190:** 217-228.

Kirszbaum L, Sharpe JA, Murphy B, d'Apice AJ, Classon B, Hudson P, Walker ID. 1989. Molecular cloning and characterization of the novel, human complement-associated protein, SP-40,40: a link between the complement and reproductive systems. *EMBO J.* **8:** 711-718.

Kiuru S. 1998. Gelsolin-related familial amyloidosis, Finnish type (FAF), and its variants found worldwide. *Amyloid.* **5:** 55-66.

Klein WL, Krafft GA, Finch CE. 2001. Targeting small Abeta oligomers: the solution to an Alzheimer's disease conundrum? *Trends Neurosci.* **24:** 219-224.

Koike H, Tomioka S, Sorimachi H, Saido TC, Maruyama K, Okuyama A, Fujisawa-Sehara A, Ohno S, Suzuki K, Ishiura S. 1999. Membrane-anchored metalloprotease MDC9 has an alpha-secretase activity responsible for processing the amyloid precursor protein. *Biochem.J.* **343 Pt 2:** 371-375.

Koo EH, Lansbury PT, Jr., Kelly JW. 1999. Amyloid diseases: abnormal protein aggregation in neurodegeneration. *Proc.Natl.Acad.Sci.U.S.A* **96:** 9989-9990.

Koudinov AR, Koudinova NV, Kumar A, Beavis RC, Ghiso J. 1996. Biochemical characterization of Alzheimer's soluble amyloid beta protein in human cerebrospinal fluid: association with high density lipoproteins. *Biochem.Biophys.Res.Commun.* **223:** 592-597.

Ksiezak-Reding H, Morgan K, Mattiace LA, Davies P, Liu WK, Yen SH, Weidenheim K, Dickson DW. 1994. Ultrastructure and biochemical composition of paired helical filaments in corticobasal degeneration. *Am.J.Pathol.* **145:** 1496-1508.

Kumar-Singh S, Cras P, Wang R, Kros JM, van Swieten J, Lubke U, Ceuterick C, Serneels S, Vennekens K, Timmermans JP, Van Marck E, Martin JJ, van Duijn CM, Van Broeckhoven C. 2002. Dense-core senile plaques in the Flemish variant of Alzheimer's disease are vasocentric. *Am.J.Pathol.* **161:** 507-520.

Kumar-Singh S, De Jonghe C, Cruts M, Kleinert R, Wang R, Mercken M, De Strooper B, Vanderstichele H, Lofgren A, Vanderhoeven I, Backhovens H, Vanmechelen E, Kroisel PM, Van Broeckhoven C. 2000. Nonfibrillar diffuse amyloid deposition due to a gamma(42)-secretase site mutation points to an essential role for N-truncated A beta(42) in Alzheimer's disease. *Hum.Mol.Genet.* **9:** 2589-2598.

Kuo YM, Beach TG, Sue LI, Scott S, Layne KJ, Kokjohn TA, Kalback WM, Luehrs DC, Vishnivetskaya TA, Abramowski D, Sturchler-Pierrat C, Staufenbiel M, Weller RO, Roher AE. 2001. The evolution of A beta peptide burden in the APP23 transgenic mice: implications for A beta deposition in Alzheimer disease. *Mol.Med.* **7:** 609-618.

Kwiatkowski DJ, Stossel TP, Orkin SH, Mole JE, Colten HR, Yin HL. 1986. Plasma and cytoplasmic gelsolins are encoded by a single gene and contain a duplicated actin-binding domain. *Nature* **323:** 455-458.

Lalowski M, Golabek A, Lemere CA, Selkoe DJ, Wisniewski HM, Beavis RC, Frangione B, Wisniewski T. 1996. The "nonamyloidogenic" p3 fragment (amyloid beta17-42) is a major constituent of Down's syndrome cerebellar preamyloid. *J Biol.Chem.* **271:** 33623-33631.

Lambert MP, Barlow AK, Chromy BA, Edwards C, Freed R, Liosatos M, Morgan TE, Rozovsky I, Trommer B, Viola KL, Wals P, Zhang C, Finch CE, Krafft GA, Klein WL. 1998. Diffusible, nonfibrillar ligands derived from Abeta1-42 are potent central nervous system neurotoxins. *Proc.Natl.Acad.Sci.U.S.A* **95:** 6448-6453.

Lammich S, Kojro E, Postina R, Gilbert S, Pfeiffer R, Jasionowski M, Haass C, Fahrenholz F. 1999. Constitutive and regulated alpha-secretase cleavage of Alzheimer's amyloid precursor protein by a disintegrin metalloprotease. *Proc.Natl.Acad.Sci.U.S.A* **96:** 3922-3927.

Lansbury PT, Jr. 1999. Evolution of amyloid: what normal protein folding may tell us about fibrillogenesis and disease. *Proc.Natl.Acad.Sci.U.S.A* **96:** 3342-3344.

Lee SC, Liu W, Brosnan CF, Dickson DW. 1994. GM-CSF promotes proliferation of human fetal and adult microglia in primary cultures. *Glia* **12:** 309-318.

Leitlein J, Aulwurm S, Waltereit R, Naumann U, Wagenknecht B, Garten W, Weller M, Platten M. 2001. Processing of immunosuppressive pro-TGF-beta 1,2 by human glioblastoma cells involves cytoplasmic and secreted furin-like proteases. *J.Immunol.* **166:** 7238-7243.

Lemere CA, Blusztajn JK, Yamaguchi H, Wisniewski T, Saido TC, Selkoe DJ. 1996. Sequence of deposition of heterogeneous amyloid beta-peptides and APO E in Down syndrome: implications for initial events in amyloid plaque formation. *Neurobiol.Dis.* **3:** 16-32.

Levy E, Carman MD, Fernandez-Madrid IJ, Power MD, Lieberburg I, van Duinen SG, Bots GT, Luyendijk W, Frangione B. 1990a. Mutation of the Alzheimer's disease amyloid gene in hereditary cerebral hemorrhage, Dutch type. *Science* **248:** 1124-1126.

Levy E, Haltia M, Fernandez-Madrid I, Koivunen O, Ghiso J, Prelli F, Frangione B. 1990b. Mutation in gelsolin gene in Finnish hereditary amyloidosis. *J.Exp.Med.* **172:** 1865-1867.

Levy E, Lopez-Otin C, Ghiso J, Geltner D, Frangione B. 1989. Stroke in Icelandic patients with hereditary amyloid angiopathy is related to a mutation in the cystatin C gene, an inhibitor of cysteine proteases. *J.Exp.Med.* **169:** 1771-1778.

Levy E, Sastre M, Kumar A, Gallo G, Piccardo P, Ghetti B, Tagliavini F. 2001. Codeposition of cystatin C with amyloid-beta protein in the brain of Alzheimer disease patients. *J.Neuropathol.Exp.Neurol.* **60:** 94-104.

Levy-Lahad E, Wasco W, Poorkaj P, Romano DM, Oshima J, Pettingell WH, Yu CE, Jondro PD, Schmidt SD, Wang K, . 1995. Candidate gene for the chromosome 1 familial Alzheimer's disease locus. *Science* **269:** 973-977.

Li F, Iseki E, Odawara T, Kosaka K, Yagishita S, Amano N. 1998. Regional quantitative analysis of tau-positive neurons in progressive supranuclear palsy: comparison with Alzheimer's disease. *J.Neurol.Sci.* **159:** 73-81.

Li JJ, McAdam KP. 1984. Human amyloid P component: an elastase inhibitor. *Scand.J.Immunol.* **20:** 219-226.

Li YM, Lai MT, Xu M, Huang Q, DiMuzio-Mower J, Sardana MK, Shi XP, Yin KC, Shafer JA, Gardell SJ. 2000. Presenilin 1 is linked with gamma-secretase activity in the detergent solubilized state. *Proc.Natl.Acad.Sci.U.S.A* **97:** 6138-6143.

Lidstrom AM, Bogdanovic N, Hesse C, Volkman I, Davidsson P, Blennow K. 1998. Clusterin (apolipoprotein J) protein levels are increased in hippocampus and in frontal cortex in Alzheimer's disease. *Exp.Neurol.* **154:** 511-521.

Lin X, Koelsch G, Wu S, Downs D, Dashti A, Tang J. 2000. Human aspartic protease memapsin 2 cleaves the beta-secretase site of beta-amyloid precursor protein. *Proc.Natl.Acad.Sci.U.S.A* **97:** 1456-1460.

Lippa CF, Smith TW, Saunders AM, Hulette C, Pulaski-Salo D, Roses AD. 1997. Apolipoprotein E-epsilon 2 and Alzheimer's disease: genotype influences pathologic phenotype. *Neurology* **48:** 515-519.

Lofberg H, Grubb AO, Nilsson EK, Jensson O, Gudmundsson G, Blondal H, Arnason A, Thorsteinsson L. 1987. Immunohistochemical characterization of the amyloid deposits and quantitation of pertinent cerebrospinal fluid proteins in hereditary cerebral hemorrhage with amyloidosis. *Stroke* **18:** 431-440.

Lopez-Perez E, Zhang Y, Frank SJ, Creemers J, Seidah N, Checler F. 2001. Constitutive alpha-secretase cleavage of the beta-amyloid precursor protein in the furin-deficient LoVo cell line: involvement of the pro-hormone convertase 7 and the disintegrin metalloprotease ADAM10. *J.Neurochem.* **76:** 1532-1539.

Love S, Duchen LW. 1982. Familial cerebellar ataxia with cerebrovascular amyloid. *J.Neurol.Neurosurg.Psychiatry* **45:** 271-273.

Lovestone S, Reynolds CH. 1997. The phosphorylation of tau: a critical stage in neurodevelopment and neurodegenerative processes. *Neuroscience* **78:** 309-324.

Ma J, Yee A, Brewer HB, Jr., Das S, Potter H. 1994. Amyloid-associated proteins alpha 1-antichymotrypsin and apolipoprotein E promote assembly of Alzheimer beta-protein into filaments. *Nature* **372:** 92-94.

Maat-Schieman ML, van Duinen SG, Bornebroek M, Haan J, Roos RA. 1996. Hereditary cerebral hemorrhage with amyloidosis-Dutch type (HCHWA-D): II--A review of histopathological aspects. *Brain Pathol.* **6:** 115-120.

Maat-Schieman ML, Yamaguchi H, van Duinen SG, Natte R, Roos RA. 2000. Age-related plaque morphology and C-terminal heterogeneity of amyloid beta in Dutch-type hereditary cerebral hemorrhage with amyloidosis. *Acta Neuropathol.(Berl)* **99:** 409-419.

Mackic JB, Stins M, McComb JG, Calero M, Ghiso J, Kim KS, Yan SD, Stern D, Schmidt AM, Frangione B, Zlokovic BV. 1998. Human blood-brain barrier receptors for Alzheimer's amyloid-beta 1- 40. Asymmetrical binding, endocytosis, and transcytosis at the apical side of brain microvascular endothelial cell monolayer. *J.Clin.Invest* **102:** 734-743.

MacRaild CA, Stewart CR, Mok YF, Gunzburg MJ, Perugini MA, Lawrence LJ, Tirtaatmadja V, Cooper-White JJ, Howlett GJ. 2004. Non-fibrillar components of amyloid deposits mediate the self-association and tangling of amyloid fibrils. *J Biol.Chem.* **279:** 21038-21045.

Mahley RW. 1988. Apolipoprotein E: cholesterol transport protein with expanding role in cell biology. *Science* **240:** 622-630.

Mann DM, Iwatsubo T, Ihara Y, Cairns NJ, Lantos PL, Bogdanovic N, Lannfelt L, Winblad B, Maat-Schieman ML, Rossor MN. 1996. Predominant deposition of amyloid-beta 42(43) in plaques in cases of Alzheimer's disease and hereditary cerebral hemorrhage associated with mutations in the amyloid precursor protein gene. *Am.J.Pathol.* **148:** 1257-1266.

Mann DM, Pickering-Brown SM, Takeuchi A, Iwatsubo T. 2001a. Amyloid angiopathy and variability in amyloid beta deposition is determined by mutation position in presenilin-1-linked Alzheimer's disease. *Am.J.Pathol.* **158:** 2165-2175.

Mann DM, Takeuchi A, Sato S, Cairns NJ, Lantos PL, Rossor MN, Haltia M, Kalimo H, Iwatsubo T. 2001b. Cases of Alzheimer's disease due to deletion of exon 9 of the presenilin-1 gene show an unusual but characteristic beta-amyloid pathology known as 'cotton wool' plaques. *Neuropathol.Appl.Neurobiol.* **27:** 189-196.

Mao M, Fu G, Wu JS, Zhang QH, Zhou J, Kan LX, Huang QH, He KL, Gu BW, Han ZG, Shen Y, Gu J, Yu YP, Xu SH, Wang YX, Chen SJ, Chen Z. 1998. Identification of genes expressed in human CD34(+) hematopoietic stem/progenitor cells by expressed sequence tags and efficient full-length cDNA cloning. *Proc.Natl.Acad.Sci.U.S.A* **95:** 8175-8180.

Marcinkiewicz M. 2002. BetaAPP and furin mRNA concentrates in immature senile plaques in the brain of Alzheimer patients. *J.Neuropathol.Exp.Neurol.* **61:** 815-829.

Masters CL, Gajdusek DC, Gibbs CJ, Jr. 1981. The familial occurrence of Creutzfeldt-Jakob disease and Alzheimer's disease. *Brain* **104:** 535-558.

Maury CP. 1991. Gelsolin-related amyloidosis. Identification of the amyloid protein in Finnish hereditary amyloidosis as a fragment of variant gelsolin. *J.Clin.Invest* **87:** 1195-1199.

Maury CP, Nurmiaho-Lassila EL, Rossi H. 1994. Amyloid fibril formation in gelsolin-derived amyloidosis. Definition of the amyloidogenic region and evidence of accelerated amyloid formation of mutant Asn-187 and Tyr-187 gelsolin peptides. *Lab Invest* **70:** 558-564.

May PC, Finch CE. 1992. Sulfated glycoprotein 2: new relationships of this multifunctional protein to neurodegeneration. *Trends Neurosci.* **15:** 391-396.

McCarron MO, Hoffmann KL, DeLong DM, Gray L, Saunders AM, Alberts MJ. 1999. Intracerebral hemorrhage outcome: apolipoprotein E genotype, hematoma, and edema volumes. *Neurology* **53:** 2176-2179.

McGeer PL, Akiyama H, Itagaki S, McGeer EG. 1989. Activation of the classical complement pathway in brain tissue of Alzheimer patients. *Neurosci.Lett.* **107:** 341-346.

McGeer PL, Kawamata T, Walker DG. 1992. Distribution of clusterin in Alzheimer brain tissue. *Brain Res.* **579:** 337-341.

McGeer PL, McGeer EG. 1995. The inflammatory response system of brain: implications for therapy of Alzheimer and other neurodegenerative diseases. *Brain Res.Brain Res.Rev.* **21:** 195-218.

McGeer PL, McGeer EG. 2001. Inflammation, autotoxicity and Alzheimer disease. *Neurobiol.Aging* **22:** 799-809.

McGeer PL, Walker DG, Akiyama H, Kawamata T, Guan AL, Parker CJ, Okada N, McGeer EG. 1991. Detection of the membrane inhibitor of reactive lysis (CD59) in diseased neurons of Alzheimer brain. *Brain Res.* **544:** 315-319.

McLaurin J, Yang D, Yip CM, Fraser PE. 2000. Review: modulating factors in amyloid-beta fibril formation. *J.Struct.Biol.* **130:** 259-270.

McLean CA, Cherny RA, Fraser FW, Fuller SJ, Smith MJ, Beyreuther K, Bush AI, Masters CL. 1999. Soluble pool of Abeta amyloid as a determinant of severity of neurodegeneration in Alzheimer's disease. *Ann.Neurol.* **46:** 860-866.

McMenemey WH. 1952. Proceedings of the first International Congress of Neuropathology, Rome. In: Turin: Rosenberg and Sellier, 432-436.

McMenemey WH. 1970. Alzheimer's Disease and related conditions: A Ciba foundation Symposium. In: Wolstenholme GEW, O'Conner M, eds. London: 132-133.

Mead S, James-Galton M, Revesz T, Doshi RB, Harwood G, Pan EL, Ghiso J, Frangione B, Plant G. 2000. Familial British dementia with amyloid angiopathy: early clinical, neuropsychological and imaging findings. *Brain* **123 (Pt 5):** 975-991.

Miravalle L, Tokuda T, Chiarle R, Giaccone G, Bugiani O, Tagliavini F, Frangione B, Ghiso J. 2000. Substitutions at codon 22 of Alzheimer's abeta peptide induce diverse conformational changes and apoptotic effects in human cerebral endothelial cells. *J.Biol.Chem.* **275:** 27110-27116.

Mirra SS, Heyman A, McKeel D, Sumi SM, Crain BJ, Brownlee LM, Vogel FS, Hughes JP, van Belle G, Berg L. 1991. The Consortium to Establish a Registry for Alzheimer's Disease (CERAD). Part II. Standardization of the neuropathologic assessment of Alzheimer's disease. *Neurology* **41:** 479-486.

Miyazono M, Kitamoto T, Iwaki T, Tateishi J. 1992. Colocalization of prion protein and beta protein in the same amyloid plaques in patients with Gerstmann-Straussler syndrome. *Acta Neuropathol.(Berl)* **83:** 333-339.

Morelli L, Llovera R, Gonzalez SA, Affranchino JL, Prelli F, Frangione B, Ghiso J, Castano EM. 2003. Differential degradation of amyloid beta genetic variants associated with hereditary dementia or stroke by insulin-degrading enzyme. *J Biol.Chem.* **278:** 23221-23226.

Morelli L, Llovera R, Ibendahl S, Castano EM. 2002. The degradation of amyloid beta as a therapeutic strategy in Alzheimer's disease and cerebrovascular amyloidoses. *Neurochem.Res.* **27:** 1387-1399.

Morgan D, Diamond DM, Gottschall PE, Ugen KE, Dickey C, Hardy J, Duff K, Jantzen P, DiCarlo G, Wilcock D, Connor K, Hatcher J, Hope C, Gordon M, Arendash GW. 2000. A beta peptide vaccination prevents memory loss in an animal model of Alzheimer's disease. *Nature* **408:** 982-985.

Mori H, Takio K, Ogawara M, Selkoe DJ. 1992. Mass spectrometry of purified amyloid beta protein in Alzheimer's disease. *J.Biol.Chem.* **267:** 17082-17086.

Morishima-Kawashima M, Hasegawa M, Takio K, Suzuki M, Yoshida H, Watanabe A, Titani K, Ihara Y. 1995. Hyperphosphorylation of tau in PHF. *Neurobiol.Aging* **16:** 365-371.

Mouton PR, Martin LJ, Calhoun ME, Dal Forno G, Price DL. 1998. Cognitive decline strongly correlates with cortical atrophy in Alzheimer's dementia. *Neurobiol.Aging* **19:** 371-377.

Muller U, Bodeker RH, Gerundt I, Kurz A. 1996. Lack of association between alpha 1-antichymotrypsin polymorphism, Alzheimer's disease, and allele epsilon 4 of apolipoprotein E. *Neurology* **47:** 1575-1577.

Nakayama K. 1997. Furin: a mammalian subtilisin/Kex2p-like endoprotease involved in processing of a wide variety of precursor proteins. *Biochem.J.* **327 (Pt 3):** 625-635.

Namba Y, Tomonaga M, Kawasaki H, Otomo E, Ikeda K. 1991. Apolipoprotein E immunoreactivity in cerebral amyloid deposits and neurofibrillary tangles in Alzheimer's disease and kuru plaque amyloid in Creutzfeldt-Jakob disease. *Brain Res.* **541:** 163-166.

Natte R, Maat-Schieman ML, Haan J, Bornebroek M, Roos RA, van Duinen SG. 2001. Dementia in hereditary cerebral hemorrhage with amyloidosis-Dutch type is associated with cerebral amyloid angiopathy but is independent of plaques and neurofibrillary tangles. *Ann.Neurol.* **50:** 765-772.

Nicoll JA, Burnett C, Love S, Graham DI, Dewar D, Ironside JW, Stewart J, Vinters HV. 1997. High frequency of apolipoprotein E epsilon 2 allele in hemorrhage due to cerebral amyloid angiopathy. *Ann.Neurol.* **41:** 716-721.

Nilsberth C, Westlind-Danielsson A, Eckman CB, Condron MM, Axelman K, Forsell C, Stenh C, Luthman J, Teplow DB, Younkin SG, Naslund J, Lannfelt L. 2001. The 'Arctic' APP mutation (E693G) causes Alzheimer's disease by enhanced Abeta protofibril formation. *Nat.Neurosci.* **4:** 887-893.

Nilsson LN, Bales KR, DiCarlo G, Gordon MN, Morgan D, Paul SM, Potter H. 2001. Alpha-1-antichymotrypsin promotes beta-sheet amyloid plaque deposition in a transgenic mouse model of Alzheimer's disease. *J.Neurosci.* **21:** 1444-1451.

Nochlin D, Bird TD, Nemens EJ, Ball MJ, Sumi SM. 1998. Amyloid angiopathy in a Volga German family with Alzheimer's disease and a presenilin-2 mutation (N141I). *Ann.Neurol.* **43:** 131-135.

Oda T, Wals P, Osterburg HH, Johnson SA, Pasinetti GM, Morgan TE, Rozovsky I, Stine WB, Snyder SW, Holzman TF, . 1995. Clusterin (apoJ) alters the aggregation of amyloid beta-peptide (A beta 1-42) and forms slowly sedimenting A beta complexes that cause oxidative stress. *Exp.Neurol.* **136:** 22-31.

Olafsson I, Thorsteinsson L, Jensson O. 1996. The molecular pathology of hereditary cystatin C amyloid angiopathy causing brain hemorrhage. *Brain Pathol.* **6:** 121-126.

Ozawa K, Tomiyama T, Maat-Schieman ML, Roos RA, Mori H. 2002. Enhanced Abeta40 deposition was associated with increased Abeta42-43 in cerebral vasculature with Dutch-type hereditary cerebral hemorrhage with amyloidosis (HCHWA-D). *Ann.N.Y.Acad.Sci.* **977:** 149-154.

Pangburn MK, Muller-Eberhard HJ. 1983. Initiation of the alternative complement pathway due to spontaneous hydrolysis of the thioester of C3. *Ann.N.Y.Acad.Sci.* **421:** 291-298.

Pasternack JM, Abraham CR, Van Dyke BJ, Potter H, Younkin SG. 1989. Astrocytes in Alzheimer's disease gray matter express alpha 1-antichymotrypsin mRNA. *Am.J.Pathol.* **135:** 827-834.

Peers MC, Lenders MB, Defossez A, Delacourte A, Mazzuca M. 1988. Cortical angiopathy in Alzheimer's disease: the formation of dystrophic perivascular neurites is related to the exudation of amyloid fibrils from the pathological vessels. *Virchows Arch.A Pathol.Anat.Histopathol.* **414:** 15-20.

Pepys MB, Rademacher TW, Amatayakul-Chantler S, Williams P, Noble GE, Hutchinson WL, Hawkins PN, Nelson SR, Gallimore JR, Herbert J, . 1994. Human serum amyloid P component is an invariant constituent of amyloid deposits and has a uniquely homogeneous glycostructure. *Proc.Natl.Acad.Sci.U.S.A* **91:** 5602-5606.

Perlmutter LS, Chui HC, Saperia D, Athanikar J. 1990. Microangiopathy and the colocalization of heparan sulfate proteoglycan with amyloid in senile plaques of Alzheimer's disease. *Brain Res.* **508:** 13-19.

Pfeifer LA, White LR, Ross GW, Petrovitch H, Launer LJ. 2002. Cerebral amyloid angiopathy and cognitive function: the HAAS autopsy study. *Neurology* **58:** 1629-1634.

Piccini A, Russo C, Gliozzi A, Relini A, Vitali A, Borghi R, Giliberto L, Armirotti A, D'Arrigo C, Bachi A, Cattaneo A, Canale C, Torrassa S, Saido TC, Markesbery W, Gambetti P, Tabaton M. 2005. beta-amyloid is different in normal aging and in Alzheimer disease. *J Biol.Chem.* **280:** 34186-34192.

Picken MM, Larrondo-Lillo M, Coria F, Gallo GR, Shelanski ML, Frangione B. 1990. Distribution of the protease inhibitor alpha 1-antichymotrypsin in cerebral and systemic amyloid. *J.Neuropathol.Exp.Neurol.* **49:** 41-48.

Pickford F, Onstead L, Camacho-Prihar C, Hardy J, McGowan E. 2003. Expression of mBRI(2) in mice. *Neurosci.Lett.* **338:** 95-98.

Pike CJ, Overman MJ, Cotman CW. 1995. Amino-terminal deletions enhance aggregation of beta-amyloid peptides in vitro. *J.Biol.Chem.* **270:** 23895-23898.

Pillot T, Goethals M, Vanloo B, Lins L, Brasseur R, Vandekerckhove J, Rosseneu M. 1997. Specific modulation of the fusogenic properties of the Alzheimer beta-amyloid peptide by apolipoprotein E isoforms. *Eur.J Biochem.* **243:** 650-659.

Pitas RE, Boyles JK, Lee SH, Foss D, Mahley RW. 1987. Astrocytes synthesize apolipoprotein E and metabolize apolipoprotein E-containing lipoproteins. *Biochim.Biophys.Acta* **917:** 148-161.

Pittois K, Deleersnijder W, Merregaert J. 1998. cDNA sequence analysis, chromosomal assignment and expression pattern of the gene coding for integral membrane protein 2B. *Gene* **217:** 141-149.

Pittois K, Wauters J, Bossuyt P, Deleersnijder W, Merregaert J. 1999. Genomic organization and chromosomal localization of the Itm2a gene. *Mamm.Genome* **10:** 54-56.

Plant GT, Revesz T, Barnard RO, Harding AE, Gautier-Smith PC. 1990. Familial cerebral amyloid angiopathy with nonneuritic amyloid plaque formation. *Brain* **113 (Pt 3):** 721-747.

Potter H, Nelson RB, Das S, Siman R, Kayyali US, Dressler D. 1992. The involvement of proteases, protease inhibitors, and an acute phase response in Alzheimer's disease. *Ann.N.Y.Acad.Sci.* **674:** 161-173.

Potter H, Wefes IM, Nilsson LN. 2001. The inflammation-induced pathological chaperones ACT and apo-E are necessary catalysts of Alzheimer amyloid formation. *Neurobiol.Aging* **22:** 923-930.

Prelli F, Levy E, van Duinen SG, Bots GT, Luyendijk W, Frangione B. 1990. Expression of a normal and variant Alzheimer's beta-protein gene in amyloid of hereditary cerebral hemorrhage, Dutch type: DNA and protein diagnostic assays. *Biochem.Biophys.Res.Commun.* **170:** 301-307.

Premkumar DR, Cohen DL, Hedera P, Friedland RP, Kalaria RN. 1996. Apolipoprotein E-epsilon4 alleles in cerebral amyloid angiopathy and cerebrovascular pathology associated with Alzheimer's disease. *Am.J.Pathol.* **148:** 2083-2095.

Probst A, Langui D, Lautenschlager C, Ulrich J, Brion JP, Anderton BH. 1988. Progressive supranuclear palsy: extensive neuropil threads in addition to neurofibrillary tangles. Very similar antigenicity of subcortical neuronal pathology in progressive supranuclear palsy and Alzheimer's disease. *Acta Neuropathol.(Berl)* **77:** 61-68.

Quist A, Doudevski I, Lin H, Azimova R, Ng D, Frangione B, Kagan B, Ghiso J, Lal R. 2005. Amyloid ion channels: a common structural link for protein-misfolding disease. *Proc.Natl.Acad.Sci.U.S.A* **102:** 10427-10432.

Revesz T, Ghiso J, Lashley T, Plant G, Rostagno A, Frangione B, Holton JL. 2003. Cerebral amyloid angiopathies: a pathologic, biochemical, and genetic view. *J.Neuropathol.Exp.Neurol.* **62:** 885-898.

Revesz T, Holton JL, Doshi B, Anderton BH, Scaravilli F, Plant GT. 1999. Cytoskeletal pathology in familial cerebral amyloid angiopathy (British type) with non-neuritic amyloid plaque formation. *Acta Neuropathol.(Berl)* **97:** 170-176.

Roebroek AJ, Umans L, Pauli IG, Robertson EJ, Van Leuven F, Van de Ven WJ, Constam DB. 1998. Failure of ventral closure and axial rotation in embryos lacking the proprotein convertase Furin. *Development* **125:** 4863-4876.

Rogers J, Cooper NR, Webster S, Schultz J, McGeer PL, Styren SD, Civin WH, Brachova L, Bradt B, Ward P, . 1992a. Complement activation by beta-amyloid in Alzheimer disease. *Proc.Natl.Acad.Sci.U.S.A* **89:** 10016-10020.

Rogers J, Schultz J, Brachova L, Lue LF, Webster S, Bradt B, Cooper NR, Moss DE. 1992b. Complement activation and beta-amyloid-mediated neurotoxicity in Alzheimer's disease. *Res.Immunol.* **143:** 624-630.

Rogers J, Webster S, Lue LF, Brachova L, Civin WH, Emmerling M, Shivers B, Walker D, McGeer P. 1996. Inflammation and Alzheimer's disease pathogenesis. *Neurobiol.Aging* **17:** 681-686.

Roher AE, Palmer KC, Yurewicz EC, Ball MJ, Greenberg BD. 1993. Morphological and biochemical analyses of amyloid plaque core proteins purified from Alzheimer disease brain tissue. *J.Neurochem.* **61:** 1916-1926.

Rostagno A, Revesz T, Lashley T, Tomidokoro Y, Magnotti L, Braendgaard H, Plant G, Bojsen-Moller M, Holton J, Frangione B, Ghiso J. 2002. Complement activation in chromosome 13 dementias. Similarities with Alzheimer's disease. *J.Biol.Chem.* **277:** 49782-49790.

Rozemuller JM, Abbink JJ, Kamp AM, Stam FC, Hack CE, Eikelenboom P. 1991. Distribution pattern and functional state of alpha 1-antichymotrypsin in plaques and vascular amyloid in Alzheimer's disease. A immunohistochemical study with monoclonal antibodies against native and inactivated alpha 1-antichymotrypsin. *Acta Neuropathol.(Berl)* **82:** 200-207.

Rozemuller JM, Eikelenboom P, Stam FC, Beyreuther K, Masters CL. 1989. A4 protein in Alzheimer's disease: primary and secondary cellular events in extracellular amyloid deposition. *J.Neuropathol.Exp.Neurol.* **48:** 674-691.

Rozemuller JM, van d, V, Eikelenboom P. 1992. Activated microglia and cerebral amyloid deposits in Alzheimer's disease. *Res.Immunol.* **143:** 646-649.

Russo C, Saido TC, DeBusk LM, Tabaton M, Gambetti P, Teller JK. 1997. Heterogeneity of water-soluble amyloid beta-peptide in Alzheimer's disease and Down's syndrome brains. *FEBS Lett.* **409:** 411-416.

Russo C, Schettini G, Saido TC, Hulette C, Lippa C, Lannfelt L, Ghetti B, Gambetti P, Tabaton M, Teller JK. 2000. Presenilin-1 mutations in Alzheimer's disease. *Nature* **405:** 531-532.

Saido TC, Iwatsubo T, Mann DM, Shimada H, Ihara Y, Kawashima S. 1995. Dominant and differential deposition of distinct beta-amyloid peptide species, A beta N3(pE), in senile plaques. *Neuron* **14:** 457-466.

Saido TC, Yamao-Harigaya W, Iwatsubo T, Kawashima S. 1996. Amino- and carboxyl-terminal heterogeneity of beta-amyloid peptides deposited in human brain. *Neurosci.Lett.* **215:** 173-176.

Sanan DA, Weisgraber KH, Russell SJ, Mahley RW, Huang D, Saunders A, Schmechel D, Wisniewski T, Frangione B, Roses AD, . 1994. Apolipoprotein E associates with beta amyloid peptide of Alzheimer's disease to form novel monofibrils. Isoform apoE4 associates more efficiently than apoE3. *J.Clin.Invest* **94:** 860-869.

Sanchez-Pulido L, Devos D, Valencia A. 2002. BRICHOS: a conserved domain in proteins associated with dementia, respiratory distress and cancer. *Trends Biochem.Sci.* **27:** 329-332.

Schalken JA, Roebroek AJ, Oomen PP, Wagenaar SS, Debruyne FM, Bloemers HP, Van de Ven WJ. 1987. fur gene expression as a discriminating marker for small cell and nonsmall cell lung carcinomas. *J.Clin.Invest* **80:** 1545-1549.

Schenk D, Barbour R, Dunn W, Gordon G, Grajeda H, Guido T, Hu K, Huang J, Johnson-Wood K, Khan K, Kholodenko D, Lee M, Liao Z, Lieberburg I, Motter R, Mutter L, Soriano F, Shopp G, Vasquez N, Vandevert C, Walker S, Wogulis M, Yednock T, Games D, Seubert P. 1999. Immunization with amyloid-beta attenuates Alzheimer-disease-like pathology in the PDAPP mouse. *Nature* **400:** 173-177.

Schmechel DE, Saunders AM, Strittmatter WJ, Crain BJ, Hulette CM, Joo SH, Pericak-Vance MA, Goldgaber D, Roses AD. 1993. Increased amyloid beta-peptide deposition in cerebral cortex as a consequence of apolipoprotein E genotype in late-onset Alzheimer disease. *Proc.Natl.Acad.Sci.U.S.A* **90:** 9649-9653.

Schmidt ML, Martin JA, Lee VM, Trojanowski JQ. 1996. Convergence of Lewy bodies and neurofibrillary tangles in amygdala neurons of Alzheimer's disease and Lewy body disorders. *Acta Neuropathol.(Berl)* **91:** 475-481.

Schmidt ML, Murray JM, Trojanowski JQ. 1993. Continuity of neuropil threads with tangle-bearing and tangle-free neurons in Alzheimer disease cortex. A confocal laser scanning microscopy study. *Mol.Chem.Neuropathol.* **18:** 299-312.

Schnittger S, Rao VV, Abrahamson M, Hansmann I. 1993. Cystatin C (CST3), the candidate gene for hereditary cystatin C amyloid angiopathy (HCCAA), and other members of the cystatin gene family are clustered on chromosome 20p11.2. *Genomics* **16:** 50-55.

Schultz J, Schaller J, McKinley M, Bradt B, Cooper N, May P, Rogers J. 1994. Enhanced cytotoxicity of amyloid beta-peptide by a complement dependent mechanism. *Neurosci.Lett.* **175:** 99-102.

Schvartz I, Seger D, Shaltiel S. 1999. Vitronectin. *Int.J.Biochem.Cell Biol.* **31:** 539-544.

Schwab C, Akiyama H, McGeer EG, McGeer PL. 1998. Extracellular neurofibrillary tangles are immunopositive for the 40 carboxy-terminal sequence of beta-amyloid protein. *J.Neuropathol.Exp.Neurol.* **57:** 1131-1137.

Schwab C, Hosokawa M, Akiyama H, McGeer PL. 2003. Familial British dementia: colocalization of furin and ABri amyloid. *Acta Neuropathol.(Berl)* **106:** 278-284.

Schwab C, Steele JC, McGeer EG, McGeer PL. 1997. Amyloid P immunoreactivity precedes C4d deposition on extracellular neurofibrillary tangles. *Acta Neuropathol.(Berl)* **93:** 87-92.

Schwab C, Steele JC, McGeer PL. 1996a. Neurofibrillary tangles of Guam parkinson-dementia are associated with reactive microglia and complement proteins. *Brain Res.* **707:** 196-205.

Schwab C, Steele JC, McGeer PL. 1996b. Neurofibrillary tangles of Guam parkinson-dementia are associated with reactive microglia and complement proteins. *Brain Res.* **707:** 196-205.

Seidah NG, Chretien M. 1994. Pro-protein convertases of subtilisin/kexin family. *Methods Enzymol.* **244:** 175-188.

Seidah NG, Chretien M. 1999. Proprotein and prohormone convertases: a family of subtilases generating diverse bioactive polypeptides. *Brain Res.* **848:** 45-62.

Selkoe DJ. 1994. Alzheimer's disease: a central role for amyloid. *J Neuropathol.Exp.Neurol.* **53:** 438-447.

Selkoe DJ. 1998. The cell biology of beta-amyloid precursor protein and presenilin in Alzheimer's disease. *Trends Cell Biol.* **8:** 447-453.

Selkoe DJ. 1999. Translating cell biology into therapeutic advances in Alzheimer's disease. *Nature* **399:** A23-A31.

Selkoe DJ. 2001. Alzheimer's disease: genes, proteins, and therapy. *Physiol Rev.* **81:** 741-766.

Shen Y, Halperin JA, Lee CM. 1995. Complement-mediated neurotoxicity is regulated by homologous restriction. *Brain Res.* **671:** 282-292.

Shen Y, Lue L, Yang L, Roher A, Kuo Y, Strohmeyer R, Goux WJ, Lee V, Johnson GV, Webster SD, Cooper NR, Bradt B, Rogers J. 2001. Complement activation by neurofibrillary tangles in Alzheimer's disease. *Neurosci.Lett.* **305:** 165-168.

Sheng JG, Mrak RE, Griffin WS. 1996. Apolipoprotein E distribution among different plaque types in Alzheimer's disease: implications for its role in plaque progression. *Neuropathol.Appl.Neurobiol.* **22:** 334-341.

Shibata M, Yamada S, Kumar SR, Calero M, Bading J, Frangione B, Holtzman DM, Miller CA, Strickland DK, Ghiso J, Zlokovic BV. 2000. Clearance of Alzheimer's amyloid-ss(1-40) peptide from brain by LDL receptor-related protein-1 at the blood-brain barrier. *J.Clin.Invest* **106:** 1489-1499.

Silkensen JR, Skubitz KM, Skubitz AP, Chmielewski DH, Manivel JC, Dvergsten JA, Rosenberg ME. 1995. Clusterin promotes the aggregation and adhesion of renal porcine epithelial cells. *J.Clin.Invest* **96:** 2646-2653.

Sinha S, Anderson JP, Barbour R, Basi GS, Caccavello R, Davis D, Doan M, Dovey HF, Frigon N, Hong J, Jacobson-Croak K, Jewett N, Keim P, Knops J, Lieberburg I, Power M, Tan H, Tatsuno G, Tung J, Schenk D, Seubert P, Suomensaari SM, Wang S, Walker D, John V, . 1999. Purification and cloning of amyloid precursor protein beta-secretase from human brain. *Nature* **402:** 537-540.

Sisodia SS, Koo EH, Beyreuther K, Unterbeck A, Price DL. 1990. Evidence that beta-amyloid protein in Alzheimer's disease is not derived by normal processing. *Science* **248:** 492-495.

Snow AD, Kinsella MG, Parks E, Sekiguchi RT, Miller JD, Kimata K, Wight TN. 1995. Differential binding of vascular cell-derived proteoglycans (perlecan, biglycan, decorin, and versican) to the beta-amyloid protein of Alzheimer's disease. *Arch.Biochem.Biophys.* **320:** 84-95.

Snow AD, Mar H, Nochlin D, Kimata K, Kato M, Suzuki S, Hassell J, Wight TN. 1988. The presence of heparan sulfate proteoglycans in the neuritic plaques and congophilic angiopathy in Alzheimer's disease. *Am.J.Pathol.* **133:** 456-463.

Snow AD, Mar H, Nochlin D, Kresse H, Wight TN. 1992. Peripheral distribution of dermatan sulfate proteoglycans (decorin) in amyloid-containing plaques and their presence in neurofibrillary tangles of Alzheimer's disease. *J.Histochem.Cytochem.* **40:** 105-113.

Snow AD, Mar H, Nochlin D, Sekiguchi RT, Kimata K, Koike Y, Wight TN. 1990. Early accumulation of heparan sulfate in neurons and in the beta-amyloid protein-containing lesions of Alzheimer's disease and Down's syndrome. *Am.J.Pathol.* **137:** 1253-1270.

Snow AD, Sekiguchi R, Nochlin D, Fraser P, Kimata K, Mizutani A, Arai M, Schreier WA, Morgan DG. 1994. An important role of heparan sulfate proteoglycan (Perlecan) in a model system for the deposition and persistence of fibrillar A beta-amyloid in rat brain. *Neuron* **12:** 219-234.

Solans A, Estivill X, de La LS. 2000. A new aspartyl protease on 21q22.3, BACE2, is highly similar to Alzheimer's amyloid precursor protein beta-secretase. *Cytogenet.Cell Genet.* **89:** 177-184.

Soto C, Golabek A, Wisniewski T, Castano EM. 1996. Alzheimer's beta-amyloid peptide is conformationally modified by apolipoprotein E in vitro. *Neuroreport* **7:** 721-725.

Stalder M, Phinney A, Probst A, Sommer B, Staufenbiel M, Jucker M. 1999. Association of microglia with amyloid plaques in brains of APP23 transgenic mice. *Am.J.Pathol.* **154:** 1673-1684.

Steiner H, Revesz T, Neumann M, Romig H, Grim MG, Pesold B, Kretzschmar HA, Hardy J, Holton JL, Baumeister R, Houlden H, Haass C. 2001. A pathogenic presenilin-1 deletion causes abberrant Abeta 42 production in the absence of congophilic amyloid plaques. *J.Biol.Chem.* **276:** 7233-7239.

Stoltzner SE, Grenfell TJ, Mori C, Wisniewski KE, Wisniewski TM, Selkoe DJ, Lemere CA. 2000. Temporal accrual of complement proteins in amyloid plaques in Down's syndrome with Alzheimer's disease. *Am.J.Pathol.* **156:** 489-499.

Strittmatter WJ, Roses AD. 1996. Apolipoprotein E and Alzheimer's disease. *Annu.Rev.Neurosci.* **19:** 53-77.

Strittmatter WJ, Saunders AM, Schmechel D, Pericak-Vance M, Enghild J, Salvesen GS, Roses AD. 1993a. Apolipoprotein E: high-avidity binding to beta-amyloid and increased frequency of type 4 allele in late-onset familial Alzheimer disease. *Proc.Natl.Acad.Sci.U.S.A* **90:** 1977-1981.

Strittmatter WJ, Weisgraber KH, Huang DY, Dong LM, Salvesen GS, Pericak-Vance M, Schmechel D, Saunders AM, Goldgaber D, Roses AD. 1993b. Binding of human apolipoprotein E to synthetic amyloid beta peptide: isoform-specific effects and implications for late-onset Alzheimer disease. *Proc.Natl.Acad.Sci.U.S.A* **90:** 8098-8102.

Strohmeyer R, Shen Y, Rogers J. 2000. Detection of complement alternative pathway mRNA and proteins in the Alzheimer's disease brain. *Brain Res.Mol.Brain Res.* **81:** 7-18.

Stromgren E. 1981. heredopathia ophthalmo-oto-encephalica. In: Vinken PJ, Bruyn GW, eds. *Handbook of clinical neurology*. Amsterdam: North-Holland Publishing Company, 150-152.

Stromgren E, Dalby A, Dalby MA, Ranheim B. 1970. Cataract, deafness, cerebellar ataxia, psychosis and dementia--a new syndrome. *Acta Neurol.Scand.* **46:** Suppl.

Su JH, Cummings BJ, Cotman CW. 1994. Early phosphorylation of tau in Alzheimer's disease occurs at Ser-202 and is preferentially located within neurites. *Neuroreport* **5:** 2358-2362.

Suzuki K, Terry RD. 1967. Fine structural localization of acid phosphatase in senile plaques in Alzheimer's presenile dementia. *Acta Neuropathol.(Berl)* **8:** 276-284.

Sykes PA, Watson SJ, Temple JS, Bateman RC, Jr. 1999. Evidence for tissue-specific forms of glutaminyl cyclase. *FEBS Lett.* **455:** 159-161.

Tacnet-Delorme P, Chevallier S, Arlaud GJ. 2001. Beta-amyloid fibrils activate the C1 complex of complement under physiological conditions: evidence for a binding site for A beta on the C1q globular regions. *J.Immunol.* **167:** 6374-6381.

Tamaoka A, Fraser PE, Ishii K, Sahara N, Ozawa K, Ikeda M, Saunders AM, Komatsuzaki Y, Sherrington R, Levesque G, Yu G, Rogaeva E, Shoji S, Nee LE, Pollen DA, Hendriks L, Martin JJ, Van Broeckhoven C, Roses AD, Farrer LA, George-Hyslop PH, Mori H. 1998. Amyloid-beta-protein isoforms in brain of subjects with PS1-linked. *Brain Res.Mol.Brain Res.* **56:** 178-185.

Taupin P, Gage FH. 2002. Adult neurogenesis and neural stem cells of the central nervous system in mammals. *J.Neurosci.Res.* **69:** 745-749.

Tekirian TL, Saido TC, Markesbery WR, Russell MJ, Wekstein DR, Patel E, Geddes JW. 1998. N-terminal heterogeneity of parenchymal and cerebrovascular Abeta deposits. *J.Neuropathol.Exp.Neurol.* **57:** 76-94.

Teller JK, Russo C, DeBusk LM, Angelini G, Zaccheo D, Dagna-Bricarelli F, Scartezzini P, Bertolini S, Mann DM, Tabaton M, Gambetti P. 1996. Presence of soluble amyloid beta-peptide precedes amyloid plaque formation in Down's syndrome. *Nat.Med.* **2:** 93-95.

Tenner AJ. 2001. Complement in Alzheimer's disease: opportunities for modulating protective and pathogenic events. *Neurobiol.Aging* **22:** 849-861.

Terry RD, Gonatas NK, Weiss M. 1964. The ultrastructure of the cerebral cortex in Alzheimer's disease. *Trans.Am.Neurol.Assoc.* **89:** 12.

Thomas G. 2002. Furin at the cutting edge: from protein traffic to embryogenesis and disease. *Nat.Rev.Mol.Cell Biol.* **3:** 753-766.

Tomidokoro Y, Lashley T, Rostagno A, Neubert T, Bojsen-Moller M, Braendgaard H, Plant G, Holton J, Frangione B, Revesz T, Ghiso J. 2005. Familial Danish dementia: Co-existence of Danish and Alzheimer amyloid subunits (ADan and Abeta) in the absence of compact plaques. *J Biol.Chem.*

Tooyama I, Kawamata T, Akiyama H, Moestrup SK, Gliemann J, McGeer PL. 1993. Immunohistochemical study of alpha 2 macroglobulin receptor in Alzheimer and control postmortem human brain. *Mol.Chem.Neuropathol.* **18:** 153-160.

Tooyama I, Kimura H, Akiyama H, McGeer PL. 1990. Reactive microglia express class I and class II major histocompatibility complex antigens in Alzheimer's disease. *Brain Res.* **523:** 273-280.

Tschopp J, Chonn A, Hertig S, French LE. 1993. Clusterin, the human apolipoprotein and complement inhibitor, binds to complement C7, C8 beta, and the b domain of C9. *J.Immunol.* **151:** 2159-2165.

Urmoneit B, Prikulis I, Wihl G, D'Urso D, Frank R, Heeren J, Beisiegel U, Prior R. 1997. Cerebrovascular smooth muscle cells internalize Alzheimer amyloid beta protein via a lipoprotein pathway: implications for cerebral amyloid angiopathy. *Lab Invest* **77:** 157-166.

Van Dorpe J, Smeijers L, Dewachter I, Nuyens D, Spittaels K, Van Den HC, Mercken M, Moechars D, Laenen I, Kuiperi C, Bruynseels K, Tesseur I, Loos R, Vanderstichele H, Checler F, Sciot R, Van Leuven F. 2000. Prominent cerebral amyloid angiopathy in transgenic mice overexpressing the london mutant of human APP in neurons. *Am.J Pathol.* **157:** 1283-1298.

van Horssen J, Otte-Holler I, David G, Maat-Schieman ML, van den Heuvel LP, Wesseling P, De Waal RM, Verbeek MM. 2001. Heparan sulfate proteoglycan expression in cerebrovascular amyloid beta deposits in Alzheimer's disease and hereditary cerebral hemorrhage with amyloidosis (Dutch) brains. *Acta Neuropathol.(Berl)* **102:** 604-614.

van Horssen J, Wesseling P, van den Heuvel LP, De Waal RM, Verbeek MM. 2003. Heparan sulphate proteoglycans in Alzheimer's disease and amyloid-related disorders. *Lancet Neurol.* **2:** 482-492.

Van Nostrand WE, Melchor JP, Cho HS, Greenberg SM, Rebeck GW. 2001. Pathogenic effects of D23N Iowa mutant amyloid beta -protein. *J.Biol.Chem.* **276:** 32860-32866.

Vassar R, Bennett BD, Babu-Khan S, Kahn S, Mendiaz EA, Denis P, Teplow DB, Ross S, Amarante P, Loeloff R, Luo Y, Fisher S, Fuller J, Edenson S, Lile J, Jarosinski MA, Biere AL, Curran E, Burgess T, Louis JC, Collins F, Treanor J, Rogers G, Citron M. 1999. Beta-secretase cleavage of Alzheimer's amyloid precursor protein by the transmembrane aspartic protease BACE. *Science* **286:** 735-741.

Velazquez P, Cribbs DH, Poulos TL, Tenner AJ. 1997. Aspartate residue 7 in amyloid beta-protein is critical for classical complement pathway activation: implications for Alzheimer's disease pathogenesis. *Nat.Med.* **3:** 77-79.

Verbeek MM, Otte-Holler I, van den BJ, van den Heuvel LP, David G, Wesseling P, De Waal RM. 1999. Agrin is a major heparan sulfate proteoglycan accumulating in Alzheimer's disease brain. *Am.J Pathol.* **155:** 2115-2125.

Verbeek MM, Otte-Holler I, Veerhuis R, Ruiter DJ, De Waal RM. 1998. Distribution of A beta-associated proteins in cerebrovascular amyloid of Alzheimer's disease. *Acta Neuropathol.(Berl)* **96:** 628-636.

Verga L, Frangione B, Tagliavini F, Giaccone G, Migheli A, Bugiani O. 1989. Alzheimer patients and Down patients: cerebral preamyloid deposits differ ultrastructurally and histochemically from the amyloid of senile plaques. *Neurosci.Lett.* **105:** 294-299.

Verkkoniemi A, Kalimo H, Paetau A, Somer M, Iwatsubo T, Hardy J, Haltia M. 2001. Variant Alzheimer disease with spastic paraparesis: neuropathological phenotype. *J.Neuropathol.Exp.Neurol.* **60:** 483-492.

Veugelers M, De Cat B, Ceulemans H, Bruystens AM, Coomans C, Durr J, Vermeesch J, Marynen P, David G. 1999. Glypican-6, a new member of the glypican family of cell surface heparan sulfate proteoglycans. *J.Biol.Chem.* **274:** 26968-26977.

Vey M, Schafer W, Berghofer S, Klenk HD, Garten W. 1994. Maturation of the trans-Golgi network protease furin: compartmentalization of propeptide removal, substrate cleavage, and COOH-terminal truncation. *J.Cell Biol.* **127:** 1829-1842.

Vickers JC, Chin D, Edwards AM, Sampson V, Harper C, Morrison J. 1996. Dystrophic neurite formation associated with age-related beta amyloid deposition in the neocortex: clues to the genesis of neurofibrillary pathology. *Exp.Neurol.* **141:** 1-11.

Vidal R, Calero M, Revesz T, Plant G, Ghiso J, Frangione B. 2001. Sequence, genomic structure and tissue expression of Human BRI3, a member of the BRI gene family. *Gene* **266:** 95-102.

Vidal R, Frangione B, Rostagno A, Mead S, Revesz T, Plant G, Ghiso J. 1999. A stop-codon mutation in the BRI gene associated with familial British dementia. *Nature* **399:** 776-781.

Vidal R, Ghiso J, Frangione B. 2000a. New familial forms of cerebral amyloid and dementia. *Mol.Psychiatry* **5:** 575-576.

Vidal R, Revesz T, Rostagno A, Kim E, Holton JL, Bek T, Bojsen-Moller M, Braendgaard H, Plant G, Ghiso J, Frangione B. 2000b. A decamer duplication in the 3' region of the BRI gene originates an amyloid peptide that is associated with dementia in a Danish kindred. *Proc.Natl.Acad.Sci.U.S.A* **97:** 4920-4925.

Vidricaire G, Denault JB, Leduc R. 1993. Characterization of a secreted form of human furin endoprotease. *Biochem.Biophys.Res.Commun.* **195:** 1011-1018.

Vinters HV. 1987. Cerebral amyloid angiopathy. A critical review. *Stroke* **18:** 311-324.

Vinters HV. 1992. Cerebral amyloid angiopathy and Alzheimer's disease: two entities or one? *J.Neurol.Sci.* **112:** 1-3.

Vinters HV, Nishimura GS, Secor DL, Pardridge WM. 1990. Immunoreactive A4 and gamma-trace peptide colocalization in amyloidotic arteriolar lesions in brains of patients with Alzheimer's disease. *Am.J.Pathol.* **137:** 233-240.

Vinters HV, Wang ZZ, Secor DL. 1996. Brain parenchymal and microvascular amyloid in Alzheimer's disease. *Brain Pathol.* **6:** 179-195.

Vonsattel JP, Myers RH, Hedley-Whyte ET, Ropper AH, Bird ED, Richardson EP, Jr. 1991. Cerebral amyloid angiopathy without and with cerebral hemorrhages: a comparative histological study. *Ann.Neurol.* **30:** 637-649.

Walker DG, McGeer PL. 1998. Vitronectin expression in Purkinje cells in the human cerebellum. *Neurosci.Lett.* **251:** 109-112.

Walsh DM, Hartley DM, Kusumoto Y, Fezoui Y, Condron MM, Lomakin A, Benedek GB, Selkoe DJ, Teplow DB. 1999. Amyloid beta-protein fibrillogenesis. Structure and biological activity of protofibrillar intermediates. *J.Biol.Chem.* **274:** 25945-25952.

Walsh DM, Lomakin A, Benedek GB, Condron MM, Teplow DB. 1997. Amyloid beta-protein fibrillogenesis. Detection of a protofibrillar intermediate. *J.Biol.Chem.* **272:** 22364-22372.

Webster S, Lue LF, Brachova L, Tenner AJ, McGeer PL, Terai K, Walker DG, Bradt B, Cooper NR, Rogers J. 1997. Molecular and cellular characterization of the membrane attack complex, C5b-9, in Alzheimer's disease. *Neurobiol.Aging* **18:** 415-421.

Wegiel J, Wisniewski HM, Dziewiatkowski J, Popovitch ER, Tarnawski M. 1996. Differential susceptibility to neurofibrillary pathology among patients with Down syndrome. *Dementia* **7:** 135-141.

Weller RO, Massey A, Newman TA, Hutchings M, Kuo YM, Roher AE. 1998. Cerebral amyloid angiopathy: amyloid beta accumulates in putative interstitial fluid drainage pathways in Alzheimer's disease. *Am.J.Pathol.* **153:** 725-733.

Westermark P, Araki S, Benson MD, Cohen AS, Frangione B, Masters CL, Saraiva MJ, Sipe JD, Husby G, Kyle RA, Selkoe D. 1999. Nomenclature of amyloid fibril proteins. Report from the meeting of the International Nomenclature Committee on Amyloidosis, August 8-9, 1998. Part 1. *Amyloid.* **6:** 63-66.

Wien TN, Sorby R, Omtvedt LA, Landsverk T, Husby G. 2004. Kinetics of glycosaminoglycan deposition in splenic AA amyloidosis induced in mink. *Scand.J Immunol.* **60:** 600-608.

Winkler DT, Bondolfi L, Herzig MC, Jann L, Calhoun ME, Wiederhold KH, Tolnay M, Staufenbiel M, Jucker M. 2001. Spontaneous hemorrhagic stroke in a mouse model of cerebral amyloid angiopathy. *J.Neurosci.* **21:** 1619-1627.

Wisniewski HM, Wegiel J. 1994. Beta-amyloid formation by myocytes of leptomeningeal vessels. *Acta Neuropathol.(Berl)* **87:** 233-241.

Wisniewski T, Castano EM, Golabek A, Vogel T, Frangione B. 1994a. Acceleration of Alzheimer's fibril formation by apolipoprotein E in vitro. *Am.J.Pathol.* **145:** 1030-1035.

Wisniewski T, Frangione B. 1992. Apolipoprotein E: a pathological chaperone protein in patients with cerebral and systemic amyloid. *Neurosci.Lett.* **135:** 235-238.

Wisniewski T, Ghiso J, Frangione B. 1991. Peptides homologous to the amyloid protein of Alzheimer's disease containing a glutamine for glutamic acid substitution have accelerated amyloid fibril formation. *Biochem.Biophys.Res.Commun.* **179:** 1247-1254.

Wisniewski T, Golabek AA, Kida E, Wisniewski KE, Frangione B. 1995. Conformational mimicry in Alzheimer's disease. Role of apolipoproteins in amyloidogenesis. *Am.J Pathol.* **147:** 238-244.

Wisniewski T, Lalowski M, Bobik M, Russell M, Strosznajder J, Frangione B. 1996. Amyloid beta 1-42 deposits do not lead to Alzheimer's neuritic plaques in aged dogs. *Biochem.J* **313 (Pt 2):** 575-580.

Wisniewski T, Lalowski M, Levy E, Marques MR, Frangione B. 1994b. The amino acid sequence of neuritic plaque amyloid from a familial Alzheimer's disease patient. *Ann.Neurol.* **35:** 245-246.

Wolfe MS, De Los AJ, Miller DD, Xia W, Selkoe DJ. 1999. Are presenilins intramembrane-cleaving proteases? Implications for the molecular mechanism of Alzheimer's disease. *Biochemistry* **38:** 11223-11230.

Wood SJ, Chan W, Wetzel R. 1996. Seeding of A beta fibril formation is inhibited by all three isotypes of apolipoprotein E. *Biochemistry* **35:** 12623-12628.

Worster C, Greenfield JG, McMenemey WH. 1940. A Form of Familial Presenile Dementia with Spastic Paralysis. *Brain* 237-254.

Worster-Drought C, Greenfield JG, McMenemey WH. 1944. A form of Familial Presenile Dementia with Spastic Paralysis. *Brain* 38-43.

Wyss-Coray T, Yan F, Lin AH, Lambris JD, Alexander JJ, Quigg RJ, Masliah E. 2002. Prominent neurodegeneration and increased plaque formation in complement-inhibited Alzheimer's mice. *Proc.Natl.Acad.Sci.U.S.A* **99:** 10837-10842.

Yamaguchi H, Nakazato Y, Hirai S, Shoji M, Harigaya Y. 1989. Electron micrograph of diffuse plaques. Initial stage of senile plaque formation in the Alzheimer brain. *Am.J.Pathol.* **135:** 593-597.

Yamaguchi H, Nakazato Y, Kawarabayashi T, Ishiguro K, Ihara Y, Morimatsu M, Hirai S. 1991. Extracellular neurofibrillary tangles associated with degenerating neurites and neuropil threads in Alzheimer-type dementia. *Acta Neuropathol.(Berl)* **81:** 603-609.

Yamaguchi H, Yamazaki T, Lemere CA, Frosch MP, Selkoe DJ. 1992. Beta amyloid is focally deposited within the outer basement membrane in the amyloid angiopathy of Alzheimer's disease. An immunoelectron microscopic study. *Am.J.Pathol.* **141:** 249-259.

Yamashiro D, Li CH. 1976. Isolation and properties of ovine [1-pyroglutamic acid]-beta-lipoprotein. *Biochim.Biophys.Acta* **451:** 124-132.

Yan R, Bienkowski MJ, Shuck ME, Miao H, Tory MC, Pauley AM, Brashier JR, Stratman NC, Mathews WR, Buhl AE, Carter DB, Tomasselli AG, Parodi LA, Heinrikson RL, Gurney ME. 1999. Membrane-anchored aspartyl protease with Alzheimer's disease beta-secretase activity. *Nature* **402:** 533-537.

Yang DS, Smith JD, Zhou Z, Gandy SE, Martins RN. 1997. Characterization of the binding of amyloid-beta peptide to cell culture-derived native apolipoprotein E2, E3, and E4 isoforms and to isoforms from human plasma. *J.Neurochem.* **68:** 721-725.

Yasojima K, Schwab C, McGeer EG, McGeer PL. 2000. Human neurons generate C-reactive protein and amyloid P: upregulation in Alzheimer's disease. *Brain Res.* **887:** 80-89.

Yin HL, Kwiatkowski DJ, Mole JE, Cole FS. 1984. Structure and biosynthesis of cytoplasmic and secreted variants of gelsolin. *J.Biol.Chem.* **259:** 5271-5276.

Zahedi K. 1997. Characterization of the binding of serum amyloid P to laminin. *J.Biol.Chem.* **272:** 2143-2148.

Zhou Z, Smith JD, Greengard P, Gandy S. 1996. Alzheimer amyloid-beta peptide forms denaturant-resistant complex with type epsilon 3 but not type epsilon 4 isoform of native apolipoprotein E. *Mol.Med.* **2:** 175-180.

Zlokovic BV. 2002. Vascular disorder in Alzheimer's disease: role in pathogenesis of dementia and therapeutic targets. *Adv.Drug Deliv.Rev.* **54:** 1553-1559.

Zlokovic BV. 2004. Clearing amyloid through the blood-brain barrier. *J Neurochem.* **89:** 807-811.

Zlokovic BV, Ghiso J, Mackic JB, McComb JG, Weiss MH, Frangione B. 1993. Blood-brain barrier transport of circulating Alzheimer's amyloid beta. *Biochem.Biophys.Res.Commun.* **197:** 1034-1040.

Zlokovic BV, Martel CL, Matsubara E, McComb JG, Zheng G, McCluskey RT, Frangione B, Ghiso J. 1996. Glycoprotein 330/megalin: probable role in receptor-mediated transport of apolipoprotein J alone and in a complex with Alzheimer disease amyloid beta at the blood-brain and blood-cerebrospinal fluid barriers. *Proc.Natl.Acad.Sci.U.S.A* **93:** 4229-4234.